University of Strathclyde

Department of Naval Architecture, Ocean and Marine Engineering

Investigation of Cavitation Influence on Propeller-Rudder-Hull Interaction

Naz YILMAZ

A thesis presented in fulfilment of the requirements for the degree of Doctor of Philosophy

2019

This thesis is the result of the Author's original research. It has been composed by the Author and has not been previously submitted for examination which has led to the award of a degree.

Signed: Date:

Acknowledgements

Undoubtedly, I have spent three invaluable and enjoyable years during my PhD studies in Glasgow. I would like to thank everyone who contributed to this and helped me for completing the most important training of my life with their support, help, assistance and companionship.

To begin with, I would like to express the deepest appreciation to my primary supervisor, Professor Mehmet Atlar, director of research, who has been always a supportive mentor for me during these three years for not only my PhD studies but also my academic journey. I have always benefited from his wide and invaluable experience in both my academic and personal life. Professor Atlar always supported and believed in me and my studies even I had some hesitations during this journey from time to time. I have always felt that I am a so lucky PhD student when I was studying with him.

Also, I would like to acknowledge the valuable support and help of my second supervisor, Patrick Fitzsimmons. I have always benefited from his boundless experience, academic and professional background on propeller cavitation. I am also indebted to Patrick who supported proofreading of my papers and thesis for spending his valuable time and effort.

Moreover, I gratefully acknowledge the sponsorship of The Ministry of National Education, Turkey, for giving the PhD Scholarship to fully support my PhD research at the University of Strathclyde, Glasgow.

I also would like to express my gratitude to Professor Noriyuki Sasaki for providing data for my propeller-rudder interaction studies and sharing his invaluable experience on marine hydrodynamics.

I also would like to thank Dr Mahdi Khorasanchi who was my primary supervisor in the first year of my PhD for sharing his immense knowledge of computational marine hydrodynamics.

I would also like to thank the University of Strathclyde Faculty of Engineering for the provision of the ARCHIE-WeSt high-performance computing facilities. The CFD results were obtained using the EPSRC funded ARCHIE-WeSt High-Performance Computer (www.archie-west.ac.uk), EPSRC grant no. EP/K000586/1.

Additionally, I would like to thank my colleagues and friends who helped me to spend three fantastic years in Glasgow, in alphabetical order: Dr Elif Oguz, Kurt Mizzi, Matthias Maasch, Dr Tahsin Tezdogan and Dr Yigit Kemal Demirel. I also would like to thank my colleagues and my officemates, Emin Ozturk and Dr Batuhan Aktas for their support and encouragement during my PhD research. I also gratefully acknowledge Dr Aktas's help and support for providing test data and sharing his experimental experience with me without any hesitation.

My many thanks extend to Sefer Anil Gunbeyaz, Zeynep Gunbeyaz, Dr Rafet Emek Kurt and Senem Kurt for making my days brighter in Glasgow.

I would also like to thank my self-sacrificing mother for always supporting my decisions and for believing in me. I would like to remember my deceased grandma, who passed away on 14th December 2017. I very much wish she could feel that I have completed my PhD!

Last, but definitely not least, I would like to thank my dear husband, Gorkem Yilmaz for his total understanding and support, completely changing his life and completing this arduous journey with me. Without his support and motivation, I would not have completed this thesis.

Naz Yilmaz, December 2018

Contents

Acknowledgements iii
Contents v
List of Figures ix
List of Tables xv
Nomenclature xvii
Abstract xxii
Chapter 1 Introduction 1
1.1 Introduction 1
1.2 General Perspectives 1
1.3 Motivation 4
1.4 Aims and Objectives 5
1.5 Thesis Layout 6
1.6 Summary 10
Chapter 2 Literature Review 11
2.1 Introduction 11
2.2 History of Propeller Cavitation 11
2.3 History of Bubble Dynamics 14
2.4 Modelling of Propeller Cavitation 17
2.5 Cavitation Investigation Methods 26
2.6 Cavitation Influence on Propeller – Rudder – Hull Interaction 31
2.7 Concluding Remarks 36
Chapter 3 Methodology 38
3.1 Introduction 38
3.2 Computational Fluid Dynamics (CFD) 38
3.2.1 Modelling Turbulence 39
3.2.2 Modelling Multiphase Flow 42
3.2.3 Modelling Cavitation 42
3.2.4 Modelling Motion 46
3.3 Experimental Fluid Dynamics (EFD) 47
3.3.1 The SJTU Cavitation Tunnel 47
3.4 Test Cases 50

3.4.1 Model Scale Propellers 51
3.4.2 Ship Model 56
3.5 Verification and Validation 58
3.5.1 Methodology and Procedure 58
3.5.2 Open Water Simulations 60
3.5.3 Cavitation Simulations 64
3.6 Concluding Remarks 72
Chapter 4 Open Water Propeller Performance 74
4.1 Introduction 74
4.2 Open Water Propeller Characteristics 74
4.3 Numerical Modelling 76
4.3.1 Computational domain 77
4.3.2 Mesh Generation 78
4.3.3 Boundary Conditions 80
4.4 Presentation and Discussion of Results 82
4.4.1 Effect of cavitation on the open water propeller performance data 88
4.5 Concluding Remarks 90
Chapter 5 Propeller Cavitation 92
5.1 Introduction 92
5.2 Computational domain 93
5.3 Mesh Generation 93
5.4 Simulation Setup and Boundary Conditions 106
5.5 Results and Discussion 110
5.5.1 *INSEAN E779A* Propeller 110
5.5.2 *PPTC VP1304* Propeller 115
5.5.3 *The Princess Royal* Propeller 130
5.6 Concluding Remarks 144
Chapter 6 Cavitation Influence on Propeller – Rudder Interaction 146
6.1 Introduction 146
6.2 Experimental Fluid Dynamics Approach (EFD) 147
6.2.1 The Emerson Cavitation Tunnel (ECT) 147
6.3 Propeller – Conventional Rudder Arrangement 149
6.3.1 Experimental Setup 149
6.3.2 Computational Fluid Dynamics Approach (CFD) 152
6.4 *The Princess Royal* Propeller – Rudder Arrangement 158
6.4.1 Experimental Setup 158

6.4.2 Computational Fluid Dynamic Approach (CFD) 161
6.5 Results and Discussions 164
6.5.1 Propeller – Conventional Rudder Arrangement 164
6.5.2 The *Princess Royal* Propeller – Rudder Arrangement 173
6.6 Concluding Remarks 192
Chapter 7 Cavitation Influence on Propeller – Rudder – Hull Interaction 195
7.1 Introduction 195
7.2 Model Scale Investigations 196
7.2.1 Experimental Fluid Dynamics Approach (EFD) 196
7.2.2 Computational Fluid Dynamics Approach (CFD) 202
7.3 Full Scale Investigations 210
7.3.1 Experimental Fluid Dynamics Approach (EFD) – Review of Full-Scale Trials 210
7.3.2 Computational Fluid Dynamics Approach (CFD) 211
7.4 Results and Discussions 217
7.4.1 Model Scale Investigations 217
7.4.2 Full Scale Investigations 228
7.5 Concluding Remarks 236
Chapter 8 Conclusions and Recommendations 238
8.1 Introduction 238
8.2 Main Conclusions and Contributions 238
8.3 Concluding Remarks 246
8.4 Recommendations for Future Work 249
References 253

List of Figures

Figure 2-1 Turbinia and its triple propeller arrangement on a shaft line 13
Figure 2-2 Parsons' world's first cavitation tunnel 13
Figure 2-3 A cavity bubble deformation during bubble collapse stage (Left: Numerical Results (Plesset, 1970), Right: CFD Results in 2D) 15
Figure 2-4 Measured radii of the cavitating core of propeller V (Kuiper, 1981) 16
Figure 2-5 Typical phase diagram (Brennen, 1995) 17
Figure 2-6 Cavitation Types (ITTC, 2002) 21
Figure 2-7 Propeller-Rudder-Hull Interaction (*The Princess Royal*) 31
Figure 3-1 The cavitation tunnel of Shanghai Jiao Tong University (SJTU) 48
Figure 3-2 Side view of the propeller dynamometer installed in the cavitation tunnel of SJTU 48
Figure 3-3 Strobodriver and stroboscopic light 49
Figure 3-4 Small water-filled tank for hydrophone 50
Figure 3-5 Hydrophone for noise measurement tests, Left; Hydrophone, Right; Sketch of test section including dynamometer & hydrophone 50
Figure 3-6 CAD geometry of the *PPTC VP 1304* Propeller (Top; PPTC with axial shaft, Bottom; PTTC with inclined shaft) 52
Figure 3-7 CAD geometry of the benchmark propeller 53
Figure 3-8 *'The Princess Royal'* Propeller Geometry 55
Figure 3-9 Left: Deep-V Hull Form Catamaran 'Princess Royal', Right: Princess Royal Propeller 56
Figure 3-10 Different Grids for V&V Studies 61
Figure 3-11 Grid Convergence Study 62
Figure 3-12 Different Grids for V&V Studies (Tip Vortex Cavitation) 64
Figure 3-13 Tip Vortex Cavitation Extension due to different grids for V&V studies 66
Figure 3-14 Different Grids for Grid Independency Study 68
Figure 3-15 Grid Convergence Study for K_T 70
Figure 3-16 Tip Vortex Cavitation Extension for V&V Studies 72
Figure 4-1 Computational Domain (Top; PPTC with shaft inclination, Bottom; INSEAN E779A propeller) 78
Figure 4-2 Generated Mesh (Top; *PPTC* with shaft inclination, Bottom; *The Princess Royal* propeller) 79

Figure 4-3 *y+* on blades, hub and shaft for *E779A* propeller 80

Figure 4-4 Computational domain and boundary conditions (Top: *PPTC* propeller with inclined shaft, Bottom: *E779A* propeller) 81

Figure 4-5 Propeller Performance Curves for *PPTC* propeller with inclined shaft case (EFD and CFD Comparison) 83

Figure 4-6 Propeller Performance Curves for the *Princess Royal* Propeller (EFD Results)..... 85

Figure 4-7 Propeller Performance Curves for the *Princess Royal* Propeller 86

Figure 4-8 Pressure Coefficient for Non-Cavitating Conditions (Top; 0.7R Bottom; 0.9R)..... 88

Figure 4-9 The effect of the cavitation on open water propeller performance 89

Figure 4-10 Pressure distribution on propeller surfaces (Left; Suction Side, Right; Pressure Side) (Top; *The Princess Royal*, Bottom; *INSEAN E779A*)..... 90

Figure 5-1 Computational Grid (Left; *PPTC VP1304* with inclined shaft, Right; *INSEAN E779A*)..... 95

Figure 5-2 Mesh Refinement using Volumetric Control (Tube) 97

Figure 5-3 Mesh Refinement using Volumetric Control (Spiral)..... 98

Figure 5-4 Absolute pressure threshold below 10000 [Pa]..... 101

Figure 5-5 Mesh refinement due to MARCS..... 102

Figure 5-6 Flow chart summarising new Mesh Adaption and Refinement approach for Cavitation Simulation (MARCS)..... 103

Figure 5-7 Absolute pressure threshold below 17000 [Pa]..... 104

Figure 5-8 Mesh generation using MARCS 104

Figure 5-9 Modified Flow chart summarising MARCS in order to reduce total number of cells 105

Figure 5-10 The *INSEAN E779A:* Comparisons cavitation pattern simulations as obtained from CFD (no tip vortex refinement) and EFD (Left; EFD, Right; CFD) 111

Figure 5-11 The *INSEAN E779A:* Stages in the improvement of modelling tip vortex cavitation extent 112

Figure 5-12 The *INSEAN E779A:* Comparisons between EFD and CFD results regarding tip vortex cavitation 114

Figure 5-13 The *INSEAN E779A*: Comparison of Results Tip Vortex Cavitation Roll-up (Left; EFD, Right; CFD, MARCS)..... 115

Figure 5-14 The *PPTC VP1304*: Cavitation Case 2.3.1 – Sheet Cavitation simulations 117

Figure 5-15 The *PPTC VP1304*: Cavitation Case 2.3.2 – Sheet Cavitation simulations 118

Figure 5-16 The *PPTC VP1304*: Cavitation Case 2.3.3 –Sheet Cavitation simulations 119

Figure 5-17 The *PPTC VP1304* with Axial Shaft; Comparisons of cavitation patterns 121

Figure 5-18 The *PPTC VP1304* with Axial Shaft: Cavitation Case 2.3.1 - Comparisons of tip vortex cavitation 123

Figure 5-19 The *PPTC VP1304* with Axial Shaft: Comparison of Tip Vortex Cavitation Roll-up Results 123

Figure 5-20 The *PPTC VP130 with* Axial Shaft: Comparison of Results Sheet and Tip Vortex Cavitation (MARCS) 124

Figure 5-21 The effect of the shaft inclination on the propeller velocity diagram (Carlton, 2002) 126

Figure 5-22 The *PPTC VP1304* with inclined Shaft: Comparisons between EFD and sheet cavitation patterns 127

Figure 5-23 *PPTC* Inclined Shaft - Comparisons between EFD and CFD results for cavitation patterns 129

Figure 5-24 *The Princess Royal* Tip Vortex Cavitation Inception (SJTU)..... 131

Figure 5-25 *The Princess Royal* Tip Vortex Cavitation Inception & Desinence Results (UNIGE & UNEW Results from Tani et al., 2017)..... 132

Figure 5-26 The *Princess Royal:* Cavitation pattern Comparisons between EFD and CFD (MARCS is not used) 135

Figure 5-27 The *Princess Royal:* Cavitation pattern Comparisons between EFD and CFD (MARCS is not used) 136

Figure 5-28 The *Princess Royal:* Cavitation pattern Comparisons between EFD and CFD (MARCS - tip vortex cavitation)..... 138

Figure 5-29 The *Princess Royal:* Cavitation pattern Comparisons between EFD and CFD (MARCS - tip vortex cavitation)..... 139

Figure 5-30 *The Princess Royal:* Comparison propeller performance coefficients (K_T, K_Q and η_0) for Open Water and Cavitation Tests 140

Figure 5-31 Tip Vortex Cavitation Extension Comparison in terms of Different Turbulence Models (From Left to Right; RANS, DES and LES) 142

Figure 5-32 Axial Velocity Comparisons between RANS and LES (0.9R Cylindrical Section) 143

Figure 6-1 Sketch of the Emerson Cavitation Tunnel..... 148

Figure 6-2 Emerson Cavitation Tunnel..... 149

Figure 6-3 Propeller-Conventional Rudder Arrangement..... 150

Figure 6-4 ECT test set-up including wake plate (Yilmaz et, al., 2018)..... 152

Figure 6-5 Flow Domain for Propeller and Conventional Rudder Configuration ... 154

Figure 6-6 Isosurface of Q-Criterion = 20000 s^{-2} 156

Figure 6-7 Generated mesh for Conventional Rudder-Propeller system 156

Figure 6-8 Wake Representation..... 159

Figure 6-9 Target Wake (Left), Simulated Wake (Right) (Aktas et. al., 2015) 160

Figure 6-10 Flow Domain including Background and Overset Mesh Regions 161

Figure 6-11 Generated Mesh for Propeller-Rudder Interaction Simulations with MARCS 162

Figure 6-12 Wake Representation in STAR-CCM+ and Boundary Conditions 164

Figure 6-13 Cavitation pattern for conventional rudder and propeller system (Left; Sheet Cavitation, Right; tip vortex cavitation) 166

Figure 6-14 Cavity Volume Change against Solution Time without and with MARCS application 166

Figure 6-15 The *Propeller-Convectional Rudder Arrangement:* Cavitation Comparisons for Conventional Rudder-propeller system (Left: EFD from tunnel tests; Right; CFD predictions) 167

Figure 6-16 The *Propeller-Convectional Rudder Arrangement:* Section Planes (z direction) at 6 spanwise positions on rudder for pressure distribution calculations 168

Figure 6-17 The *Propeller-Convectional Rudder Arrangement:* Chordwise pressure distribution at 6 spanwise positions for rudder (MARCS) (From top to bottom; S1-S6) (Red: Back, Blue: Face) 170

Figure 6-18 The *Propeller-Convectional Rudder Arrangement:* The deformation of the TVC in the presence of the rudder 171

Figure 6-19 The *Propeller-Convectional Rudder Arrangement:* Vortex Interaction with Rudder Leading Edge (From Top View) 172

Figure 6-20 The *Princess Royal Propeller – Rudder Arrangement*: Comparison of cavitation viewings (Left; Model test, Right; Full Scale Observations for Condition 4) (Top; EFD Results, Bottom; CFD Results) 174

Figure 6-21 *The Princess Royal Propeller – Rudder Arrangement*: Cavitation pattern for *The Princess Royal* propeller and rudder (Left; Sheet Cavitation, Right; tip vortex cavitation (MARCS)) 176

Figure 6-22 *The Princess Royal Propeller – Rudder Arrangement*: Cavity Volume Change against Solution Time without and with MARCS application 177

Figure 6-23 The *Princess Royal Propeller*: Cavitation Pattern Comparisons including TVC between the propeller without and with rudder arrangements 178

Figure 6-24 The *Princess Royal Propeller – Rudder Arrangement*: Condition 4 – EFD Results; High Speed Video Captures from Inward Camera 180

Figure 6-25 The *Princess Royal Propeller – Rudder Arrangement*: Condition 4 – CFD Results; Cavitation Pattern including extended TVC 181

Figure 6-26 The *Princess Royal Propeller – Rudder Arrangement*: Condition 4 – EFD Results; High Speed Video Captures from Outward Camera 182

Figure 6-27 The *Princess Royal Propeller – Rudder Arrangement*: Condition 4 – CFD Results; Cavitation Pattern including extended TVC 183

Figure 6-28 The *Princess Royal Propeller – Rudder Arrangement*: Vortex Interaction with Leading Edge 184

Figure 6-29 The *Princess Royal Propeller – Rudder Arrangement*: Section Planes (z direction) for pressure distribution calculations 185

Figure 6-30 Rudder Profiles (Left; Conventional Rudder, Right; The Princess Royal Rudder) 186

Figure 6-31 2D Pressure Distribution Plots over 3D rudder surfaces 187

Figure 6-32 The *Princess Royal Propeller – Rudder Arrangement*: Chordwise pressure distribution at 6 spanwise positions for rudder (From top to bottom; S1-S6) 188

Figure 6-33 The *Princess Royal Propeller – Rudder Arrangement*: The deformation of the TVC in the presence of the rudder and pressure distribution on the rudder (Port side view) 190

Figure 6-34 The Princess Royal Propeller – Rudder Arrangement: The deformation of the TVC in the presence of the rudder and pressure distribution on the rudder (Starboard side view) 191

Figure 7-1 The Large Circulating Channel of CNR INSEAN 197

Figure 7-2 The Princess Royal research Vessel and the Propeller 197

Figure 7-3 Stroscobic lights and camera arrangement 200

Figure 7-4 Cavitation observations: set up arrangement 200

Figure 7-5 Nomenclature of Pressure sensors and relative position 201

Figure 7-6 Computational Flow Domain Dimensions (Model Scale) 203

Figure 7-7 The Flow domain including Rotating (Sliding and Overset Mesh) and Stationary (Background) regions (Model Scale) 204

Figure 7-8 Isosurface of Q-Criterion = 10000 s^{-2} (Side view) (Model Scale) 205

Figure 7-9 Generated mesh using MARCS (Model Scale) 206

Figure 7-10 Boundary Conditions (Model Scale) 207

Figure 7-11 Flow chart summarising Simulation Procedure in the presence of the tip vortex cavitation (MARCS application) 210

Figure 7-12 Computational Flow Domain (Full Scale) 212

Figure 7-13 Flow domain including Rotating (Sliding and Overset Mesh) and Stationary (Background) regions (Full Scale) 213

Figure 7-14 The *Princess Royal Propeller-Rudder-Hull Interaction:* Isosurface of Q-Criterion = 10000 s^{-2} (Side view) (Full Scale) 214

Figure 7-15 Generated mesh using MARCS (Full Scale) 215

Figure 7-16 Boundary Conditions (Full Scale) (Left; Perspective view, Right; Front view) 217

Figure 7-17 Free surface representation (Model-Scale) 218

Figure 7-18 EFD Results - Cavitation observations @ V_M=2.61 m/s and n=20.96 rps 220

Figure 7-19 CFD Results - Cavitation Patterns including tip vortex cavitation 221

Figure 7-20 Cavitation pattern Comparisons (Model Scale) between EFD and CFD (Backward; EFD, Forward; CFD) (MARCS - tip vortex cavitation)..... 223

Figure 7-21 CFD Results- Cavitation pattern (Left; Sheet Cavitation, Right; tip vortex cavitation (MARCS) (Model Scale)..... 224

Figure 7-22 CFD Results Cavity Volume Change against to Solution Time without and with MARCS application (Model Scale) 224

Figure 7-23 Hull Pressure Fluctuations Comparisons between EFD (Red) and CFD (Black) Results (Sheet Cavitation, From Top to Bottom; P1, P2 and P3)..... 226

Figure 7-24 Hull Pressure Fluctuations Comparisons between EFD (Red) and CFD (Black) Results (Sheet Cavitation, From Top to Bottom; P5, P6 and P7)..... 227

Figure 7-25 Free surface representation (Full Scale) (Top; Volume Fraction of Air, Bottom; Volume Fraction of Water including sheet cavitation on propeller blades) 229

Figure 7-26 Cavitation pattern Comparisons between Sea Trials and CFD (Full Scale) (Top; Sea Trials, Bottom; CFD) (MARCS - tip vortex cavitation) 231

Figure 7-27 Cavitation pattern Comparisons between Sea Trials and CFD (Full Scale) (Top; Sea Trials, Bottom; CFD) (MARCS - tip vortex cavitation) 232

Figure 7-28 Cavitation pattern Comparisons between Sea Trials and CFD (Full Scale) (Top; Sea Trials, Bottom; CFD) (MARCS - tip vortex cavitation) 233

Figure 7-29 Cavitation pattern Comparisons between Sea Trials and CFD (MARCS - tip vortex cavitation) (Top; Sea Trials, Condition 3: 1200 rpm, Bottom; CFD; Condition 4: 2000 rpm)..... 235

List of Tables

Table 3-1 Particulars of the *PPTC* Propeller 52
Table 3-2 Particulars of the Propeller 53
Table 3-3 The *Princess Royal* Propeller Main Particulars 55
Table 3-4 The Princess Royal Research Vessel Main Particulars 57
Table 3-5 Grid Convergence Study in Non-Cavitating Conditions 61
Table 3-6 Time Step Convergence Study in Non-Cavitating Conditions 62
Table 3-7 Numerical Uncertainty Calculations from Grid and Time Step Convergence 62
Table 3-8 Validation of Thrust Coefficient (K_T) 63
Table 3-9 Validation of Torque Coefficient (K_Q) 63
Table 3-10 Grid Convergence Study for Cavitating Conditions 65
Table 3-11 Grid Uncertainty Study Results in Cavitating Conditions 65
Table 3-12 Numerical Uncertainty Calculations from Grid Convergence 65
Table 3-13 Validation of Thrust (K_T) and Torque Coefficient (K_Q) 67
Table 3-14 Grid Convergence Study in Cavitating Conditions 68
Table 3-15 Grid Convergence Study in Cavitating Conditions 69
Table 3-16 Time Step Convergence Study in Cavitating Conditions 69
Table 3-17 Numerical Uncertainty Calculations from Grid and Time Step Convergence 70
Table 3-18 Validation of K_T 71
Table 3-19 Validation of $10K_Q$ 71
Table 4-1 Boundary Conditions for Open Water Simulations 81
Table 4-2 EFD and CFD Comparisons for *PPTC* propeller with inclined shaft 83
Table 4-3 EFD and CFD Comparisons for the *Princess Royal* propeller 86
Table 4-4 EFD and CFD Comparisons for *INSEAN E779A* Propeller 87
Table 5-1 Mesh details for sheet cavitation simulations 95
Table 5-2 Mesh Details 99
Table 5-3 Mesh details for tip vortex cavitation simulations 106
Table 5-4 The *INSEAN E779A* Propeller Cavitation Conditions 108
Table 5-5 The *PPTC VP1304* Propeller Cavitation Conditions 109
Table 5-6 The *Princess Royal* Propeller Cavitation Conditions 109

Table 5-7 The *INSEAN E779A:* Comparison between CFD and EFD results for different mesh refinement approaches 113
Table 5-8 The *PPTC VP1304*: Thrust Coefficient Comparison between EFD &CFD 116
Table 5-9 The *PPTC VP1304*: Thrust Coefficient Comparison for mesh refinement methods 117
Table 5-10 Thrust Coefficients (Sheet vs Tip Vortex Cavitation Simulations)..... 141
Table 5-11 Propeller Performance Coefficients (Tip Vortex Cavitation Simulations) 141
Table 5-12 Propeller Performance Comparisons in terms of Different Turbulence Models..... 142
Table 6-1 General Specifications of the ECT 149
Table 6-2 Test Conditions..... 151
Table 6-3 EFD and CFD Conditions..... 153
Table 6-4 Mesh Details for propeller-conventional rudder arrangement..... 157
Table 6-5 Full Scale vs. Model Scale Operating Conditions 160
Table 6-6 Mesh Details for *The Princess Royal* propeller- rudder arrangement 163
Table 6-7 EFD and CFD Results Comparisons for conventional rudder-propeller arrangement..... 165
Table 6-8 Hydrodynamic Propeller Performance Interacting with Rudder 175
Table 6-9 Propeller Performance Coefficients (Sheet vs Tip Vortex Cavitation Simulations) 176
Table 6-10 Hydrodynamic Propeller Performance with and without rudder..... 178
Table 7-1 General Specifications of the Princess Royal Research Vessel..... 198
Table 7-2 Test Matrix..... 199
Table 7-3 Mesh Details for the *Princess Royal* propeller-rudder-hull arrangement (Model Scale) 205
Table 7-4 Mesh Details for the different computational regions (Model Scale) 205
Table 7-5 Exact positions of the each pressure sensor..... 208
Table 7-6 Full Scale Operating Conditions from *The Princess Royal* Sea Trials.... 211
Table 7-7 Mesh Details for the *Princess Royal* propeller-rudder-hull arrangement (Full Scale)..... 214
Table 7-8 Mesh Details for the different computational regions (Full Scale) 214
Table 7-9 Hydrodynamic Propeller Performance for Propeller-Rudder-Hull Interaction 218
Table 7-10 Hydrodynamic Propeller Performance for Propeller-Rudder-Hull Interaction 228

Nomenclature

Symbols

Item	*Description*	*Units*
A_E/A_0	*Expanded Blade Area Ratio*	*Non-dimensional*
a_v	*Volume Fraction of Vapour*	*Non-dimensional*
B	*Breadth*	*m*
C_P	*Pressure Coefficient*	*Non-dimensional*
C_{Pmin}	*Minimum Pressure Coefficient*	*Non-dimensional*
D	*Propeller Diameter*	*m*
D	*Experimentally Determined Value*	*Non-dimensional*
E	*Error*	*Non-dimensional*
g	*Gravitational Acceleration*	m/s^2
H	*Height*	*m*
J	*Advance Coefficient*	*Non-dimensional*
K_Q	*Torque Coefficient*	*Non-dimensional*
K_T	*Thrust Coefficient*	*Non-dimensional*
L	*Length*	*m*
n	*Propeller Revolution Speed*	*rps*
N	*Number of Bubbles*	*Non-dimensional*
n_0	*Number of Bubble per Unit Volume of Liquid*	*Non-dimensional*
η_0	*Open Water Efficiency*	*Non-dimensional*
P	*Tunnel Pressure*	*Pa*
P/D	*Pitch to Diameter Ratio*	*Non-dimensional*
P_0	*Reference Pressure*	*Pa*
P_M	*Local Pressure*	*Pa*
P_{min}	*Minimum Pressure*	*Pa*
P_{sat}	*Saturated Vapour Pressure*	*Pa*
P_{ST}	*Static Pressure*	*Pa*
P_{tun}	*Tunnel Pressure*	*Pa*
P_v	*Saturated Vapour Pressure*	*Pa*
P_{vac}	*Vacuum Pressure*	*Pa*

Q	*Torque*	*Nm*
Q	*Q-Criterion*	s^{-2}
Q_V	*Source Term for Volume Fraction of Vapour*	*Non-dimensional*
R	*Radius of One Bubble*	*m*
r	*Refinement ratio*	*Non-dimensional*
Re_n	*Reynolds Number*	*Non-dimensional*
S	*Simulated Determined Value*	*Non-dimensional*
S	*Strain Rate Tensors*	s^{-1}
S_L	*Upper Value in the Convergence h History of Parameter*	*Non-dimensional*
S_U	*Upper Value in the Convergence History of Parameter*	*Non-dimensional*
T	*Thrust*	*N*
t	*Time*	*s*
T	*Temperature*	^oC
U	*Cruising Speed*	*m/s*
u^*	*Reference Velocity*	*m/s*
U_D	*Experimental Uncertainty*	*Non-dimensional*
U_G	*Grid Uncertainty*	*Non-dimensional*
U_I	*Iteration Uncertainty*	*Non-dimensional*
U_k	*Uncertainty*	*Non-dimensional*
U_P	*Parameter Uncertainty*	*Non-dimensional*
U_{SN}	*Simulation Uncertainty*	*Non-dimensional*
U_T	*Time step Uncertainty*	*Non-dimensional*
U_V	*Validation Uncertainty*	*Non-dimensional*
V	*Velocity*	*m/s*
V	*Volume*	m^3
V_A	*Advance Velocity*	*m/s*
V_b	*Volume of One Bubble*	m^3
V_l	*Liquid Volume*	m^3
V_M	*Model Test Velocity*	*m/s*
V_R	*Reference Velocity*	*m/s*
v_r	*Bubble Growth Velocity*	*m/s*
V_S	*Ship Speed*	*m/s*

V_V	*Vapour Volume*	m^3
y	*the Normal Distance from the Centroid to the Wall*	*m*
y^+	*y plus*	*Non-dimensional*
z	*Number of Blades*	*Non-dimensional*
α_l	*Volume Fraction of Liquid*	*Non-dimensional*
γ	*Scaling Factor*	*Non-dimensional*
Δt	*Time Step*	*s*
λ	*Scale Factor*	*Non-dimensional*
μ	*Dynamic Viscosity of the Fluid*	*Kg/ms*
ν	*Kinematic Viscosity*	m^2/s
ρ	*Density*	Kg/m^3
ρ_l	*Liquid Density*	Kg/m^3
σ	*Cavitation Number*	*Non-dimensional*
σ_i	*Cavitation Inception Number*	*Non-dimensional*
σ_n	*Cavitation Number Based on Rotational Speed of Propeller*	*Non-dimensional*
τ	*Stress Tensor*	*Pa*
Ω	*Spin Rate Tensors*	s^{-1}

Abbreviations

2D	*2-Dimensional*
3D	*3-Dimensional*
AMT	*International Conference on Advanced Model Measurement Technology for The Maritime Industry*
AP	*Aft Perpendicular*
BEM	*Boundary Element Method*
BHP	*Break Horse Power*
CAD	*Computer Aided Design*
CFD	*Computational Fluid Dynamics*
CL	*Centreline*
CPP	*Controllable Pitch Propeller*
DES	*Detached Eddy Simulations*
DFBI	*Dynamic Fluid-Body Interaction*
DNS	*Direct Numerical Simulations*
DTMB	*David Taylor Model Basin*

ECT	*Emerson Cavitation Tunnel*
EFD	*Experimental Fluid Dynamics*
ESD	*Energy Saving Devices*
FCM	*Full Cavitation Model*
FP	*Forward Perpendicular*
FPP	*Fixed Pitch Propeller*
HTF	*Hydro Testing Forum*
INSEAN	*Instituto Nazionale di Studi ed Esperienze di Architettura Navale*
ITTC	*International Towing Tank Conference*
ITU	*Istanbul Technical Umiversity*
LDV	*Laser Doppler Velocimetry*
LES	*Large Eddy Simulations*
MARCS	*Mesh Adaption Refinement for Cavitation Simulations*
MARIN	*Maritime Research Institute Netherlands*
MAST	*School of Marine Science and Technology*
MRF	*Moving Reference Frame*
N/A	*Not Available*
PhD	*Doctor of Philosophy*
PIV	*Particle Image Velocimetry*
POT	*Propeller Open Water Tests*
PPTC	*Postdam Propeller Test Case*
RANS	*Reynolds Averaged Navier-Stokes*
RBM	*Rigid Body Motion*
SCAT	*Samsung Cavitation Tunnel*
SJTU	*Shanghai Jiao Tong University*
SMP	*Symposium of Marine Propulsors*
SONIC	*Supression of Underwater Noise Induced by Cavitation*
SSPA	*Statens Skeppsprovnings Anstalt (Acronym for SSPA Sweden AB)*
SST	*Shear Stress Transport*
SVA	*Schiffbau-Versuchsanstalt Postdam*
TVC	*Tip Vortex Cavitation*
UK	*United Kingdom*
UNEW	*Newcastle University*
UNIGE	*University of Genoa*
UoS	*University of Strathclyde*

URN	*Underwater Radiated Noise*
V&V	*Verification and Validation*
VIRTUE	*The Virtual Tank Utility in Europe*
VOF	*Volume of Fluid*
WALE	*Wall-Adapting Local-Eddy Viscosity*
WWI	*World War II*

Abstract

Computational modelling of tip vortex cavitation of a ship propeller has its challenges particularly to extend the cavitating tip vortex trajectories in the propeller's slipstream for investigating their influence on the propeller-rudder-hull interaction. Although the prediction of sheet cavitation on the propeller blade surfaces has been tackled successfully by many researchers, the research to extend the prediction model for the tip vortex cavitation from all propeller blades simultaneously and throughout the rudder is rather scarce. This PhD study, therefore, aims to contribute in this area of research to investigate the cavitation influence on propeller-rudder-hull interaction, especially due to the tip vortex cavitation, by using a commercial Computational Fluid Dynamics (CFD) code.

To achieve the above aim, an investigation on the propeller-rudder-hull system is conducted in steps; first by modelling the propeller performance and cavitation in CFD for the isolated propeller case, and next to continue with the propeller-rudder system and finally by modelling the propeller-rudder-hull combination case to represent the ship system. The CFD modelling for these cases are conducted using the commercial CFD software STAR-CCM+ and validated by the available Experimental Fluid Dynamics (EFD) data for three benchmark propellers including the Potsdam Propeller Test Case *(PPTC) VP1304*, *INSEAN E779A* model propeller and *The Princess Royal* research vessel model propeller which are all tested in different experimental facilities.

The cavitation model used in the commercial software is the Schnerr–Sauer model based on the Rayleigh-Plesset equation. This model together with the new meshing technique called **MARCS**, which is developed by the Author as an advanced **M**esh **A**daption **R**efinement procedure for **C**avitation **S**imulations, is applied successfully to simulate the cavitating tip vortices from all blades simultaneously in the propeller's slipstream beside other cavitation types. The cavitation simulations are conducted to test and validate the MARCS procedure to include the presence of the rudder and to study the interaction between the propeller and rudder including the effect of the hull

wake in the model scale. The simulation results are validated for two different types of propeller-rudder arrangements involving a typical container ship propeller-rudder arrangement and *The Princess Royal* propeller-rudder arrangement with an inclined shaft and flat rudder section tested in the Emerson Cavitation Tunnel.

Further cavitation simulations with the commercial code using the MARCS procedure are also conducted for the scaled full-model of *The Princess Royal* research vessel to simulate the model tests conducted in the depressurised large circulating water channel of CNR-INSEAN and to validate the simulation results with the EFD measurements available from this facility. Finally, the same computational tool and procedure are used for the cavitation simulations of *The Princess Royal* in full-scale, and the simulation results are compared with the cavitation observation images available from sea-trials with this vessel.

In spite of various shortcomings, which can be further improved, implementation of the new meshing procedure developed has proven that using a state-of-the-art commercial CFD code can be a practical and attractive analysis tool to investigate the influence of cavitation on propeller-rudder-hull interaction in the model and full-scale with confidence. Furthermore, it is feasible, and may be more attractive, to simulate the propeller cavitation directly in full-scale in order to save the additional time, effort and expense required for model tests. Due respect is given to the invaluable contributions made by the EFD in the validation stage of the CFD methods.

Chapter 1 Introduction

1.1 Introduction

Chapter 1 presents an introduction to the research study conducted in this thesis. Firstly, the general perspectives of the research study is given, and this is followed by the Author's motivation behind the research. The aim and objectives of the study are the next presented in this chapter while the layout of the thesis summarising the work conducted in each chapter of the thesis is explained. The chapter finally concludes with a summary of the work presented in this chapter.

1.2 General Perspectives

The present research study focuses on cavitation investigations relating to propeller, rudder and hull interaction. Cavitation investigations date back to the early 20^{th} century (see Chapter 2) with the experiments in the bubble dynamics field. Then these fundamental studies evolved into cavitation studies directly related to marine propeller applications.

Despite cavitation investigations having been started with experiments, various numerical models have been developed and used commonly in the past 40 years. Cavitation phenomena can be investigated for marine propellers with existing methods such as lifting surface, Boundary Element Methods (BEM) and even more accurately with computational fluid dynamics (CFD) methods due to better modelling of the physics of the flow, and developing computational power and technology.

Although the international marine research community recognizes experimental fluid dynamics (EFD) method, perhaps, as the most reliable approach for many cavitation investigations, CFD methods have other advantages for designers and researchers. The accessibility of commercial CFD software and open source codes can be verified and validated by using existing sets of EFD results, especially in benchmarking. CFD

methods also have some benefits in terms of time and cost compared to experiments such as cavitation observations tests in the cavitation tunnels.

CFD simulations of any physical phenomena include three important stages; namely, pre-processing, solving and the post-processing, which can provide very detailed results, images and videos for the better evaluation of the phenomena being investigated. Additionally, the use of CFD also allows users to easily change parameters and the conditions for the investigations of the phenomena in various physical configurations.

While the CFD approach is commonly used by many researchers for modelling complex flows such as cavitation, various open source codes and commercial CFD software have been developed in recent years. Although the open source codes offer the users more freedom to control the mathematical equations and physical models, these are still unreliable and need to be validated for extraordinarily complex flows. In contrast to open source codes, commercial CFD software are used by many design and research groups from various areas of expertise and also provide ever-growing platforms to test and validate their models. In the present study, one of the most widely used commercial CFD codes for marine applications (STAR-CCM+) has been used for the propeller performance simulations in non-cavitating and cavitating conditions of various propeller types in open water condition and behind the hull condition including the rudder in model and full-scale.

By the nature of the propeller cavitation phenomena, different types of cavitation were investigated within the scope of the present study, namely, sheet, bubble, tip and hub vortex cavitation, etc.) Each type of cavitation affects the propeller performance differently. While some sheet and tip vortex cavitation cause erosive effects on propeller blade surfaces, tip vortex cavitation is generally associated with radiated noise, particularly for naval, survey and cruise ships. Nowadays it is accepted that the extent and variation of the sheet cavitation on propeller blades can be predicted reasonably accurately with existing methods. However, computational modelling of the cavitating tip vortices of a propeller remains challenging, in particular for extending the cavitation trajectories from the blade tips up to and onto a rudder in the

wake of a ship with relatively large propeller-rudder separation, and thus interacting with the rudder.

In contrast to the Reynolds Average Navier-Stokes (RANS) model, scale-resolving simulations can model small-scale motions and resolve the large scales of turbulence. Within this context, there are two popular approaches for scale-resolving simulations, namely, Detached Eddy Simulations (DES) and Large Eddy Simulations (LES) models. Recently, the turbulence models based on these two approaches have been preferred widely by the CFD community for simulating complex physical phenomenon such as cavitation and especially for simulating the tip vortex cavitation.

From the ship propulsion point of view, traditionally, the propeller performance with its detailed hydrodynamic characteristics can be computed and investigated in two conditions; in “open water” and “behind the hull” conditions. This also applies for experiments with the propellers. Although some experiments for propeller cavitation investigations are conducted in open water with uniform flow (if the propeller is not operating in an inclined condition), the majority of investigations involves the assessment of propeller performance behind the hull to include the non-uniform effect of the hull flow. Thus, consistent with this tradition, in this study the cavitation, especially tip vortex cavitation, has been investigated using EFD and CFD methods firstly for the isolated propeller in open water, and later including the presence of the rudder to investigate the propeller-rudder interaction, and finally introducing the presence of the hull to investigate this interaction further, including the effect of the hull wake.

The influence of the cavitation on the propeller, rudder and hull interaction is a complex phenomenon. Although the cavitation can be predicted and presented for isolated propellers using EFD and CFD approaches, its accurate modelling on the propeller-rudder-hull interaction using CFD methods still requires to be developed further, verified and validated, especially for modelling tip vortex cavitation. Hence, cavitating propeller flows should be appropriately evaluated including the effect of rudder and hull geometries in non-uniform flow conditions and the condition which is the closest to the reality can be simulated using CFD methods.

Throughout this thesis, the commercial CFD software STAR-CCM+ version 12.04.10, which was developed by CD-Adapco, is used wherever unsteady RANS, DES and LES models have been applied. All the complex CFD simulations in this study were conducted through the University of Strathclyde's access to the High-Performance Computing facility for the West of Scotland (ARCHIE-WeSt).

1.3 Motivation

The following provides the Author's motivation behind the present research study; including how the research study may fill gaps in the literature, which are identified in Chapter 2, to make a worthwhile contribution to the state-of-the-art.

- ✓ Although the EFD approaches are still the most reliable and accurate method to predict propeller performance in non-cavitating and cavitating conditions, access to the test facilities such as towing tanks and cavitation tunnels and conducting some experiments is still too limited and expensive for many researchers.

- ✓ Nowadays it is accepted that hydrodynamic performance of marine propellers can be predicted reasonably accurately with CFD methods due to better modelling of the physics of the flow, and developing computational power and technology. In contrast to experiments, CFD methods are accessible, easy to use, cheap and suitable for the various physical problems. (Chapter 3)

- ✓ In contrast to open source codes, although the commercial codes have some limitations interfering the background of the physical phenomenon, they are still preferred by many researchers with different expertise and from different disciplines and applications throughout the world. Early in her professional career the Author had the opportunity to become familiar with and, have access to, one of the most widely used commercial CFD codes for marine applications. One of the challenging tasks of this career has been to use the limited resources of such commercial software wisely for the investigation of the complex

engineering problems such as the propeller cavitation phenomenon. (Chapter 3)

- ✓ The prediction of sheet cavitation sometimes gives unstable convergence due to the lack of more accurate tip vortex cavitation modelling. Hence a new method has to be developed by the Author for the propeller cavitation investigations for the better accuracy and the performance predictions of the propellers in cavitating conditions. (Chapter 2 and Chapter 5)

- ✓ To the best of the Author's knowledge, no CFD model exists to be able to simulate tip vortex cavitation, simultaneously from all blades, in the propeller's slipstream up to and interacting with the rudder; also including the investigation of the deformation of tip vortices in uniform and non-uniform flow conditions. (Chapter 2, Chapter 6)

- ✓ The modelling of the cavitation influence on the propeller, rudder and hull interaction is a real challenge including the propeller cavitation (with interacting phases of water and vapour) and the free surface (between air and water); in particular for extending the tip vortices from the blades up to a rudder in the wake of a ship hull and interacting with the rudder. (Chapter 7)

1.4 Aims and Objectives

The aim of this research study is to make contribution in the field of the cavitation influence on the propeller-rudder-hull interaction, especially by better modelling of tip vortex cavitation and fully exploiting the use of commercial CFD codes.

Within the above framework, and considering the traditional approach to analyse the hydrodynamic performance of a propeller in the presence of the rudder and hull in non-cavitating and cavitating conditions, the specific objectives of this research are listed as follows:

1. To review the state-of-the-art literature regarding the propeller cavitation, in particular its effect on the interaction due to the propeller, rudder and hull, and to identify the associated research gaps.
2. To develop a rational methodology for investigating propeller cavitation including the tip vortex cavitation using computational and experimental fluid dynamics methods.
3. To predict propeller performance in open water conditions to verify and validate the methodology and its implementation.
4. To predict propeller performance especially in cavitating conditions in open water conditions.
5. To develop a new mesh refinement technique to improve the simulation process of propeller performance and cavitation with better accuracy including the tip vortex cavitation simultaneously from all blades.
6. To investigate the cavitation influence on the propeller-rudder combination including the tip vortex cavitation from all blades extending in the propeller's slipstream.
7. To simulate the performance of the ship propulsion system including the propeller, rudder and hull in model and full-scale to investigate cavitation influence on the combined system as realistically as possible.

1.5 Thesis Layout

In achieving the above-stated aim and objectives, this research study is presented in the eight chapters of the thesis, described as follows:

- Chapter 1 - **Introduction**: In this chapter the general perspectives of the research study, the Author's motivation to conduct this study together with its aim and objectives are presented. The layout of the thesis, which describes a brief summary of the work conducted in the thesis to achieve the aim and objectives of the research, is also presented together with a brief summary of the chapter.

- Chapter 2 - **Literature Review**: The main objective of this chapter is to identify research gap(s) in open literature and hence to justify the aim and objectives of this research study. The chapter therefore provides a detailed state-of-the-art literature review on propeller cavitation regarding to the propeller, rudder and hull interaction. To begin with, the chapter presents the historical background to the cavitation studies. It then continues with a specific review on propeller cavitation, different types of the propeller cavitation and their investigations by using the CFD and EFD methods with a view to reflect on the influence of cavitation on the propeller-rudder-hull interaction. This review chapter finally concludes with a set of research gaps identified from the survey which forms the basis for the aim and objectives of the present study.

- Chapter 3 – **Methodology**: This chapter presents detailed information about the methods which have been developed and used step by step in this thesis for the investigations of the propeller cavitation regarding to the propeller, rudder and hull interaction phenomena. The chapter therefore presents the CFD and EFD methods, that have been used, to analyse the hydrodynamic performance of propellers including the rudder and hull effects. The model test cases used for the study are presented in detail. Validation and verification studies for the CFD simulations are presented and the chapter concludes with a brief summary of the chapter findings.

- Chapter 4 - **Open Water Propeller Performance**: As the first building brick of the propeller-rudder-hull system, this chapter concentrates on the isolated propeller case, and presents the details and results of the CFD simulations for the standard (benchmark) test propellers such as *PPTC VP1304*, *INSEAN E779A* and *The Princess Royal* model propellers in "non-cavitating" conditions. The comparison of the simulations with the benchmark test data are presented in detail and results are discussed regarding the propeller performance coefficients in non-cavitating and open water conditions. The chapter includes some concluding remarks based on the results of the investigations in this chapter.

- Chapter 5 - **Propeller Cavitation**: This chapter presents CFD simulations for the above stated standard test propellers and their performance predictions in "cavitating" conditions. In addition to the CFD simulations, cavitation tests were also conducted by the Author in the Shanghai Jiao Tong University (SJTU) cavitation tunnel for further experimental investigation of the open-water cavitation performance of *The Princess Royal* model propeller. The corresponding EFD and CFD results for this propeller are presented in this chapter. For the comparisons of the EFD and CFD results of the other standard test propellers, the EFD data have been obtained from the open literature and results are presented and discussed in this chapter. Additionally, in the same chapter, a new meshing technique, which utilizes a **M**esh **A**daption **R**efinement procedure for **C**avitation **S**imulations (MARCS), has been developed and applied successfully to simulate the tip vortex cavitation from all blades simultaneously, and particularly to trace their extensions in the propeller's slipstream. The MARCS procedure has also been used for the propeller-rudder and propeller-rudder-hull interaction simulations presented in subsequent Chapter 6 and 7. The chapter concludes with the final remarks of the findings from the investigations in this chapter.

- Chapter 6 – **Cavitation Influence on Propeller-Rudder Interaction**: This chapter presents the computational investigations of the cavitation influence on the propeller-rudder interaction including the tip vortex cavitation extension using the MARCS technique. For this investigation, two different propeller-rudder interaction cases were simulated; for the first case, a typical Container ship model propeller with a level shaft and a profile section of rudder in uniform flow was simulated, while for the second case *The Princess Royal* model propeller with an inclined shaft and flat-plated rudder in non-uniform flow was simulated. The simulation results for the first and second test cases were compared with the experimental data of the cavitation tunnel tests conducted in the Emerson Cavitation Tunnel (ECT). The results of the findings from both simulations cases and their comparisons with the experiments were discussed regarding the effect of the tip vortex cavitation and different types of

these propeller-rudder arrangements. The chapter concludes with the final remarks on the findings from this chapter.

- Chapter 7 – **Cavitation Influence on Propeller – Rudder – Hull Interaction**: This chapter presents the CFD simulations for the propeller cavitation behind the full hull with the rudder and in the presence of the free-surface. This is the ultimate case to study the cavitation influence on propeller-rudder-hull interaction and hence addressing the aim of this research study at model and full-scale. For this purpose two sets of simulation cases were presented with *The Princess Royal*. Firstly, the cavitation tunnel tests conducted in the depressurised Large Circulating Water Channel of CNR-INSEAN with the scaled model of *The Princess Royal* were simulated and results were compared with the test data for one of the test conditions which displayed the strongest tip vortex cavitation presence. This was followed by further CFD simulations in the full-scale for the cavitation performance of *The Princess Royal*, and comparing the results with the full-scale data. In both simulations the MARCS technique developed in Chapter 5 were used to improve the accurate simulation of the tip vortex cavitation and hence its influence on the propeller-rudder-hull interaction phenomena in the most realistic scenario. The chapter finally ends with the concluding remarks on the main findings obtained in the chapter.

- Chapter 8 - **Conclusions and Recommendations for Future Work**: This chapter starts with the presentation of an overall review of the research study regarding the contributions made to the state-of-the-art. This is in particular by the development of the MARCS methodology for better simulation of the cavitating propeller performance and hence to further understand the propeller, rudder and hull interaction in the presence of the tip vortex cavitation of all blades. The chapter continues with the statement of the main results and conclusions, that support the aim and objectives of the research study and how these objectives are addressed. The chapter concludes with the recommendations for future work that could not be achieved due to the scope and time limitations of this research study.

1.6 Summary

This chapter presented an introduction to the research study conducted in this thesis. Hence the general perspectives of the research study, Author's motivation behind the research and the aim and objectives of the study are presented as well as the layout of thesis to describe the work conducted in each chapter of the thesis.

Chapter 2 Literature Review

2.1 Introduction

Chapter 2 presents a critical literature review of the state-of-the-art related to propeller cavitation and its effect on the propeller, rudder and hull interaction. The review aims to identify the research gaps to justify the aim and objectives of this research study, and to support the computational and experimental approach to be developed and used in the study to achieve the aim and objectives.

The chapter initially presents a historical review of the propeller cavitation, bubble dynamics and different types of propeller cavitation in relation to the numerical modelling of two main types of propeller cavitation; sheet cavitation and tip vortex types. It then continues with the survey of the literature regarding the cavitation investigations and modelling methods using both EFD and the low-fidelity numerical and the CFD methods. The remaining part of the review and Chapter 2 is focused on the presence of cavitation regarding the propeller, rudder and hull interaction phenomena and hence on the identification of the associated research gaps in this area. The chapter finally concludes with the overall findings from the literature survey including the associated research gaps.

2.2 History of Propeller Cavitation

The history of the cavitation studies, which may be stretched back to the middle of the eighteenth century, has started with early study of the Swiss mathematician Euler (Euler, 1756) who reported the cavitation phenomena on a water wheel for the first time and discussed its effect on the performance of the water wheel. Following his reporting, the cavitation, which was directly related to the marine applications, was also mentioned by Osborne Reynolds in the mid-nineteenth century when he discussed the causes of engine racing in screw propelled steamers (Reynolds, 1873).

Although these two scientists were the foremost runners of the cavitation research, the term ‘cavitation’ was first introduced to the literature by R. E. Froude and after that cited by Barnaby and Thornycroft in 1895 (Thornycroft & Barnaby, 1895). However, the cavitation phenomena on marine propellers was discovered by Barnaby and later by Parsons during the sea trials of a British high-speed warship HMS Daring in 1885 and those of the first steam turbine driven ship, “*Turbinia*” in 1895 (Figure 2-1), respectively.

The propeller cavitation phenomenon, as we know today and study its effects on the hydrodynamic performance of a propeller, was discovered and demonstrated clearly by Sir Charles Parsons with his famous steam turbine yacht *Turbinia.* Whereas Parsons was expecting to achieve very high ship speeds by installing an axial steam turbine onboard a ship for the first time as the prime mover, he faced the problem of cavitation while the steam turbine was able to provide *Turbinia* with the required power. Parsons was able to explain this problem by thrust breakdown due to the excessive cavitation developed on the propeller blades in consulting with his contemporaries and conducting his own investigations. In parallel to the ship trials in 1895-1897, Parsons also investigated the phenomena by constructing the world’s first cavitation tunnel in 1895, as an enclosed small circulating water channel, by which he was able to demonstrate the cavitation on a inch diameter model propeller of *Turbinia* (Figure 2-2). This first cavitation tunnel and the Turbinia hull are now kept at the Discovery Museum of Newcastle upon Tyne, and are marked as the beginning of propeller cavitation research as well as cavitation testing with model propellers (Atlar, 2000).

The first experimental sea trials with *Turbinia* were conducted in 1894 (Parsons, 1897) when the vessel originally had a single screw and even not being able to achieve twenty knots on these trials while Parsons was expecting almost double this speed. In 1895, seven various types of the propellers were tried and failed achieving a maximum of 19.75 knots. After these experiments, it had been realized that the density of the thrust loading on the Turbinia’s single screw was too high resulting in severe cavitation, and to remedy this the blade surface area of the propeller needed to be increased. In consultation with others including Barnaby, Thornycroft, R.E Froude and after further sea trials and cavitation tunnel tests, Parsons modified the propulsion system of

Turbinia from single shaft drive arrangement to a triple shaft drive configuration with three screws on each shaft (see Figure 2-1- right). This configuration would increase the blade surface area to absorb the required power at a desirable thrust density to avoid the excessive cavitation and hence the thrust breakdown. The new configuration, indeed, provided Turbinia with the full power absorption at a required level of thrust density and to reach a 32.75 knot ship speed during the sea trials in April 1897. Following this achievement, Parsons started to investigate the nature of the cavitation phenomena with a series of propeller models in a second, much larger, cavitation tunnel built (3 feet diameter) in Wallsend in 1910, and which was also constructed by himself.

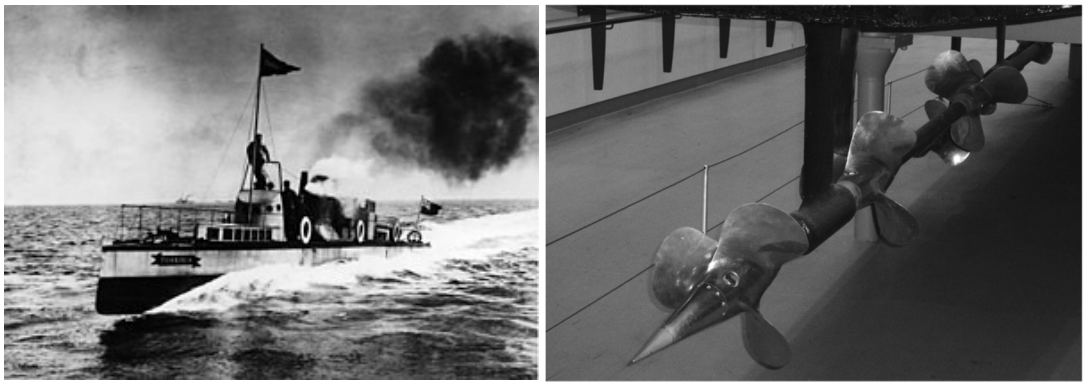

Figure 2-1 Turbinia and its triple propeller arrangement on a shaft line

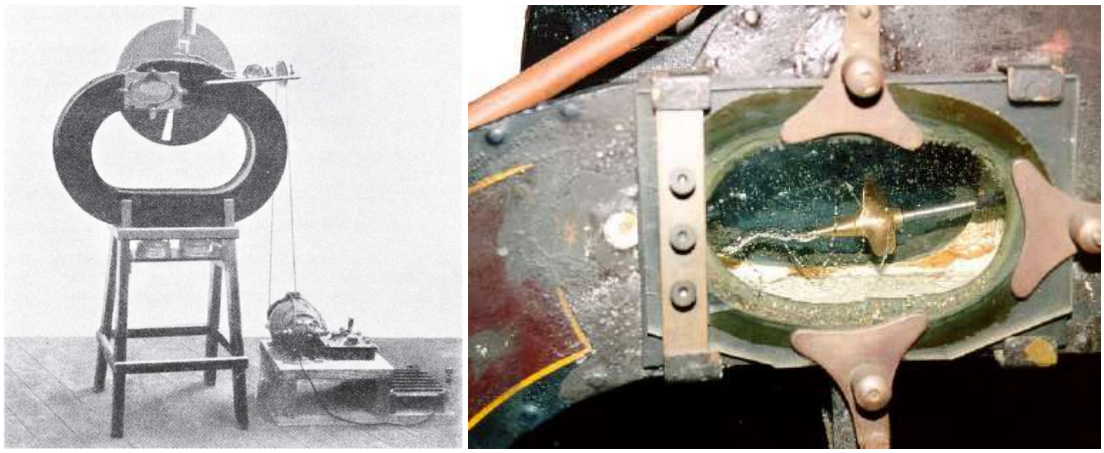

Figure 2-2 Parsons' world's first cavitation tunnel
(Courtesy of E.-A. Weitendorf and M. Atlar, respectively)

Although Parsons conducted the first most detailed and scientific investigations on propeller cavitation at that time, he was not able to publish the details of his activities

in those years while his achievements were mentioned by others in some memorial lectures e.g. Burril (1951), (Weitendorf, 2001).

After the second cavitation tunnel had been constructed in 1910, other larger tunnels were built in Europe and America during the 1920s and 1930s, each incorporating the lessons learned from their predecessors (Carlton, 2007). Recently, very large cavitation facilities have been built and run in various locations all around the world, where propeller cavitation investigations still continue with experimental, numerical and recently with the computational fluid dynamic (CFD) approaches. Gaps still exist to be investigated in this complex phenomena which is also the main driver of the present research study by using the latest computational and experimental tools.

2.3 History of Bubble Dynamics

Within the framework of the cavitation phenomena and associated modelling, the cavitation bubble collapse is one of the most important and complex aspects of the phenomena and hence has been the topic of considerable research. Apart from its numerical modelling, the undesirable consequences of the bubble collapse regarding the material erosion and underwater radiated noise of marine propeller have been the main drivers for research on bubble collapse which depends on the pressure, velocity, temperature, bubble shape and its deformation etc.

The beginning of the scientific investigation on the bubble dynamics was started with Lord Rayleigh who presented the theoretical formulations of the cavitating spherical bubble collapse in a liquid (Rayleigh, 1917). In the 1940s, Knapp was able to observe the details of the cavity collapse by using high-speed movie cameras capable of 20,000 frames per second at the California Institute of Technology (Knapp and Hollander 1948). Based on these developments, Plesset (1948), Parkin (1952), and many other researchers began to model the cavity collapse by making use of the observation details of the growth and collapse of the cavitating bubbles and modifying Rayleigh's motion equations for a spherical bubble collapse (Brennen, 1995).

Although the shape of a vapour bubble was generally accepted to be spherical in the past, the later numerical and experimental studies have claimed that the shape of the

collapsing bubble does not remain spherical during the collapse process near a rigid wall (Plesset, 1970 and Lauterborn & Bolle, 1975) (Figure 2-3).

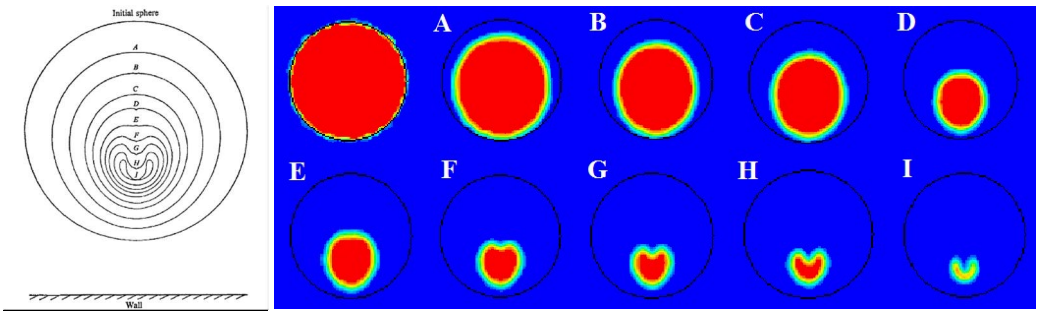

Figure 2-3 A cavity bubble deformation during bubble collapse stage (Left: Numerical Results (Plesset, 1970), Right: CFD Results in 2D)

Despite this claim, Plesset and Prosperetti (1977) represented the Rayleigh-Plesset equation for modelling the bubble growth and collapse by neglecting the bubble-bubble interaction and retaining the bubble spherical shape, and this model is one of the most commonly used approaches in numerical modelling of cavitation in the CFD studies.

For example, based on the Rayleigh-Plesset equation, a new dispersed volume of fraction method was developed for time dependent growth and collapse of bubbles by Schnerr and Sauer (2001). This cavity model, which is based on the Rayleigh-Plesset equation, is also built into the commercial CFD code (STAR-CCM+) which is used in this research study, but neglecting the viscous effects, bubble growth acceleration and surface tension (STAR-CCM+ User Guide, 2018).

In complementing the cavity modelling in CFD studies, detailed mesh generation techniques have been investigated for the accurate capture of cavitating bubbles and cavitation inception which are related to bubble radius and cavitation dynamics. As far as the cavity modelling in STAR-CCM+ is concerned, although the motion of each bubble seed in space cannot be modelled and tracked, the phenomena can be investigated profoundly through the wise use of the software and mesh generation capabilities as will be conducted in this research study.

In this research study, it is envisaged to develop a new meshing technique which can be based on the relationship between the generated mesh size and bubble radius.

Although the sheet cavitation could be simulated with large surface size of the generated meshes, such sizes are often too large to capture tip vortex cavitation. Hence studies relating to cavitating bubble radius have been investigated in the literature. Within this framework, e.g. Kuiper (1981) performed extremely useful cavitation tests using a model scale propeller (Propeller V) at advance coefficient, J = 0.3, 0.4 and 0.5 and focusing on tip vortex cavitation. During these tests, the radii of the cavitating core corresponding to various cavitation index values (i.e. cavitation number based on rotational speed) values were measured and a relationship between the cavitation index and the core radius was established as shown in Figure 2-4. Based on this kind of study, the semi-empirical relationship between the bubble radius and mesh size for simulating the tip vortex cavitation can be propounded for developing an adaptive mesh refinement technique as proposed in this research study.

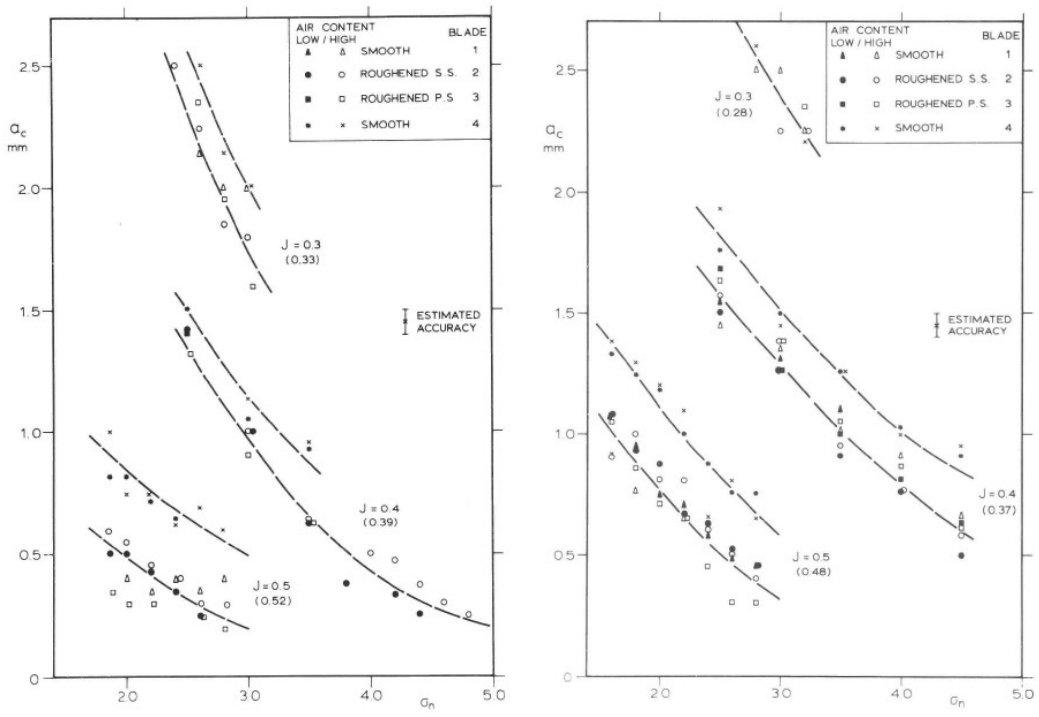

Figure 2-4 Measured radii of the cavitating core of propeller V (Kuiper, 1981)
(Left; Re_n=1.38x10^6, Right; Re_n=2.76x10^6)

2.4 Modelling of Propeller Cavitation

As described in many text books (e.g., Carlton 2007), cavitation is a complex physical phenomenon that occurs when a machine is operating in a liquid induced by pressure and temperature fluctuations. These machines might be pumps, turbines, propellers and etc. Cavitation generally occurs when the local pressure in the fluid suddenly drops at the level of saturated vapour pressure of that fluid and below at the given temperature. This definition of cavitation can be shown on the phase diagram of water (Figure 2-5). When the temperature raises or the pressure reduces, this process cause a phase change from liquid to vapour. While the liquid will "boil" eventually when the temperature is increased at the given pressure the cavitation, which is also known as "cold boiling", can also take place when the pressure is reduced to the level of the saturated vapour pressure of the liquid at almost constant temperature.

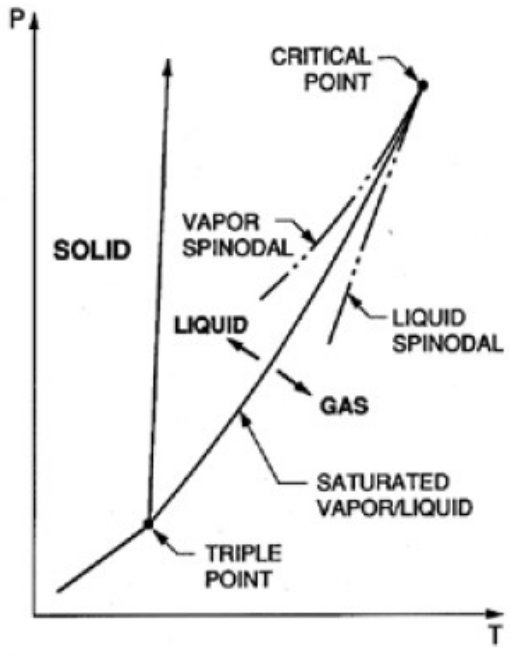

Figure 2-5 Typical phase diagram (Brennen, 1995)

Although there are many non-dimensional parameters in existence to characterize the flow and forces in a hydrodynamic system, the two parameters such as the pressure coefficient (C_P) and cavitation number (σ) are the most important parameters for defining the inception point of cavitation. For a given body in a flow field, the pressure

field map around the body allows the determination of points susceptible to cavitation. The pressure coefficient, which characterizes the forces acting on the body and enables calculation of the pressure field around the body (i.e. at point M), can be given by Equation 2.1. On the other hand, from the dimensional analysis, the fundamental non-dimensional parameter regarding the pressure and hence dominating the cavitation phenomenon is given by $P/\rho V^2$. When this parameter is related to the saturated vapour pressure of any liquid, the cavitation number (σ) can be described as given by Equation 2.2.

$$C_P = \frac{p_M - p_{ST}}{0.5\rho {V_R}^2} \quad [2.1]$$

$$\sigma = \frac{p_{ST} - p_v}{0.5\rho {V_R}^2} = \frac{static\ pressure\ head}{dynamic\ pressure\ head} \quad [2.2]$$

where P_M is the local pressure, P_{ST} is the static pressure, P_v is the saturated vapour pressure, ρ is the density of the fluid, and V_R is the reference velocity.

Theoretically, when the minimum value of the local pressure, P_{min}, on the body reaches at the saturated vapour pressure of the fluid, P_v, i.e.

$$P_{min} = P_v \quad [2.3]$$

the cavitation inception may be assumed to occur and this is represented by cavitation inception number σ_i as given in Equation 2.4.

$$\sigma_i = -C_{Pmin} \quad [2.4]$$

Although the above definition of the inception for cavitation is a theoretical assumption, the cavitation inception, in practice, is extremely complex phenomenon involving many parameters of bubble dynamics and viscous effects for different cavitation types and hence leading into the well-known scale effect problems of cavitation.

From the early works of Parsons, Barnaby and Thornycroft on models and at full scale it was correctly concluded that extreme back or suction side cavitation of the type

causing thrust breakdown could be avoided by increasing the blade surface area. Criteria were subsequently developed by relating the mean thrust to the required blade surface area in the form of a limiting thrust loading coefficient. The first such criterion (e.g. 77.57 kPa) was derived in the latter part of the last century by R.E. Froude. Following this much development work was undertaken in the first half of the century in deriving refined forms of these thrust loading criteria for design purposes and two of the best known practical criteria are those derived by Burrill and Keller.

At the basic design stage of the propellers, the risk of erosion or the required area to minimise the risk of erosion can be obtained by using the Burrill diagram, which was presented first in 1943, or later versions of his diagrams including the cavitation tests conducted at the King's College Cavitation Tunnel (Emerson Cavitation Tunnel today) of Newcastle University. The essence of the Burrill Diagram is the simple criterion line(s) as function of the thrust loading coefficient (for the thrust density) and the cavitation number (for operational condition). This line was recommended based on the annual drydock observations of many full-scale propellers designed by his company, for which he was the chief designer, regarding the risk of erosive cavitation. The Burrill diagram was first published in 1943 (Burrill, 1943) but has stood the test of time. Also shown on the diagram are the results of the observations made later in the Emerson Cavitation Tunnel (ECT) for different percentage of coverages for the back cavitation.

Another popular design tool with Dutch origin, which is still used for checking the cavitation risk on propellers for preliminary design purposes, is the semi-empirical formula given by Keller (1966). Based upon the necessary blade area required to avoid the high thrust density and hence excessive cavitation, Keller formula mainly relates the expanded blade area ratio of a propeller to the thrust developed by the propeller.

Within the framework of propeller design and analysis regarding cavitation, one of the practical tools is the cavitation Bucket Diagrams for the blade section design and analysis. In a typical cavitation bucket diagram the combinations of angle of attack for a section or advance velocity ratio (J) for a propeller can be related to cavitation number (σ) at the regions, where cavitation may occurs, with associated inception

boundaries for different types of cavitation, and where cavitation is not expected within the bucket.

The cavitation prediction criteria such as the Burrill diagram and the Keller formula as well as the cavitation bucket diagrams can be used for practical design purposes involving the risk of cavitation with the lack of the reflection for the effect of hull wake and blade geometry details as well as other important parameters e.g. regarding the water quality. Hence, this has been the main drivers for the development of the numerical tools to model the propeller flow after the introduction of the vortex theory in early 20^{th} century and progressed further by the developments of the potential flow based procedures. These procedures started with the development of the lifting line methods (e.g. Prandtl & Tietiens, 1934) towards the mid of that century and have progressed with the introduction the lifting surface (e.g Hill, 1949 and Strscheletsky, 1950) in 1950s and later with the panel methods (e.g. Hess & Valarezo, 1985) by using the boundary element methods (BEM). While these methods have been still used by many researchers for the propeller flow modelling, especially the lifting surface and panel methods regarding the cavitation effects, the introduction of the CFD and its power for accurate modelling the flow physics especially for the viscous effects regarding certain types of propeller cavitation, which are discussed next, has been the main attraction for many researchers as well as for the Author.

Cavitation Types

Cavitation may affect the propeller performance adversely causing; undesirable performance breakdown if it is excessive, blade or other appendage erosion if it is erosive, fluctuating hull and shaft vibrations as well as the underwater radiated noise. Knapp et al., (1970) categorized hydrodynamic cavitation in general into the following sections; travelling, fixed, vortex and vibratory. Besides, the cavitation on marine propellers can be categorized mainly as the fixed and vortex type (Manen & Oassanen, 1988). As shown in Figure 2-6, for practical purposes and recommended by (ITTC, 2002), cavitation can be also classified according to the location on the propeller, where cavitation may occur, as well as the form or nature of the cavitation such as; sheet, bubble, cloud, tip vortex and hub vortex cavitation since each type of cavitation

affects the propeller performance distinctly. While some sheet cavitation causes erosive effects on propeller blade surfaces, tip vortex cavitation is associated with underwater radiated noise, particularly for naval, survey and cruise ships. The requirements for efficient propeller design and higher ship speed and power mean that avoiding cavitation may not possible, without a big compromise, but must often be managed under challenging circumstances.

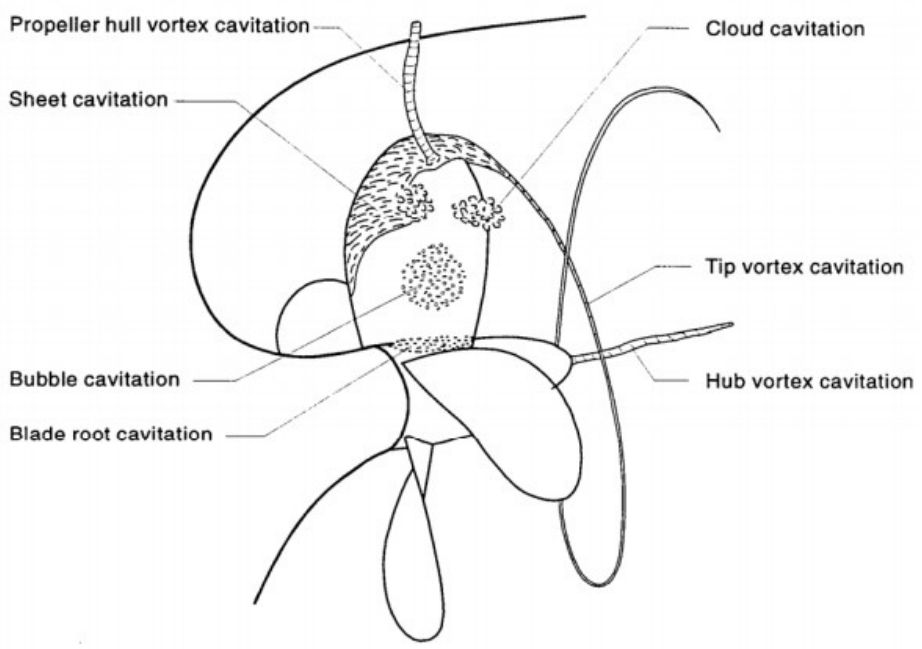

Figure 2-6 Cavitation Types (ITTC, 2002)

Sheet cavitation first occurs at the leading edge of the blades on the suction side (positive angle of attack) and on pressure side (negative angle of attack). This cavity form may develop to cover the complete suction side of the blade, spreading from leading edge in a sheet form. If the propeller is operating under wake, sheet cavitation generally shows an unstable characteristic. Bubble cavitation first occurs at the mid chord or at the position of maximum blade thickness section in non-separated flows. The bubble cavitation appears as individual bubbles growing and contracting rapidly. Cloud cavitation occurs behind developed stable sheet cavitation and appears as a mist or a cloud of very small bubbles. The vortex type of cavitation occurs at the tip and hub of the propellers. The flow around the propeller tip region from pressure to the suction side causes an unstable tip vortex. Tip vortex cavitation usually starts behind

the propeller tip and in unattached form in the early stage of the cavitation. Then the tip vortex becomes stronger (while the fluid pressure is reduced) and attached to the blade. The hub vortex cavitation is formed by the combined vortices from the blades at the blade root, which by themselves are too weak to cavitate. With a converging hub form this vortex can be very stable and strong.

In this research study, within the limitation of the methodology to be developed, and the commercial CFD code to be used, the main focus will be on the sheet and tip vortex type of cavitation. A new mesh refinement approach needs to be developed, especially to capture and simulate the tip vortex cavitation at longer extents to apply on some aft end arrangements of ships with larger propeller-rudder separations, to interact with the rudder for investigating the propeller, rudder and hull interaction. Hence the literature review is focused on the modelling of the sheet and tip vortex type propeller cavitation in the next section.

Sheet Cavitation

In the past 40 years, studies of propeller cavitation have focused on sheet cavitation largely, as this type of cavitation is the main responsible for propeller excited hull vibrations. Thus, the numerical methods such as lifting surface and panel methods have been developed and used to predict propeller performance including sheet cavitation. Lee (1979) developed a numerical lifting surface procedure to predict both the steady and unsteady performance of sub-cavitating propellers. Due to the mainly more accurate representation of the three-dimensional effect, panel method was implemented by Fine and Kinnas (1993) for the analysis of the flow around 3-D cavitating hydrofoils. Kinnas and Hsin (1992) analysed unsteady flow around a marine propeller using a potential-based low-order panel methods with flat surfaces. Afterwards, cavity shapes were validated using the same method by Kinnas and Fine (1994) for a cavitating marine propeller. In later years, Young and Kinnas (2001) analysed sheet cavitation on a propeller using the panel method and predicted forces and cavity shapes that showed good agreement with experimental results. The BEM based panel method was implemented in the PROCAL code by Vaz and Bosschers (2006) and applied to the benchmark DTMB P4119 and Seiun-Maru propeller in non-

cavitating conditions, and applied to the MARIN S-propeller and the *INSEAN E779A* propellers in cavitating conditions.

Nowadays it is accepted that sheet cavitation for marine propellers can be predicted reasonably accurately with existing low-fidelity computational methods such as lifting surface and panel methods, and even more accurately with Computational Fluid Dynamics methods (CFD) due to better modelling of the physics of the flow, thanks to further increase on computational power and speed as well as the capacity of storage. However, simulating the sheet cavitation in the presence of the tip vortex cavitation of a propeller can be still challenging for propeller cavitation research. Fine (1992) mentioned that the prediction of sheet cavitation using BEM based procedures sometimes gives unstable convergence due to the lack of tip vortex cavitation modelling. On the other hand, Lee (2002) applied a low order potential-based panel method in his PhD dissertation for not only sheet cavitation but also for the tip vortex cavitation. Lee and Kinnas (2004) investigated the tip vortex cavitation with the two-dimensional and three-dimensional hydrofoils as well as with a marine propeller using the panel method and concluded that convergence studies and comparisons were satisfactory for the foils while the method required further development for marine propellers.

Beside the above developments, it is worthwhile to review some benchmark propeller test cases and associated propellers which have been used for many researchers to validate and verify their methods and computational tools regarding propeller cavitation, sheet cavitation especially. Amongst them, the *INSEAN E779A* propeller, which will be also used in this research study, was presented in the Rome Workshop for the VIRTUE Project. This model propeller, which is a four-bladed FPP (Fixed Pitch Propeller) with small skew, was designed in 1959 and was tested by INSEAN (Instituto Nazionale di Studi ed Esperienze di Architettura Navale) in non-cavitating and cavitating conditions. The results of the Rome Workshop on this propeller, including cavitating cases, were presented by Salvatore et al. (2009). Different computational models based on the BEM and CFD methods were used for comparison in non-cavitating and cavitating conditions for the propeller performance including pressure distributions and cavitation patterns for the latter condition on the blades. As

fas as the cavitation phenomenon is concerned, only the sheet cavitation could be predicted using the *INSEAN E779A* propeller in the above studies.

Another benchmark propeller test case, which has recently become popular for many researchers, is the Postdam Propeller Test Case (*PPTC VP1304*) without and with shaft inclination including non-cavitating and cavitating conditions. For example, Guilmineau et al. (2015) investigated this benchmark propeller with inclined shaft in cavitating and non-cavitating conditions using k-ω SST model in solver ISIS-CFD. Pressure distribution and cavitation pattern on the blade surfaces were evaluated as well as the propeller performance characteristics. Lloyd et al. (2015) reported the results of the pressure pulses and cavitation patterns using the CFD code ReFRESCO with various mesh density (course, medium and fine) for both open water and cavitating conditions for the same test case. Morgut and Nobile (2012) also studied cavitation of the *PPTC VP1304* and *INSEAN E779A* propellers in a uniform flow using Ansys CFX software. Three different mass transfer models, i.e. Kunz, Zwart and FCM (Full Cavitation Model) were implemented.

Similar to the *INSEAN E779A* test propeller, the *PPTC VP1304* was used by many researchers for the predictions of sheet cavitation phenomenon with lack of the accurate modelling tip vortex cavitation. The *INSEAN E779A* and the *PPTC VP1304* propeller will be also used in this research study for validation and verification of the cavitation modelling for both sheet and tip vortex cavitation investigations.

Tip Vortex Cavitation

Computational modelling of a tip and hub vortex cavitation in a propeller's slipstream is a real challenge for CFD users. Although prediction of cavitation on the propeller blade surfaces has been tackled by many researchers, the efforts for extending the model to include the tip vortex cavitation from all blades simultaneously leaving the propeller and reaching rudder, especially at large rudder-propeller separations, are rather scarce.

There are many low-fidelity numerical and CFD studies to predict tip vortex cavitation in literature e.g. (Lee, 2002, Hsiao and Pauley, 1998, Lee and Kinnas, 2004, Hsiao and Chahine, 2008, Park et al., 2009, Peng et al., 2013), using especially CFD methods in

which RANS based models for the simulation of tip vortex cavitation of marine propellers are preferred (Gaggero et al., 20114). Although the RANS model is recognized as a reliable method for sheet cavitation simulations, further studies are still required particularly for accurate predictions of tip vortex cavitation (Gaggero et al., 2014).

Recently, numerical modelling of the tip vortex cavitation phenomenon has been the focal point by some researchers using CFD methods and commercial codes by creating mesh refinement regions around the propeller's tip area for capturing cavity bubbles in the slipstream. Amongst them, Windt and Bosschers applied an adaptive mesh refinement approach by using the jump based estimator with the in-house CFD code ReFRESCO for a wing and a propeller. Although adaptive mesh refinement improved the accuracy of the predictions for the wing, good results could not be obtained from this application for the propeller, which required further investigations (Windt & Bosschers, 2015). By using the same code, another adaptive mesh refinement approach, was recently used by Lloyd et al. (2017) for the cavitation simulations on a propeller. In this study, the tip vortex cavitation was simulated for the key blade only and not from all the blades simultaneously.

Viitanen and Siikonen have also simulated a single blade of a model-scale marine propeller in cavitating conditions with a novel compressible homogenous flow model and by solving phase volume fractions (Viitanen & Siikonen, 2017). The results showed good agreement regarding not only the propeller performance coefficient and local flow phenomena but also the tip vortex cavitation extension in the propeller slipstream.

Budich et al. (2015) applied a mesh alignment technique to improve the accuracy of the propeller wake structure for capturing the tip vortex cavitation including compressible shock wave dynamics. This method also helped to investigate the surface loads due to cavity dynamics, collapse phenomena and its effects on erosion risks. Phillips and Turnock have also applied an improved version of the Vortfind algorithm increasing the mesh resolution to have sufficient mesh density for capturing vortex cores to investigate the propeller, rudder and hull interaction (Phillips & Turnock, 2011). However, this study is not for cavitating vortex flow.

To this end, Fujiyama et al. (2011) created a fine mesh region around the tip area of the *PPTC VP1304* propeller with level shaft to capture tip vortex cavitation using RANS model and SC/Tetra CFD software. With this mesh refinement, the cavitation pattern was simulated on blade surfaces and moreover a small extension of tip vortex cavitation was observed.

In spite of the above reviewed recent studies the full simulation of the propeller tip vortex cavitation from all propeller blades in simultaneous manner has not been satisfactorily demonstrated in the open literature as an important research gap. The present study, therefore, aims to make contribution in this gap by modelling the tip vortex cavitation from all blades of a propeller simultaneously by developing a new and efficient meshing approach in combination with a state-of-the-art commercial CFD code.

2.5 Cavitation Investigation Methods

Experimental Fluid Dynamics Methods (EFD)

Although this research study is mainly based on the CFD methods to investigate the propeller cavitation on the propeller-rudder-hull interaction, the CFD methods need to be validated by supporting experimental data to be produced by using EFD methods. Since the focus of this research study is on cavitation, the main bulk of such data is generated in cavitation tunnels using EFD methods.

There are various types of cavitation tunnels around the world that have been used for the cavitation observations, hull vibrations and noise measurement tests. Within the framework of this research study, the experimental data for validating the CFD were obtained from five different cavitation tunnels. The *PPTC VP1304* propeller test data was generated in the medium size cavitation tunnel of SVA Potsdam without a free surface (Potsdam Evaluation Reports, 2015) while the test data with the *INSEAN E779A* propeller was at the Italian Navy Cavitation Tunnel (CEIMM, Rome, Italy), (Salvatore at al., 2009). Another tunnel which is the Large Circulating Water Channel of CNR-INSEAN with free surface was used for generating the data for *The Princess*

Royal propeller operating behind the full demi-hull model of *The Princess Royal* research vessel of Newcastle University to investigate the propeller-hull-rudder interaction in cavitating condition (SONIC Project Report, 2012). *The Princess Royal* propeller was also tested in the Emerson Cavitation Tunnel of Newcastle University, which is a medium size cavitation tunnel with no free surface (Atlar, 2011). These tests were in the open water of the propeller as well as behind the dummy hull based simulated wake of *The Princess Royal* demi-hull to generate the validation test data for the propeller-rudder-hull interaction. Finally, the Author produced further validation test data for *The Princess Royal* propeller in open water condition by conducting tests in the large cavitation tunnel of SJTU Shanghai (SJTU – The Princess Royal Propeller Test Report, 2017).

Apart from the above described data, in recent years there has been increased EFD activities regarding propeller cavitation and associated underwater radiated noise involving cavitation tunnels and depressurised wave basin. In the recently completed European Framework (FP7) sponsored collaborative research project SONIC (SONIC Project Report, 2012), Newcastle University's catamaran research vessel, "*The Princess Royal*" (Atlar et al., 2013), was used to investigate the underwater radiated noise induced by its cavitating propellers. Comprehensive model tests and full-scale trials were conducted and associated data were collected to be used as the benchmark data. A continuation of this collaborative research has seen the model propeller of *The Princess Royal* being tested by eight major cavitation tunnels and wave basin facilities around the world, under a major round robin test campaign organised by Hydro Testing Forum (HTF) including the Emerson Cavitation Tunnel where the first set of the round robin tests were conducted e.g. (Aktas et al, 2016, Tani et al, 2017). Results from the Emerson Cavitation Tunnel (ECT) have been published and also compared with tests conducted in the University of Genoa (UNIGE) Cavitation Tunnel by Tani et al. (2017a). Similar cavitation tests and noise measurement studies using *The Princess Royal* propeller were published in a recent conference (AMT, 2017) by the major cavitation tunnel and marine research facilities. Amongst them Lafeber and Lloyd (2017) performed the tests in MARIN's Depressurized Wave Basin to evaluate propeller performance in open water and cavitating conditions and to measure the underwater radiated noise characteristic of this propeller. Besides these measurements,

they have also evaluated the effect of nuclei generated by the electrolysis process on cavitation inception (Lafeber & Lloyd, 2017). Tani et al, (2017b) conducted the similar cavitation and noise measurement test at the UNIGE cavitation tunnel and compared the results with those from the Emerson Cavitation Tunnel, (Aktas et al., 2016). A similar study was also published by Hallander, (2017) including open water, cavitation and noise measurement tests conducted in the large SSPA cavitation tunnel as a part of the above mentioned round robin test campaign.

Further tests were also conducted in non-uniform flow in the Emerson Cavitation Tunnel by using scaled models of the propeller, a dummy hull model of *The Princess Royal* and its rudder. The results of the cavitation tests and noise measurements were published by Aktas et al., (2016) including the comparison of the cavitation images and the extrapolated noise with the results from the full scale trials. *The Princess Royal* propeller has also been recommended recently by the ITTC to be used as a benchmark propeller for test ranging from open water tests to noise measurements studies (ITTC, 2017a).

Within the context of studying the dynamics of sheet and tip vortex cavitation by using the EFD methods it is worthwhile to include Konno et al., (2002). In that study, the modern propeller design tendency was considered using highly skewed propellers for lowering pressure fluctuations. However, the skew distribution created a strong cavitating tip vortex which emitted high levels of acoustic pressure when deforming within the wake peak.

Recently, Pennings et al., (2016) conducted cavitation tunnel test for investigating the effects of tip vortex cavitation on the underwater radiated noise while the main purpose of this investigation was to extrapolate the results to full-scale propellers. Their tests showed that the dominant sound frequency is directly related to the resonance of the tip vortex cavitation.

A theoretical and experimental study was conducted in uniform flow for propeller performance and cavitation observations with the *INSEAN E779A* propeller by Pereira et al. (2004). Another experimental study was carried out in a cavitation tunnel in non-

uniform flow by Pereira et al. (2016) for describing a correlation between the cavitation patterns on blades and near-field pressures.

Above mentioned studies regarding the sheet and tip vortex cavitation investigations using EFD methods showed the importance of the modelling of tip vortices with CFD approaches for the more accurate cavitation and noise predictions.

Computational Fluid Dynamics Methods (CFD)

Although the developments in CFD methods have been reviewed in Section 2.4 of this chapter within the framework of tip vortex cavitation, here in this section, a short and focused review is given on further details of the CFD methods from the modelling point of view.

CFD methods have been progressing to be more efficient and reliable tools with the ultimate ambition of replacing or removing the need for EFD methods, especially for complex physical phenomena including the propeller cavitation. Regarding the methods, as already highlight earlier, while the RANS based modelling appears to be adequate for the simulation of sheet cavitation, the complex tip vortex cavitation may require for the advanced CFD methods such as LES, DNS and Euleraian/Lagrangian approach.

In the past decade, CFD methods have become more common, superseding the potential flow based BEM methods, and with RANS primarily being preferred by many researchers due to computational time and costs. Amongst them, Hsiao and Pauley (1998) used incompressible RANS computations with the Baldwin-Barth turbulence model for simulating tip vortex cavitation. They also tested a modified tip propeller which delayed cavitation inception without reducing propeller performance. Tip vortex cavitation inception was simulated for a marine propeller using RANS including the investigations of scaling effect by Hsiao and Chahine (2008). Lately, a RANS method with the Schnerr–Sauer cavitation model was implemented by Gaggero et al. (2014) for simulating tip vortex cavitation for two ducted propellers. Although RANS was proved to be a reliable tool for the prediction of sheet cavitation, further studies - especially for tip vortex cavitation- are still required (Gaggero et al., 2014). In particular, tip vortex cavitation extent can be highly sensitive to the choice of the

RANS turbulence model in non-cavitating (Guilmineau et al., 2015) and cavitating flows (Viitanen & Siikonen, 2017).

In contrast to the RANS model, scale-resolving simulations can model small-scale motions and hence resolve the large scales of turbulence. Within the scope of the scale-resolving simulations, there are two popular approaches to simulate complex physical phenomena including cavitation; namely DES and LES models which are also available in the STAR-CCM+ as will be used in this research study, (STAR-CCM+ User Guide, 2018).

As stated previously, the *INSEAN E779A* propeller had been the subject of numerous simulations studies by using CFD methods and comparisons with the experimental results as a benchmark propeller. For example, Vaz et al. (2015) used RANS and RANS-BEM coupled approaches in non-cavitating and cavitating conditions to predict propeller performance, pressure distributions and cavitation volume for the latter condition. Bensow and Bark also simulated the *INSEAN E779A* propeller in cavitating conditions to predict cavity extent on the blade surface as well as tip vortex development and its interaction with the sheet cavity using an LES model in OpenFOAM (Bensow and Bark, 2010). Guilmineau et al. (2015) discussed various turbulence closures such as RANS SST k-ω, Algebraic Reynolds Stress Model (EARSM) and DES k-ω model to predict the wake of the *INSEAN E779A* propeller. Although the instabilities of the wake cannot be predicted with RANS, the evaluation of the tip vortices and the prediction of the instabilities of the wake can be achieved using a DES model.

Although the above reported simulations succeed in validating propeller performance and cavitation patterns on the blade surfaces of the *E779A* propeller, an accurate simulation of the tip vortex cavitation from all blades, especially, including its extension in the propeller's slipstream appears to be missing which is an important element of investigating the propeller-rudder interaction.

2.6 Cavitation Influence on Propeller – Rudder – Hull Interaction

Having reviewed the developments focused on the propeller cavitation and its modelling in the previous sections of this chapter, the following presents the literature review specific to the propeller-rudder-hull interaction within the framework of the aim of this research study.

The propeller and rudder are the major components of the propulsion system of a ship as such; while the propeller is generating the thrust to keep the ship at speed, the rudder is trying to keep the ship on route. Hence both components interact with each other and the hull. Due to this reason, perhaps it is more logical that each component needs to be investigated invidually and then the mutual interaction effect between them.

While the propeller and rudder are placed behind a hull and hence work together in the wake field, all components of this complex system interact each other more or less strongly as represented in Figure 2-7.

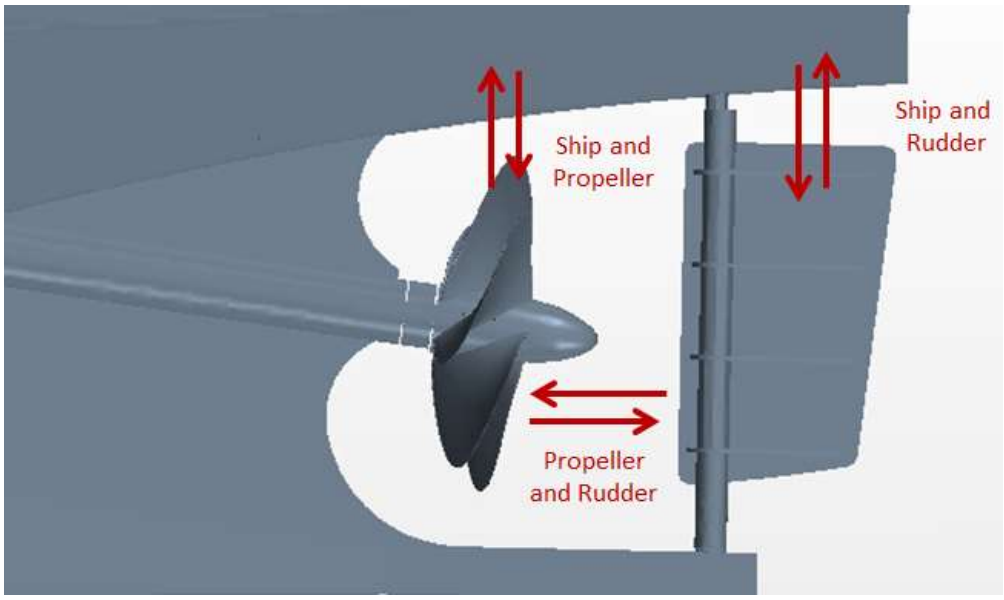

Figure 2-7 Propeller-Rudder-Hull Interaction (*The Princess Royal*)

For a better understanding of the physics of the complex interaction phenomenon due to all components, the mutual interaction effect of two isolated components are

described as “ship and rudder”, “hull and rudder”, and “propeller and rudder” interaction by Kracht, (1995) as also depicted in Figure 2-7. Although the interaction between the ship and rudder may be considered somewhat weak, if the gap between hull and rudder is quite small and both are immersed deeply enough, the hull prevents the flow around the rudder root which improves the rudder force (Kracht, 1995). On the other hand, the interaction between the propeller and hull, depending on the aft end arrangements, is generally very strong and this has been the classical topic of research for many investigators in the history of ship propulsion. Although the modelling of the propeller-hull interaction will be inherently taken into account during the numerical/experimental representation. Therefore the detailed analysis of this interaction is not the main interest of this study.

As it has been highlighted previously, while the propeller cavitation is an essential phenomenon to predict the propeller’s performance and evaluate its undesirable effects, its interaction with the rudder is also important and complex from both the propeller and rudder point of view. As a result, the mutual interaction effect due to the propeller – rudder combination will be explored in details as the main interest of this study regarding the propeller cavitation, and tip vortex cavitation in particular.

Most propellers induce tip vortices. These are the regions of low pressure, often cavitating. Behind the propeller they form spirals which intersect the rudder. Cavitation erosion is often observed at the upper and sometimes lower part of the intersection zones; mainly on the upper starboard side of the rudder for right-turning propellers. The best means to reduce these effects is to decrease gradually the propeller loading towards the blade tips by appropriately reducing the pitch, and to use a high propeller skew. Such an approach can also reduce propeller-induced vibrations. It is also common to see a vortex forming behind a faired propeller hub, which can often cavitate, and may strip paint off the rudder. If it is not aggressive, however, the hub vortex cavitation seems to cause fewer problems at the rudder than the tip vortices, possibly due to the lower axial velocity behind the propeller hub (Bertram, 2012).

The propeller-rudder interaction phenomenon may be investigated in two parts: (1) The influence by the rudder on the back-pressure distribution, where the propeller is operating in the flow in front of the rudder. (2) The effect of the propeller flow field

on the rudder which sometimes manifests itself in cavitation erosion of the rudder structure (Carlton, 2007). These two parts may be investigated using existing experimental and numerical methods including CFD.

In the past 30 years, the propeller-rudder interaction has been investigated experimentally by many researchers. An experimental propeller-rudder interaction study was conducted by Molland and Turnock for the investigation of the influence of the propeller loading on ship rudder performance in the wind tunnel of the Southampton University (Molland and Turnock, 1991). While the early study of Goodrich et al., (1979) and later Molland and Turnock (1992) have contributed to the development of the semi-empirical expressions of the propeller-rudder interaction based on the wind tunnel experiments at the Berlin Model Basin, this interaction phenomenon was explored by Kracht (1995) including cavitation aspects. Kracht also investigated cavitation on rudders in the presence of strong interaction between propeller and rudder.

The EFD data produced from the wind tunnel experiments (of Molland and Turnock) has been used several times as a validation case for the BEM and RANS studies conducted by the same research group at Southampton e.g. (Phillips, 2010).

Another related experimental investigation on the propeller-rudder interaction phenomena for hub vortex cavitation was carried out by Atlar and Patience (1998) to investigate the effect of the various boss cap designs on the phenomenon. While the effect of different boss-cap designs on the hub vortex cavitation and propeller performance was investigated with and without the presence of the rudder, the study indicated a weakening of the hub vortex strength (cavitation) due to the introduction of the rudder in the propeller's slipstream.

Perhaps the most comprehensive EFD study on propeller-rudder interaction, including the effect of cavitation was conducted by Felli and his colleagues (Felli et al., 2008) at the INSEAN large cavitation channel facility. This study involved detailed flow measurements using laser based measurement devices on an isolated free-running propeller-rudder arrangement using the *INSEAN E779A* model propeller. In these experiments Felli et al. captured images of the tip vortex and rudder interaction with

particular emphasis on the instability mechanism of the propeller slipstream and on its correlation with the blade-to-blade interaction phenomenon. Following the initial tests, the propeller tip and hub vortex dynamics were investigated in a further test campaign by using the same model propeller and rudder geometries in a different arrangement (Felli and Falchi, 2011) in which the propeller and rudder were located at the same axial plane in contrast with the arrangement used by Felli in 2008. In 2011 Felli reported on the results of the analysis of the complex interaction between the propeller wake structures and the rudder based on PIV and LDV based measurement techniques on the *INSEAN E779A* propeller. The experimental data allowed the authors to investigate complex flow features around the rudder operating within the propeller wake i.e the spiral breakdown of the tip vortices, their rejoining mechanism behind the rudder and the mechanisms governing the different spanwise misalignment of the vortex filaments on the pressure and suction sides of the appendage (Felli & Falchi, 2011).

In addition to the above investigations, further combined studies including low-fidelity numerical methods, EFD and CFD methods have been reported to investigate the propeller-rudder interaction phenomena over the last two decades. Amongst these investigations, Han, et al. (2001) used a mixed numerical approach involving a classical vortex lattice method with a surface panel method to predict propeller cavitation interacting with a horn-type rudder. Natarajan developed an iterative method which coupled a finite volume method with a combination of a vortex-lattice and a panel method to analyse a marine propeller in cavitating conditions in the presence of a rudder (Natarajan, 2003). In the same year, Lee et al., also presented a similar coupled method including a vortex lattice method, a finite volume method and a panel method to predict rudder sheet cavitation, including interaction with the propeller and tunnel wall affects (Lee et al., 2003).

In another low-fidelity but useful investigation the mutual hydrodynamic interaction between the propeller and rudder was investigated using numerical models including lifting surface and panel methods for representing the propeller and rudder geometries, respectively, by (Szantyr, 2007a). Szantyr also investigated the dynamic interaction between the tip vortex cavitation and the rudder using a numerical model based on the

Rankine vortex and the potential solution of the cylindrical sections of the cavitating kernel passing through the strongly varying pressure distribution in the vicinity of the rudder leading edge (Szantyr, 2007b).

Carlton et al investigated propeller-rudder-hull interaction based on sea trails results, CFD studies for different rudder geometries and model tests. His study underlined the importance of rudder-propeller-hull interaction in terms of the flow characteristics around the rudder geometry and also the implications for the rudder's contribution to the overall propulsion efficiency (Carlton et al., 2009).

With an increasing use of CFDs in ship applications, there have been recent investigations by using CFD methods for better understanding of the cavitation phenomenon including the effect of rudder regarding the sheet cavitation developed on the blades and tip vortex cavitation. Amongst them Boorsma and Whitworth discussed potential improvements in the prediction of cavitation using CFD methods and their ability to predict small-scale motions in the flow using DES. Such studies were important for determining the erosive potential of both sheet and vortex cavitation on propeller and rudder geometries respectively (Boorsma and Whitworth, 2011).

Simulation of cavitating flow and its effect on the fluctuating hull pressures have also been investigated using RANS methods for the propeller operating behind the hull and in cavitating conditions by Paik et al. This investigation reported good agreement not only for the cavitation pattern, but also for the fluctuating hull pressures induced by the propeller when the simulation results were compared with corresponding experiments carried out in Samsung Cavitation Tunnel (SCAT) (Paik, et al., 2013). Finally Mascio et al., (2015) also investigated by CFD methods the interaction of the vortex systems detached from a propeller with a rudder installed in its wake.

Perhaps the essence of the information, that can be obtained from the above review in the field of the propeller-rudder-hull interaction is that; although there have been pockets of useful EFD and numerical studies involving low-fidelity and CFD based numerical modelling, there is a clear gap to model the interaction phenomenon by taking advantage of today's commercial CFD codes, especially including the effect of

tip vortex cavitation from all blades of the propeller, behind the hull and in cavitating operation conditions. This presented the Author with a challenge, as proposed in this research study, by making use of the recently published EFD data and recent progress made in the modelling of propeller cavitation by using the state-of-the-art commercial CFD codes.

2.7 Concluding Remarks

Chapter 2 has reviewed the literature relating to propeller cavitation and its modelling to tackle the aim of this research study, namely, to make a contribution to propeller-rudder-hull interaction phenomena, including the effect of cavitation.

The literature survey presented a historical review of propeller cavitation, bubble dynamics and different types of propeller cavitation in relation to the numerical modelling of the two main types of propeller cavitation; sheet cavitation and tip vortex types.

Since the main focus of this research study is to investigate interaction phenomena using CFD methods, which need to be validated by using credible data created using EFD methods, the review continued with a survey of the literature relating to cavitation investigations and modelling methods using both EFD and CFD.

Finally propeller cavitation investigations were revisited by surveying the relevant EFD and numerical studies including low-fidelity and CFD methods for the propeller, rudder and hull interaction phenomenon.

Within the framework of the review study it became clear that:

- Although sheet cavitation for marine propellers can be predicted reasonably accurately both with existing low-fidelity numerical methods and CFD, simulating the tip vortex cavitation of a propeller is still challenging for propeller cavitation research.
- There has been no CFD study involving simultaneous modelling of cavitating vortices from all of the blade tips and the hub, including the effect of hull wake. This is identified as one of the clear research gaps in the literature.

- Current commercial CFD codes may provide a basis to tackle the above stated research gap but requires efficient mesh refinement approaches. Although there have been limited attempts to develop and apply such approaches using in-house codes, no attempt has been reported for a widely used commercial CFD code to tackle the above challenge.
- Although there have been pockets of useful EFD and computational studies involving the low-fidelity and CFD based modelling, there is another clear research gap to model the propeller-rudder-hull interaction phenomenon by taking the advantage of readily available commercial CFD codes, especially including the effect of simultaneously modelling tip vortex cavitation from all blades of a propeller, operating behind a hull and in self-propelling conditions.
- The above stated gaps encouraged the Author to tackle the challenge of closing them by making use of the recently published EFD data and recent progress made in the modelling of propeller cavitation by using the state-of-the-art commercial CFD codes and hence to confirm the aim and objectives of this research study.

Chapter 3 Methodology

3.1 Introduction

This chapter presents the methodology used and further developed, where required, for investigating the propeller cavitation during propeller, rudder and hull interaction. Firstly, the computational fluid dynamics (CFD) and experimental fluid dynamics (EFD) methods are presented. Subsequently, the experimental test cases used for the validation and verification of the numerical simulations conducted in this study are explained together with the details of the models used in these test cases. The chapter also includes the description of the validation and verification methodology as well as its application for the computational simulations and concludes with a summary of the work conducted in the chapter.

3.2 Computational Fluid Dynamics (CFD)

In the scope of this study, CFD methods were mainly used to investigate propeller performance including the cavitation phenomena. The cavitation simulations were conducted using one of the widely used commercial CFD codes for marine applications, STAR-CCM+. The flow actions around the propeller and ship geometries used for the test cases selected in the study have been simulated in this code for non-cavitating and cavitating conditions. While RANS turbulence models were preferred for the non-cavitating test conditions, DES and LES turbulence models were preferred for the cavitating test conditions. The mass and continuum conservation equations solved during the simulations are given below in the most general way (Ferziger & Peric, 2002).

$$\frac{\partial \rho}{\partial t} + div(\rho v) = 0 \qquad [3.1]$$

$$\frac{\partial \rho}{\partial t} + \frac{\partial (\rho u_i)}{\partial x_i} = \frac{\partial \rho}{\partial t} + \frac{\partial (\rho u_x)}{\partial x} + \frac{\partial (\rho u_y)}{\partial y} + \frac{\partial (\rho u_z)}{\partial z} = 0 \quad [3.2]$$

$$\frac{\partial (\rho u_i)}{\partial t} + \frac{\partial \rho (u_j u_i)}{\partial x_j} = \frac{\partial \rho (\tau_{ij})}{\partial x_j} - \frac{\partial p}{\partial x_i} + \rho g_i \quad [3.3]$$

where x, y and z are the Cartesian coordinates and u_x, u_y and u_z are the Cartesian components of the velocity, ρ is the density, τ_{ij} is the viscous part of the stress tensor and g_i is the component of the gravitational acceleration in the direction of the cartesian coordinate x_i.

3.2.1 Modelling Turbulence

Most engineering problems focus on solving turbulent flows at small scales and high frequencies. However, resolving them in time and space can incur high computational costs.

To solve the exact governing equations of turbulent flows – i.e. Direct Numerical Simulation (DNS) - needs too much computational time, effort and costs. For practical purposes, less expensive solution methods, involving turbulence models, were developed by averaging or neglecting some quantities in order to reduce computational times and high costs of CFD simulations. The turbulence models implemented in STAR-CCM+ for solving the governing equations are:

- Reynolds-Averaged Navier-Stokes (RANS) methods
- Scale-resolving Methods
  - Detached Eddy Simulation (DES)
  - Large Eddy Simulation (LES)

3.2.1.1 Reynolds Averaged Navier-Stokes (RANS)

Despite of the complexity of flow turbulence, closure relations are available for the RANS equations which govern the transport of the averaged flow quantities. All the uncertainties of the turbulence are averaged for solving the governing equations in an easier way by using the Reynolds averaged approaches. Although RANS models may

be preferred for the engineering applications, their inherent simplifications do not allow the accuracy required in solutions for scientific laws and academic researches.

The averaged continuity and momentum equations can be written in tensor notation and Cartesian coordinates as follow:

$$\frac{\partial(\rho\overline{u_i})}{\partial x_i} = 0 \qquad [3.4]$$

$$\frac{\partial(\rho\overline{u_i})}{\partial t} + \frac{\partial}{\partial x_i}\left(\rho\overline{u}_i\overline{u}_j + \rho\overline{u_i'u_j'}\right) = -\frac{\partial\overline{p}}{\partial x_i} + \frac{\partial\overline{\tau_{ij}}}{\partial x_j} \qquad [3.5]$$

where p is the mean pressure, $\rho\overline{u_i'u_j'}$ is the Reynolds stresses, ρ is the fluid density and μ is the dynamic viscosity and the $\overline{\tau_{ij}}$ are the mean viscous stress tensor components, is calculated from Equation 3.6:

$$\overline{\tau_{ij}} = \mu\left(\frac{\partial\overline{u_i}}{\partial x_j} + \frac{\partial\overline{u_j}}{\partial x_i}\right) \qquad [3.6]$$

As it can be seen from Equation 3.5, some approximations and additional models are required to solve the equations due to the Reynolds stresses and the turbulent scalar flux in the conservation equations. There are many models such as Spalart-Allmaras, K-Epsilon, K-Omega, and Reynolds Stress Transport and so on for solving RANS equations in STAR-CCM+.

In this research study, for turbulence modelling, the Shear Stress Transport (SST) k-omega model has been preferred for the RANS solver applied to non-cavitating simulations.

3.2.1.2 Detached Eddy Simulations (DES)

DES is a combined method of RANS and LES models which can resolve the turbulent flow around the wall surfaces by RANS and the outside of the wall region by LES. This hybrid method allows the users to model the turbulent flow without the very expensive meshes required to generate a LES turbulence model.

In the scope of this study, the DES turbulence model has been used for cavitation simulations to model sheet cavitation and predict propeller performance in cavitating conditions. The LES turbulence model has been preferred for the simulation of the tip vortex cavitation, in order to extend the tip vortex cavitation in the propeller slipstream. Having compared the cavitation pattern results from the DES and LES turbulence models with the same mesh refinement with each other, it was concluded that the tip vortex cavitation could be extended further using the LES model instead of the DES model.

3.2.1.3 Large Eddy Simulations (LES)

In contrast to RANS and DES models, the LES turbulence model is able to resolve large scales of the turbulence directly everywhere in the flow domain and also to model small scale motions. Although the LES model is time dependent, three-dimensional (3D) and more expensive computationally than the RANS and DES models, it is still less expensive and feasible than the DNS approach.

In contrast to the RANS equations, the equations that are solved for LES are obtained by a spatial filtering rather than an averaging process. According to filtering the quantities, especially velocity field to have only large scale components removing smaller eddies, the filtering method of Leonard, (1979) was used. For LES model, the Navier-Stokes equation are filtered and became very similar with RANS turbulence model equations as follows:

$$\frac{\partial(\rho\overline{u_\iota})}{\partial t}+\frac{\partial(\rho\overline{u_\iota u_j})}{\partial x_j}=-\frac{\partial\bar{p}}{\partial x_i}+\frac{\partial}{\partial x_j}\left[\mu(\frac{\partial\overline{u_\iota}}{\partial x_j}+\frac{\partial\overline{u_j}}{\partial x_i})\right] \qquad [3.7]$$

Filtering does not change the continuity equation which is linear, as shown in Equation 3.4.

Hence, it is important to note the inequality as shown in Equation 3.8.

$$\overline{u_i u_j}\neq\overline{u_i}\,\overline{u_j} \qquad [3.8]$$

The left hand side of Equation 3.8 is not easily computed, an approximation for modelling of this difference must be introduced as in Equation 3.9.

$$\tau_{ij}{}^{S} = -\rho\left(\overline{u_i u_j} - \overline{u_i}\,\overline{u_j}\right) \quad [3.9]$$

where $\tau_{ij}{}^{S}$ is the subgrid-scale Reynolds stress.

In this research study, for turbulence modelling, the SST k-omega DES model and the Wall-Adapting Local-Eddy Viscosity (WALE) subgrid scale model were respectively used for the DES and LES turbulence models in cavitating conditions. Details of the implementation of these turbulence models used in these simulations are fully described in STAR-CCM+ User Guide (2018).

For all CFD calculations, the first-order scheme was used for time discretization. For LES computations, the bounded-central differencing scheme which provides a good compromise between accuracy and robustness was used for discretizing the governing equations in space. This scheme is recommended for LES of complex turbulent flows such as cavitation in STAR-CCM+ User Guide, (2018).

3.2.2 Modelling Multiphase Flow

3.2.2.1 Volume of Fluid (VOF)

For cavitation modelling, a Volume of Fluid (VOF) model, that is a simple multiphase model, was used for describing two flow phases; water and vapour. The basic VOF equations and VOF model are described in the user guide of STAR-CCM+, User Guide (2018).

3.2.3 Modelling Cavitation

For cavitation models, STAR-CCM+ uses the same homogeneous seed-based approach described in Muzaferija et al., (2017). Although this approach is not able to capture all of the physical phenomena present, it is a proven method for use in academic and industrial studies. Seed-based mass transfer models are commonly used for gas dissolution and cavitation. For cavitation phenomena, two interacting phases are described as the liquid (water) and gas (vapour) transferring the mass between water and vapour (STAR-CCM+, User Guide 2018).

In the software, the Schnerr-Sauer cavitation model (Schnerr and Sauer, 2001), which is based on the Rayleigh-Plesset equation (Plesset and Prosperetti, 1977), was used for the cavitation simulations. As reviewed in Chapter 2, in this model the bubbles are considered to be spherical, uniformly distributed in the flow and all seeds have the same radius at the beginning of the simulations. Since each bubble cannot be modelled individually, the cavitation is modelled using a number of bubbles in a control volume. According to this approach, the number of bubbles can be calculated at any time from Equation 3.10.

$$N = n_0 a_l V \qquad [3.10]$$

where V is volume, a_l is volume fraction of liquid and n_0 is the number of bubble per unit volume of liquid. The total vapour volume inside the control volume V_V is calculated from Equation 3.11.

$$V_v = N V_b \qquad [3.11]$$

where V_b is the volume of one bubble.

The volume of one bubble can be calculated from Equation 3.12.

$$V_b = \frac{4}{3}\pi R^3 \qquad [3.12]$$

where R is the radius of one bubble.

Volume fraction of vapour, a_v , can be described as in Equation 3.13, including the bubble radius.

$$a_v = \frac{V_v}{V} = \frac{N V_b}{V} = \frac{4}{3}\pi R^3 n_0 a_l \qquad [3.13]$$

The radius of a bubble can be calculated if the volume fraction is known from Equation 3.13.

While the bubbles are moving with the flow and the time is changing, the change of volume of every bubble can be computed from Equation 3.14 as follows.

$$\frac{dV_b}{dt} = 4\pi R^2 \frac{dR}{dt} = 4\pi R^2 v_r \qquad [3.14]$$

where v_r is the bubble growth velocity. At this stage, to calculate the bubble growth velocity, an additional model is required. This term can be calculated from the following models in STAR-CCM+:

- The Schnerr-Sauer cavitation model
- The Rayleigh–Plesset cavitation model
- The Gas Dissolution model

Before describing the bubble growth velocity, for growth and collapse of the bubbles in a control volume, a source term Q_V for volume fraction of vapour is given in Equation 3.15.

$$Q_V = N \frac{dV_b}{dt} = 4\pi n_0 (1 - a_v) V R^r v_r \qquad [3.15]$$

The volume fraction of vapour can be calculated as:

$$a_v = \frac{V_v}{V} = \frac{V_v}{V_v + V_l}$$
$$a_v = \frac{n_0 \frac{4}{3}\pi R^3}{1 + n_0 \frac{4}{3}\pi R^3} \qquad [3.16]$$

where V is the control volume, and V_v and V_l denote the respective parts of the volume that the vapour and the liquid phases occupy.

The vapour bubble radius can be computed from the Equation 3.16 and hence the seed diameter.

The cavitation number based on the rotational speed of the propeller is defined as in Equation 3.17.

$$\sigma_n = \frac{p - p_{sat}}{0.5\rho_l (nD)^2} \qquad [3.17]$$

where p is the tunnel pressure, p_{sat} is the saturated vapour pressure, ρ_l is the density of the fluid, n is the rotation rate and D is the diameter of the propeller.

The variables, such as seed diameter and seed density, used the STAR-CCM+ default values which are 1.0E-6 m and 1.0E12 /m^3, respectively. The tunnel pressure was calculated from the rotational cavitation number using Equation 3.17 and used as a reference pressure value in the software.

In using the Schnerr-Sauer model for the cavitation modelling, the bubble growth rate is estimated from Equation 3.18.

$$(\frac{dR}{dt})^2 = \frac{2}{3}(\frac{p_{sat} - p_\infty}{\rho_l}) \quad [3.18]$$

When the simulation results from this model are to be compared with observed experimental results, scaling the bubble growth rate might be used by specifying the appropriate scaling factors (positive or negative). Such factors may be required when the generated mesh is not sufficient for calculating the pressure drop accurately and to resolve sharp corners that consequently cause STAR-CCM+ to under-predict the minimum pressure. As such, positive scaling factors might be used to increase the cavitation rate to model cavitating bubbles properly. Negative scaling factors might be also used to delay bubble collapse while the cavitating bubbles are travelling inside the turbulent flow where the local pressure is calculated to be smaller than the averaged pressure calculated by STAR-CCM+. In these circumstances, the bubble collapse phenomenon is occurring more slowly than it is predicted by the cavitation model. In such a simulation case, scaling factor (positive and negative) value might be changed until the simulation results and images are perfectly matched with the experiments. This method has some disadvantages if the users do not have the experimental results while they are trying to predict propeller performance in cavitating conditions.

The scaling factor, γ, is applied to the source term (Equation 3.15) as in Equation 3.19:

$$Q_V = \gamma\beta^* \frac{dR}{dt} \quad [3.19]$$

The scaling factor γ can be described as a ratio of the new to the existing multiplier of *dR/dt* , which then causes the current multiplier to cancel out, as in Equation 3.20:

$$\gamma = \frac{\beta^{New}}{\beta^{*}} \qquad [3.20]$$

3.2.4 Modelling Motion

STAR-CCM+ enables the users to simulate a wide range of applications using motion models such as; Moving Reference Frame (MRF), Rigid Body Motion (RBM), Dynamic Fluid-Body Interaction (DFBI) and Vertex Based Motion (Morphing). RBM model which is used for the transient simulations that require the resolution of changing the position of a component (e.g. propeller blades) within a region has been used for describing rotation in this study.

For given described motion models, different mesh models to complement the motion models can be used in STAR-CCM+ such as, sliding mesh, mesh morphing and overset mesh. As will be shown later, the sliding mesh, overset mesh and a combined model (including the sliding and overset mesh) was used for the cavitation simulations of the isolated propeller case, the propeller-rudder combination case and the propeller-rudder-hull combination case, respectively.

Sliding Mesh

This mesh model is used where two or more regions, connected via an ordinary contact interface, are moved (as rigid bodies) relative to one another either in translation and/or rotation. Simple motions such as rotation or translation can be modelled by moving mesh regions as rigid bodies using the sliding mesh approach. The interface between regions is intersected at each time step. The sliding mesh model was used for the simulations in non-cavitating and cavitating conditions for the isolated propellers in this research study.

Overset Mesh

The overset mesh model is a coupled approach where the moving region is defined separately to a background region. The two regions are then coupled together via a hole-cutting algorithm with overlapping cells deactivated.

The overset mesh, is also known as Chimera or Overlapping Mesh, provides the objects to move independently (i.e. mesh separately), by superimposing on the background mesh. When the overset mesh is used, all regions are meshed separately while there will be still an overlapping mesh zone in the same space. As the overset body moves within the background region, the overlapping zone changes at the same time. The data is transferred between the two regions through the overlapping cells. Overset mesh model was used for the propeller-rudder combination case simulations to be able to transfer the data (i.e. tip vortices) from the rotating overset region (including propeller) to the stationary background region (including rudder).

3.3 Experimental Fluid Dynamics (EFD)

Although the most majority of the experimental data used in this study were obtained from the experiments conducted by others, the Author was fortunate to generate additional experimental data for the model propeller of *The Princess Royal* by conducting further tests in the cavitation tunnel of the Shanghai Jiao Tong University (SJTU) as part of her PhD study training. General dimensions, specifications and limitations of the cavitation tunnel are given in §3.3.1.

3.3.1 The SJTU Cavitation Tunnel

As shown in Figure 3-1, SJTU has a test section is 6.1 m in length, and its cross section is 1×1 m^2 with rounded corners. The axial flow velocity over the test section ranges from 0.5 m/s to 15.8 m/s, and the static pressure at the centreline of the test section ranges from 25 kPa to 300 kPa. The non-uniformity of the axial flow velocity in the test section is below 1%.

Figure 3-1 The cavitation tunnel of Shanghai Jiao Tong University (SJTU)

Figure 3-2 shows the propeller dynamometer used in the cavitation tests. The measuring range for thrust is ±1500 N while for the torque is ±75 Nm. The non-linearity and repeatability of the measured thrust and torque are both better than 0.2% FS. The propeller model is driven by an AC servo motor via bevel-geared shafts, within a rotating speed range of ±1998 rpm.

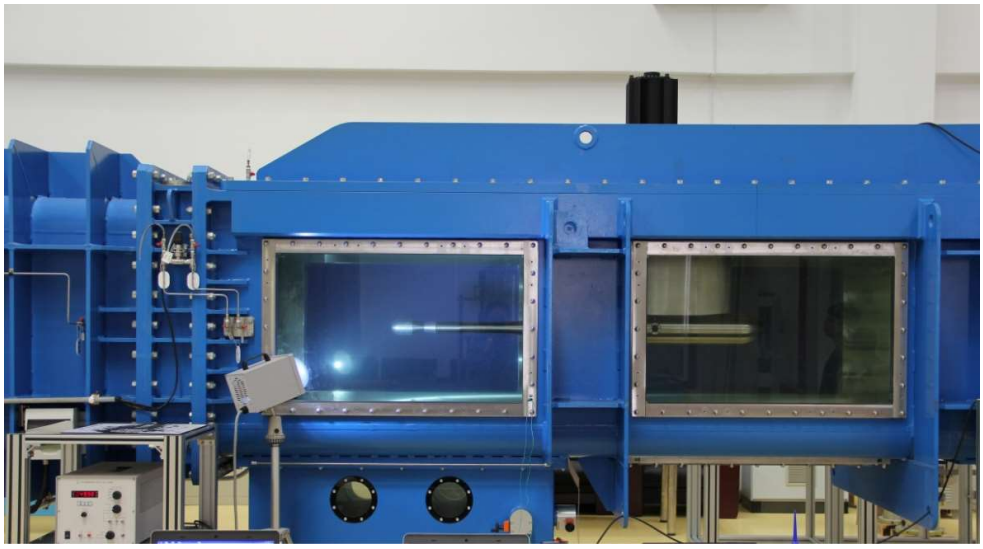

Figure 3-2 Side view of the propeller dynamometer installed in the cavitation tunnel of SJTU

The cavitation observations were recorded using a camera aided by stroboscopic lighting which was synchronized with the shaft position signal. Figure 3-3 shows the strobodriver, stroboscopic light and the camera used during the cavitation tests.

Figure 3-3 Strobodriver and stroboscopic light

Figure 3-3 (left) shows the test arrangement required for the cavitation observations where **A** indicates the test section, while **B** and **C** show the digital camera and stroboscopic light for recording and capturing cavitation images respectively. **D** indicates the Plexiglas material between the test section and a separate water-filled tank **E** which houses a hydrophone. This arrangement allows the environmental conditions of the water to remain the same for measuring noise as if the hydrophone were in the tunnel (Figure 3-4 and Figure 3-5). Although the results are not included in this thesis due to the scope of this research, the Author also conducted noise measurements as part of her training. For this purposes the noise data was measured by using a Brüel & Kjær (B&K) 8103 hydrophone (Figure 3-5). The frequency range of the hydrophone is 0.1 Hz ~ 180 kHz, and the sensitivity is -211 dB re 1 V/µPa ±2 dB. Data acquisition and analysis was made using a B&K LAN-XI model type 3161 as shown in Figure 3-5.

Figure 3-4 Small water-filled tank for hydrophone

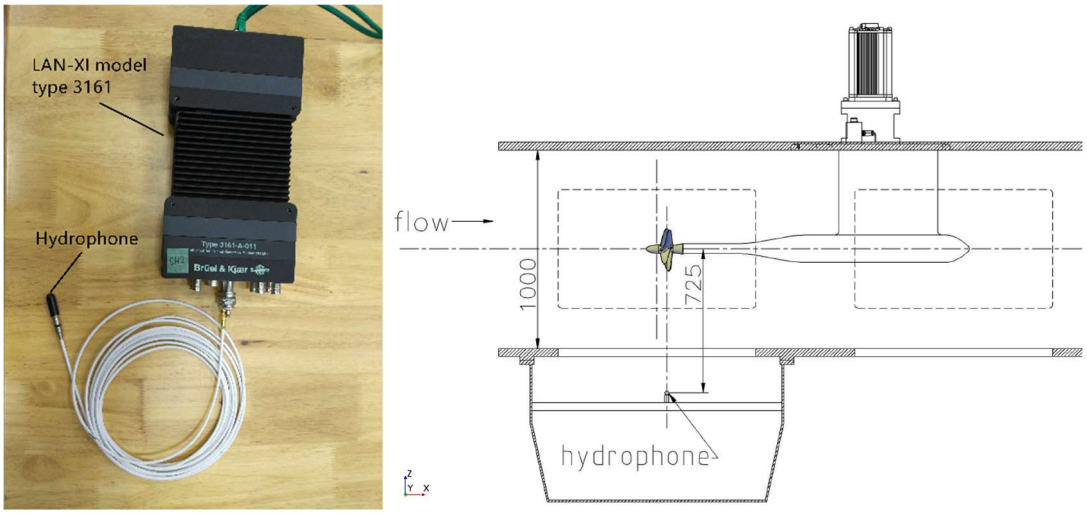

Figure 3-5 Hydrophone for noise measurement tests, Left; Hydrophone, Right; Sketch of test section including dynamometer & hydrophone

Figure 3-5 also shows a sketch of the test section including dynamometer and hydrophone with the dimensions from propeller origin. The hydrophone was placed 725 mm from propeller origin at the z axis while the flow is coming from x axis direction.

3.4 Test Cases

Within the scope of this research study, as reviewed in Chapter 2 already, three different benchmark test propellers – *PPTC VP1304, INSEAN E779A* and *The Princess Royal* Propellers – and a ship geometry – *The Princess Royal* Catamaran Research Vessel of Newcastle University– were used for the investigation of propeller cavitation in connection with the propeller, rudder and hull interaction. In the following section

of this chapter, the details of these benchmark propellers and the hull geometry are presented.

3.4.1 Model Scale Propellers

3.4.1.1 The *PPTC VP1304* Propeller

The *PPTC* (Potsdam Propeller Test Case) propeller, which is a five-bladed, right handed CPP (Controllable Pitch Propeller), was used as a benchmark test case presented in the propeller workshops at the SMP'11 and SMP'15, for predicting hydrodynamic performance in open water and cavitating conditions. The corresponding experimental data was provided by SVA Potsdam. The *PPTC VP1304* propeller has further been used for propeller open water performance investigations by the ITTC Propulsion Committee (ITTC, 2017b).

At SMP'11, several investigations on the *PPTC* propeller were conducted including open water tests, cavitation tests and LDV measurements. These were provided to the workshop participants to test and validate their numerical tools. (Potsdam Propeller Test Case Reports, 2011).

Subsequent to SMP'11, the same propeller geometry was tested on an open water rig set with 12 degrees shaft inclination to provide a test case for the SMP'15 Propeller Workshop in 2015 (Potsdam Evaluation Reports, 2015). The complete experimental data for the *PPTC* propeller, including cavitation observations and hull pressure pulses have been used by many researchers for validation studies.

Table 3-1 and Figure 3-6 show the main particulars and CAD geometries of the *PPTC* propeller for axial and inclined shaft respectively.

Table 3-1 Particulars of the *PPTC* Propeller

Parameters	**Value**
Propeller Diameter (D)	0.25 [m]
Number of Blades (z)	5
Pitch to Diameter Ratio at 0.7R (P/D)	1.635
Expanded Blade Area Ratio (A_E/A_0)	0.77896
Chord Length at 0.7R (c)	0.10417 [m]
Hub Ratio (d/D)	0.30
Skew Angle	18.837º
Propeller Type	Controllable Pitch Propeller
Direction of Rotation	Right Turning

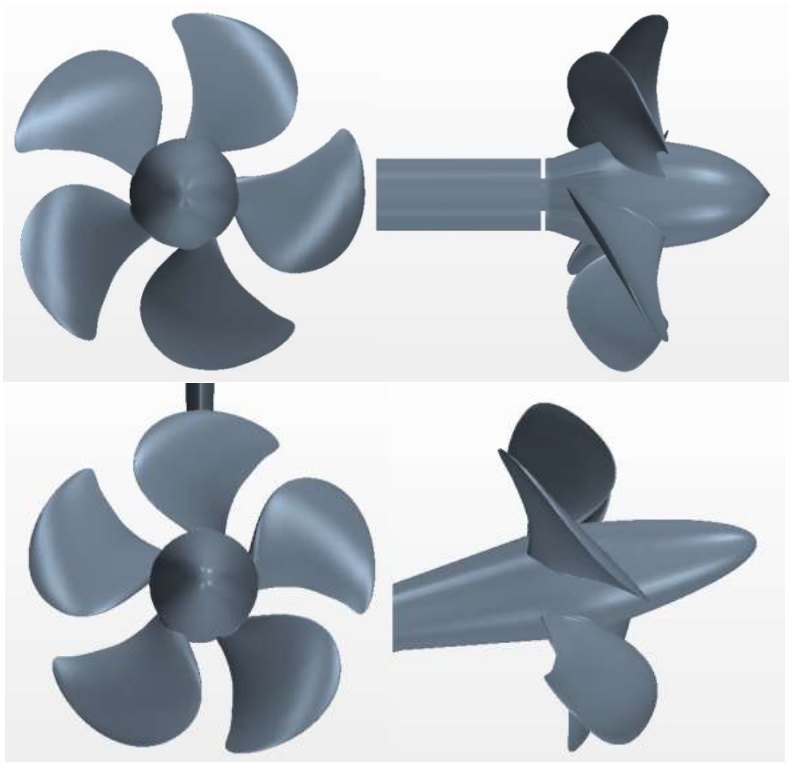

Figure 3-6 CAD geometry of the *PPTC VP 1304* Propeller (Top; PPTC with axial shaft, Bottom; PTTC with inclined shaft)

3.4.1.2 The *INSEAN E779A* Propeller

The *INSEAN E779A* propeller is a four-bladed FPP with small skew. It was designed in 1959 and was tested by INSEAN (Instituto Nazionale di Studi ed Esperienze di Architettura Navale) under cavitating and non-cavitating conditions. This propeller was also used as a benchmark propeller in the Rome Workshop for the VIRTUE Project. Salvatore et al. (2009) presented corresponding experimental and numerical results, including cavitation, obtained from the Workshop participants. Figure 3-7 and Table 3-2, respectively, present the geometry and main particulars of the *INSEAN E779A* propeller.

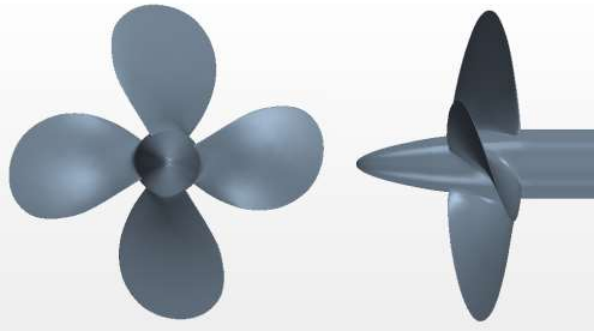

Figure 3-7 CAD geometry of the benchmark propeller

Table 3-2 Particulars of the Propeller

Parameters	**Value**
Propeller Diameter (D)	0.22727 [m]
Number of Blades (z)	4
Pitch to Diameter Ratio (Nominal)	1.1
Expanded Blade Area Ratio (A_E/A_0)	0.689
Skew Angle at Blade Tip	4.48^o [deg] (positive)
Rake (Nominal)	4.35^o [deg]
Propeller Type	Fixed Pitch Propeller
Hub Diameter	0.04553 [m]
Hub Length	0.06830 [m]

3.4.1.3 *The Princess Royal* Propeller

The recently completed collaborative European research project, SONIC (Aktas, 2016), utilized the Newcastle University catamaran research vessel, *The Princess Royal,* as the target vessel to investigate underwater radiated noise from her cavitating propellers. As a result, comprehensive model tests and full-scale trials were conducted and associated data were collected to be used as the benchmark data. As the continuation of this research, currently, the model propeller of *The Princess Royal* is being tested by 8 major cavitation tunnels/basin facilities around the world under a major round robin test campaign (Tani, 2017). This includes the Emerson Cavitation Tunnel where the first set of the round robin tests were conducted.

Within the scope of this research study, the model propeller of *The Princess Royal* has been also investigated. The data for the *Princess Royal* propeller was also recommended by the ITTC Specialist Committee on Hydrodynamic Noise as the benchmark propeller for cavitation noise measurements (ITTC, 2017a).

As part of the ongoing round robin campaign and conducting the cavitation tests and noise measurements, the propeller model was manufactured by Shanghai Jiao Tong University (SJTU) using a propeller data table and CAD file provided by the University of Strathclyde (UoS). The model propeller was manufactured for SJTU using a scale factor (λ) of 3.41, resulting in model diameter of 0.22 m model propeller. Figure 3-8 and Table 3-3 show the geometry and main particulars of this propeller model, respectively (Atlar et al., 2013).

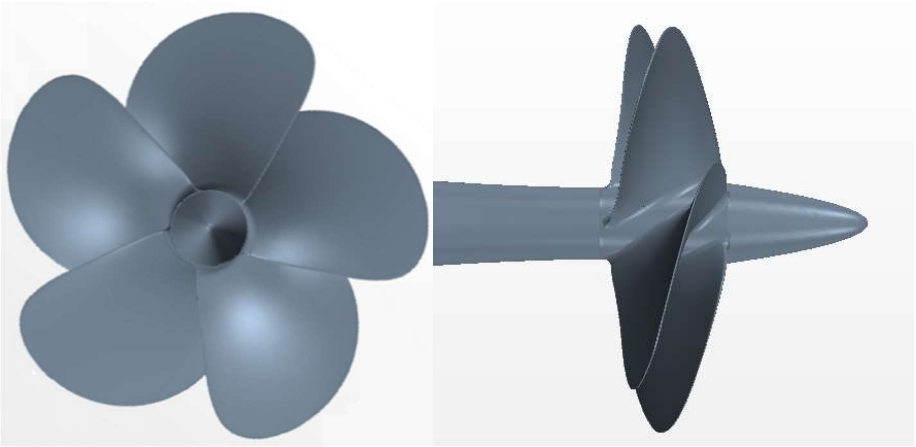

Figure 3-8 *'The Princess Royal'* Propeller Geometry

Table 3-3 The *Princess Royal* Propeller Main Particulars

Parameters	**Full Scale**	**Model Scale**
Propeller Diameter	0.75 [m]	0.22 [m]
Number of Propellers	2	
Number of Blade	5	
Pitch to Diameter Ratio at 0.7R	0.8475	
Expanded Blade Area Ratio	1.057	
Hub to Propeller Diameter Ratio	0.18	
Rake Angle	0 [deg]	
Skew Angle	190 [deg]	
Propeller Type	Fixed Pitch Propeller	
Blade Loading Distribution	NACA a=0.8	
Thickness Distribution	NACA 66 modified	
Material	Ni-Al-Br	
Direction of Rotation	Port-Left Turning	

3.4.2 Ship Model

3.4.2.1 Research Vessel '*The Princess Royal*'

Newcastle University designed and built a catamaran research vessel, *"The Princess Royal",* to support marine research, teaching and consultancy activities to operate mainly in the North East coast of England. The hull form of this vessel was designed by the staff and students of the School of Marine Science and Technology (MAST). The catamaran design was based on displacement-type, Deep-V hull forms with a novel anti-slamming bulbous bow and a tunnel stern as described in details by Atlar et al. (2013). The main particulars of the ship and the pictures of the vessel, propeller and the rudder are shown in Figure 3-9 and Table 3-4.

Within the scope of this research study, various operational conditions of *The Princess Royal* was simulated to investigate the propeller, rudder and hull interaction in Chapter 7.

Figure 3-9 Left: Deep-V Hull Form Catamaran 'Princess Royal', Right: Princess Royal Propeller

Table 3-4 The Princess Royal Research Vessel Main Particulars

Main Particulars of the Ship	
Length overall	18.88 [m]
Length BP	16.45 [m]
Breadth Moulded	7.03 [m]
Breadth Extreme	7.34 [m]
Depth moulded	3.18 [m]
Demi-hulls separation (CL to CL)	4.9 [m]
Displacement (Lightship)	36.94 [tonnes]
Draught (Lightship)	1.65 [m]
Deadweight data	7.32 [tonnes]
Engine particulars	
Number of engines & Type	2 & QSM11-610 HO Cummins Mercruiser Diesel
Power rating (each)	449 [kW] (602 BHP) @ 2300 [rpm]
Cylinder-Displacement-Bore-Stroke	6 - 10.8 [lt] – 125 [mm] – 147 [mm]
Fuel system	CELECT
Aspiration	Turbocharged – seawater after cooled
Fuel consumption at rated speed	117 [lt/hr]
Gearbox particulars	
Number of gearbox & Type	2 & QuickShift (Twin disc marine transmission) – MGX 5114 A (intermediate duty)
Reduction ratio	1.75:1
Input speed limits	330 [rpm] (min) 3000 [rpm] (max)

3.5 Verification and Validation

In this section (3.5) and its following sub-sections, the methodology and procedure for the verification and validation of the CFD simulations are described and this followed by the application of the methodology to the simulation of non-cavitating and cavitating cases for the two of the benchmark model propellers in uniform and open water conditions.

3.5.1 Methodology and Procedure

Verification and validation (V&V) studies were conducted for non-cavitating and cavivating conditions using the two-part methodology described by Stern et al. (2001) and Wilson et al. (2001). This section (3.5.1), therefore, presents the methodology for the verification and validation study of the CFD simulation, while the following section (3.5.2) presents the application of the methods for RANS simulation of a propeller in open water to verify and validate the results. Following this, the same procedure was applied on two above described test propellers in cavitating conditions using LES turbulence model.

The uncertainty of a numerical simulation includes the uncertainties of the number of iterations *(U_I)*, generated grid *(U_G)*, time step *(U_T)* and other parameters *(U_P)* and can be calculated as in Equation 3.21.

$$U^2_{SN} = U^2_I + U^2_G + U^2_T + U^2_P \qquad [3.21]$$

To determine if the simulation has been validated, the error *(E)* between the CFD and EFD results is compared for the validation of uncertainty which is calculated as in Equation 3.22.

$$U^2_V = U^2_D + U^2_{SN} \qquad [3.22]$$

where U_V is the validation uncertanity, U_D is the experimental test uncertanity and U_{SN} is the numerical simulation uncertainty.

The error *(E)* between the results from experiments and simulations can be calculated as in Equation 3.23.

$$E = D - S \quad [3.23]$$

where D is the experimentally determined value while S the simulated (computationally) determined value.

According to this validation method, if $|E|<U_V$, the simulation is validated at the U_V level. Otherwise, where $(U_V<<|E|)$, the sign and magnitude of E can be used for making improvements (Stern et al., 2001).

According to Stern's verification procedures, iterative and parametric convergence studies should be applied using multiple solutions (at least 3). These studies are also conducted using systematic parameters while the other parameters are kept constant. A uniform refinement ratio can be calculated as in Equation 3.24.

$$r = {\Delta x_2}/{\Delta x_1} = {\Delta x_3}/{\Delta x_2} \quad [3.24]$$

A sufficient and a good alternative for the refinement ratio may be $\sqrt{2}$ as discussed by Roache (1998). According to Roache's study, $r = 2$ may be too big for industrial CFD simulations. The verification and validation studies were conducted for this study using $r = \sqrt{2}$ and 2 for grid and time step convergence study, respectively, in non-cavitating and cavitating conditions.

Convergence studies must be done for a minimum of three solutions to evaluate the convergence. Two solutions are not sufficient to assess the sensitivity and convergence. The type of convergence or divergence, which are defined as fine (S_1), medium (S_2) and coarse (S_3), can be determined by using Equation 3.25.

$$\begin{gathered} \varepsilon_{21} = S_2 - S_1 \text{ (Medium-Fine)} \\ \varepsilon_{32} = S_3 - S_2 \text{ (Coarse-Medium)} \\ R = \varepsilon_{21}/\varepsilon_{32} \end{gathered} \quad [3.25]$$

Two different types of convergence and divergence are possible if;

(1) Monotonic Convergence: $0 < R < 1$

(2) Oscillatory Convergence: $R < 0$

(3) Divergence: $R > 1$

The errors and uncertainties can be calculated according to the type of convergence and divergence.

For monotonic convergence, generalised Richardson Extrapolation, with correction and safety factor methods are used for the evaluation. This method is fully described by Stern et al (2001).

For oscillatory convergence, uncertainties can be calculated by using Equation 3.26.

$$U_k = \frac{1}{2}(S_U - S_L) \qquad [3.26]$$

where S_U is the upper and S_L is the lower value in the convergence history of the parameter, respectively.

For divergence, there is no method to calculate the error and uncertainties. These values cannot be estimated.

3.5.2 Open Water Simulations

3.5.2.1 The *INSEAN E779A* Propeller

Verification

For the V&V studies in non-cavitating conditions, simulations were made with four different grids (coarse, medium, fine and very fine) and for three time step conditions (for the fine grid). Figure 3-10 shows images and Table 3-5 shows details of the different grids for the grid independence study. In Table 3-5, 'Surface Size Blade' and 'Surface Size Refinement' demonstrate the surface size of the mesh generated on the propeller blade surface and the surface size of the mesh in the refinement region around the propeller tip, respectively. The grid convergence study was conducted with the RANS method at J=0.71, using r = √2. For the time step convergence study, three-time step conditions were prepared; namely, Coarse (2Δt), Medium (Δt) and Fine (Δt/2). The medium time step was defined as $\Delta t=1.25 \times 10^{-4}$. This time step corresponds to 1.62 deg of propeller rotation.

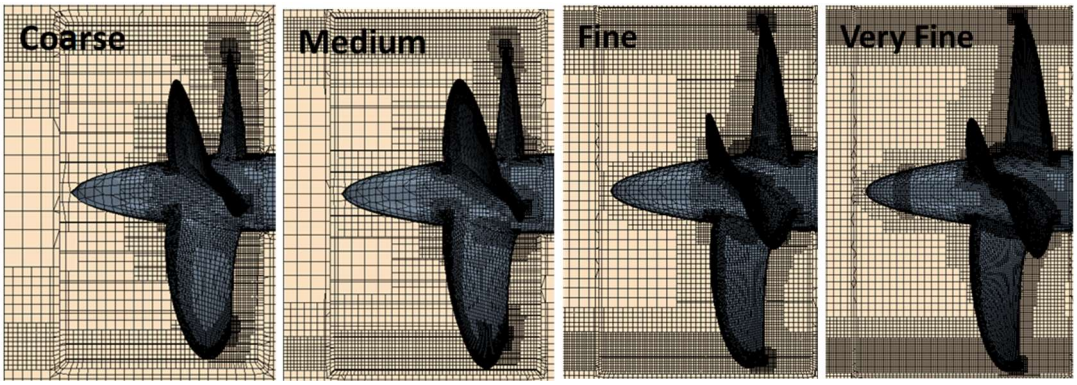

Figure 3-10 Different Grids for V&V Studies

Table 3-5 Grid Convergence Study in Non-Cavitating Conditions

Grid Convergence	**Surface Size Blade [mm]**	**Surface Size Refinement [mm]**	**Number of Cells**
Coarse	1.4	4.2	2,022,542
Medium	1	3	3,690,159
Fine	0.7	2.1	6,478,455
Very Fine	0.5	1.5	13,054,684

Figure 3-11 shows propeller performance coefficients computed for the different grids, together with experimental results. The oscillatory convergence types for "coarse (C), medium (M) and fine (F)" meshes are also indicated in the same figure. The propeller performance coefficients for the time step convergence study are given in detail in Table 3-6. For oscillatory of convergence as shown in Figure 3-11, the uncertainties given in Table 3-7 were calculated using the upper and lower values of K_T and K_Q in the time history. The time step uncertainty was calculated using Equation 3.26 as shown in Table 3-7.

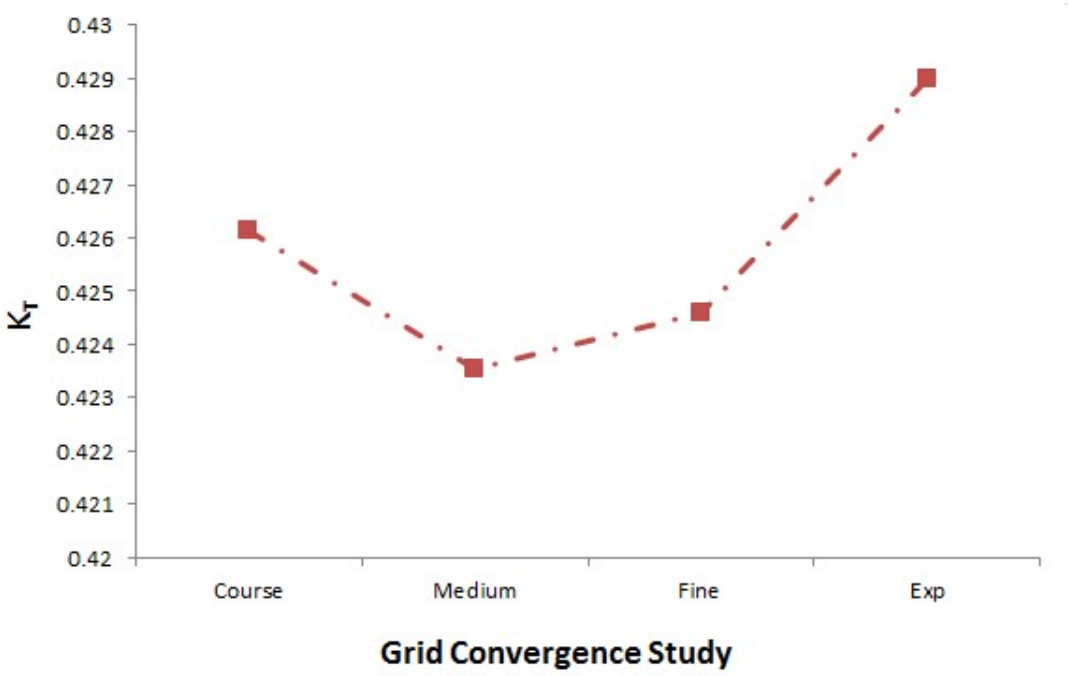

Figure 3-11 Grid Convergence Study

Table 3-6 Time Step Convergence Study in Non-Cavitating Conditions

Time Step	**J**	**K_T**	**$10K_Q$**	**η_0**
$2\Delta t$	0.71	0.22910	0.4245	0.6097
Δt	0.71	0.22909	0.4243	0.6101
$\Delta t/2$	0.71	0.22929	0.4244	0.6105
Exp	0.71	0.23800	0.4290	0.6269

Table 3-7 Numerical Uncertainty Calculations from Grid and Time Step Convergence

Uncertainties	**K_T%**	**$10K_Q$%**
Grid Uncertainty (Coarse, Medium and Fine)	0.05457	0.07494
Grid Uncertainty (Medium, Fine and Very Fine)	0.02931	0.04777
Time Step Uncertainty	0.17262	0.24710

Validation

The error between the CFD and EFD results *(E)*, uncertainties of validation (U_V), and that of experiments (U_D) and numerical simulations (U_{SN}) are given for K_T and K_Q in Table 3-8 and Table 3-9**,** respectively. For these calculations, Equation 3.21 was used, and previous data uncertainty and iterative uncertainty were neglected. The iteration errors and iterative uncertainties are accepted to be negligible compared with the grid and time step uncertainties with regards to the thrust and torque coefficient.

It is observed that the deviations between calculated and measured values in non-cavitating conditions are small, 4% for thrust and 1% for torque coefficients. Although the deviation is small between the EFD and CFD results, the uncertainty for experimental tests was assumed as 1%, $|E| > U_V$ such that K_T is not validated due to a small U_V value for grid 1 and 2. On the other hand, K_Q is validated for both grids. ($|E| < U_V$)

Table 3-8 Validation of Thrust Coefficient (K_T)

Grid	**E%**	**U_{SN}%**	**U_D%**	**U_V%**
1 (Coarse, Medium and Fine)	-4	0.18	1	1.032
2 (Medium, Fine and Very Fine)	-4	0.175	1	1.030

Table 3-9 Validation of Torque Coefficient (K_Q)

Grid	**E%**	**U_{SN}%**	**U_D%**	**U_V%**
1 (Coarse, Medium and Fine)	-1	0.258	1	1.066
2 (Medium, Fine and Very Fine)	-1	0.251	1	1.063

3.5.3 Cavitation Simulations

3.5.3.1 The *INSEAN E779A* Propeller

Verification

For the verification and validation studies in cavitating conditions, three different grids (coarse, medium, and fine) and three-time step conditions (for the medium grid) have been simulated following the same V&V procedure presented at §3.5.1. While Figure 3-12 presents the images of different grids for the grid uncertainty studies, Table 3-10 demonstrates the details of refined meshes using the MARCS method developed and described at §5.3.1.2 in Chapter 5. The V&V studies have been conducted for cavitating conditions with an LES model which is particularly recommended by STAR-CCM+ to solve complex turbulent flows such as, tip vortex type cavitation. Three-time step conditions have been simulated for the medium grid as described in the V&V studies for cavitating conditions using the coarse, medium and fine time step $\Delta t/2=5x10^{-5}$ which corresponds to 0.64 deg of propeller rotation.

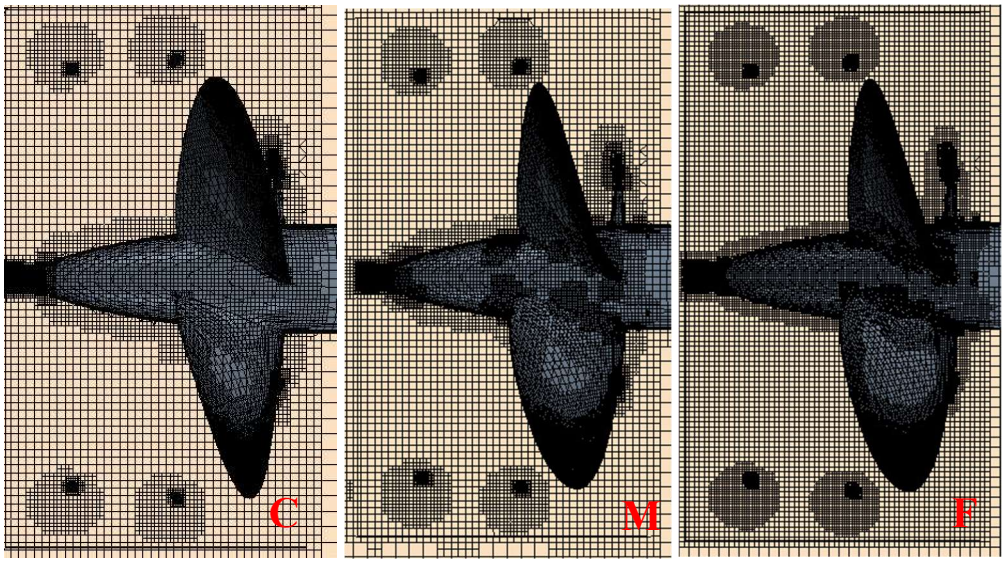

Figure 3-12 Different Grids for V&V Studies (Tip Vortex Cavitation)

Table 3-10 Grid Convergence Study for Cavitating Conditions

Grid Convergence	**Surface Size Blade** [mm]	**Surface Size Refinement** [mm]	**Refinement Factor MARCS** [-]	**Number of Cells** [-]
Coarse	1.0	2.0	Cell Width / 1.5	8,548,852
Medium	0.7	1.4	Cell Width / 2.0	15,702,802
Fine	0.5	1.0	Cell Width / 3.0	28,912,661

The results of the grid uncertainty studies have been given in Table 3-11 regarding the propeller hydrodynamic performance characteristics. Besides K_T, K_Q and η_0, the numerical uncertainties have also been calculated for cavitating volume with regards to different type of cavitation as presented in Table 3-12.

Table 3-11 Grid Uncertainty Study Results in Cavitating Conditions

	K_T	**$10K_Q$**	**η_0**
Coarse	0.2473	0.4593	0.6084
Medium	0.2453	0.4406	0.6292
Fine	0.2470	0.4435	0.6295
Exp	0.255	0.460	0.626

Table 3-12 Numerical Uncertainty Calculations from Grid Convergence in terms of K_T, K_Q and different types of cavitation

Uncertainty	**K_T%**	**$10K_Q$%**	**Cavity Volume%** (Total)	**Cavity Volume%** (Sheet)	**Cavity Volume%** (Tip)
Grid Uncertainty	0.1345	0.2232	348.92	41.15	307.77

In complimenting the uncertainty calculations for cavity volume, Figure 3-13 shows the cavitation pattern including tip vortex cavitation extend in the propeller slipstream due to the different mesh refinements.

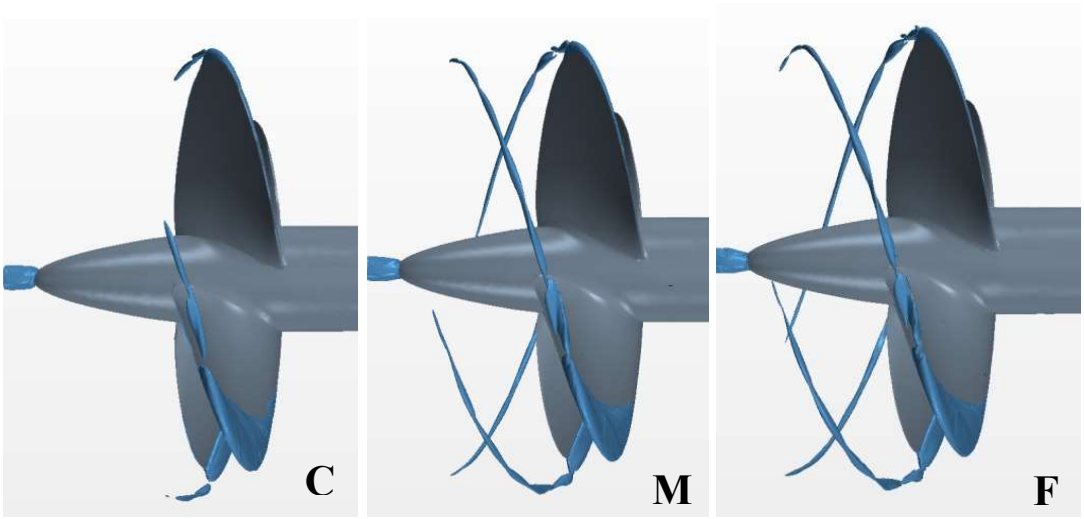

Figure 3-13 Tip Vortex Cavitation Extension due to different grids for V&V studies

Table 3-12 and Figure 3-13 also present that the uncertainty values for the tip vortex cavitation predictions are much higher than the sheet cavitation and adaptive mesh refinement is required to solve the tip vortex cavitation accurately. The images of the cavity extent also prove that smaller grid size (Cell Width / 3.0) is essential to be able to extend tip vortex type cavitation.

Validation

The same validation procedure has been followed with the non-cavitating simulation as described in §3.5.1 and Table 3-13 has been prepared including results (E), uncertainties of numerical simulations *(U_{SN}),* experiments *(U_D)* and validation *(U_V)* respectively. Table 3-13 shows that although the deviation is small between the EFD and CFD results (3% for thrust and 3% for torque coefficients) the uncertainty for experimental tests in cavitating conditions was assumed to be 2%, $|E| > U_V$ such that K_T and K_Q are not validated due to a small U_V value for the grid convergence study.

Table 3-13 Validation of Thrust (K_T) and Torque Coefficient (K_Q)

	E%	**U_{SN}%**	**U_D%**	**U_V%**
K_T	3	0.1815	2	2.008
K_Q	3	0.3042	2	2.023

3.5.3.2 *The Princess Royal* Propeller

Verification

After the V&V study was conducted for non cavitating and cavitating conditions using the *INSEAN E779A* propeller, another V&V study was performed for propeller simulation in cavitating conditions for *The Princess Royal* Propeller. For the cavitation simulations, four different grids (course, medium fine and very fine) and three time step conditions (for fine grid) were simulated. While Figure 3-14 shows the images of the different grids applied, Table 3-14 shows details of these different grids for the grid independency study. The grid convergence study was conducted at J=0.4 using r = √2 and LES turbulence model which gave the best results comparing with the RANS and DES models regarding the accuracy of the propeller performance coefficients in cavitating conditions and for an effective extension of the tip vortex cavitation. For the time step convergence study, the three time step conditions were applied for the fine mesh; Course (2Δt), Medium (Δt) and Fine (Δt/2). The Medium time step was defined as $\Delta t=1.0x10^{-4}$. The results for the propeller performance coefficients from the V&V studies for grid and time independency are shown in Table 3-15 and Table 3-16 respectively.

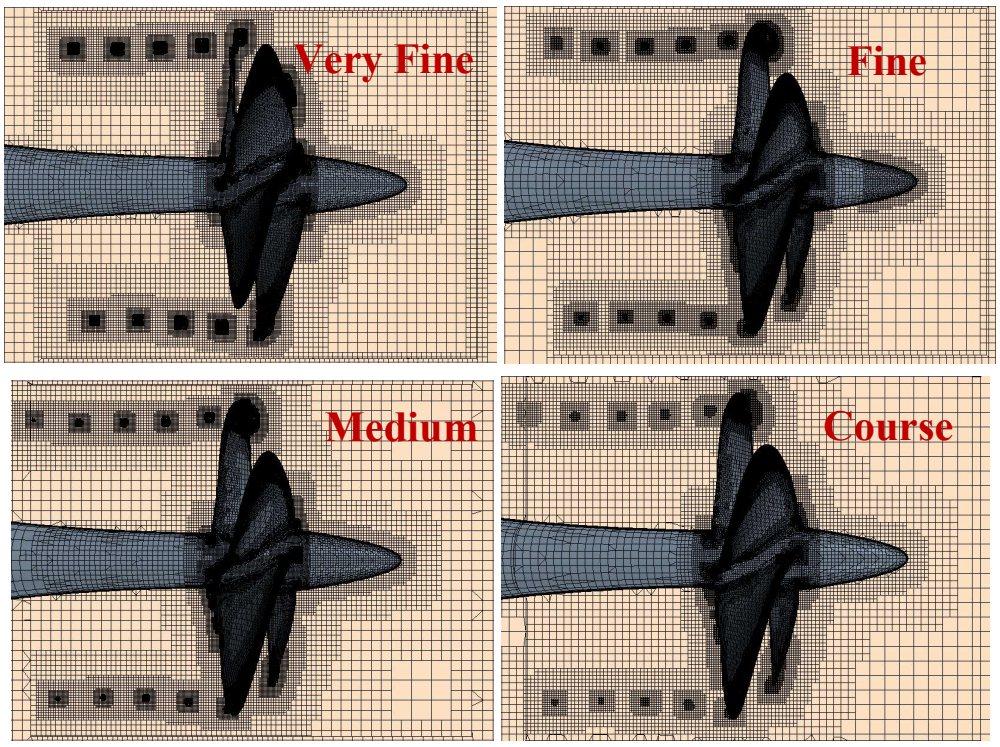

Figure 3-14 Different Grids for Grid Independency Study

Table 3-14 Grid Convergence Study in Cavitating Conditions

Grid Convergence	**Min Blade Surface Size [mm]**	**Surface Size Field Function [mm]**	**Surface Size Refinement [mm]**	**Number of Cells**
Coarse	1.4	1.00	0.618	6,216,885
Medium	1.0	0.70	0.437	9,531,418
Fine	0.7	0.50	0.312	15,877,834
Very Fine	0.5	0.35	0.218	27,154,939

Table 3-15 Grid Convergence Study in Cavitating Conditions

	J	**K_T**	**$10K_Q$**	**h_0**
Coarse	0.4	0.2672	0.3482	0.4884
Medium	0.4	0.2664	0.3470	0.4886
Fine	0.4	0.2661	0.3466	0.4887
Very Fine	0.4	0.2666	0.3475	0.4884

Table 3-16 Time Step Convergence Study in Cavitating Conditions

	J	**K_T**	**$10K_Q$**	**h_0**
$2\Delta t$	0.4	0.2660	0.3466	0.4887
Δt	0.4	0.2655	0.3459	0.4886
$\Delta t/2$	0.4	0.2661	0.3466	0.4887
Exp	0.4	0.2588	0.3699	0.4453

Figure 3-15 also presents the convergence type for the grid independency study in terms of K_T. It can be seen that while the V&V study for coarse, medium and fine mesh shows the monotonic-type convergence, the results for the medium, fine and very fine mesh cases demonstrate an oscillatory convergence behaviour.

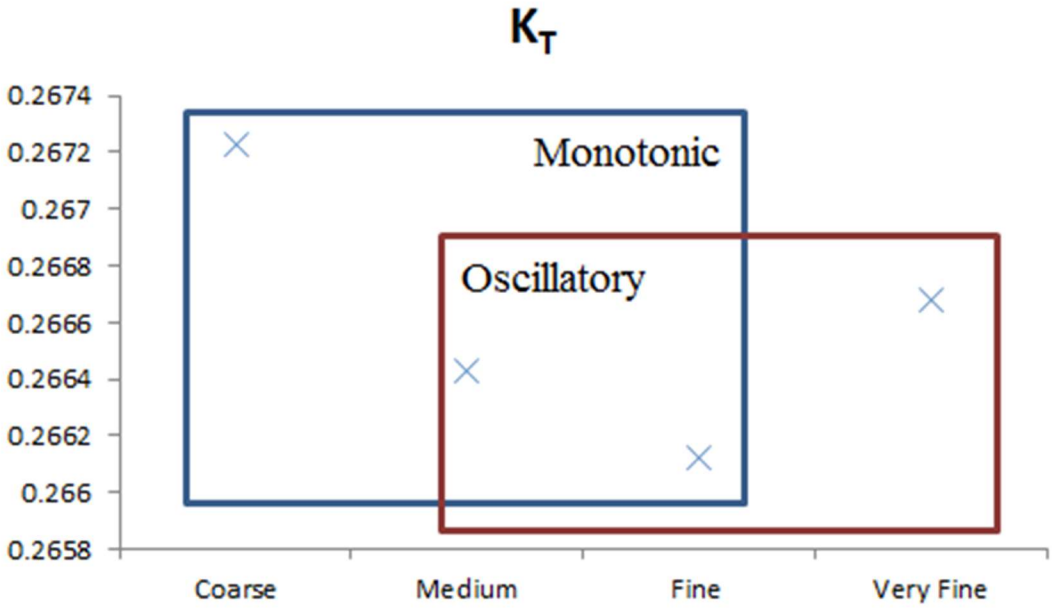

Figure 3-15 Grid Convergence Study for K_T

Due to the differences of the convergence types, the uncertainty values have been calculated using the Generalised Richardson Extrapolation for the monotonic convergence, and the upper and lower limits for the oscillatory convergence as described in §3.5.1. Table 3-17 shows the numerical uncertainty calculations for the grid and time step convergence studies.

Table 3-17 Numerical Uncertainty Calculations from Grid and Time Step Convergence

	K_T%	**$10K_Q$%**
Grid Uncertainty (Coarse, Medium and Fine)	0.1468	0.1656
Grid Uncertainty (Medium, Fine and Very Fine)	0.0613	0.0570
Time Step Uncertainty	0.0466	0.0605

Validation

The error between CFD and EFD results *(E)*, uncertainties of validation (U_V), experimental tests (U_D) and numerical simulations (U_{SN}) were given for K_T and K_Q in Table 3-18 and Table 3-19 respectively. For these calculations, $U^2{}_V = U^2{}_D + U^2{}_{SN}$ equation was used and previous data uncertainty and iterative uncertainty was neglected. It is observed that the deviations between calculated and measured values in cavitating conditions are not too great, 2.8% for thrust and 6.2% for torque coefficients. Despite the deviation being small between EFD and CFD results, uncertainty for the experimental tests was assumed to be 2%, $|E| > U_V$ and as such, K_T and K_Q not validated for grid 1 and 2 due to a small U_V value. On the other hand, K_T can be accepted for both grids due to the small error values between the EFD and CFD results. Besides, the simulations must be evaluated critically by taking into consideration the error in K_Q values which is still higher than 5%. Although K_T and K_Q values cannot be validated at the U_V level, Figure 3-16 demonstrates that smaller surface size and mesh refinement, where the cavitation may possibly occur in propeller's slipstream, helps to improve the accuracy of the tip vortex cavitation extent as will be discussed in details later in Chapter 5.

Table 3-18 Validation of K_T

	E%	**U_{SN}%**	**U_D%**	**U_V%**
Grid 1 (Coarse, Medium and Fine)	-2.8207	0.16229	2	2.00673
Grid 2 (Medium, Fine and Very Fine)	-2.8207	0.17685	2	2.01651
Time Step (2Δt, Δt, Δt/2)	-2.8207	0.13444	2	2.00956

Table 3-19 Validation of $10K_Q$

Grid	**E%**	**U_{SN}%**	**U_D%**	**U_V%**
Grid 1 (Coarse, Medium and Fine)	6.2944	0.17214	2	2.0074
Grid 2 (Medium, Fine and Very Fine)	6.2944	0.16444	2	2.0142
Time Step (2Δt, Δt, Δt/2)	6.2944	0.17454	2	2.0160

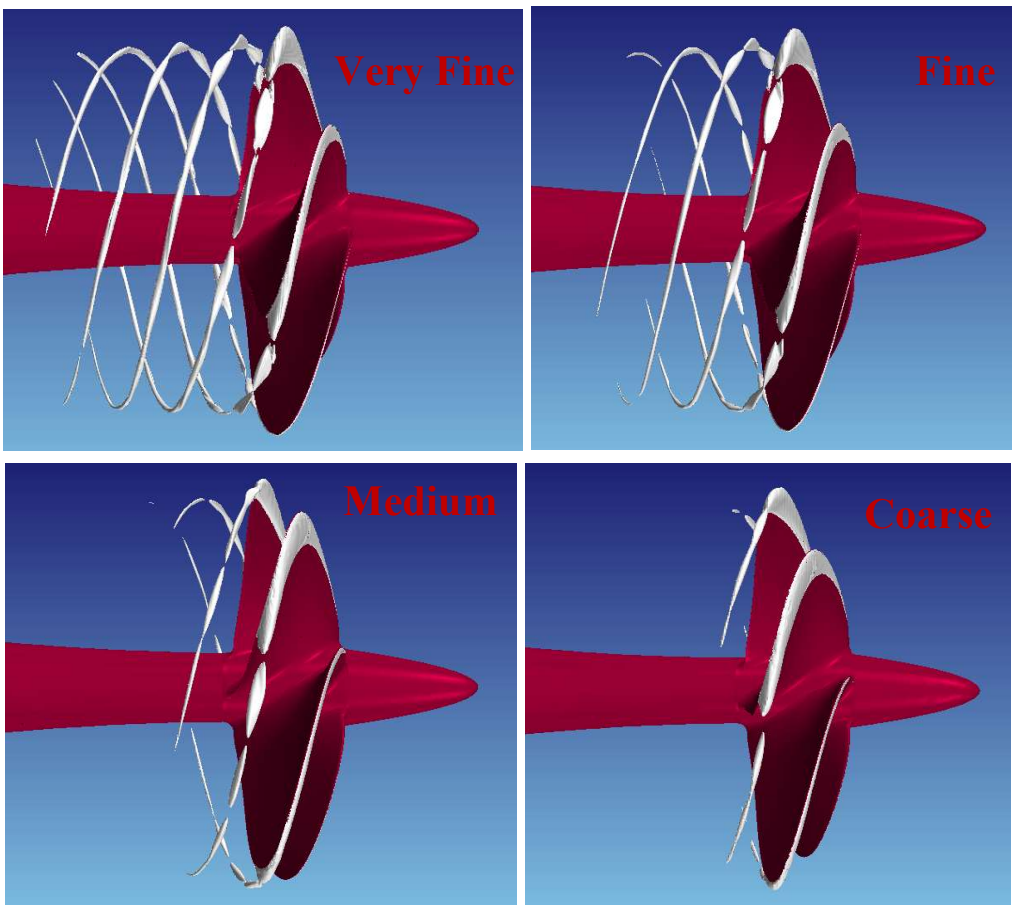

Figure 3-16 Tip Vortex Cavitation Extension for V&V Studies

3.6 Concluding Remarks

The basis methodologies (i.e. CFD and EFD) to be followed and further developed during this research study are presented in this chapter in relation to the propeller, rudder and hull interaction. The details of the three different propeller models and one hull geometry to be used for these investigations are also presented. The required validation and verification studies for the CFD calculations were conducted for the two propeller models for non-cavitating and cavitating conditions.

It was concluded that although the deviations between calculated and measured values in non-cavitating and cavitating conditions are small (less than 5%) for thrust and torque coefficients for all validation and verification studies, K_T and K_Q values could not be validated for each simulation case due to the small U_V values for different grids and time-step configurations.

The conclusions for validation and verification studies of cavitation simulations also presented that the uncertainty values for the tip vortex cavitation predictions were much higher than the sheet cavitation and adaptive mesh refinement is required to solve the tip vortex cavitation accurately.

Chapter 4 Open Water Propeller Performance

4.1 Introduction

Chapter 4 provides details of the non-cavitating open water propeller performance simulations of the model propellers introduced in Chapter 3. The main purpose of this chapter is to investigate propeller performance by using CFD and compare these with the results from experiments (EFD). While the experimental results were from the open literature for the PPTC propeller and the INSEAN E779A propellers, the experimental results for The Princess Royal Propeller were obtained from the cavitation tunnel tests that the Author was involved in at the SJTU cavitation tunnel as described in Chapter 3.

This chapter, therefore, first describes the performance characteristics of a propeller operating in open water. This is followed by the details of the CFD simulations for the above-mentioned three benchmark model propellers including their numerical modelling regarding the computational domain, mesh generation and boundary conditions. The chapter then continues with the presentations and discussions of the simulation results including the comparisons with the EFD results in terms of the propeller performance coefficients for the thrust, torque and propeller efficiency. Finally, the concluding remarks are presented based on the overall findings obtained from the chapter.

4.2 Open Water Propeller Characteristics

Traditionally, the propeller performance and associated characteristics can be investigated in two parts; open water and the behind hull conditions. The open water propeller characteristics indicate the forces and the moments on the propellers when they are operating in a uniform flow without the presence of any other object (e.g. hull

etc.) and boundaries (e.g. free surface etc.). Within the scope of this chapter, this condition is also called the non-cavitating condition; however, the main focus of this research study is the effect of cavitation. Although the open water condition assumes that the propeller is operating in uniform flow (if the propeller is not operating in an inclined condition), a typical ship propeller generally operates behind the hull and hence in a non-uniform wake field.

Separately from the behind hull conditions, the open water propeller characteristics are concentrated in this chapter, and hence the associated terminology for presenting the results are described in the following in terms of the propeller thrust, torque and efficiency.

Thrust and torque coefficients which are the functions of thrust and torque values respectively and can be calculated as in Equation 4.1:

$$K_T = \frac{T}{\rho n^2 D^4}$$
$$K_Q = \frac{Q}{\rho n^2 D^5} \qquad [4.1]$$

where T is propeller thrust, Q is propeller torque, ρ is density of liquid, n is rotational speed of the propeller shaft and D is the diameter of the propeller.

The advance ratio is defined as in Equation 4.2:

$$J = \frac{V_A}{nD} \qquad [4.2]$$

where V_A is the advance velocity of the fluid.

The open water efficiency of a propeller is defined as the ratio between the thrust power and power delivered to the propeller which manifests itself as the function of the previously defined three non-dimensional coefficients as given in Equation 4.3.

$$\eta_0 = \frac{J}{2\pi}\frac{K_T}{K_Q} \qquad [4.3]$$

Reynolds and cavitation numbers are also important non-dimensional parameters in representing the general performance characteristics, and they are described in Equation 4.4 and 4.5, respectively.

$$Re = \frac{\rho n D^2}{\mu} \quad [4.4]$$

$$\sigma_0 = \frac{p_0 - p_v}{0.5\rho(nD)^2} \quad [4.5]$$

where μ is the dynamic viscosity of the fluid, p_O is the reference pressure and p_V is the saturated vapour pressure of the water.

The Reynolds and cavitation numbers are non-dimensionalized by the blade tip rotational speed (nD). Alternatively, these numbers can also be non-dimensionalized by using advance velocity (V_A) instead of the rotational speed as follows:

$$Re = \frac{\rho V_A D}{\mu} \quad [4.6]$$

$$\sigma_0 = \frac{p_0 - p_v}{0.5\rho(V_A)^2} \quad [4.7]$$

4.3 Numerical Modelling

Although the main focus of this research study is on the cavitating performance of the propellers, as stated earlier, it is traditional and less complex to validate the CFD used and the methodology implemented for simulating the non-cavitating conditions first. Therefore the water is the only phase used for the non-cavitating simulations as opposed to the multiphase flow for the cavitation simulations.

As stated in the General Perspective of Chapter 1, the commercial CFD Code, STAR-CCM+, has been used throughout this research study including the open water propeller performance simulations. The validation studies were conducted using the three benchmark propellers (i.e. *PPTC* with inclined shaft, *INSEAN E779A* and *The*

Princess Royal) in non-cavitating conditions. The details of the experimental data for these three benchmark propellers were taken from; Postdam Evaluation Reports Case 1 (2015) for the *PPTC* propeller with shaft inclination, Salvatore et al. (2009) for the *E779A* propeller and *The Princess Royal* Propeller Test Report (2017) for *The Princess Royal* Propeller by the Author**.**

Simulations of the *PPTC* propeller with the inclined shaft were carried out at five different flow speeds using the RANS k-ω SST turbulence model and the sliding mesh technique for describing the rotation. The analyses were conducted with the five blades of the propeller (full propeller model included all blades) and using two computational domains, i.e. rotating and stationary domains.

The similar simulation study was also carried out for the *INSEAN E779A* propeller at only one flow speed. In addition, as already presented in Chapter 3 (Section 3.5.2.1) within details, the validation and verification including the grid and time step independency studies were conducted for this propeller in non-cavitating conditions.

Lastly, the same simulations were conducted for *The Princess Royal* propeller by using the same turbulence model and the rotation technique. The CFD results have been compared with the experiments conducted at the cavitation tunnel of SJTU as described in Chapter 3 including the V&V studies in the same chapter.

4.3.1 Computational domain

For the computational domain, a rotating domain was modelled around the propeller geometry together with a stationary domain. This was achieved using the CAD software, Rhinoceros 5.0. The same dimensions of the cavitation tunnel, as provided in the Propeller Workshop of SMP'15, were used to prepare a flow domain for the *PPTC VP1304* propeller and inclined shaft case. That is approximately *1.5D* from the centre of the propeller to the sides and, *8D* and 2*D* from the outlet and inlet respectively; the propeller, shaft and bracket geometries are shown in Figure 4-1.

For the *INSEAN E779A* propeller, another flow domain was modelled using the axial distances of the propeller centre from the inlet and outlet of 5*D* and 13*D,* respectively,

according to the recommendation of the STAR-CCM+ user guide (STAR-CCM+ User Guide, 2018) (Figure 4-1).

The same guideline was followed to prepare the ideal flow domain for *The Princess Royal* propeller in open water conditions.

Figure 4-1 shows the computational flow domains for open water propeller simulations of the *PPTC* propeller with inclined shaft and the *INSEAN E779A* propeller cases at the top and bottom of the figure, respectively.

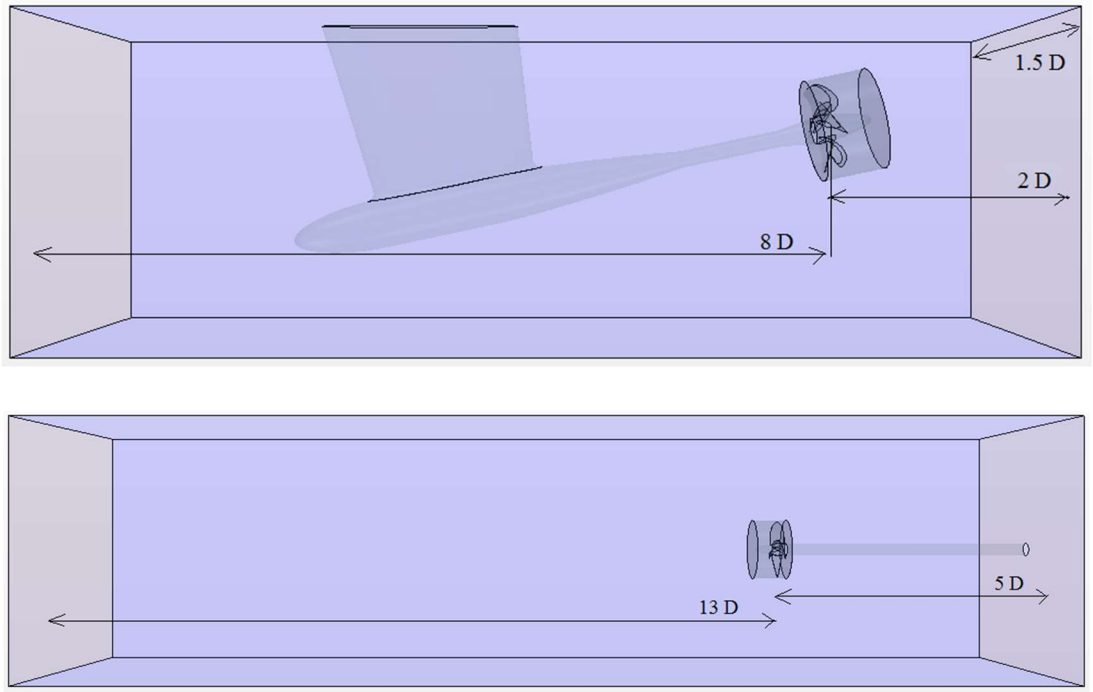

Figure 4-1 Computational Domain (Top; PPTC with shaft inclination, Bottom; INSEAN E779A propeller)

4.3.2 Mesh Generation

After the preparation of the flow domains for each simulation, a suitable mesh was generated for each propeller case with small surface size (approximately 0.004D) on the blade surfaces for the open water simulations. Figure 4-2 demonstrates the grid for the *PPTC* and *The Princess Royal* propellers, at the top and bottom, respectively. For the mesh generation, the surface size on the blade surfaces must be small enough to be able to capture edge curvatures especially at the tip, and the leading and trailing edges

of the blades. For the *INSEAN E779A* propeller a hexahedral trimmed mesh of 3.2M cells was also generated for non-cavitating conditions.

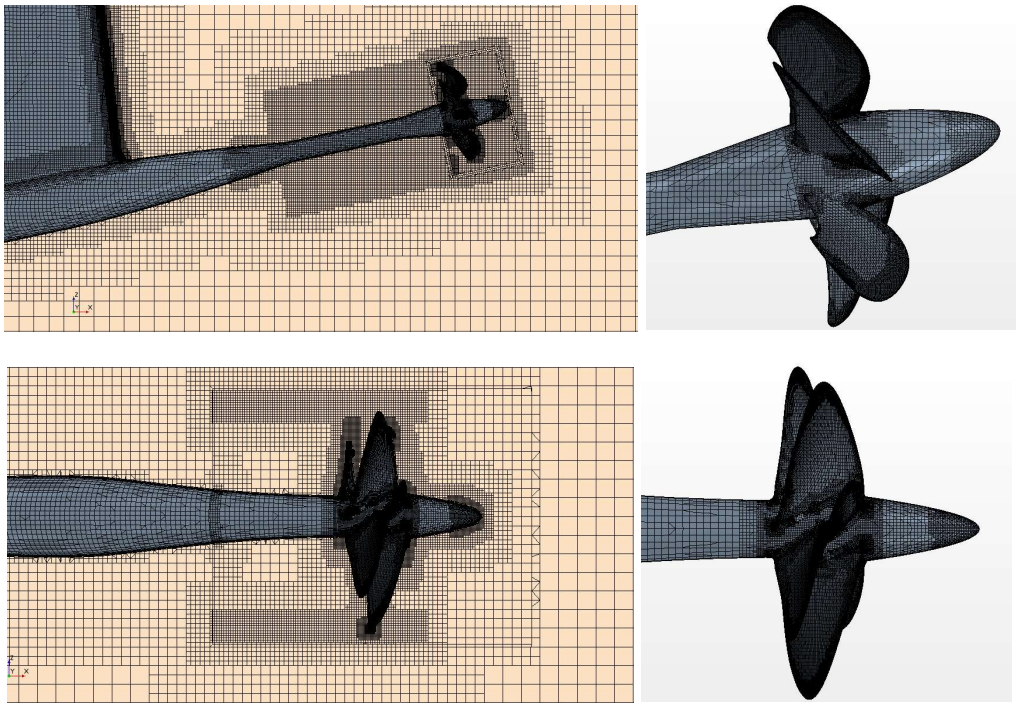

Figure 4-2 Generated Mesh (Top; *PPTC* with shaft inclination, Bottom; *The Princess Royal* propeller)

The average *y*+ value (Figure 4-3) was around 1 and less for blades and shaft respectively of the propellers using 12 prism layers and approximately 1 mm total thickness. Wall y+ is a scalar field in STAR-CCM+ that presents the non-dimensional wall distance. This value is defined as given in Equation 4.8 as follows:

$$y^+ = \frac{u^* * y}{\nu} \qquad [4.8]$$

where u^* is the reference velocity, y is the normal distance from the centroid to the wall surface and ν is the kinematic viscosity (STAR-CCM+ User Guide, 2018).

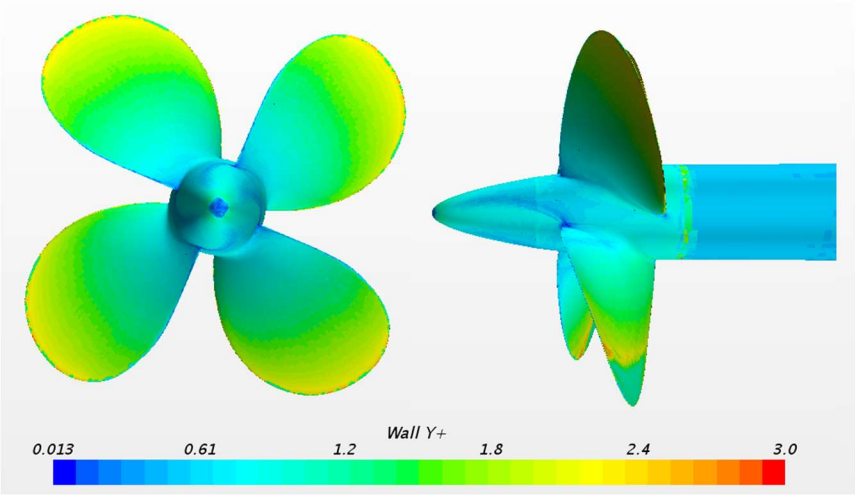

Figure 4-3 *y+* on blades, hub and shaft for *E779A* propeller

4.3.3 Boundary Conditions

Having modelled the propeller, shaft, bracket and flow domain geometries, a suitable mesh was generated for each simulation setting. According to the flow direction, the boundary conditions based on the velocity inlet and pressure outlet have been defined on the patches where the flow enters and leaves the domain, respectively. The top, bottom and side patches of the flow domain were described as the wall boundary conditions to simulate the wall effect of the cavitation tunnel. The propeller, shaft and the bracket geometries were also defined as the wall boundary conditions. The surfaces between the rotating and stationary domains are interface boundaries. The flow direction and the position of the propeller blades were replicated as in the open water tests in cavitation tunnel for each propeller. Figure 4-4 and Table 4-1 illustrates the boundary conditions applied for the open water simulations.

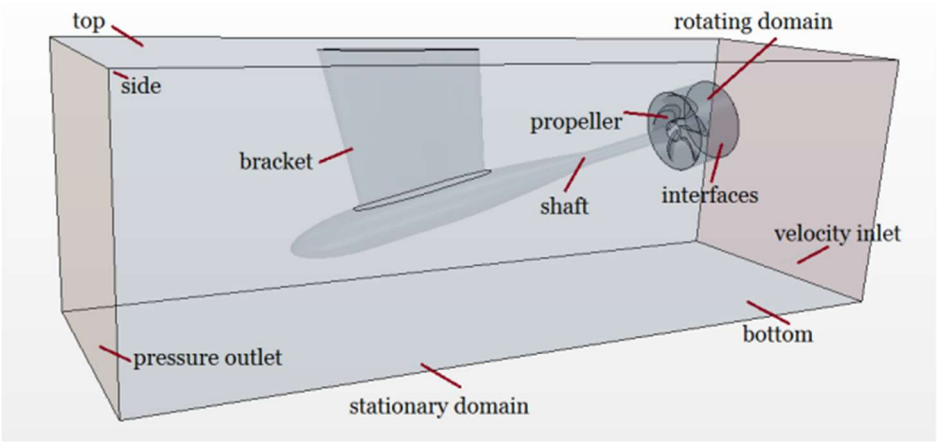

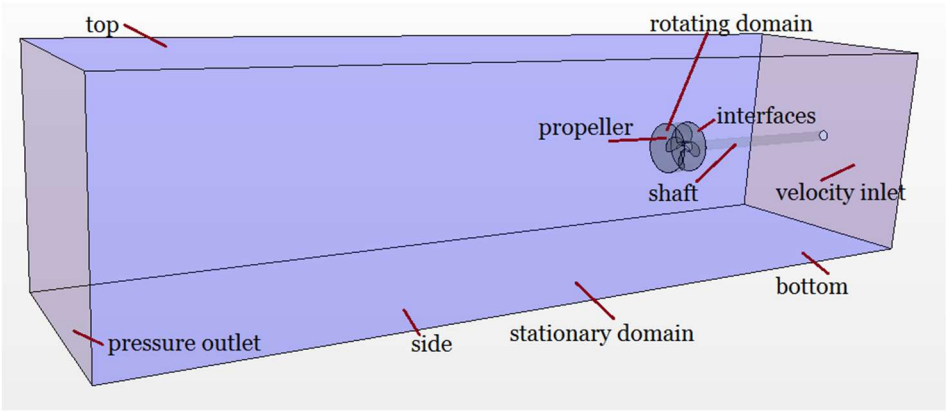

Figure 4-4 Computational domain and boundary conditions (Top: *PPTC* propeller with inclined shaft, Bottom: *E779A* propeller)

Table 4-1 Boundary Conditions for Open Water Simulations

Patches	Boundary Conditions	Descriptions
Inlet	Velocity Inlet	m/s, associated with the flow speed in the cavitation tunnel according to the simulation condition
Outlet	Pressure Outlet	0 Pa
Top, Bottom and Side	Wall	Replicating the wall effect of the tunnel walls
Geometry Surfaces	Wall	Propeller's blade, shaft, hub and bracket
Interfaces	Interface	Surface between rotating and stationary domain

4.4 Presentation and Discussion of Results

The simulations for the three model propellers were run until the thrust and torque values converged. The converged values were used to calculate the results for the associated thrust and torque coefficients given in Equation 4.1, and for the propeller efficiency in Equation 4.3, respectively. The results are presented in typical open water diagrams as described next.

Figure 4-5 and Figure 4-7 shows the open water performance data for the *PPTC* propeller with inclined shaft and *The Princess Royal* Propeller, respectively, while Table 4-2 and Table 4-3 also show the same data in a tabulated format, respectively. Both in these diagrams and the tables the data from the EFD are shown for the comparisons including the deviations between the EFD and CFD results in the tabulated data.

Table 4-2 shows the results and the deviations between the CFD and EFD for the *PPTC* propeller, presented at five different advance ratios (0.6-1.4). Although the difference in thrust and torque coefficients was 1% at J=1.0, this increased to 8% for J=1.4. The increment can be explained with the y+ values due to the generated mesh. The same mesh was used for all the advance ratios which are the results of the different advance velocities. To achieve closer results to the experiments different meshes might need to be generated keeping the y+ values around 1 and less for each flow velocity condition. While this issue affects the calculations of the thrust and torque values, the open water propeller efficiency is still below 3% for all advance ratio values due to the ratio of thrust and torque coefficients (Equation 4.3).

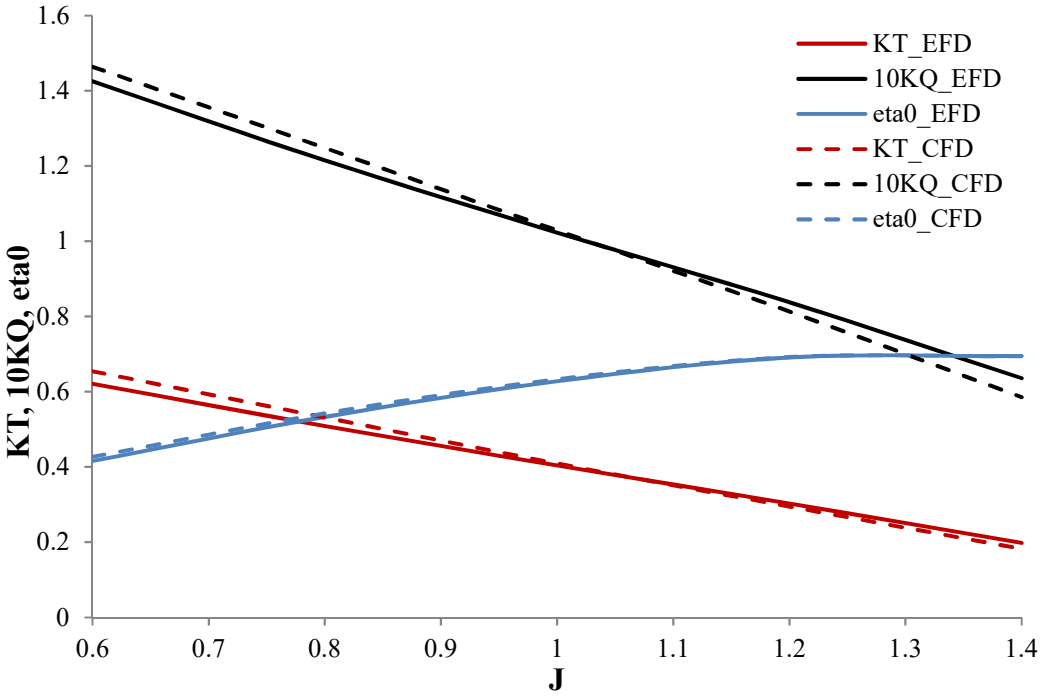

Figure 4-5 Propeller Performance Curves for *PPTC* propeller with inclined shaft case (EFD and CFD Comparison)

Table 4-2 EFD and CFD Comparisons for *PPTC* propeller with inclined shaft

Methods	J	K_T	$10K_Q$	$\eta 0$	Deviations		
					$\%K_T$	$\%10K_Q$	$\eta 0$
CFD	0.6	0.654	1.463	0.426	5	3	3
EFD		0.621	1.425	0.416			
CFD	0.8	0.531	1.248	0.542	4	3	2
EFD		0.509	1.212	0.533			
CFD	1.0	0.409	1.028	0.633	1	1	1
EFD		0.404	1.023	0.628			
CFD	1.2	0.294	0.813	0.692	-3	-3	0
EFD		0.303	0.838	0.691			
CFD	1.4	0.182	0.585	0.694	-8	-8	0
EFD		0.198	0.636	0.695			

As stated earlier, the EFD data used for the comparison of *The Princess Royal* propeller in this chapter was produced by the Author in tests conducted in the SJTU cavitation tunnel. Hence, it is appropriate to give a brief insight into the nature of the data.

Before starting the open water tests, a dummy hub (without the propeller blades) was tested and base levels of the thrust and torque values were recorded to calculate subsequent propeller performance coefficients correctly. Following this, the runs were performed using 3 different shaft speeds, namely 18, 25 and 33.3 [rps]; the last being the maximum value for the SJTU dynamometer. The results of the open water test measurements were evaluated and compared for each shaft speed to obtain the propeller performance coefficients K_T, $10K_Q$ and η_0 shown in Figure 4-6.

The open water test runs were repeated 3 times for the uncertainty calculations. Although, generally, open water tests are conducted in a towing tank using an open-water boat, propeller performance calculations can be also conducted in cavitation tunnels at the same conditions, but with higher Reynolds numbers due to shaft and advance speeds. Besides the open water tests at the cavitation tunnel, *The Princess Royal* propeller was also simulated at the same conditions for the comparison. For the CFD simulations, 25 rps was used as the propeller revolution speed. And the CFD results were compared with the experimental data that were obtained at the same revolution speed.

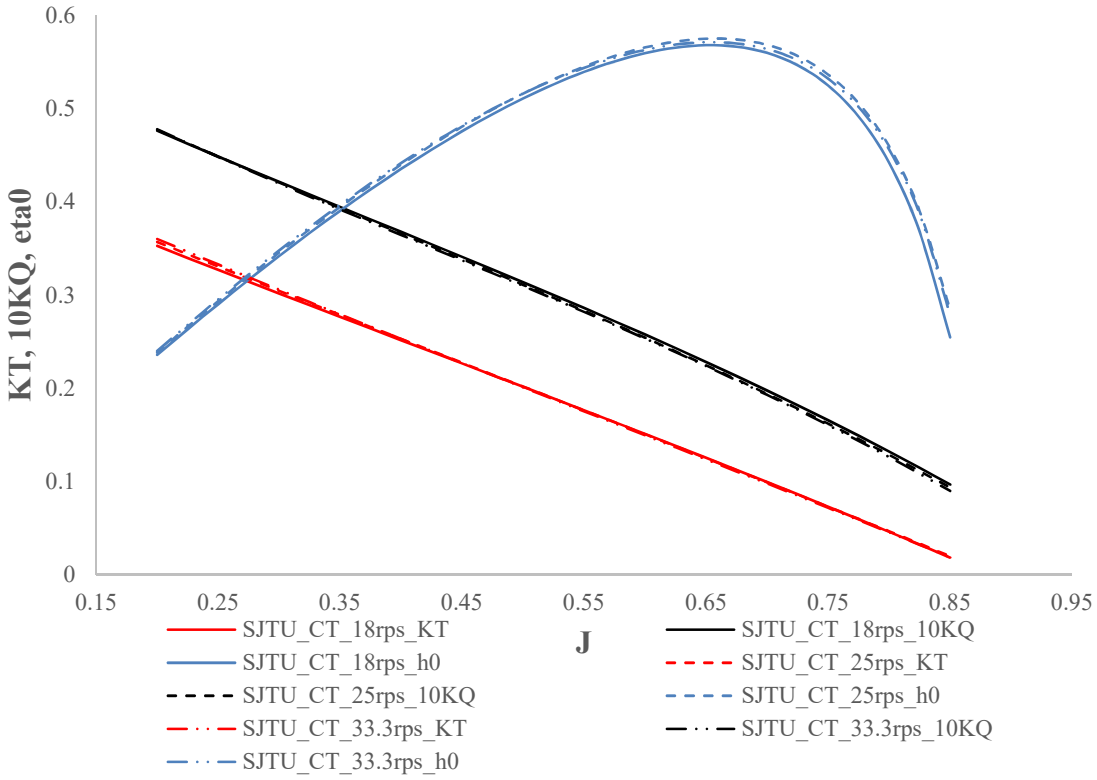

Figure 4-6 Propeller Performance Curves for the *Princess Royal* Propeller (EFD Results)

Similar to the *PPTC* case results analysis, the simulation results for *The Princess Royal* propeller test case are presented in Figure 4-7 and Table 4-3 in graphical and tabulated format, respectively, including the EFD data for comparison. As shown in Table 4-3 the deviation between the CFD and EFD is generally better for the torque than the thrust coefficient which has a maximum deviation of 3.9% for the propeller efficiency.

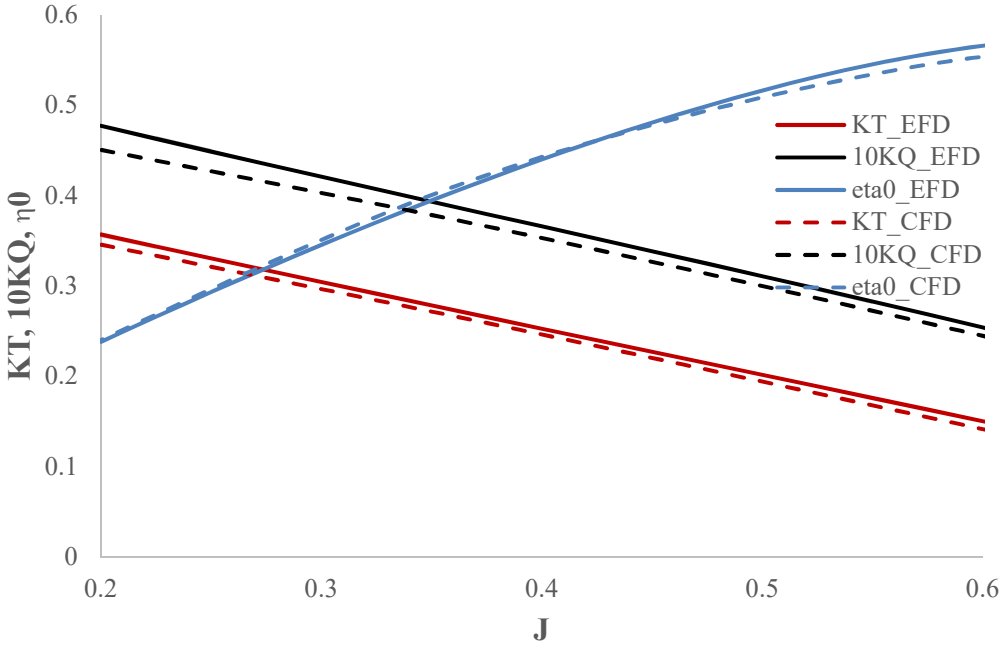

Figure 4-7 Propeller Performance Curves for the *Princess Royal* Propeller

(EFD and CFD Comparison)

Table 4-3 EFD and CFD Comparisons for the *Princess Royal* propeller

Methods	J	K_T	$10K_Q$	η_0	Deviations		
					$\%K_T$	$\%10K_Q$	$\eta 0$
CFD	0.138	0.3762	0.4801	0.1721	-2.8	-3.9	1.1
EFD		0.3872	0.4995	0.1702			
CFD	0.375	0.2589	0.3657	0.4230	-2.6	-2.3	-0.3
EFD		0.2658	0.3742	0.4244			
CFD	0.595	0.1443	0.2476	0.5520	-5.5	-1.7	-3.9
EFD		0.1528	0.2518	0.5746			

Finally, the simulation results for the open water performance of the *INSEAN E779A* propeller are given in Table 4-4 in a tabulated format only, since the data was only for a single operation point i.e. J=0.71, including the comparison with the EFD data. As

stated earlier, the V&V study for this propeller was already conducted and presented in Chapter 3, Section 3.5.2.1, including the grid and time-step independency investigations.

Table 4-4 EFD and CFD Comparisons for *INSEAN E779A* Propeller

Methods	J	K_T	$10K_Q$	$\eta 0$	Deviations		
					$\%K_T$	$\%10K_Q$	$\eta 0$
CFD	0.71	0.229	0.424	0.610	-3.8	-1.2	-2.6
EFD		0.238	0.429	0.626			

In Table 4-4, while the accuracy of the CFD simulation is less than a maximum of 3.8% under prediction for the thrust coefficient compared to the EFD data, the under prediction for the torque coefficient and efficiency is 1.2% and 2.6%, respectively.

In complementing the performance data for the same advance coefficient, the chord-wise distributions of the non-dimensional pressure coefficient at two blade section of the same propeller, which are taken at a fractional radius of 0.7 and 0.9, are also shown in Figure 4-8 for further information.

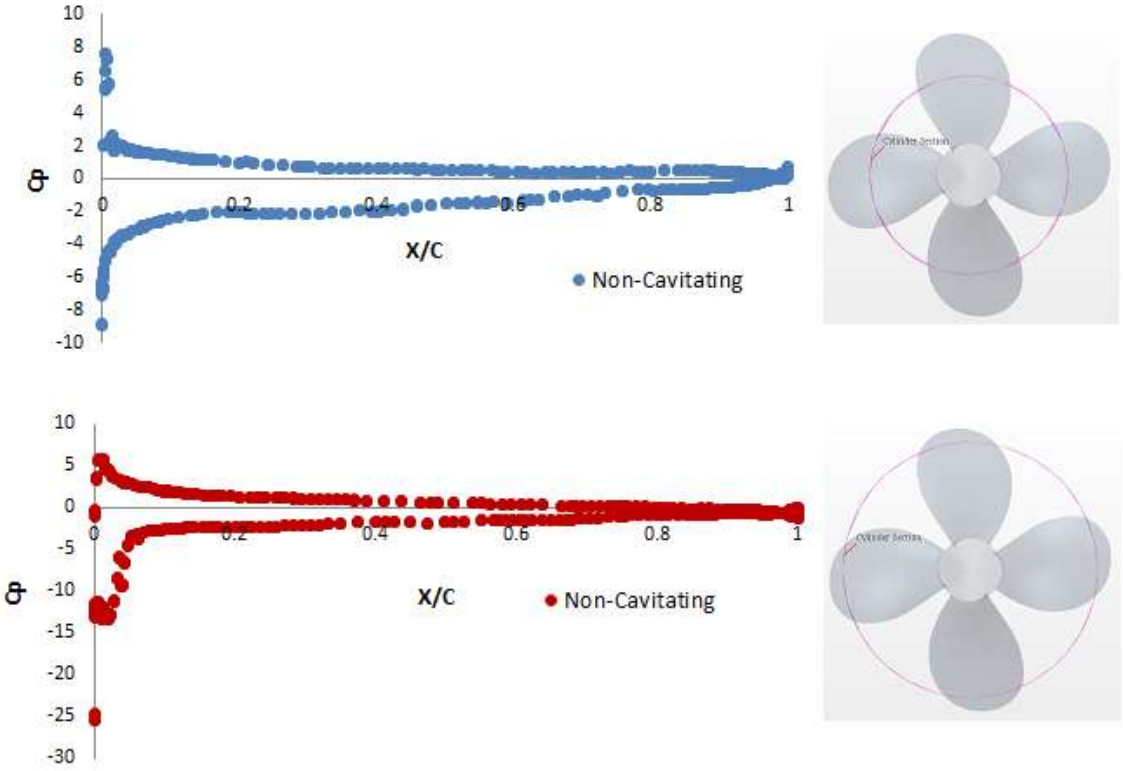

Figure 4-8 Pressure Coefficient for Non-Cavitating Conditions (Top; 0.7R Bottom; 0.9R)

4.4.1 Effect of cavitation on the open water propeller performance data

Although the detailed modelling the cavitation and its effect will be presented and discussed in Chapter 5, a basic insight is given here as an introduction to the effect of the cavitation on the propeller open water performance characteristics.

A non-cavitating flow condition can be described simply if; $p_0 - p_v \gg 0.5\rho(nD)^2$; i.e the cavitation number (σ_0) is large based on Equation 4.5. As the cavitation number decreases, typically, inception of the tip vortex cavitation may occur in the low pressure core of the vortex and be followed by the inception and formation of the sheet cavitation which may start to affect the propeller performance. This means that if the cavitation number and the extent of cavitation is moderate, the cavitation will not significantly affect the propeller performance in a negative way. On the other hand, if

the cavity extent becomes significant, it will affect the propeller performance leading, ultimately, to the thrust and torque breakdown as shown in Figure 4-9.

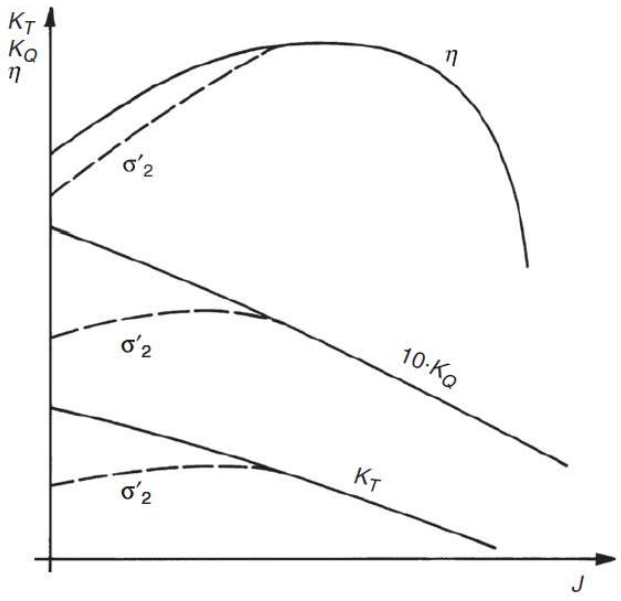

Figure 4-9 The effect of the cavitation on open water propeller performance (Thrust breakdown shown dotted, Bertram, 2000)

Figure 4-10 demonstrates the pressure distribution on the blade surfaces of *The Princess Royal* and the *INSEAN E779A* propellers, at the top and bottom figure, respectively. While the left images of Figure 4-10 show the suction side of the propeller blades, the right ones show the pressure sides. As expected the values of the pressure on the pressure side of the blades are higher than the suction sides. It is also obvious that the leading edge and the tip regions of the blades are the possible regions where cavitation may occur due to having lower pressure value than the saturated vapour pressure of the water. Although the propellers were simulated in non-cavitating conditions with only a liquid phase modelling, instead of a multiphase flow modelling, the cavitation regions on the blade surfaces can still be estimated. However, this is misleading since the proper modelling of the phenomenon is not implemented and hence the open water simulations cannot present the accurate results for cavitation prediction. Such images may offer a preliminary indication of the potential cavitation region on the blades. Cavitation simulations with the proper modelling of the phenomenon, therefore, are essential not only for the prediction of the cavitation with

correct physics but also for the accurate prediction of the propeller performance in cavitating conditions since the excessive cavitation would affect the propeller performance, especially at the low to medium J values, as shown representatively in Figure 4-9. Such cavitation simulations, therefore, are presented in the subsequent chapters for the same propellers.

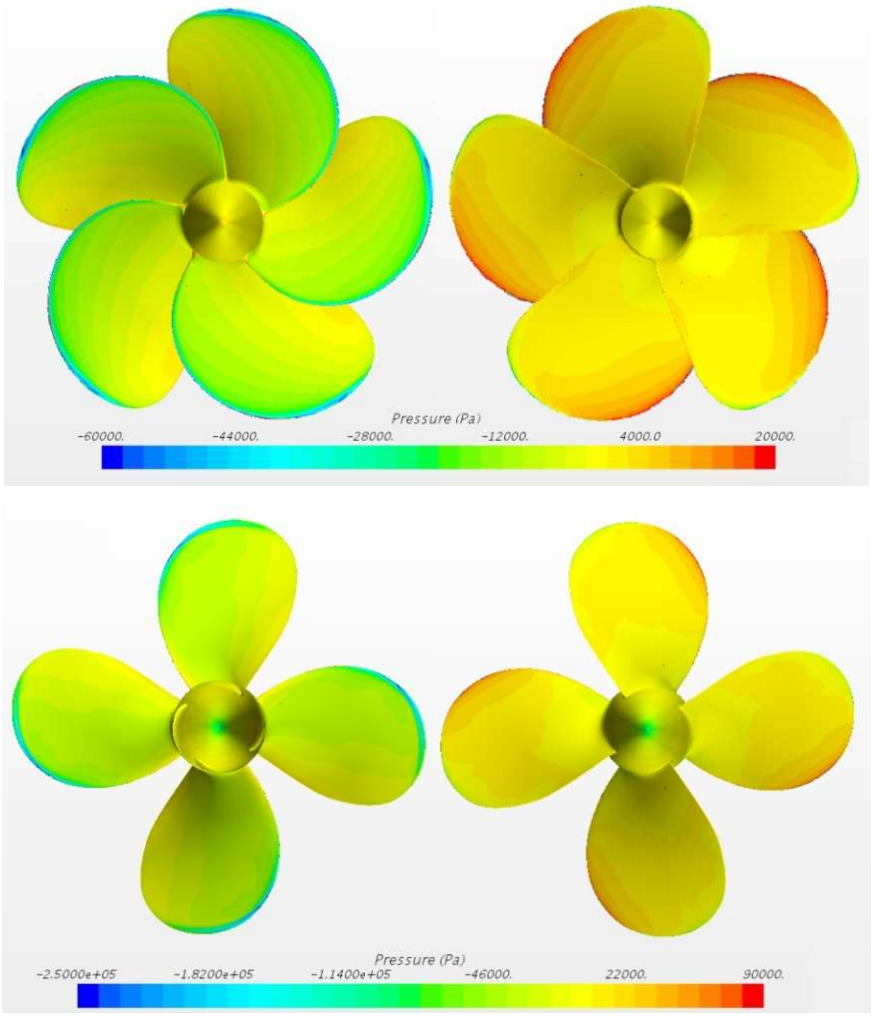

Figure 4-10 Pressure distribution on propeller surfaces (Left; Suction Side, Right; Pressure Side) (Top; *The Princess Royal*, Bottom; *INSEAN E779A*)

4.5 Concluding Remarks

This chapter presented the applications of the methodology by using the STAR-CCM+ code to calculate the non-cavitating open water performance characteristics of the three benchmark propellers described in Chapter 3.

The results of the performance predictions for the three propeller models are presented and compared successfully with the available experimental data. While the experimental data for the *PPTC VP1304* model and the *INSEAN E779A* model propellers were obtained from the open literature, the data for *The Princess Royal* model propeller was generated by the Author during model tests conducted at the SJTU cavitation tunnel.

The chapter described the application of the numerical modelling for the computational domain preparation, mesh generation, boundary conditions and simulation setup for each of the benchmark propeller test cases. The typical validation and verification study for the CFD simulations for the *INSEAN E779A* propeller was conducted and presented previously in Chapter 3 including the grid and time step uncertainty investigations.

The results of the simulations for each test propeller case were represented in graphical format (i.e. by the typical open water performance curves) as well as in tabulated form including comparisons with the experimental data for the thrust, torque and propeller efficiency.

Comparison of the CFD predictions for the performance data of the three test case propellers indicated good correlations with the EFD data, and hence provided initial confidence in the commercial code used and methodology implemented in using the code.

The chapter also included a brief discussion on the necessity of correct modelling of the propeller cavitation by using the two phase flow and its effect on the propeller open water performance characteristics. This leads on to the implementation of accurate cavitation modelling and its application to predict the performance of the same test propellers under cavitating conditions as will be focused in the next Chapter.

Chapter 5 Propeller Cavitation

5.1 Introduction

The main objective of this chapter is to develop an effective methodology for the efficient use of a commercial CFD code that will allow simultaneous modelling of the sheet and cavitating vortices from all of the blade tips and the hub from the propeller to the rudder. This capability will facilitate the propeller-rudder-hull interaction which is the main purpose of this research study.

The chapter therefore presents the implementation and further development of such methodology to model the effect of cavitation on propeller performance by using the commercial CFD code (STAR-CCM+) and applying it to simulate the actions of the three benchmark model propellers described in Chapter 3 and used in Chapter 4. The details of the CFD simulations with respect to the computational domain, mesh generation and boundary conditions are described for each propeller test case with a specific emphasis on modelling of the two main types of cavitation; sheet and tip vortex cavitation. Two different mesh refinement approaches are developed, namely, volumetric control (tube and spiral) and mesh adaption. These are used to extend the tip vortex cavitation in the propeller slipstream and to improve the propeller hydrodynamic performance predictions. Ultimately a new Mesh Adaption Refinement Approach for tip vortex Cavitation Simulations (MARCS) is developed and applied in this chapter.

By using the methodology described and applied to the three benchmark propeller cases, the chapter continues with the presentations and discussions of the simulation results for each case including comparisons with the results of the EFD methods for cavitation inception, cavitation patterns (and dynamics) as well as propeller performance coefficients wherever is appropriate or available. Finally, concluding remarks are given based on the overall findings obtained from this chapter.

5.2 Computational domain

In this section, details are presented of the computational model for the effect of cavitation on propeller performance are presented to simulate the performance of the earlier described three benchmark model propellers; namely, the *PPTC VP1304* propeller with the axial (level) shaft and inclined shaft, the *INSEAN E779A* and *The Princess Royal* model propellers in a range of cavitating conditions. For the simulations, four different computational domain geometries were prepared. The flow domains were modelled using the CAD software, RhinoCeros 5.0 and STAR-CCM+. The domain dimensions were defined using the dimensions of the actual testing environment for each propeller test case (i.e. cavitation tunnels), described in Chapter 4, by following the STAR-CCM+ User Guide recommendations for the cavitating flow simulations (STAR-CCM+ User Guide, 2018). Following the preparations of the flow domains, suitable meshes were generated for each simulation case as described in the following sections.

5.3 Mesh Generation

To begin with the simulations of the three propeller cases, first, the effect of varying parameters (mesh surface size, total number of cells, turbulence models, time step etc.) was investigated, by simulating the action of the *INSEAN E779A* propeller. Bearing in mind the important literature review finding in Chapter 2 concerning the lack of accurate modelling of the tip vortex cavitation and its interaction with the sheet cavitation, it was obvious that the CFD methods could provide great advantage over the low-fidelity methods, and within this context the selection of the appropriate mesh refinement approaches for this vortex type would be critical. Hence, different mesh refinement approaches were investigated in the STAR-CCM+ and the best mesh refinement approach, was sought to provide the largest extension of tip vortex cavitation in the propeller slipstream for the propeller-rudder-hull interaction.

At this stage, the Author would like to give an additional guidance to the Reader to follow this section; in this research study, the ultimate methodology developed to

model the tip vortex cavitation has required the development of a new mesh adaption refinement approach for the tip vortex cavitation simulation (MARCS) that is described in detail later in Section 5.3.2.1. The development of MARCS has been gradual, initially starting with the routine meshing techniques available and checking the accuracy of the simulation results from these techniques, before moving on to further advanced methods (e.g. volumetric control methods) and again checking the simulation results and so on. In this process, the Author started with modelling the PPTC propeller and then moved onto the INSEAN propeller and then gradually to The Princess Royal propeller behind the hull. Therefore, when the Reader will be reading this mesh generation selection section, the reader will be referred to the results of the simulations with these three benchmark propellers which are presented and discussed in Section 5.5 for the convenience of the thesis presentation. The Author therefore has felt making this statement necessary to inform the Reader in advance to avoid possible confusion.

By considering the two major types of cavitation patterns on a ship propeller, namely, sheet cavitation and tip vortex cavitation, first a suitable but coarse mesh was generated for the sheet cavitation simulations for the three test case propellers without any refinement around the propeller tip regions. For this purpose, a mesh arrangement was selected having a smaller size (0.002D) on the blade surfaces than the previously used mesh size for the non-cavitating case studies (in Chapter 4) was selected. These mesh arrangement are shown in Figure 5-1 for *the PPTC VP1304* and *INSEAN E779A* propeller are listed in Table 5-1 for all three propellers including *The Princess Royal* propeller model. The finer meshes were generated for the cavitation cases and used approximately 6 and 14 million cells for the *PPTC* and *E779A* propeller, respectively.

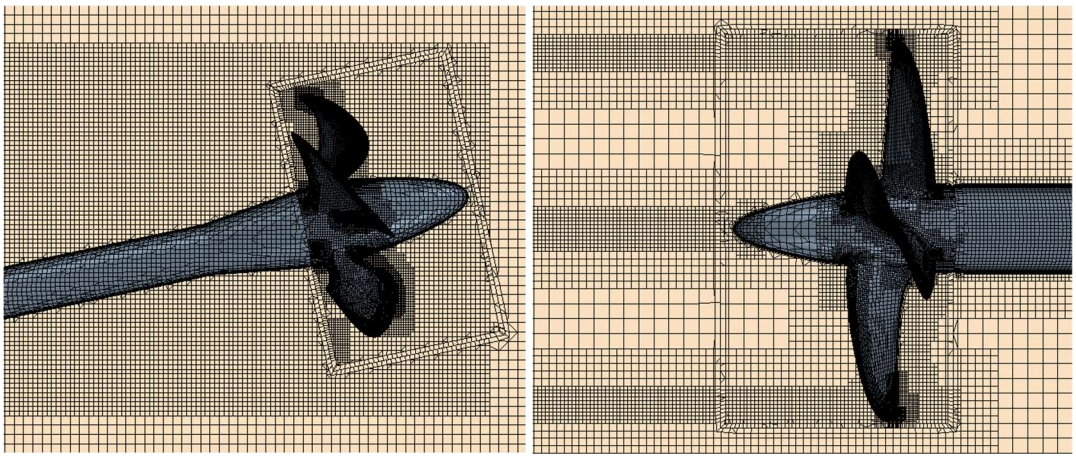

Figure 5-1 Computational Grid (Left; *PPTC VP1304* with inclined shaft, Right; *INSEAN E779A*)

Although similar grid sizes were used on the blade surfaces, the difference in the total number of cells between two meshes is due to the different domain sizes and volumetric control geometries. The average y+ value was around 1 and less for blades and shaft, respectively, of these propellers using 12 prism layers and with a total thickness of approximately 1 mm.

Table 5-1 Mesh details for sheet cavitation simulations

Mesh Details	Model Scale Test Propellers			
	PPTC VP1304		INSEAN E779	Princess Royal
	Axial Shaft	Inclined Shaft		
Surface Size on Blade (min/max)	0.5/1.5	0.5/1.5	0.5/1.5	0.5/1.5
Total Number of Cells	5,845,837	5,613,662	11,879,457	15,113,854

As presented in Section 5.5 and shown in Figure 5-10 and Figure 5-14, despite using the fine mesh and a DES model, a satisfactory agreement with the EFD cavitation patterns was only observed on the *E779A* and *PPTC VP1304* blade surfaces and their hubs (Pereira et al. 2004, Salvatore et al. 2009), (Potsdam Evaluation Reports Case 2, 2015).

However, it was concluded that this mesh and analysis method were not sufficient to capture the tip vortex cavitation and to predict propeller performance accurately.

As already concluded in Chapter 2 of this study, while the sheet cavitation of marine propellers can be predicted accurately by the CFD methods, computational modelling of their cavitating tip vortices has its challenges, in particular for extending these vortices from the blades aft to, and interacting with, the rudder in the non-uniform wake field of a ship hull. In order to capture the sudden pressure drop within the tip vortex core and the development of cavitating bubbles, the mesh must be refined in the region where the tip vortex type cavitation may occur. For this purpose, different mesh refinement approaches have been developed such as volumetric control and mesh adaption as used and discussed in the following sections.

5.3.1.1 Volumetric Control

Tube Geometry

The Author first introduced an early version of the advanced mesh refinement technique in which a tube geometry was imposed around the tip region of the propeller for capturing the tip vortex cavitation in a propeller slipstream (Yilmaz et al. 2017). The helical tube, as shown in Figure 5-2, was created to accommodate a very fine mesh around the tip area where the tip vortex cavitation occurs in the low pressure core. The simulations were conducted with approximately 11 million cells, including mesh refinement within the tube geometry. The average y+ value was kept the same since the prism layer settings were not changed in the new mesh. In addition to the tip helical tube geometry, a cylinder geometry was also prepared at the shaft axis to create a volumetric control region for capturing the extension of the hub cavitation as shown in Figure 5-2.

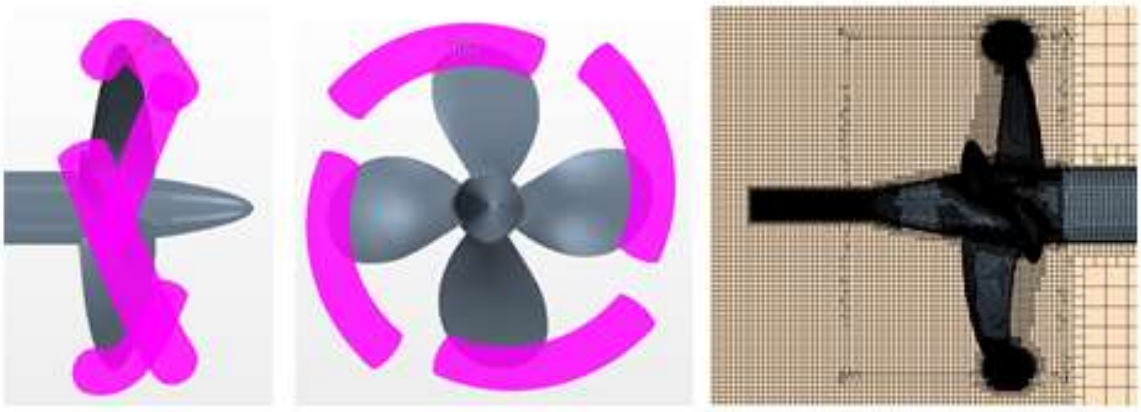

Figure 5-2 Mesh Refinement using Volumetric Control (Tube)

(Left; Tube geometry around propeller tip, Right; Generated Mesh)

These refined mesh arrangements allowed an extension of the tip vortex and hub vortex cavitation to appear. When the simulated cavitation patterns using this improved mesh arrangement was compared with the EFD results, it was observed that improvements in the visualisation of the tip vortex cavitation was directly related to the sequence of mesh refinement procedures developed in this thesis (Figure 5-11). In this first case, the mesh size in the volumetric control region around the tip was selected as 0.002D after a few iterations. With the introduction of the helical tube geometry and using it for the mesh refinement, the extension of the tip vortex could successfully be simulated. Moreover, the thrust and torque coefficients were improved by approximately 2% due to better modelling of the cavitation and its impact of the propeller performance as seen in Table 5-7 for the *INSEAN* Propeller.

As a result of the application of the tube geometry, improvements were obtained not only for tip vortex cavitation but also predicted propeller performance coefficients. However, it was concluded that this mesh arrangement system needed to be improved further in order to fully capture the EFD-observed extent of the cavitating tip vortex in the propeller's slipstream as discussed in Section 5.5.

Spiral Geometry

Following a reasonable success of the tube geometry for refining the mesh in the tip region, a new meshing approach had to be applied to rectify the "tube" deficiencies. This involved to extend the tube geometry helicoidally from the propeller tip region all the way through the propeller slipstream. The details of this method are described below, as applied to the *INSEAN E779A* propeller. This technique is the building block of the new advanced approach with its helical tube and spiral geometry extending the existing tube through the tip vortex trajectories.

In further developing the mesh refinement technique, firstly, the simulations were run with the mesh arrangement without any refinement (i.e. as in the sheet cavitation simulations). From this simulation, the pressure distribution behind the propeller was obtained to create the contracting spiral geometry of the propeller's slipstream in the rotating domain region. The pitch and the contraction of the slipstream diameter were calculated from the results of this first run. Figure 5-3 shows the spiral geometry which is starting from the propeller tip region through the propeller's slipstream.

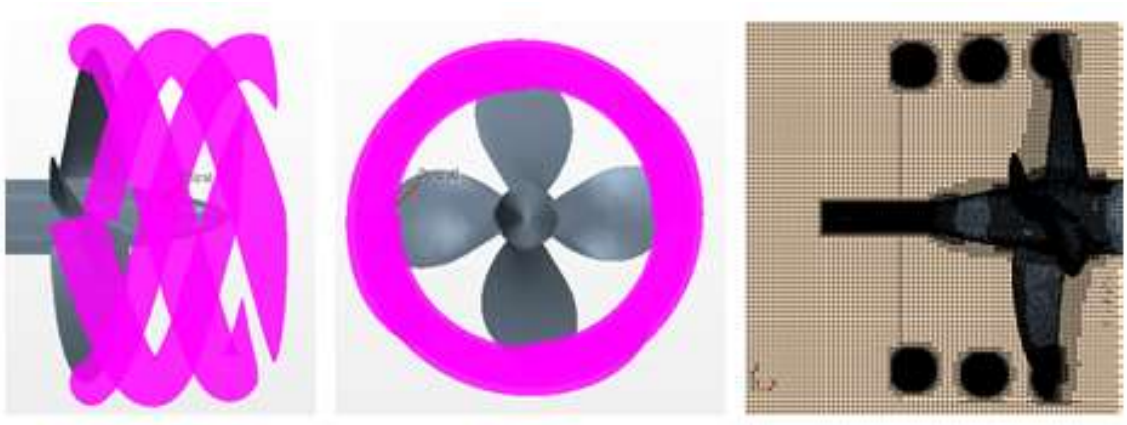

Figure 5-3 Mesh Refinement using Volumetric Control (Spiral)

(Left; Spiral geometry around propeller tip, Right; Generated Mesh)

Figure 5-3 also illustrates the mesh generated (Right) using the spiral (Left) geometry for the cavitation simulations. This geometry was used as a *"volumetric control"* to generate a more refined mesh in the region where the cavitation bubbles are moving with the flow and where the tip vortex cavitation may occur. The fine mesh was generated with approximately 0.002D surface size for the refinement area (for the

spiral geometry) with 19 million cells for the spiral geometry refinement. The average y+ value was around 1 for the propeller geometry using 12 prism layers and approximately 1 mm total thickness of prism layer. Table 5-2 also presents the mesh details for the tube and spiral geometry refinements.

Table 5-2 Mesh Details

Mesh Parameters	Mesh Refinement	
	Tube	Spiral
Surface Size (Blade)	0.5/1.5 mm	0.5/1.5 mm
Surface Size (Refinement)	0.5 mm	0.5 mm
Number of Cells	14,001,552	19,242,589

5.3.1.2 A New Mesh Adaption Refinement Approach (MARCS)

Following a distinct improvement in cavitation modelling by using the tube and spiral geometry based refinement approach, further improvement in mesh adaption was required for its adaptability and hence efficiency. This was because, although the spiral method was useful for extending the tip vortex cavitation in the propeller slipstream, it was not self-adaptive for different operating conditions and propeller geometries. However, the parameters of the spiral geometry -such as pitch, diameter and so on- must be changed efficiently for each different rotational speed and advance velocity as well as for different propeller types. Additionally, redundant cells were generated outside the area where the tip vortex cavitation occurs due to the use of a large diameter for the spiral section. Consequently, a new *"adaptive mesh refinement"* method had to be developed to improve the existing solution.

The Author therefore has proposed a new adaptive mesh refinement approach which is called MARCS (*Mesh Adaption Refinement approach for Cavitation Simulations)* especially to enhance the capture of tip vortex cavitation in a propeller slipstream. In this method the adaptive mesh refinement was created only in the region where the tip vortex cavitation may occur. At the beginning of this application, the upper limit of absolute pressure in the solution was determined by creating a threshold region in

STAR-CCM+. In such cavitation simulations, the volume fraction of vapour shows the volume where the absolute pressure is below the saturated vapour pressure of water, thus identifying the cavitating volume. A threshold region was created by increasing the saturation pressure from the STAR-CCM+ default value of 3169 [Pa] to a higher value, 10000 [Pa] thus generating, the pink region as shown in Figure 5-4. This artifice provides an indication of the volumetric trajectory on which to generate a fine mesh for accurately capturing the pressure-drop correctly and tracking the cavity bubbles in the propeller slipstream. This is something similar to applying vacuum in a cavitation tunnel to be able to detect the cavitation inception although here the saturated vapour pressure value is increased.

In applying this idea on a generated mesh, two field functions, which are described below, were created to prepare a table including the coordinates and the surface size of the new refined mesh for generating the adaptive mesh. These were needed to extend the tip vortex cavitation, within the identified volumetric trajectory of the propeller slipstream, much as shown in Figure 5-4.

Field Function 1:

Cellwidth = pow($Volume, (1/3))

Field Function 2:

Refinement = ${AbsolutePressure} < 10000 && ${AbsolutePressure} > 3169 ? ${cellwidth}/3 : 0

One of the two field functions, called “Cell Width”, specifies the one dimension of each cubic cell. The other field function termed “Refinement” is defined for creating a refinement table which includes coordinates of each cell in x, y and z directions and the surface size of the new mesh to be used while an adaptive mesh is being generated. The “Refinement” field function represents each mesh cell, where the absolute pressure, below 10000 [Pa] and above 3169 [Pa], is sub-divided by three in the three dimensions. The upper limit of absolute pressure was defined by creating a threshold (10000 [Pa]) and checked visually as shown in Figure 5-4. The lowest limit of the pressure was determined by the saturation pressure (3169 [Pa]). Figure 5-4 and Figure

5-5 show, respectively, the threshold below 10000 [Pa] and mesh generated using the new approach, MARCS.

Perhaps the most important part of the new approach was to determine the surface size of the each cubic cell in the tip vortex region for capturing cavity bubbles in the slipstream. As reviewed in Chapter 2, Kuiper (1981) investigated and measured cavitation inception, including tip vortex cavitation, using a model scale propeller (Propeller V) at J-values of 0.3, 0.4 and 0.5. Additionally, he defined an experimental relationship between the cavitating core radius (a_c) and cavitation index (σ_n) by preparing equations and graphs in this range of J values. In his study, the minimum radius of each bubble (a_i) was consistently found to be about 0.25 mm on a model scale propeller at the cavitation inception stage. According to these investigations, the core radius (a_c) always tends to go to the minimum core radius (a_i). On the basis of Kuiper's study, similar relations between bubble radius, mesh size and simulating tip vortex cavitation are determined within the new adaptive mesh approach. The mesh size was always required to be maintained below 0.25 mm (it is approximately 0.22 mm for this case) for capturing the tip vortex cavitation structure in the propeller slipstream. Using a mesh size larger than 0.25 mm, the tip vortex cavitation extension as shown in Figure 5-11 could not be simulated.

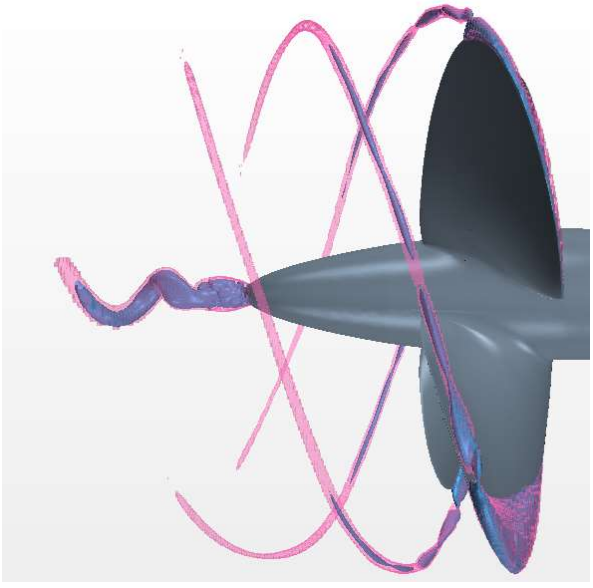

Figure 5-4 Absolute pressure threshold below 10000 [Pa]

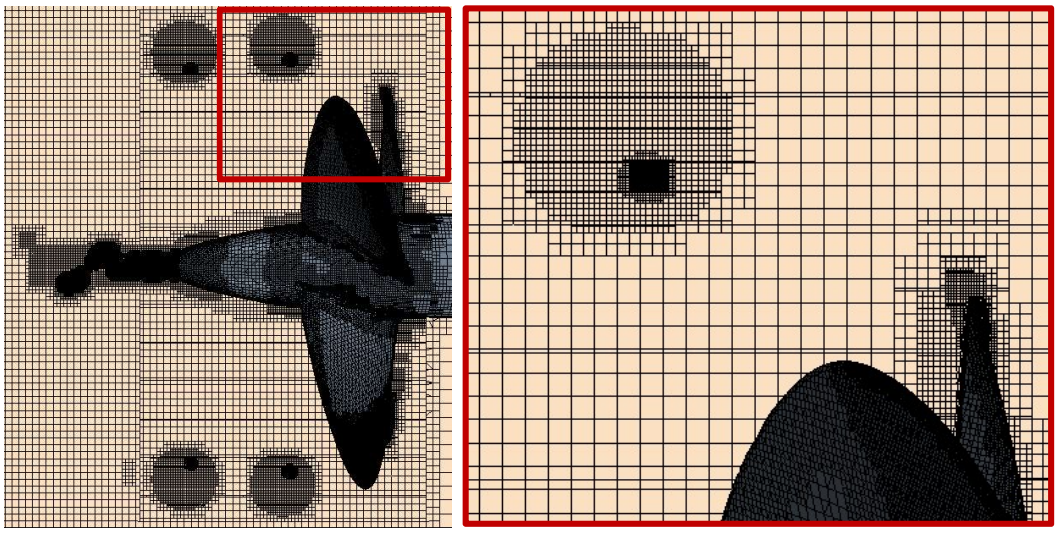

Figure 5-5 Mesh refinement due to MARCS

Having described the basis of MARCS, its step-by-step application is defined in the flowchart, Figure 5-6. This approach is implemented in using STAR-CCM+ and applied to simulate the performance of cavitating ship propellers especially for the accurate simulation of the tip vortex cavitation trajectories.

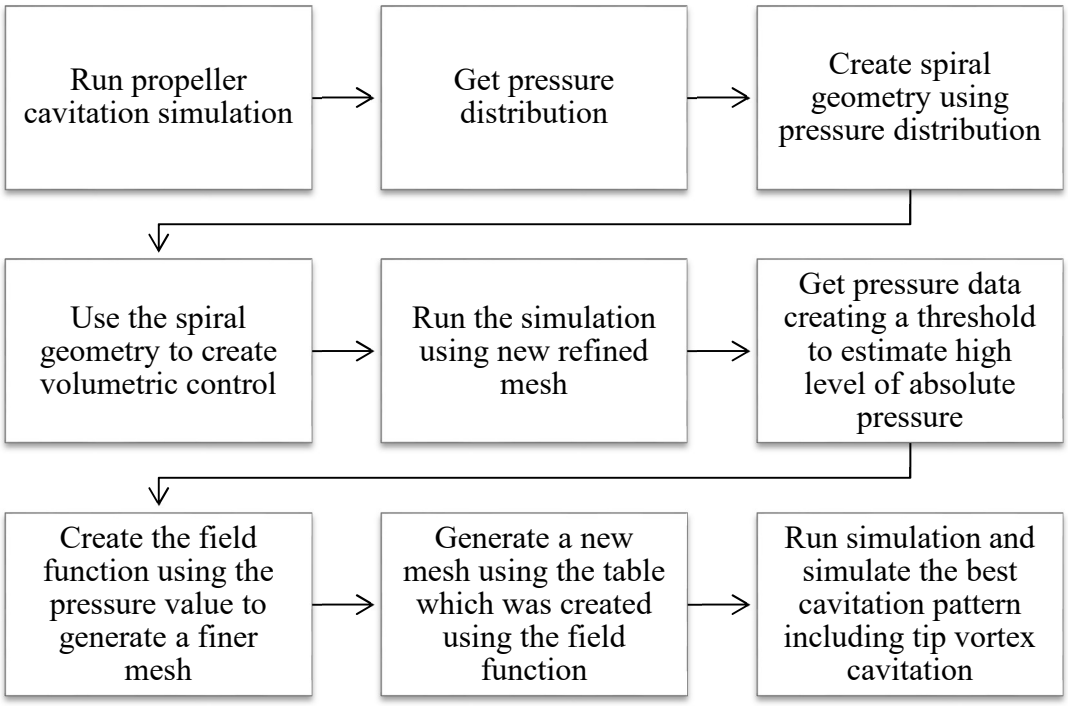

Figure 5-6 Flow chart summarising new Mesh Adaption and Refinement approach for Cavitation Simulation (MARCS)

Modifications to MARCS

While MARCS has been applied successfully to simulate the tip vortex cavitation trajectories of the *INSEAN E779A* propeller, (e.g. Figure 5-11) the approach needed to be improved further on two accounts. The first improvement was to reduce the total number of cells while the refinement region needed to be extended in the slipstream for *The Princess Royal* Propeller. This was because of more demanding modelling requirements of *The Princess Royal* propeller due to the large clearance between the propeller and rudder.

As a result, firstly, the volumetric control region (spiral geometry) was removed from the settings of the mesh generation. Secondly, having defined the required surface (less than 0.25 mm), "*cell width"* was also removed from the refinement process. The *"refinement"* field (i.e. Field Function 2) therefore was modified as follows:

Refinement = ${AbsolutePressure} < 17000 && ${AbsolutePressure} > 3800 ? 0.00035 : 0

Following this modification, the threshold below 17000 [Pa] and mesh generated using the MARCS approach is presented in Figure 5-7 and Figure 5-8, respectively.

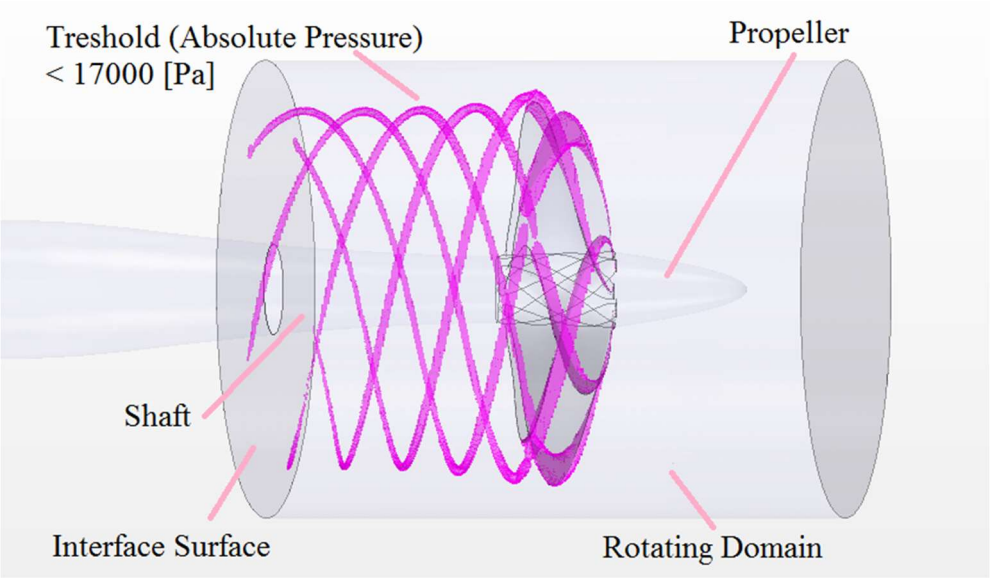

Figure 5-7 Absolute pressure threshold below 17000 [Pa]

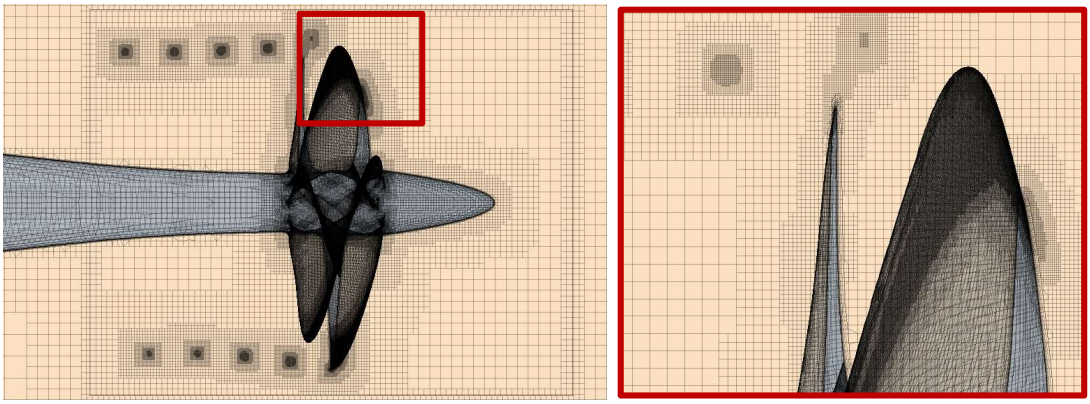

Figure 5-8 Mesh generation using MARCS

Figure 5-9 presents the modified flow chart summarising the new MARCS approach for cavitation simulations removing the volumetric control region and modifying the field function as stated earlier.

Having conducted the 1st modification on MARCS, the next modification was made on the mechanism to detect the tendency for cavitation. As stated earlier, the initial mechanism used for this purpose was the increase in the default value of the saturated vapour pressure. However, this can be replaced by using a vorticity based approach (Q-Criterion) according to the requirements of the simulations, especially for more complex applications (e.g. non-uniformity due to hull wake, inclined shaft and propeller-rudder-hull interaction etc.) as well as for better representation of the flow physics regarding the nature of cavitation inception. These two modifications therefore were applied to MARCS as further developments and the associated flow chart was updated as shown in Figure 5-9.

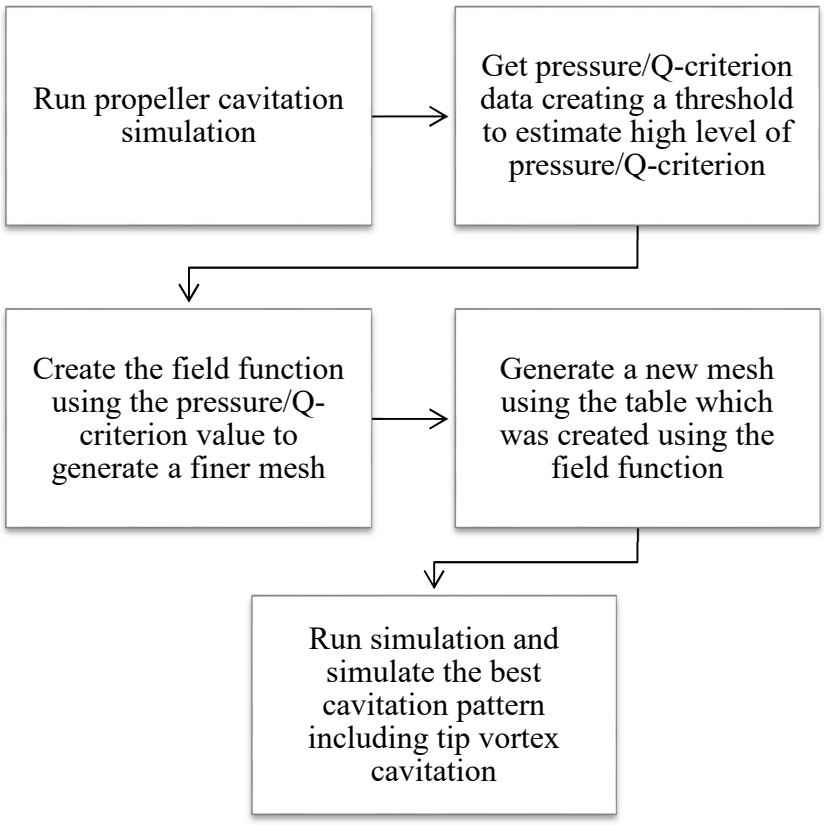

Figure 5-9 Modified Flow chart summarising MARCS in order to reduce total number of cells

Finally, within the framework of the mesh generation, Table 5-3 is included to list the total number of cells for the cavitation simulations of the three benchmark propellers in using MARCS. Less than 30 million meshes have been used with 0.22 mm surface

size for the refinement region in the propeller slipstream in applying the MARCS and to improve the tip vortex cavitation extent as shown in Figure 5-12, Figure 5-20, and Figure 5-28, and as discussed in Section 5.5.

Table 5-3 Mesh details for tip vortex cavitation simulations

	PPTC VP1304	INSEAN E779A	Princess Royal
Surface Size (Blade)	0.5/1.5	0.5/1.5	0.5/1.5
Surface Size (Refinement)	0.22	0.22	0.22
Number of Cells	27,646,573	23,416,640	27,154,939

5.4 Simulation Setup and Boundary Conditions

All parameters such as total number of mesh cells, surface size, suitable time step, and turbulence model were investigated for the cavitation simulation of marine propellers using the *INSEAN E779A* propeller. Following this, the validated and verified approach was applied for the other two test case propellers.

As stated earlier, although the RANS turbulence model was sufficient for modelling the open water performance of the propellers, the scale resolving models such as DES and LES were preferred for the cavitation simulations; LES is also recommended in the user guide of STAR-CCM+ for complex turbulent flows such as in modelling cavitation, and particularly tip vortex cavitation.

During the cavitation simulations of the *INSEAN E779A* propeller, different turbulence models were applied and compared with each other, not only for the propeller performance coefficients but also for cavitation patterns and tip vortex cavitation extents.

At the beginning of the cavitation simulations, the DES turbulence model was sufficient to simulate sheet cavitation on the blade surfaces. After the MARCS application was applied for simulating the tip vortex extension in the propeller slipstream, DES and LES turbulence models were compared each other using the same refined mesh for extension of the tip vortex. The results showed that while the mesh

refinement method helped to extend the cavitation pattern, particularly the tip vortex cavitation, the LES model also improved the accuracy of the predicted propeller performance characteristics (i.e. K_T, K_Q and η_0).

For the cavitation simulations, the SST k-omega DES model and the Wall-Adapting Local-Eddy Viscosity (WALE) subgrid-scale model were used for the DES and LES turbulence models, respectively. LES with WALE was the final set of models used for the sheet and tip vortex cavitation modelling.

With this selection of the suitable turbulence model for the tip vortex cavitation simulations of the *INSEAN E779A* propeller, different time step values were tried based on the time steps recommended by ITTC and others in the open literature. Hence the time step was calculated such that the propeller rotates between 0.5 and 2 degrees per time step, ITTC (2014). Finally, a time step value of $\Delta t=5x10^{-5}$ s, corresponding to 0.648 deg of propeller rotation, was used for the *INSEAN E779A* propeller simulations. The same time step value was also applied for the other cavitation simulations of the *PPTC VP1304* and *The Princess Royal* propellers due to the similar diameters of the propellers, surface size of the meshes and the shaft speed of the propellers. As stated earlier, the validation and verification studies including the grid and time-step uncertainty investigations were conducted for the *INSEAN E779A* propeller in non-cavitating and cavitating conditions, and presented in Chapter 3.

For cavitation modelling, while a Volume of Fluid (VOF) model was used in describing the multiphase flow, the Schnerr-Sauer model was used as a cavitation model in STAR-CCM+ as described in Chapter 3 of this thesis as well as in the STAR-CCM+ User Guide (2018).

For cavitation simulations, including sheet and tip vortex cavitation, a sliding mesh approach was used to model the motion describing the rotation of the propeller. The method for modelling this motion was replaced with the overset mesh approach in the next chapters to be able to simulate the more complex propeller-rudder and the propeller-rudder-hull cases to eliminate the data transfer problem on the interface surfaces between the rotating and stationary domains.

The same flow domain and boundary conditions used in Chapter 4 for the non-cavitating simulations were also used for the cavitation simulations presented in this chapter.

The propeller performance coefficients for the cavitation simulations were calculated by using the converged thrust and torque values corresponded to at least four revolutions of the propeller.

The simulations for the *INSEAN E779A* propeller was conducted for three different cavitating conditions for which the EFD data was available in the open literature regarding the propeller performance characteristics and cavitation images as reported (Pereira et al. 2004, Salvatore et al. 2009). Table 5-4 includes the details of three cavitating conditions, which are described as Case 1, Case 2 and Case 3, and simulated in STAR-CCM+ to predict this propeller's performance in cavitating conditions. These conditions were simulated initially without any advanced mesh refinement approaches, and hence for the sheet cavitation only. Following this Case 2, which had the strongest cavitation dynamics, was further simulated by applying the advanced mesh refinement approaches such as the volumetric control and MARCS described earlier.

Table 5-4 The *INSEAN E779A* Propeller Cavitation Conditions

Cavitation Test Conditions	**J [-]**	**σ_n [-]**	**n [1/s]**
Case 1	0.65	0.528	36.00
Case 2	0.71	1.763	36.00
Case 3	0.77	2.082	36.00

Following the *INSEAN* propeller simulations, the advanced meshing approaches were applied for the *PPTC VP1304* and *The Princess Royal* test case propellers for the conditions listed in Table 5-5 and Table 5-6 respectively.

Table 5-5 The *PPTC VP1304* Propeller Cavitation Conditions from SMP'11 and SMP'15 Workshops

Cavitation Test Conditions	**Shaft Angle**	**J [-]**	**σ_n [-]**	**n [1/s]**
Case 2.3.1	Axial Shaft (0 deg)	1.019	2.024	24.987
Case 2.3.2		1.269	1.424	24.986
Case 2.3.3		1.408	2.000	25.014
Case 2.1	Inclined Shaft (12 deg)	1.019	2.024	20.000
Case 2.2		1.269	1.424	20.000
Case 2.3		1.408	2.000	20.000

Table 5-6 The *Princess Royal* Propeller Cavitation Conditions

Cavitation Test Conditions		**J**	**σ_n [-]**	**σ_V [-]**	**n [1/s]**
J Equivalent	Case 1	0.4	2.22	13.93	33.3
	Case 2		1.28	8.05	33.3
	Case 3		0.87	5.52	33.3
	Case 4	0.5	3.45	13.83	33.3
	Case 5		2.02	8.12	33.3
	Case 6		1.11	4.45	33.3
K_T Equivalent	Case 7	0.4	2.44	13.42	33.3
	Case 8		1.51	8.09	33.3
	Case 9		1.03	5.52	33.3
	Case 10	0.5	3.79	13.96	33.3
	Case 11		2.19	8.00	33.3
	Case 12		1.26	4.53	33.3

As shown in Table 5-5, six-test conditions, in terms of varying advance coefficients and cavitation numbers, were analysed for the *PPTC VP1304* propeller for the level (axial) and inclined shaft configurations. The test conditions and other related details were obtained from the workshop reports presented to SMP'11 and SMP'15.

Table 5-5 also shows the cavitation conditions tested at the SVA Postdam Model Basin, which was the home of this data, as also presented in these workshops.

Finally, *The Princess Royal* propeller was simulated in various cavitating conditions shown in Table 5-6 by following cavitation tunnel tests conducted at the SJTU cavitation tunnel in Shanghai which was presented at Chapter 3.

As listed in Table 5-6, the cavitation test matrix followed that of Tani et al. (2017a). Twelve different conditions were defined at two different advance ratios (J = 0.4 & 0.5) and three different cavitation number values (σ_V = 13.9, 8.1 and 4.5-5.5), and corresponding conditions of J and K_T similarities (six for each). Cavitation tests were carried out at the highest revolution speed achievable and changing the inflow speed of the water in the cavitation tunnel.

Simultaneously, the sheet cavitation simulations were conducted for each condition, while tip vortex cavitation simulations were run for Case 1, 2 and 3 of *The Princess Royal* Propeller.

5.5 Results and Discussion

5.5.1 *INSEAN E779A* Propeller

Three different cavitating conditions for the sheet cavitation simulations were conducted for the *INSEAN E779A* propeller with various J and σ values shown in Table 5-4. The results of these simulations showed good agreement with the experiments for the propeller performance coefficients and sheet cavitation patterns on the blade surface as shown in Figure 5-10. However, tip vortex cavitation could not be simulated.

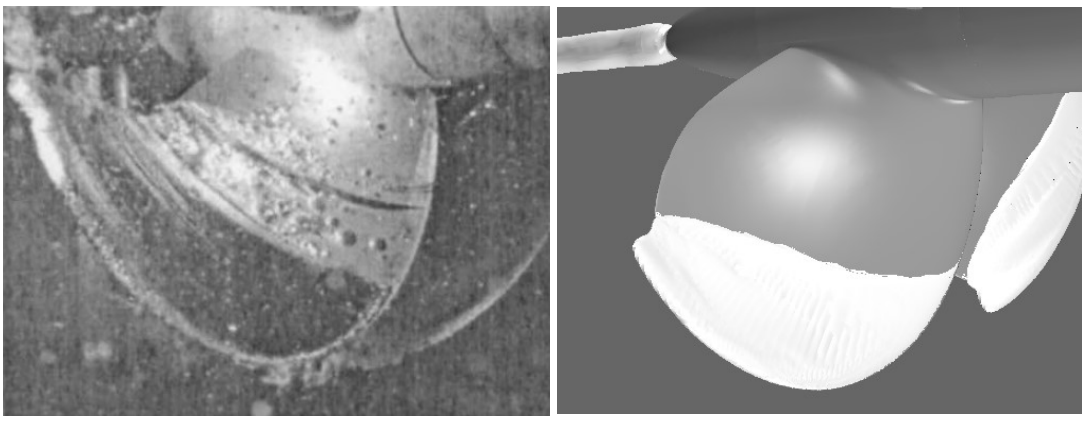

C1; J=0.65, σ_n=0.528

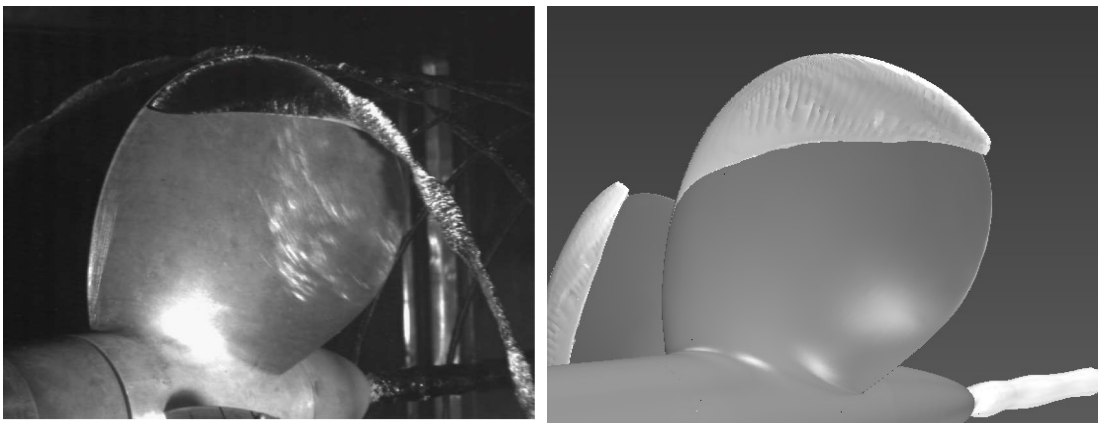

C2; J=0.71, σ_n=1.763

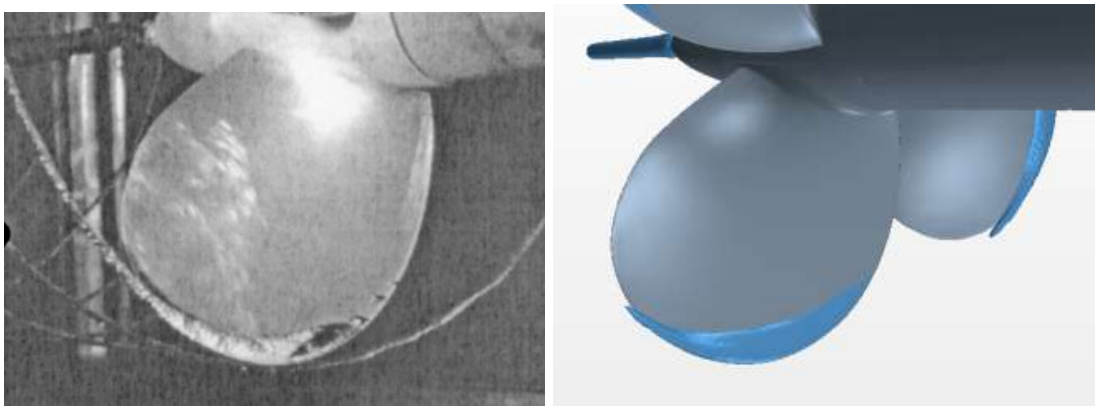

C3; J=0.77, σ_n=2.082

Figure 5-10 The *INSEAN E779A:* Comparisons cavitation pattern simulations as obtained from CFD (no tip vortex refinement) and EFD (Left; EFD, Right; CFD)

In order to fully simulate the known (EFD) cavitation phenomena, i.e. including tip vortex cavitation in the propeller slipstream, a different and advanced mesh refinement method was developed, as described earlier in this chapter. The preliminary version of this advanced method, which used a tube geometry for capturing particularly tip vortex cavitation in a propeller slipstream, achieved reasonable success in simulating the limited extension of the tip vortex cavitation for this propeller, as described in Section 5.3.1.1 and also reported in (Yilmaz et al. 2017). Although the method is based on the mesh refinement of a spiral geometry in tracking the tip vortex, this itself was not sufficient to extend the cavitating tip vortex trajectory further into the slipstream to match EFD results. Hence the method was further developed by using computed pressure distributions along the slipstream to track the tip vortex cavitation, and applied a newly refined mesh adaption approach (MARCS) as described in detail at Section 5.3.1.2, also reported in (Yilmaz et al., 2019). This enhanced method helped to extend the tip vortex cavitation until the interface between the rotating and stationary domains in the slipstream. Figure 5-11 shows the stage improvements in simulating the tip vortex cavitation extension during this study, thus demonstrating the effectiveness of the MARCS approach for tip vortex cavitation simulations.

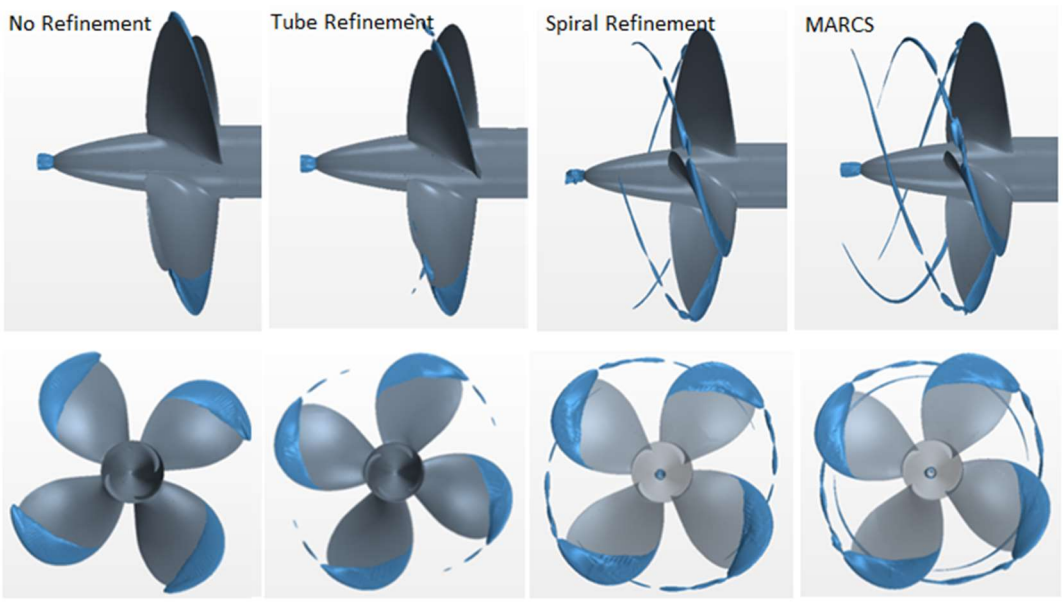

Figure 5-11 The *INSEAN E779A:* Stages in the improvement of modelling tip vortex cavitation extent

Table 5-7 presents the comparison between results without refinement, with tube, spiral geometry, mesh adaption refinement (MARCS) and experimental (EFD) results. The deviation between EFD and CFD results is approximately 3-4% for thrust and torque coefficients, respectively, using the MARCS refinement approach. Furthermore, the new mesh adaption method shows better results for predicting tip vortex cavitation extent compared to the other mesh refinement approaches and the calculated thrust and torque coefficients are closer to the EFD results.

Table 5-7 The *INSEAN E779A:* Comparison between CFD and EFD results for different mesh refinement approaches

Performance Coefficient					**Difference (CFD & EFD)**		
	J	**K_T**	**$10K_Q$**	**$\%\eta_0$**	**K_T**	**$10K_Q$**	**η_0**
Sheet (No Refinement)	0.71	0.230	0.435	0.601	-10%	-6%	-4%
Tip (Tube)	0.71	0.234	0.436	0.607	-8%	-5%	-3%
Tip (Spiral)	0.71	0.244	0.439	0.627	-4%	-4%	0%
Tip (MARCS)	0.71	0.246	0.443	0.629	-3%	-4%	1%
EFD Results	0.71	0.255	0.429	0.626	-	-	-

Figure 5-12 demonstrates the details of the sheet and the tip vortex cavitation using MARCS, thus presenting the effectiveness of this approach for tip vortex cavitation simulations.

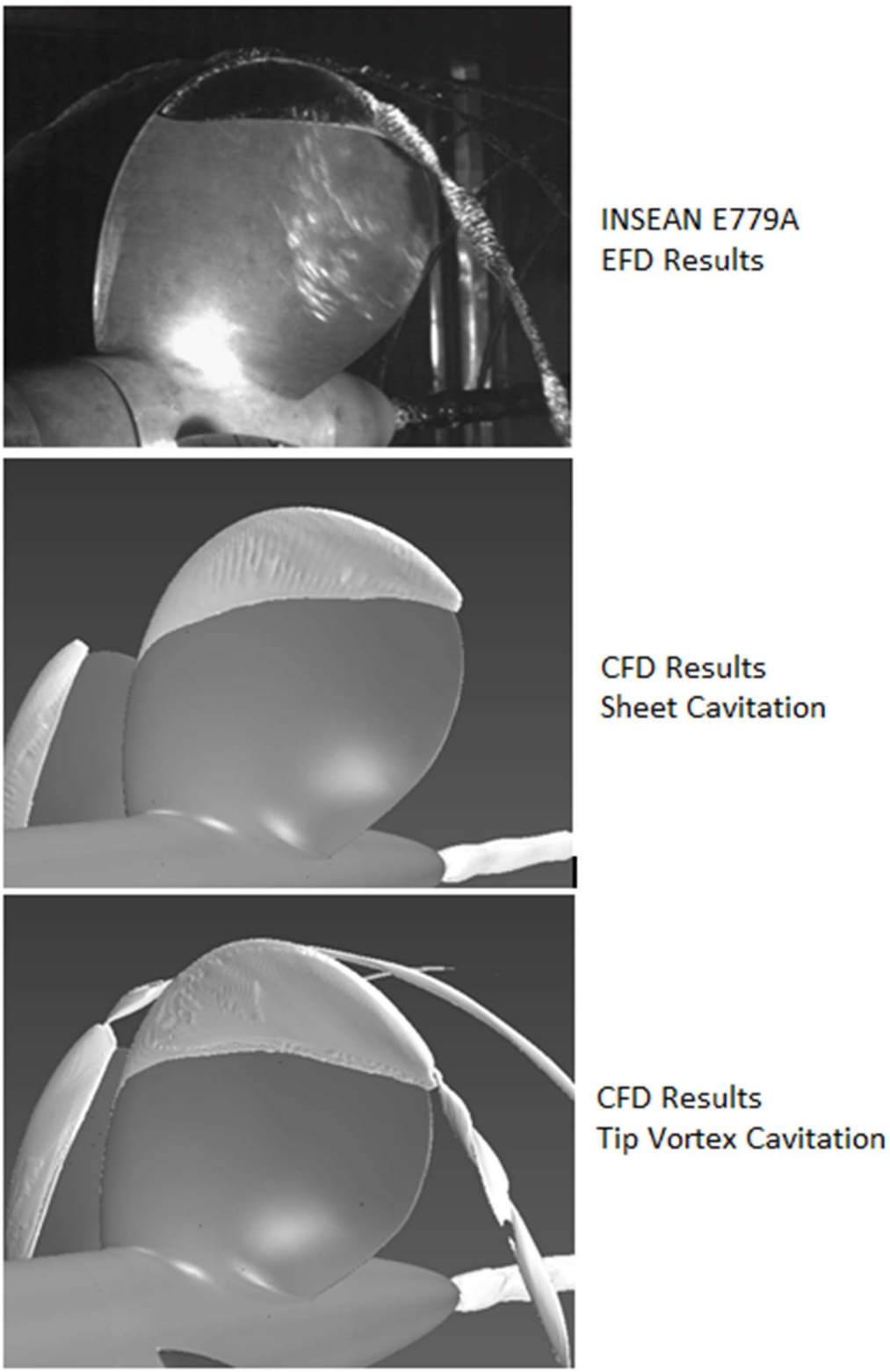

Figure 5-12 The *INSEAN E779A:* Comparisons between EFD and CFD results regarding tip vortex cavitation

Finally, Figure 5-13 shows enlarged comparative images of the cavitating tip vortices, which also include the complex roll-up phenomena in nodes. The EFD picture (on the left of Figure 5-13), illustrates the interaction between the sheet and tip vortex cavitation, which is due to a decrease of the vortex strength or increase of the pressure, causing roll-up "nodes" close to the blade trailing edge. These have become cylindrical in shape after translating one pitch downstream of the propeller plane (Kuiper, 1981). The CFD simulation image (on the right of Figure 5-13) shows that the phenomenon has been well captured by MARCS for the tip vortex although the interaction between the sheet and tip vortex cavitation is still not modelled since each cavitation type was not modelled separately.

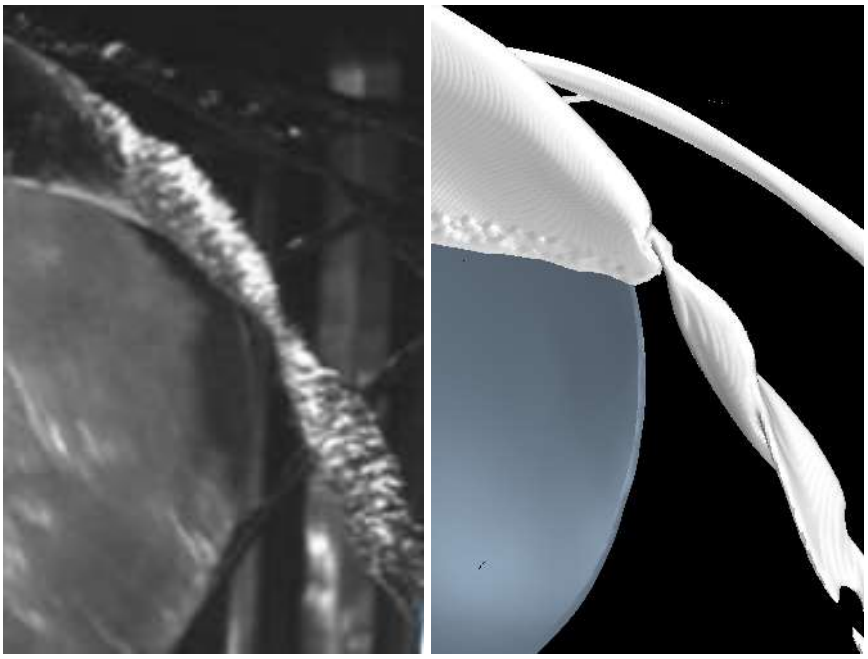

Figure 5-13 The *INSEAN E779A*: Comparison of Results Tip Vortex Cavitation Roll-up (Left; EFD, Right; CFD, MARCS)

5.5.2 *PPTC VP1304* Propeller

5.5.2.1 The *PPTC VP1304* Propeller with Axial Shaft Case

The *PPTC VP1304* propeller with the axial shaft (i.e. with zero shaft inclination) case was simulated at three different cavitating conditions as shown in Table 5-5. These simulation results were compared with the experimental data (EFD) (Potsdam

Evaluation Reports Case 2, 2015). The results showed good agreement not only for the propeller performance coefficients and but also for the sheet cavitation patterns on the propeller blades. Table 5-8 compares the thrust coefficient of the *PPTC VP1304* propeller at the various cavitation tunnel conditions predicted by the CFD using MARCS and compared with the results of EFD. The difference between the CFD and EFD were also included in the same table with a maximum of 4% for the different cavitation conditions.

Table 5-8 The *PPTC VP1304*: Thrust Coefficient Comparison between EFD &CFD

	CFD (MARCS)	**EFD**	**Difference (CFD & EFD)**
Test Condition	**K_T**	**K_T**	**%K_T**
Test Case 2.3.1	0.3890	0.3725	4.4
Test Case 2.3.2	0.2066	0.2064	0.1
Test Case 2.3.3	0.1402	0.1362	2.9

Although the sheet cavitation extent was predicted accurately, tip vortex cavitation was not simulated adequately without advanced mesh refinement around the propeller tip region and in the propeller slipstream. The MARCS approach was also necessarily applied for this propeller to be able to capture the sudden pressure drop and the cavitating bubbles in the propeller slipstream.

Table 5-9 shows the thrust coefficient differences between the different mesh applications for one of the conditions. Using the MARCS approach proved to produce the most accurate thrust coefficient as well as the tip vortex extent. While the deviation between the EFD and CFD results is approximately 5% for the sheet cavitation analyses, the difference decreased to about 4% using the MARCS methods due to accurate simulation of the tip vortex cavitation (Table 5-9).

Table 5-9 The *PPTC VP1304*: Thrust Coefficient Comparison for mesh refinement methods

Prediction Methods		**Performance Coefficient**	**Deviation**
		K_T	**%K_T**
Test Case 2.3.1	CFD - Sheet	0.3921	5.3
	CFD - MARCS	0.3890	4.4
	EFD Results	0.3725	-

Figure 5-14, Figure 5-15 and Figure 5-16 presents the cavitation pattern comparisons between the EFD and CFD results for sheet cavitation simulations without mesh refinement for Cases 2.3.1, 2.3.2 and 2.3.3 respectively which are described in Table 5-5.

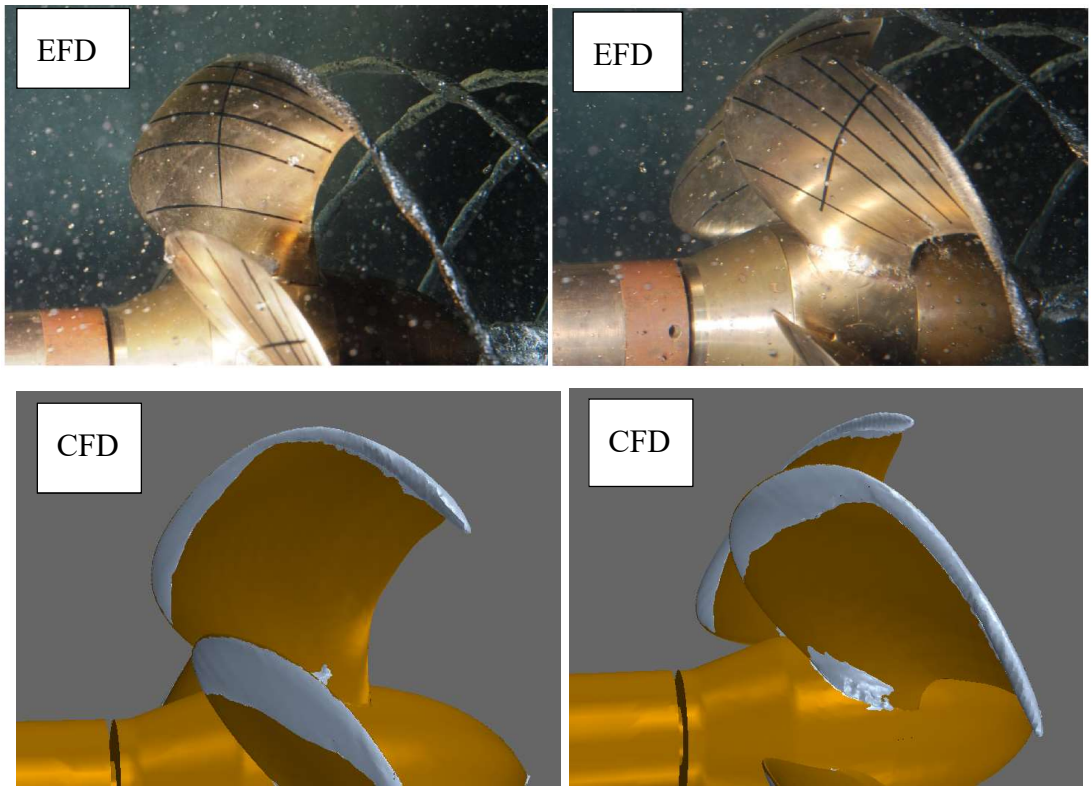

Figure 5-14 The *PPTC VP1304*: Cavitation Case 2.3.1 – Sheet Cavitation simulations
(No mesh refinement)

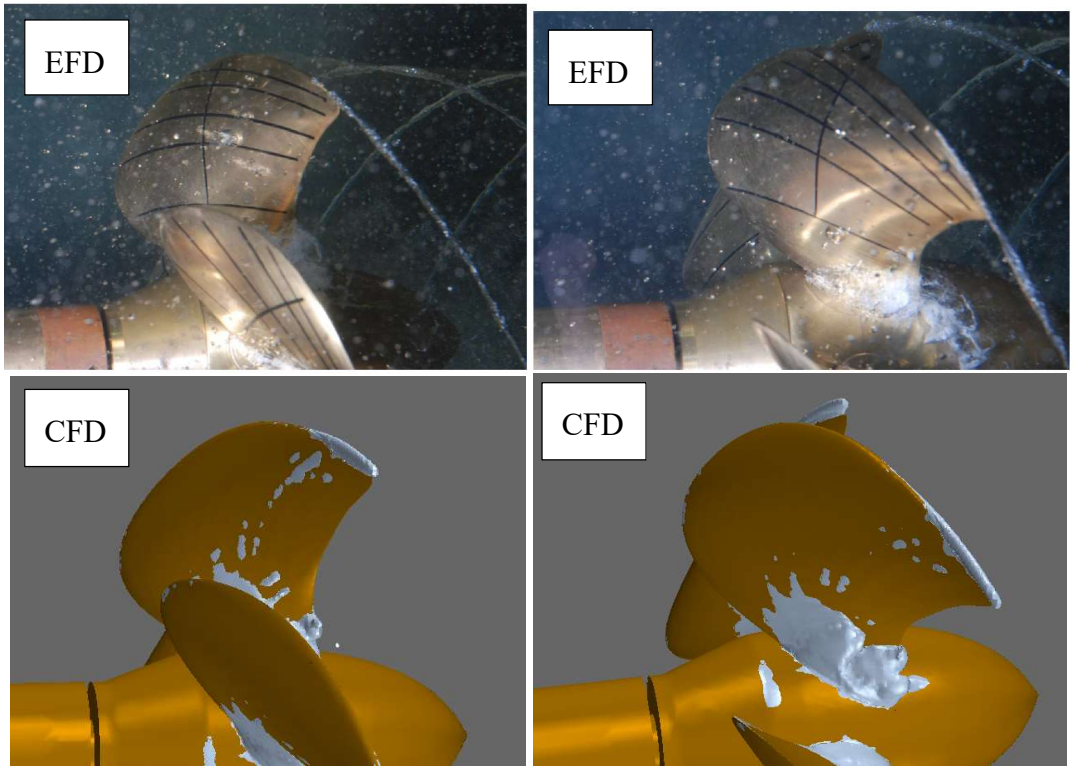

Figure 5-15 The *PPTC VP1304*: Cavitation Case 2.3.2 – Sheet Cavitation simulations

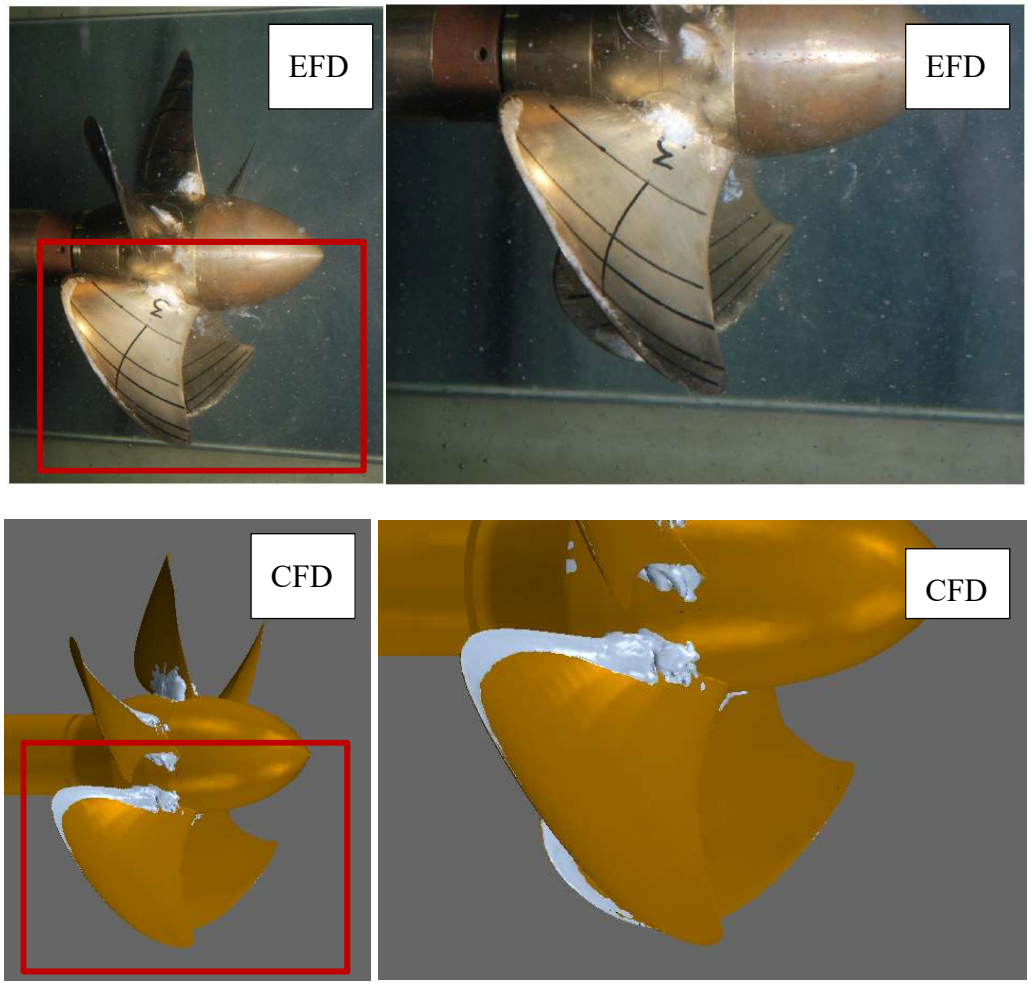

Figure 5-16 The *PPTC VP1304*: Cavitation Case 2.3.3 –Sheet Cavitation simulations

When the EFD images for Test Condition 2.3.1 and 2.3.2 were examined, it was observed that the tip vortex cavitation begins behind the propeller blade tip region. The beginning and end of the tip vortex cavitation are characterised by intermittent tip vortex cavitation. The beginning of the tip vortex cavitation on the propeller blade was defined as the point where the cavitating tip vortex appears about 5% of the observation time.

When the images from the CFD simulations were compared with the EFD images, as shown in Figure 5-14, Figure 5-15 and Figure 5-16, the CFD sheet cavitation patterns show good agreement with the experimental data especially for the propeller tip regions. Leading edge cavitation was simulated for Case 2.3.1 and tip cavitation (without tip vortex cavitation extension) was simulated for Case 2.3.2. For the same cavitating condition, the cloud and bubble type of the cavitation was simulated

successfully around the roots of the blades, while for the last cavitating case (Case 2.3.3), the sheet cavitation patterns appear throughout the leading edge of the blade, but on the pressure side instead of the suction side of the blades. The cloud cavitation around the blade roots regions has also been observed for both sides of the blades.

Figure 5-17 also presents the cavitation patterns on the blade surfaces for three different cavitating conditions. Although the cavitation on blade surfaces could be simulated including the prediction of the propeller performance successfully, tip vortex cavitation could not be simulated as appears in the experimental images. Besides the failure of the simulating tip vortex and the lack of the observation, propeller performance can only be calculated without the effect of the tip vortex cavitation extension in the propeller slipstream.

After the evaluation of the results from the sheet cavitation simulations, it was concluded that the additional mesh refinement approach was required for simulating tip vortex cavitation extension. Thus, MARCS approach was developed and applied to the same propeller with the axial shaft case. This approach was applied only for Case 2.3.1 which had the strongest tip vortex cavitation dynamics amongst the all cavitation conditions.

Figure 5-18 and Figure 5-19 presents the cavitation patterns including tip vortex cavitation extension in the downstream of the propeller for Case 2.3.1. While the results from the CFD simulations were compared with the experiments, it was observed that not only the sheet cavitation on the blade surfaces but also the tip vortex cavitation could be simulated as it was observed in the experimental images.

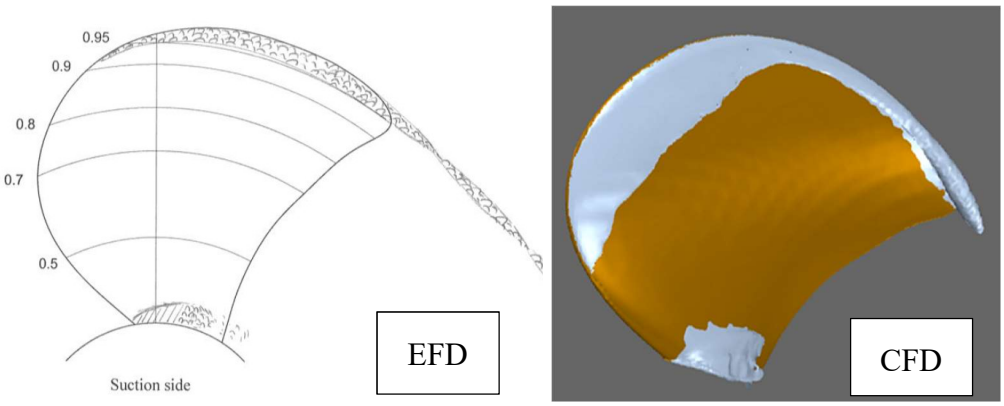

Case 2.3.1; J=1.019, σ_n=2.024

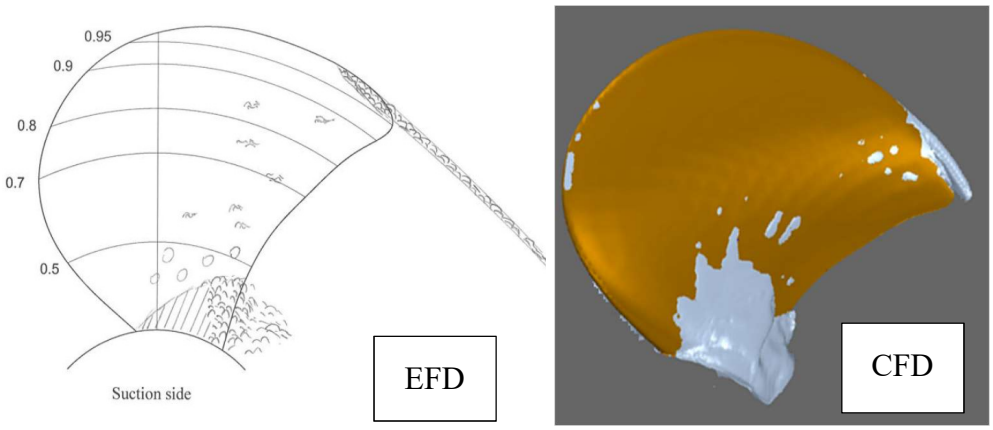

Case 2.3.2; J=1.269, σ_n=1.424

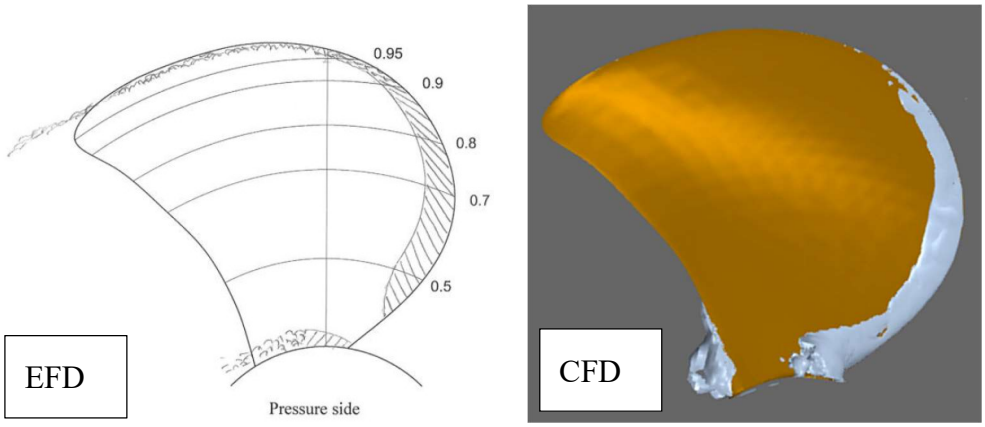

Case 2.3.3; J=1.408, σ_n=2.000

Figure 5-17 The *PPTC VP1304* with Axial Shaft; Comparisons of cavitation patterns

Figure 5-18 compares the EFD and CFD results for cavitation patterns, including the tip vortex cavity extent. It can be observed that the tip vortex and hub vortex cavitation can be both extended successfully in the propeller's slipstream with the MARCS application.

Figure 5-19 shows the detailed images the cavitating tip vortices by zooming into the blade tip and hence showing the complex roll-up phenomena in CFD and EFD simulations. These comparative images show that these complex phenomena can be well simulated in CFD with the aid of MARCS approach.

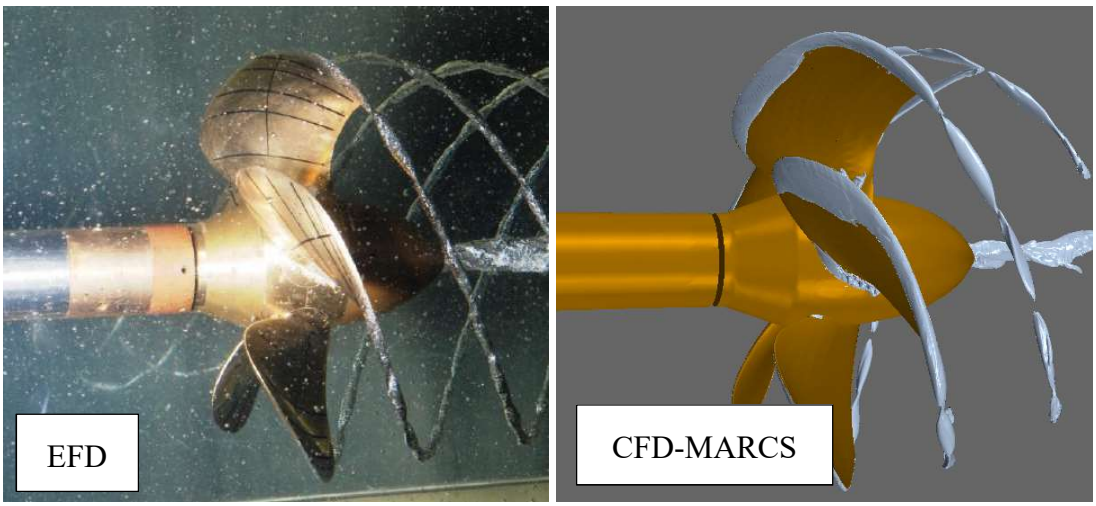

Figure 5-18 The *PPTC VP1304* with Axial Shaft: Cavitation Case 2.3.1 - Comparisons of tip vortex cavitation

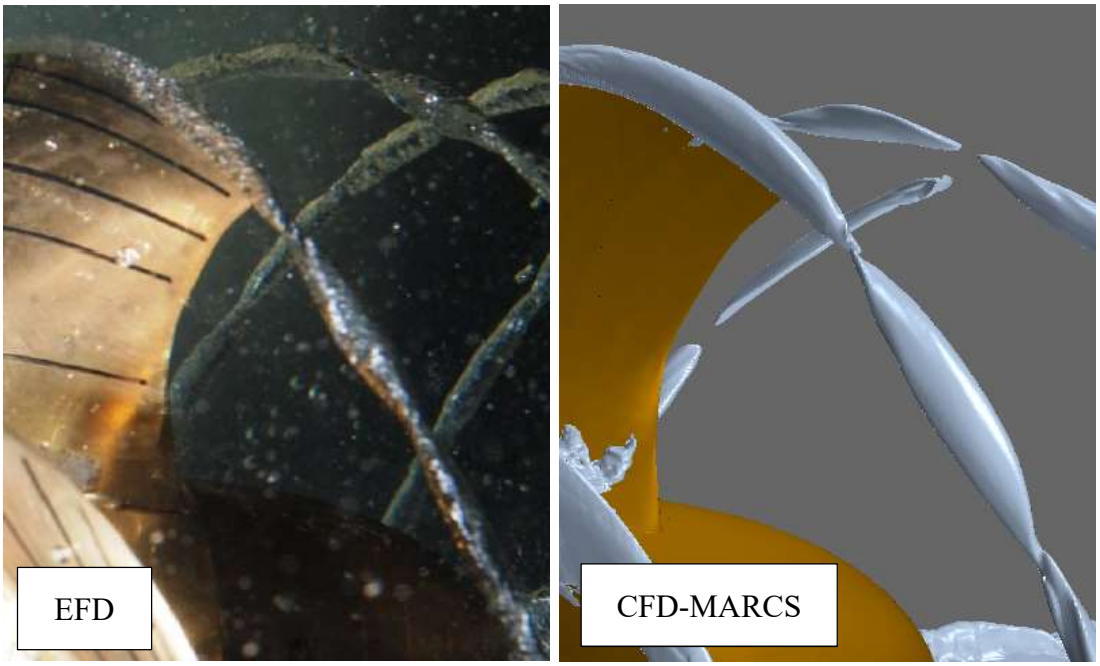

Figure 5-19 The *PPTC VP1304* with Axial Shaft: Comparison of Tip Vortex Cavitation Roll-up Results

Finally, Figure 5-20 presents the progression of the cavitation simulations from sheet cavitation to tip vortex cavitation using the MARCS approach which helps to extend the tip vortex cavitation until the interface between the rotating and stationary domains in the slipstream and thus demonstrates the effectiveness of the new approach for tip vortex cavitation simulations.

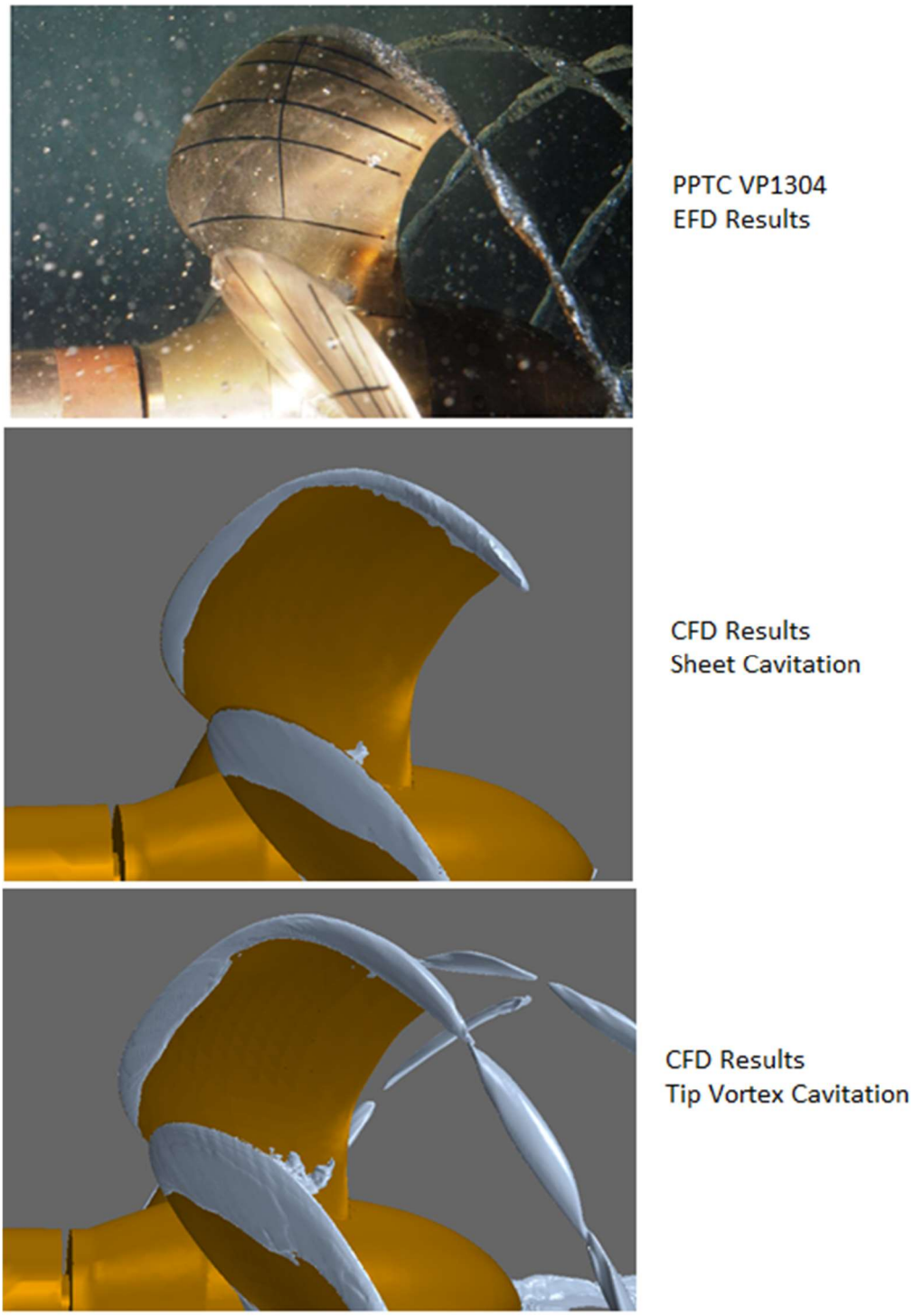

Figure 5-20 The *PPTC VP130 with* Axial Shaft: Comparison of Results Sheet and Tip Vortex Cavitation (MARCS)

5.5.2.2 The *PPTC VP1304* Propeller with Inclined Shaft Case

After the success of the first workshop at SMP'11, where the *PPTC VP1304* propeller tests were reported for an axial shaft in homogenous flow conditions, new test cases were generated for the following workshop in SMP'15, with 12^{o} shaft inclination thus producing inhomogeneous inflow conditions.

The test matrix, as given in Table 5-5, was prepared using the same cavitating conditions (same J and σ) at both workshops. The only difference between the two sets of workshop results was being the shaft inclination, hence non-uniformity of the flow.

Within the scope of this research study, the *PPTC VP1304* propeller was also modelled for the same inclined shaft configurations in order to compare the results of the CFD simulations with the EFD results reported in SMP'15 to evaluate the effect of the shaft inclination. This is a critical topic for investigation within this thesis, because *The Princess Royal* propeller also operates with an inclined shaft and in the more complex non-uniform flow condition due to the presence of the hull (wake). Such studies are essential validation cases for achieving accurate modelling of the propeller-rudder and propeller-rudder-hull interaction which are the aim of this research study.

Figure 5-21 presents a schematic of the local inflow velocities at the propeller plane for an inclined shaft configuration causing unsteady flow. In many cases, shaft inclination is inevitable due to the stern shape, engine configuration and motions of the vessel. It is also used as a means of increasing the clearence between the propeller tip and the hull, thus improving the propeller wake.

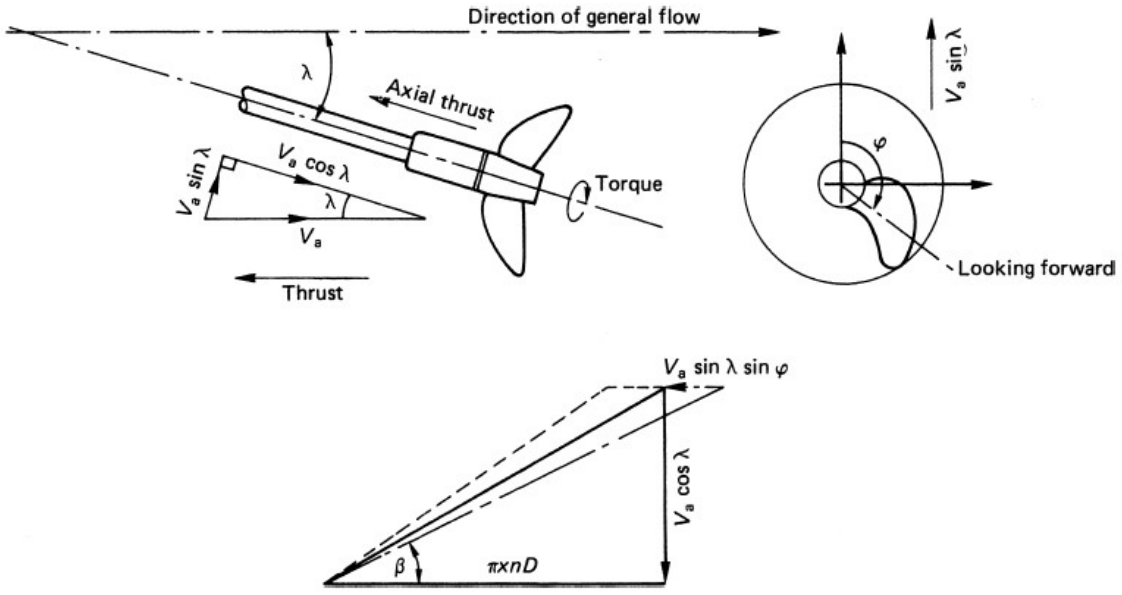

Figure 5-21 The effect of the shaft inclination on the propeller velocity diagram (Carlton, 2002)

Figure 5-22 shows the different cavitation and loading conditions corresponding to the conditions indicated by Case 2.1, 2.2 and 2.3, respectively.

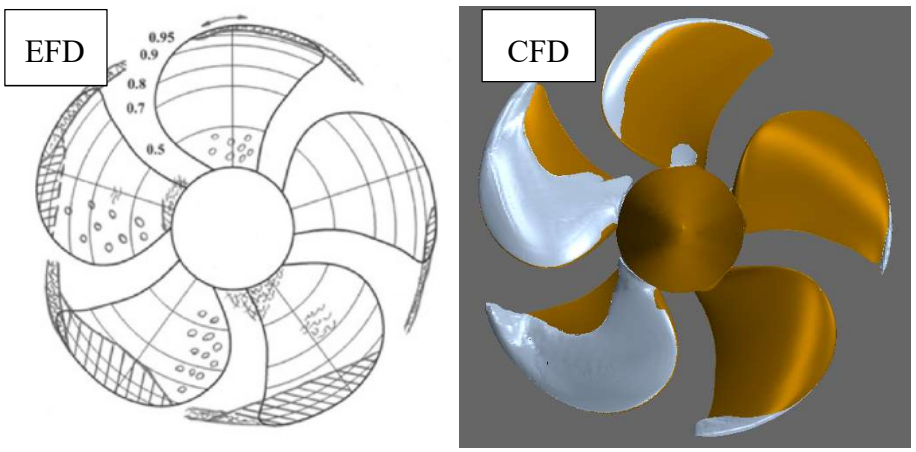

Case 2.1, J = 1.02, Suction Side

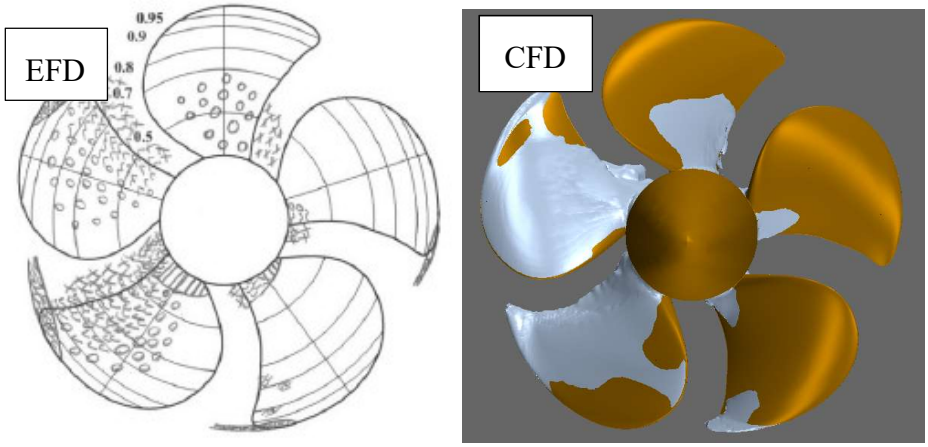

Case 2.2, J = 1.27, Suction Side

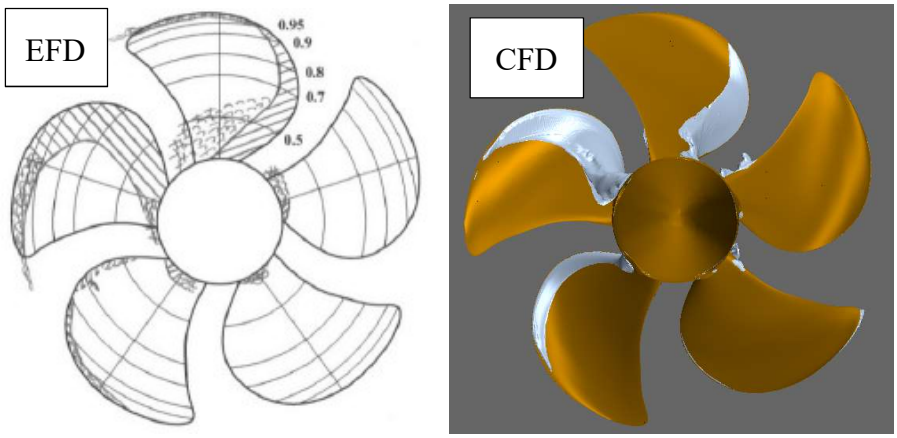

Case 2.3, J = 1.41, Pressure Side

Figure 5-22 The *PPTC VP1304* with inclined Shaft: Comparisons between EFD and sheet cavitation patterns

Figure 5-21 shows that the cross-flow component (i.e. $V_a \sin\lambda$) of the axial velocity due to the shaft inclination, changes the angles of attack (β) of the flow to the blade sections which results in changes in the cavitation behaviour and resulting noise characteristics of the propellers. This also produces a differential loading on the blades as they rotate in the propeller disc, which causes a thrust eccentricity and side force components. Due to the effect of the shaft inclination, although the propeller was at the same cavitation conditions in both workshops, the cavitation patterns on the suction and pressure surfaces of the blades were observed to be completely different as shown in Figure 5-17 and Figure 5-22 for the level shaft and inclined shaft condition, respectively.

For EFD Case 2.1, while sheet cavitation can be observed at the tip region, bubble type of cavitation appears behind the leading edge on three blades. Cloud cavitation can also be seen at the root of the blades. The cavitation pattern can be observed at the suction side of the propeller for this case.

For Case 2.2, at a higher J-value, cloud cavitation almost covers two blades with bubble cavitation on the suction side of the propeller.

For Case 2.3, the J-value is highest, the blades are least loaded creating pressure side sheet cavitation with small amounts of cloud cavitation. The pressure side cavitation occurs on the blades which are rotating in the same direction as the cross-flow velocity component. Thus producing the lowest angles of attack and suction on the “pressure” surfaces.

Additionally, different types of the cavitation cannot be simulated individually due to the limitation in the modelling of the cavitation in STAR-CCM+. Therefore, the cavitation was modelled using a number of bubbles in a control volume. As a result, e.g. individual bubble type cavitation pattern can be simulated as a continuous cavity pattern over the region where bubble cavitation is spread shown in Figure 5-23.

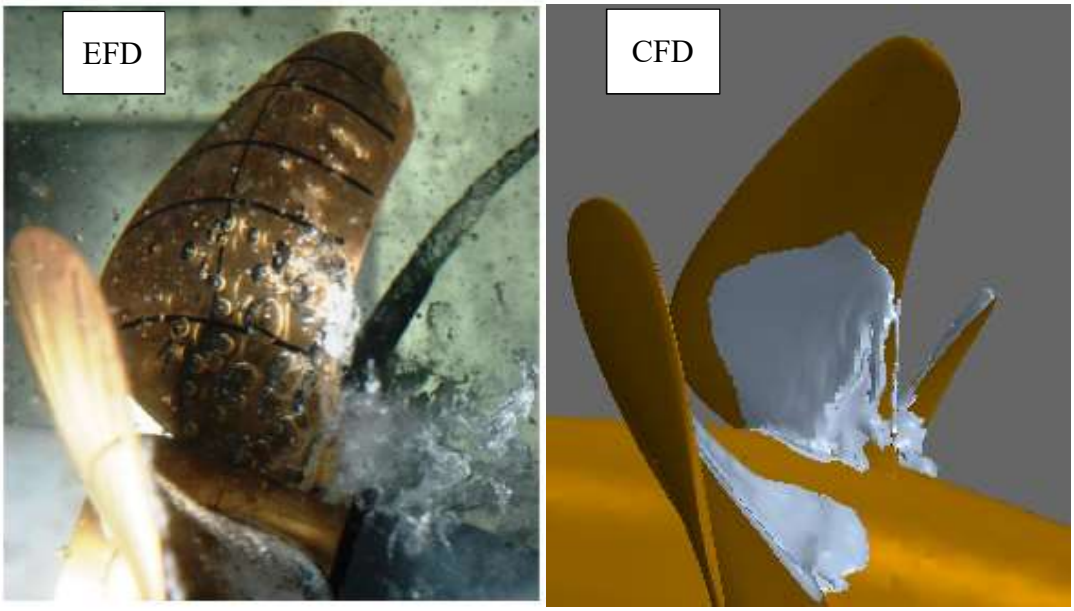

Case 2.2, J = 1.27, Suction Side (0 deg)

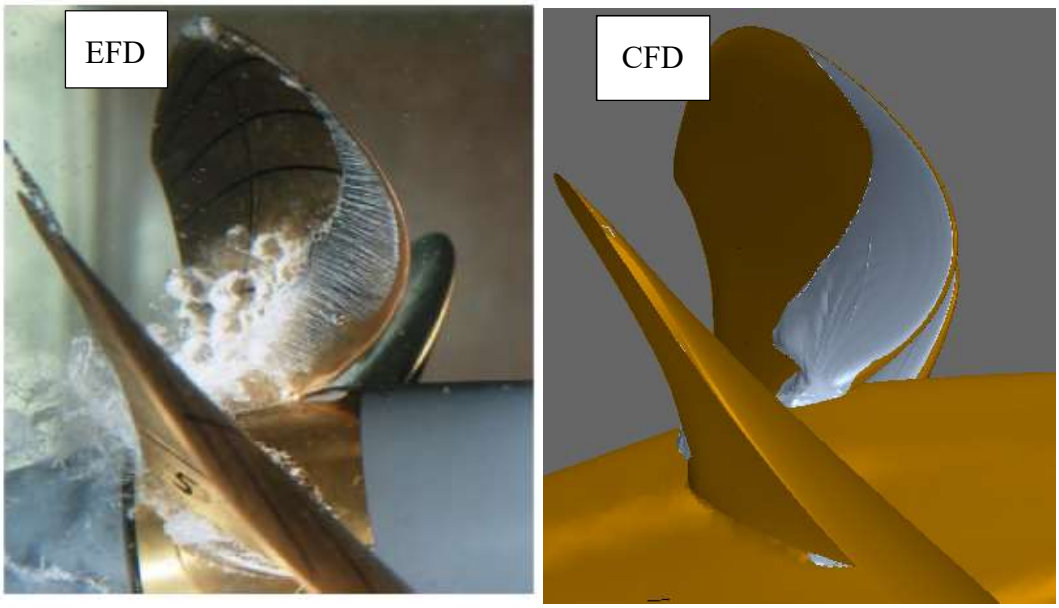

Case 2.3, J = 1.41, Pressure Side (0 deg)

Figure 5-23 *PPTC* Inclined Shaft - Comparisons between EFD and CFD results for cavitation patterns

CFD simulations for the *PPTC VP1304* propeller with inclined shaft case was conducted only for the sheet cavitation to compare with the EFD images without the application of MARCS for tip vortex cavitation simulations.

5.5.3 *The Princess Royal* Propeller

Following the evaluation of the CFD modelling of cavitation on the *INSEAN* and *PPTC* test propellers, the next was *The Princess Royal* model propeller for the conditions given in Table 5-6. As stated earlier, *The Princess Royal* propeller was tested extensively in open water condition at the cavitation tunnel of SJTU by the Author and hence comprehensive EFD data was generated.

The experimental and computational investigations with this propeller are also very important part of this research study, since this propeller and hull form has been tested in several facilities in open water, inclined flow and behind the hull and dummy hull configurations as part of the EU-FP7 Project SONIC (2012) as well as other collaborative investigations as reviewed in Chapter 2. Thus verification and validation data exist for investigations of propeller cavitation under conditions of the complex interaction between propeller, rudder and hull as will be further investigated in Chapter 6 and 7. As stated earlier, *The Princess Royal* propeller has also been recommended by the ITTC for propeller cavitation and cavitating noise investigations.

The SJTU experiments included open water performance experiments, cavitation tests, tip vortex cavitation inception and desinence tests, and the underwater radiated noise measurements. While the propeller performance results in open water and comparisons with the CFD simulation results were presented in Chapter 4, the results of the inception and desinence tests and cavitation observations are presented and discussed in the following sections. Corresponding CFD simulation results in the same cavitating conditions are also compared with the experiments in relation to hydrodynamic propeller performance and cavitation patterns including tip vortex cavitation (using the MARCS application).

Tip vortex cavitation inception and desinence tests were conducted and recorded visually as shown in Figure 5-24. The results are documented in the literature and were compared with the results from the cavitation tunnel tests at UNIGE and UNEW (Tani et al., 2017). Figure 5-25 compares the inception and desinence curves from SJTU, UNIGE and UNEW tests. This comparison shows a significant difference in terms of K_T against cavitation number. The differences can be explained by the differences in

propeller leading edge geometry, gas contents, water quality and the turbulent intensity of the cavitation tunnel flows and Reynolds number effects (Korkut, 1999). Also, the methods of recording the inception and desinence data and cavitation images differ from one institute to another (Tani et. al., 2017). Although, the cavitation images, inception and desinence data were recorded by high speed video camera in UNIGE and UNEW, the same data has been recorded with naked eye in the SJTU cavitation tunnel. It should be considered that capturing the inception and desinence with the naked eye is very difficult while small bubbles cannot be seen properly in the propeller slipstream. Therefore, inception and desinence can be determined in three different ways; the first is when cavitation bubbles attach to the propeller (surface or attached type), and the second is when cavity bubbles appear and disappear the in propeller slipstream without attaching to the propeller blades (travelling type) and the third is the appearance of the vortex either at the blade tip or just downstream (Arakeri, 1979). For this test, tip vortex cavitation inception was recorded when the cavitating bubbles are attaching to the propeller tip as it can be seen in Figure 5-24.

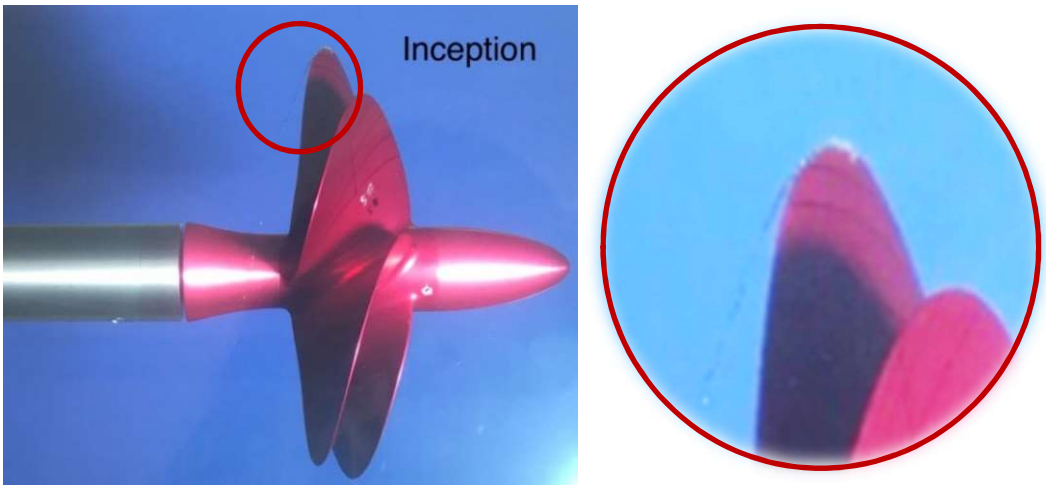

Figure 5-24 *The Princess Royal* Tip Vortex Cavitation Inception (SJTU)

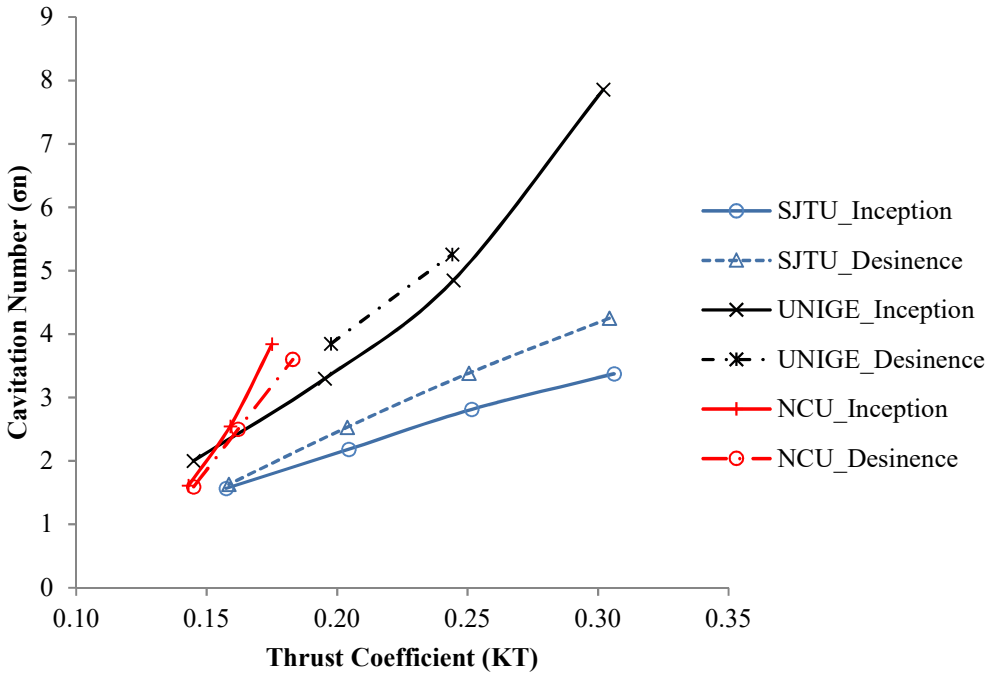

Figure 5-25 *The Princess Royal* Tip Vortex Cavitation Inception & Desinence Results (UNIGE & UNEW Results from Tani et al., 2017)

The SJTU cavitation observations were made with a still camera and stroboscopic lighting, synchronized with a shaft position signal.

During the cavitation tests, the test matrix of Tani et al. (2017) was followed. Twelve different conditions were determined at two different J (0.4 & 0.5) and three different σ_V values (13.9, 8.1 and 4.5-5.5) based on the J and K_T similarities (six for each). The observed sheet cavitation patterns on the propeller blades and the tip vortex cavitation extents showed good agreement when compared with the results from "Round Robin" participants, MARIN, SSPA, UNIGE and UNEW (Hallander, 2017, Lafeber & Lloyd, 2017 and Tani et. al, 2017), although the comparisons do not exist in this thesis.

Figure 5-26 (J=0.4) and Figure 5-27 (J=0.5) shows the EFD based cavitation images (including sheet and tip vortex) together with CFD simulations for three gradually reducing cavitation numbers. During the cavitation tests, the revolutions of the propeller was kept the same (n = 33.3 rps) and the tunnel flow velocity was changed according to the cavitation test matrix and different test conditions. At the lower J value (0.4) the EFD results, as expected, displayed more sheet and stronger tip vortex

cavitation on the propeller blades. The CFD results (without the use of MARCS) were in good agreement with the EFD for the sheet cavitation pattern.

For Condition C1 (Top, Fig 5-26), combined leading edge and sheet cavitation can be observed unless the leading edge cavitation was of a distinct vortex type. As cavitation number was reduced, the sheet cavitation became thicker and extended more chord wise (from C1 to C3). A thin, but visible tip vortex was observed in propeller's slipstream.

For condition C2 (Middle, Fig 5-26), where the cavitation number was lower, the sheet cavitation spreaded to lower radii and extended farther in the chord-wise direction. Condition C2 also displayed a stronger, more stable tip vortex, with sheet cavitation rolling up into the tip vortex which extended far downstream.

For Condition C3 (Bottom, Fig 5-26), the largest extent and thickness of the sheet cavitation was observed. Here the tip vortex cavitation and the super-cavitating sheet were shed off the blade at slightly different pitches, thus causing them to interact and produce mutual diffusion and dispersion.

Condition C4 (Top, Fig 5-27), showed the least amount of cavitation with incipient streak cavitation at about 0.95R. C4 differed from C1 in that the J-value is 0.5 and so the blade loading (K_T) is less.

The EFD cavitation patterns showed good agreement with other (HTF Round Robin) studies in various research facilities using the same propeller geometry (Hallender, 2017, Lafeber & Lloyd, 2017 and Tani et. al, 2017). Although the cavitation tests were conducted with different shaft angle conditions by the other partners of the Hydro Testing Forum (HTF), as a part of the round robin tests, only the 0^o shaft angle configuration was tested due to the limitations in the SJTU facility.

CFD investigations of the cavitation on *The Princess Royal* propeller were first applied to simulate the sheet cavitation dynamics and hydrodynamic propeller performance. Figure 5-26 and Figure 5-27 showed and compared the predicted sheet cavitation patterns obtained from CFD calculations for two different J and three different σ

values. The CFD calculations presented in these figures did not include the MARCS refinement technique.

For both J-values good agreement was achieved for sheet cavitation dynamics on the blade surfaces. At the same J level, while the cavitation number (σ) has been decreased, sheet cavity extent increases (Figure 5-26 from top to bottom) due to the nature of the cavitation phenomena presented in Chapter 2. Besides, at the same σ, sheet cavitation pattern decreases increasing J values (Figure 5-26 and Figure 5-27).

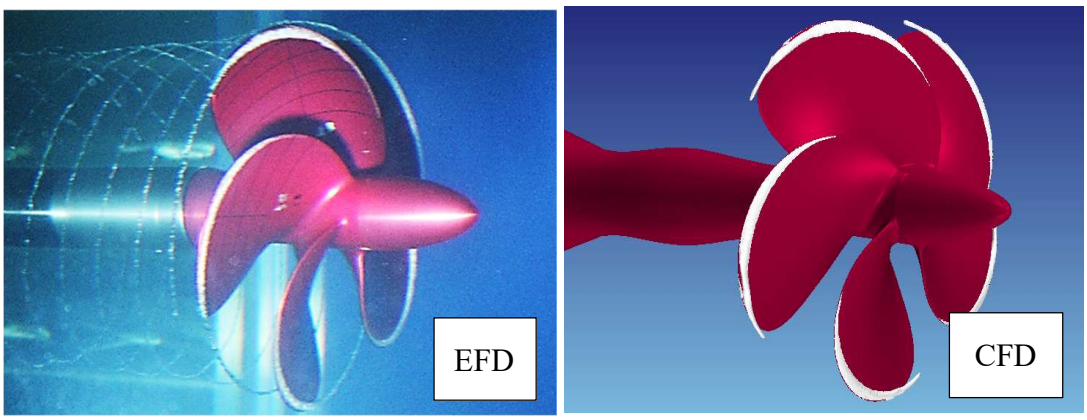

C1; J=0.4, σ_{VA}=13.93 (Left; EFD, Right; CFD)

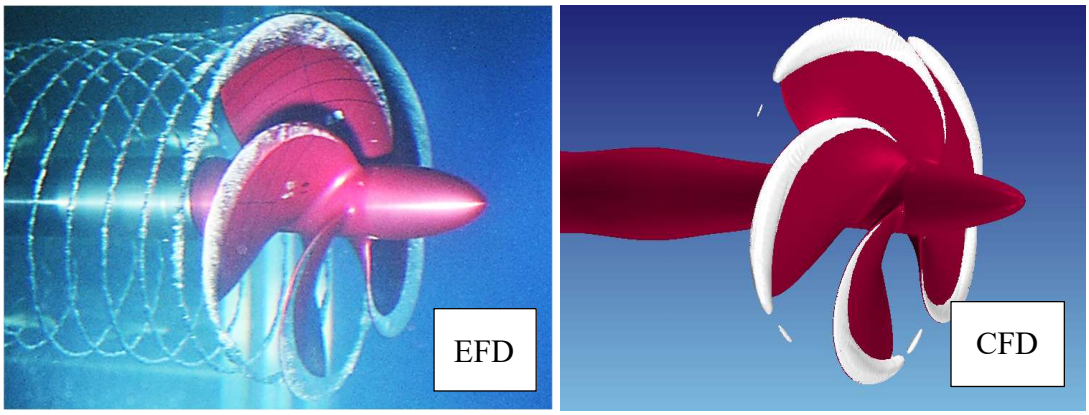

C2; J=0.4, σ_{VA}=8.05 (Left; EFD, Right; CFD)

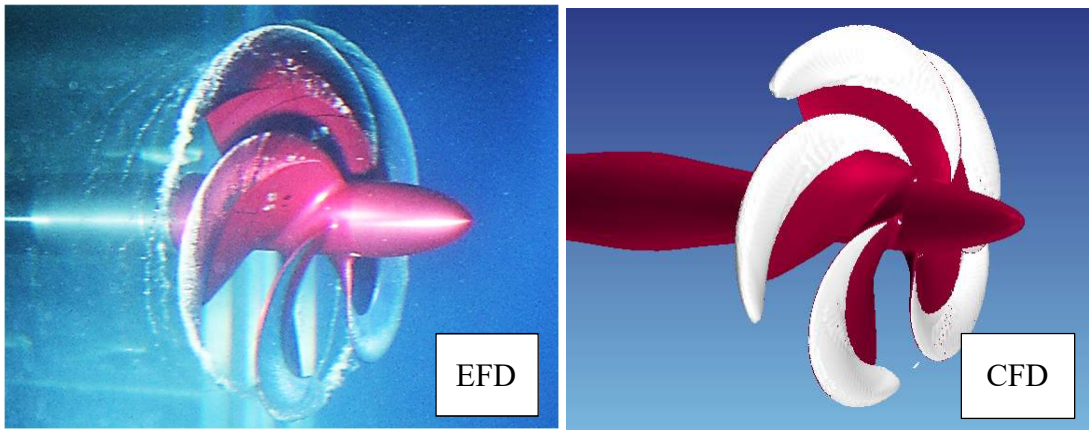

C3; J=0.4, σ_{VA}=5.52 (Left; EFD, Right; CFD)

Figure 5-26 The *Princess Royal:* Cavitation pattern Comparisons between EFD and CFD (MARCS is not used)

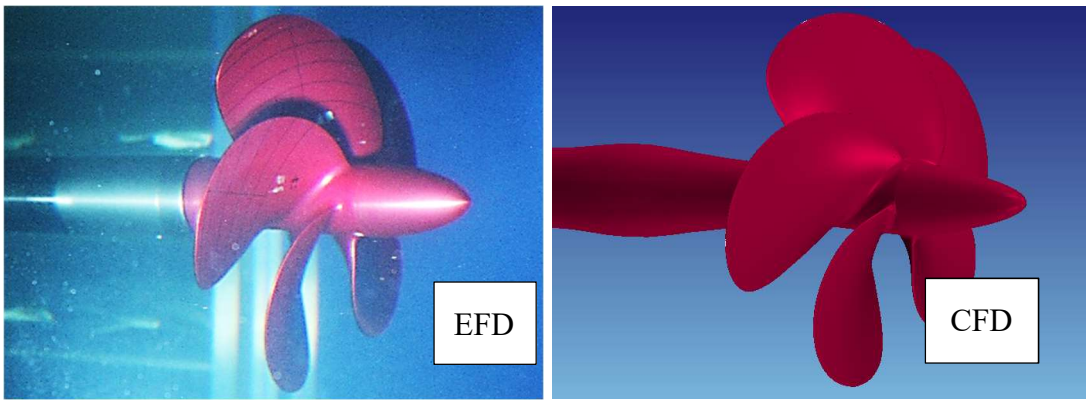

C4; J=0.5, σ_{VA}=13.83 (Left; EFD, Right; CFD)

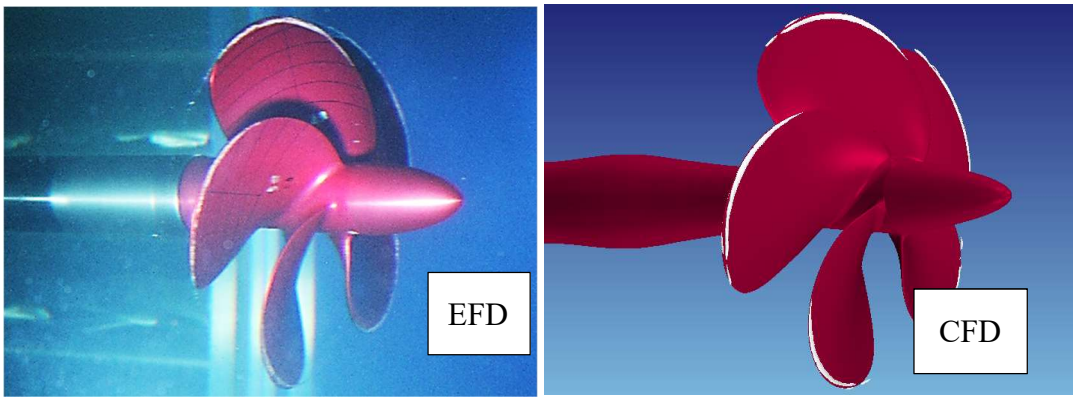

C5; J=0.5, σ_{VA}=8.13 (Left; EFD, Right; CFD)

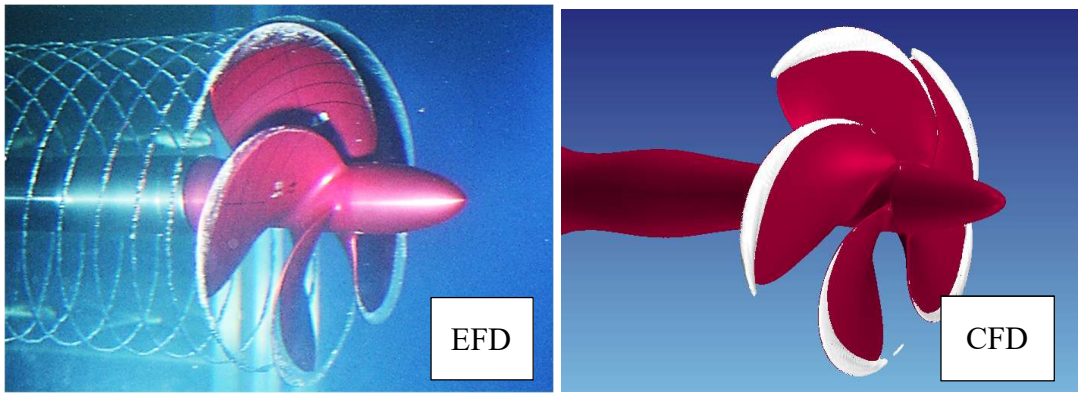

C6; J=0.5, σ_{VA}=4.45 (Left; EFD, Right; CFD)

Figure 5-27 The *Princess Royal:* Cavitation pattern Comparisons between EFD and CFD (MARCS is not used)

Following the sheet cavitation simulations, the MARCS approach was switched on in the simulations for *The Princess Royal* propeller to include tip vortex cavitations into the propeller slipstream as shown in Figure 5-28 and Figure 5-29. This mesh refinement approach was applied only for three conditions; C1, C2 and C3**,** where the tip vortex cavitation was clearly observed.

Condition 2 (EFD) (Middle, Figure 5-28) shows largest axial extent of the tip vortices due to the stronger and more stable tip vortex dynamics in the slipstream. This was captured by CFD (MARCS). The less extended tip vortices for C1 and C3 were also simulated. In Figure 5-28, the cavitation images showed that C1 produced weaker tip vortex cavitation than that in C2 (smaller diameter of the vortex core). Due to the difference of the tip vortex volume, while the refined surface size (0.22 mm) was sufficient to capture tip vortices for C2, this value was not small enough for capturing weaker cavity dynamics for C1. For C3 (Bottom, Figure 5-28), The EFD showed a disappearing tip vortex cavitation in the dispersion and eventual dissipation phenomenon with a cloudy cavitation phenomenon. Such dynamics could not be fully simulated in the CFD runs due to insufficient surface mesh size in the refinement region.

Although the tip vortex cavitation could be simulated for all these 3 conditions using the MARCS method, as opposed to the much faster sheet cavitation simulation method, the tip vortex cavitation could only be extended until the interface between rotating and stationary domain for the C2 condition and with the limited extension for C1 and C3. However, the comparisons shown in Figure 5-28 and Figure 5-29 demonstrated clearly that the MARCS methodology could capture a substantial amount of the EFD sheet and tip vortex characteristics.

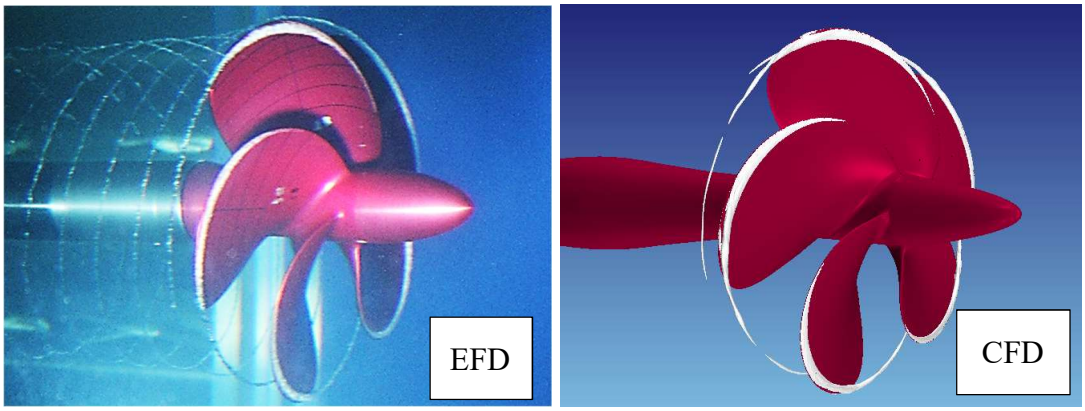

C1; J=0.4, σ_{VA}=13.93 (Left; EFD, Right; CFD)

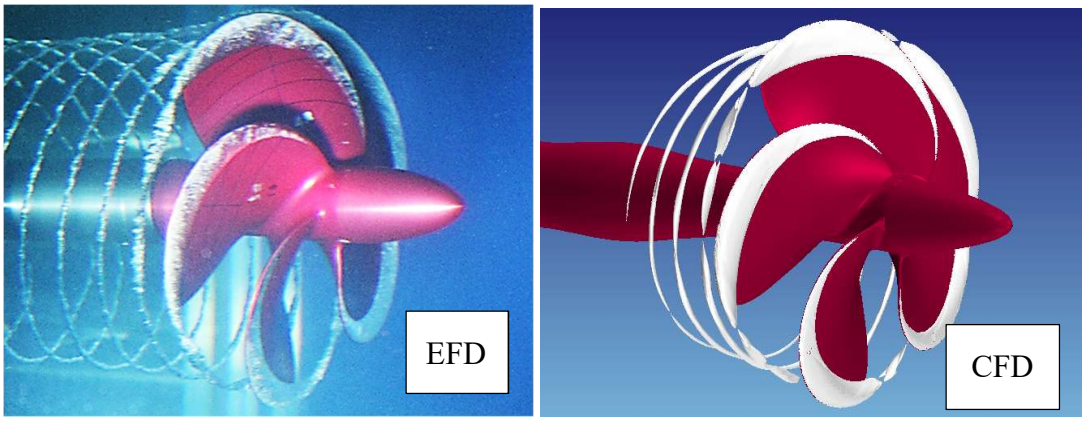

C2; J=0.4, σ_{VA}=8.05 (Left; EFD, Right; CFD)

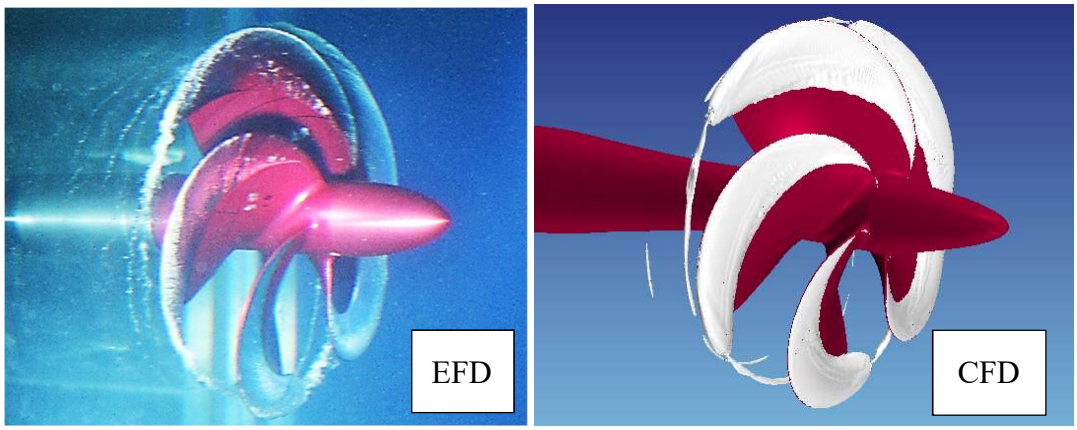

C3; J=0.4, σ_{VA}=5.52 (Left; EFD, Right; CFD)

Figure 5-28 The *Princess Royal:* Cavitation pattern Comparisons between EFD and CFD (MARCS - tip vortex cavitation)

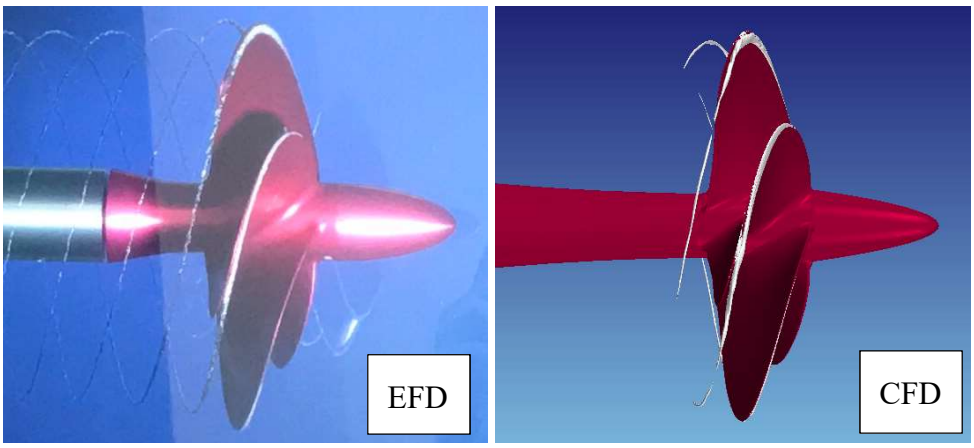

C1; J=0.4, σ_{VA}=13.93 (Left; EFD, Right; CFD)

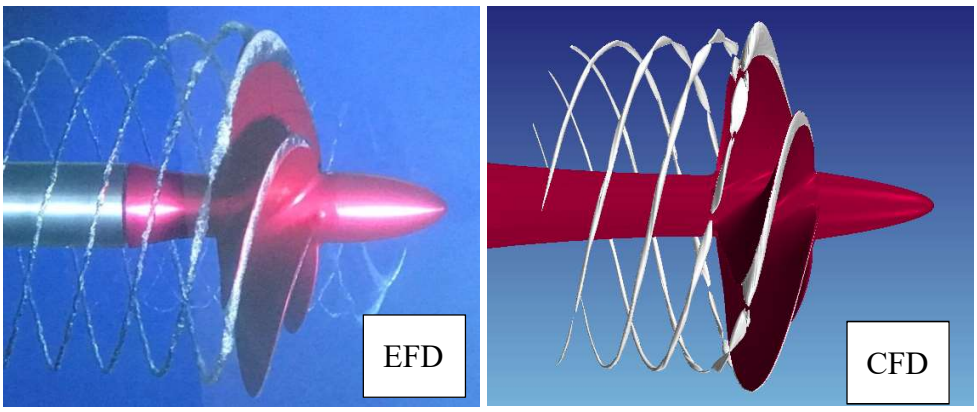

C2; J=0.4, σ_{VA}=8.05 (Left; EFD, Right; CFD)

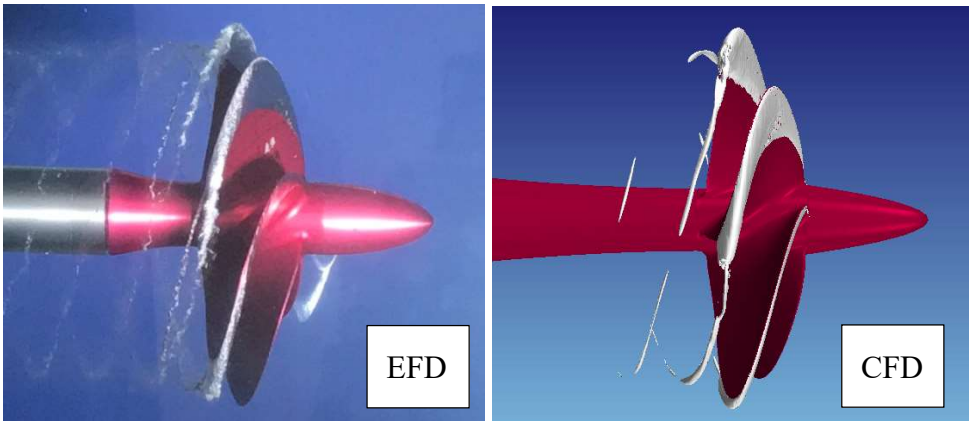

C3; J=0.4, σ_{VA}=5.52 (Left; EFD, Right; CFD)

Figure 5-29 The *Princess Royal:* Cavitation pattern Comparisons between EFD and CFD (MARCS - tip vortex cavitation)

Finally, Figure 5-30 shows cavitating propeller performance coefficients (EFD) calculated from cavitation test results and compared to those obtained from the non-cavitating open water tests. Thrust and torque values were measured during the cavitation observation tests. For the propeller rotating in the cavitation tunnel, an extra force was generated in the opposite direction to the thrust force due to the presence of the dynamometer. When the negative effect of the dynamometer on the propeller thrust was taken into account, a big difference between non-cavitating and cavitation conditions results was not expected in terms of the propeller performance characteristics, K_T, K_Q and η_0. When the results were compared between non-cavitating and cavitating conditions, K_T, K_Q and η_0 showed a difference but with the same trend without causing too much thrust breakdown that was expected (Figure 5-30).

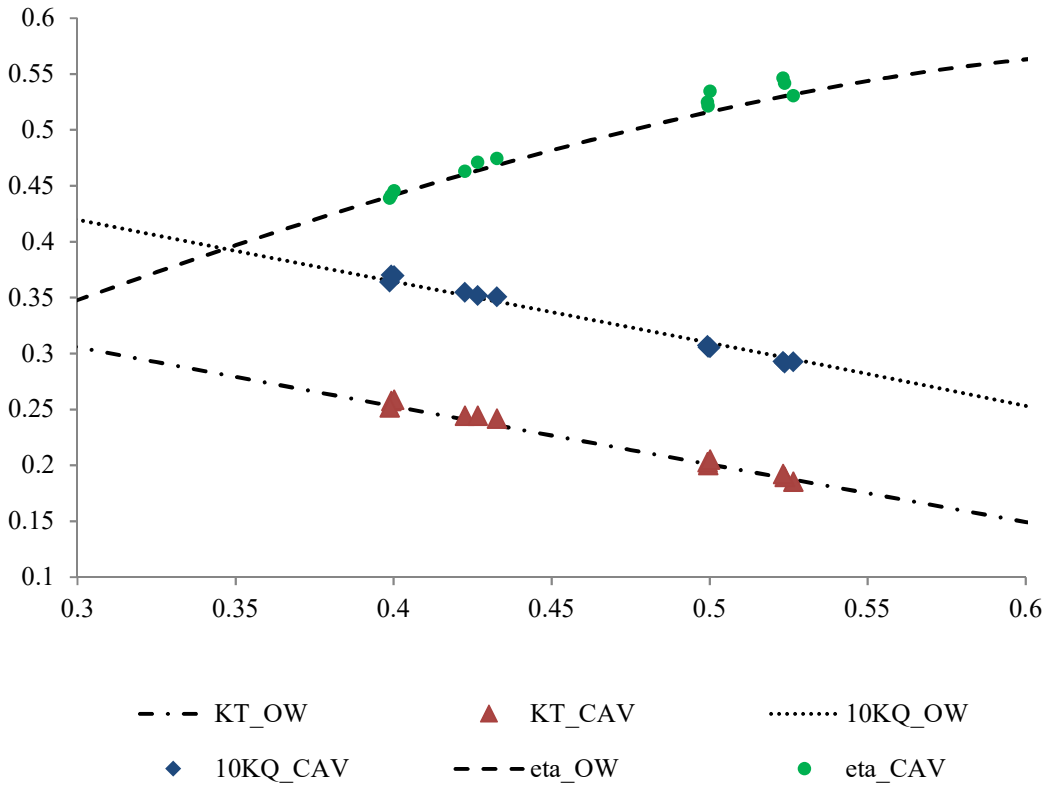

Figure 5-30 *The Princess Royal:* Comparison propeller performance coefficients (K_T, K_Q and η_0) for Open Water and Cavitation Tests

Table 5-10 compares the propeller thrust coefficients from EFD and CFD simulations including the sheet and tip vortex cavitation. From the compared values it can be concluded that while the MARCS approach could improve the tip vortex cavitation extension, it did not help to improve the propeller thrust.

Table 5-10 Thrust Coefficients (Sheet vs Tip Vortex Cavitation Simulations)

Conditions	Sheet		Tip Vortex (MARCS)	
	CFD - K_T	**Deviation between EFD-CFD %K_T**	**CFD - K_T**	**Deviation between EFD-CFD %K_T**
C1	0.2647	2.8	0.2666	3.5
C2	0.2639	1.9	0.2655	2.5
C3	0.2534	0.5	0.2440	-3.2

Table 5-11 also compares propeller performance coefficients (K_T and K_Q) between the EFD and CFD results including the tip vortex cavitation. While the comparisons showed good agreement for thrust (2.5-3.5%), torque was less predicted for these simulations with 6.0-7.6% deviation.

Table 5-11 Propeller Performance Coefficients (Tip Vortex Cavitation Simulations)

Conditions	CFD - K_T	CFD -10K_Q	Deviation between EFD-CFD %K_T	Deviation between EFD-CFD %10K_Q
C1	0.2666	0.3422	3.5	-7.6
C2	0.2655	0.3480	2.5	-6.0
C3	0.2440	0.3412	-3.2	-6.3

On the other hand, any meaningfull trend (increasing or decreasing) could not be found between cavitating conditions (J and σ) and propeller performance coefficients in using the MARCS approach for this propeller.

Figure 5-31 (from left to right) compares the extension of the tip vortex cavitation in the propeller slipstream in terms of different turbulence models; RANS, DES and LES respectively. From the compared images it can be concluded that while the most extended tip vortex cavitation extension could be obtained using LES model with MARCS approach, TVC could be predicted with less extension using DES and RANS approaches. When RANS and DES results were compared each other, it can be also concluded that DES model provides more extended TVC cavitation due to the effect of resolving the turbulent flow outside of the wall region by LES model.

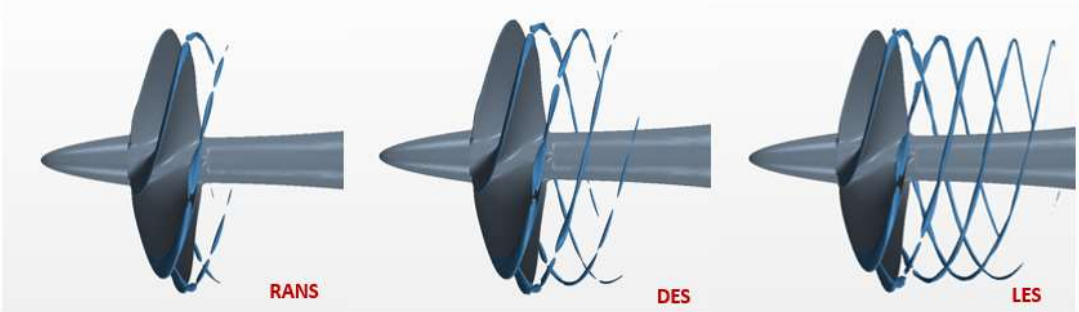

Figure 5-31 Tip Vortex Cavitation Extension Comparison in terms of Different Turbulence Models (From Left to Right; RANS, DES and LES)

Table 5-12 also compares propeller performance coefficients (K_T and K_Q) from RANS, DES and LES simulations with deviations between the EFD and CFD results including the tip vortex cavitation. While the comparisons showed very good agreement for thrust (less than 1%) and torque coefficients (less than 3%) for RANS and DES computations, torque was less predicted using LES with 6.0% deviation.

Table 5-12 Propeller Performance Comparisons in terms of Different Turbulence Models

Conditions	**CFD - K_T**	**CFD -10K_Q**	**Deviation between EFD-CFD %K_T**	**Deviation between EFD-CFD %10K_Q**
RANS	0.2587	0.3612	-0.2	-2.5
DES	0.2599	0.3638	0.3	-1.8
LES	0.2655	0.3480	2.5	-6.0

Lastly, Figure 5-32 compares RANS and LES simulation results in terms of axial velocity contour on 0.9R blade section. This figure also shows the difference between RANS and LES models in terms of flow separation on the trailing edge of the propeller blades. The deviations between RANS, DES and LES for the propeller performance predictions can be explained with the use of different turbulence models resolving the turbulent flow, especially near wall surfaces.

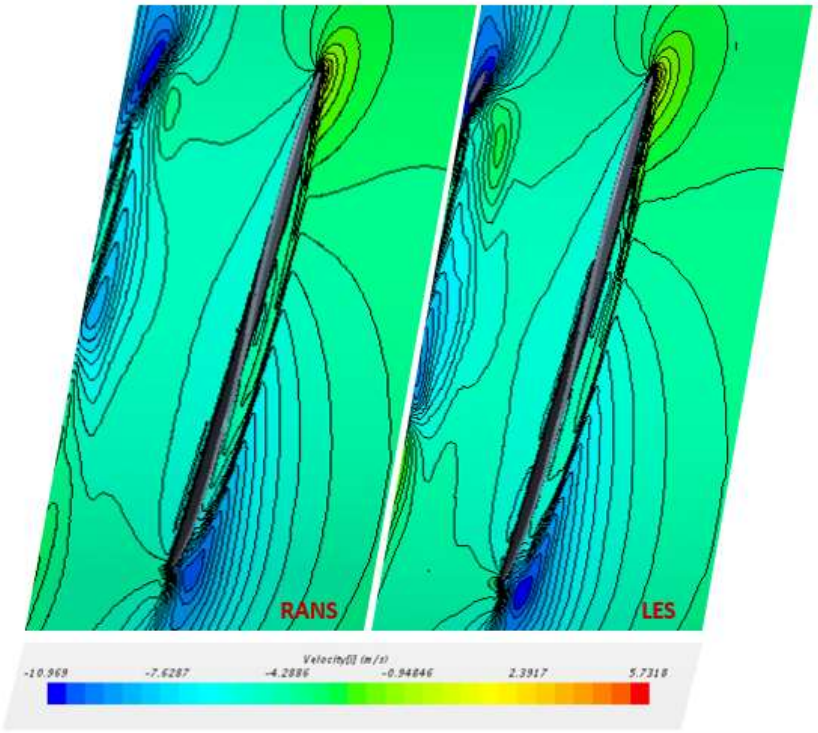

Figure 5-32 Axial Velocity Comparisons between RANS and LES (0.9R Cylindrical Section)

Nevertheless, the main purpose of the CFD modelling needs to be taken into account, while the correct turbulence model corresponding the simulations should be selected by the researchers. For this study, although LES model cannot predict propeller performance coefficients as successful as RANS and DES models, LES was still preferred due to the better modelling of the flow characteristics and the tip vortex cavitation extension in the propeller's slipstream.

5.6 Concluding Remarks

This chapter presented and compared the results from both experimental and CFD modelling research for cavitation development on three model scale propeller geometries and test configurations. A CFD model coupled with an advanced adaptive grid has been developed and applied to all of the blades of three propellers for the prediction of cavitation dynamics, including tip vortex cavitation and hydrodynamic performance coefficients, in cavitating conditions and uniform flow.

Three benchmark model propellers; the *INSEAN E779A*, the *PPTC VP1304* and *The Princess Royal* propellers and cavitating test conditions were used for the CFD investigations, since detailed experimental results (EFD) were available in open literature for these propellers concerning open water performance data and cavitation observations. Then, all the CFD variables such as number of mesh, mesh size, time step, and turbulence model were investigated for cavitation simulations on the *INSEAN E779A* propeller.

These investigations confirmed the identified a gap in the literature concerning the accurate modelling of the tip vortex cavitation and initiated further development into different mesh refinement approaches for the tip vortex cavitation in order to resolve issues of the tip vortex extent.

Two different mesh refinement approaches were developed, namely, volumetric control (tube and spiral) and mesh adaption. These were used to extend the prediction of tip vortex cavitation in the propeller slipstream and to improve the propeller hydrodynamic performance predictions. Use of the tube and spiral geometries as volumetric control regions from the propeller tip into the slipstream slightly improved tip vortex extent as well as propeller performance coefficients. However, modelling the largest tip vortex cavity extent for the *INSEAN E779A* propeller was achieved only by employing the refined mesh adaption (MARCS) approach developed by the author, in this study. MARCS also helped to model fine structures of the tip vortex cavitation, including complex roll-up phenomena and “nodes”. In spite of this success, close interaction between the sheet cavitation and tip vortex cavitation still needs to be investigated since the current model neglects this interaction.

Following the development of the MARCS approach, the same mesh refinement procedure was applied to the *PPTC VP1304* (with axial shaft) and *The Princess Royal* propellers, respectively. The MARCS approach successfully simulated the observed tip vortex cavitation extensions for all propeller cavitation cases and the validation studies were in fairly good agreement with the EFD results for cavitation dynamics and hydrodynamic performance coefficients.

Although the MARCS application helped to improve propeller performance predictions for the *INSEAN E779A* propeller (i.e. thrust coefficient deviations between EFD and CFD were decreased from 10% to 3%), similar tendencies, unexpectedly, could not be achieved with *The Princess Royal* propeller.

The main advantage of the proposed (MARCS) approach is that the economy of the refined mesh adaption process, allows simultaneous modelling of the cavitating vortices from all of the blade tips and the hub in the slipstream region from the propeller to the rudder. This capability facilitates propeller-rudder-hull interaction which is the main purpose of this research study. It has the further possibility of allowing investigation of vortex-vortex interactions between the propeller tips and the rudder.

Finally, these investigations have proven that the new mesh refinement approach is particularly effective and practically attractive in tracing the tip vortex cavitation trajectories from all-blades of the 5-bladed heavily cavitating propellers in uniform cavitating flow conditions. The method has been successful in predicting propeller performance and the dynamics of the tip vortex cavitation in comparison with model test data.

This developed mesh refinement procedure (MARCS) is further applied in Chapters 6 and 7 in the investigation of propeller-rudder and propeller-rudder-hull interaction on *The Princess Royal*, respectively, while also observing tip vortices interacting with the modelled rudder.

Chapter 6 Cavitation Influence on Propeller – Rudder Interaction

6.1 Introduction

This chapter deals with the investigation into cavitation phenomenon for marine propellers with reference to propeller-rudder interaction using EFD and CFD methods. For this investigation two different propeller-rudder configurations, without the presence of the hull, were simulated. The first configuration involved a highly skewed, 4-bladed propeller and a conventional rudder. The rudder section thickness of a 2400 GT container ship was simulated in uniform flow condition. The second configuration is of the Princess Royal Propeller and its own simplified plate rudder geometry (non-aerofoil sections) operating with an inclined shaft in non-uniform flow conditions. These two propeller-rudder configurations allow investigation of the propeller-rudder interaction in cavitating flow conditions with strong tip vortex cavitation but also the effect of flow non-uniformity, inclination and rudder profile on this complex phenomenon.

Within the above framework, firstly, the conventional rudder configuration was simulated in STAR-CCM+ in one of the cavitating conditions tested at the Emerson Cavitation Tunnel (ECT). The CFD simulation results were then compared with corresponding EFD results for the propeller performance coefficients and cavitation patterns using the MARCS approach. Then, the Princess Royal propeller and its rudder were simulated using the similar CFD procedures developed for the isolated propellers in Chapter 5. The results were compared with the experiments conducted in ECT using the simulated wake conditions with the aid of a dummy hull and the wake screens. Also, these two propeller-rudder arrangements were simulated without the rudder geometries to investigate the effect of the presence of the rudder on the propeller hydrodynamic performance coefficients and the cavitation dynamics.

The benefits of using the overset mesh method and MARCS application for the investigations of the propeller-rudder interaction are discussed and the main findings from the chapter are included in the concluding remarks.

6.2 Experimental Fluid Dynamics Approach (EFD)

This section presents the EFD approach used for the investigation of propeller-rudder interaction related to propeller cavitation, particularly, to tip vortex cavitation by using two contrasting propeller-rudder arrangements.

The first propeller-rudder arrangement is a conventional rudder and propeller configuration for a typical container vessel tested in a reverse Propeller Open Water Test (POT) condition in the Emerson Cavitation Tunnel (ECT) in parallel with the CFD simulations in similar cavitating conditions (Turkmen et al, 2018). This test was part of an ongoing research on the development of a new Energy Saving Device (ESD) and the Author had the opportunity to attend and observe this test as well as contributing in this research, (Yilmaz et al, 2018).

The second arrangement used is the propeller-rudder configuration of *The Princess Royal* tested in simulated wake conditions with the aid of a dummy hull and the wake screens. The EFD results were extracted from these prior experiments conducted by the Emerson Cavitation Tunnel research group of Newcastle University (UNEW) in the scope of the SONIC project and compared with CFD results in the same cavitating conditions with the sea trials of full scale vessel.

6.2.1 The Emerson Cavitation Tunnel (ECT)

Newcastle upon Tyne has been a centre for cavitation research for more than 100 years and, as reviewed in Chapter 2, it is credited with being the birthplace of the world's first cavitation tunnel built by Charles Parsons in 1895 (Burrill, 1963). In 1910, Parsons built the first large tunnel (500mm square section) at Wallsend and following WWII a modern tunnel was erected at the University in 1949. This was subsequently named the Emerson Cavitation Tunnel (ECT) (Atlar, 2000). The tunnel has served the British ship building industry and contributed to international research continuously

since its inauguration in 1950, and it has undergone several major upgrades and modifications to maintain its status within the hydrodynamic research community. A major upgrade in 2008 saw significant portions of the facility modified to ensure that state of the art experiments, of high accuracy, could be carried out. Lastly, the tunnel was re-located to a purpose built facility at the UNEW Blyth Campus in 2017.

ECT is a closed circuit depressurized tunnel with a measuring section of 3.1m x 1.21m x 0.8m (L x B x H), as shown in Figure 6-1 and Figure 6-2. More detailed information about the tunnel in detail after the recent upgrade is given by Atlar (2011) and general specifications can be found in Table 6-1.

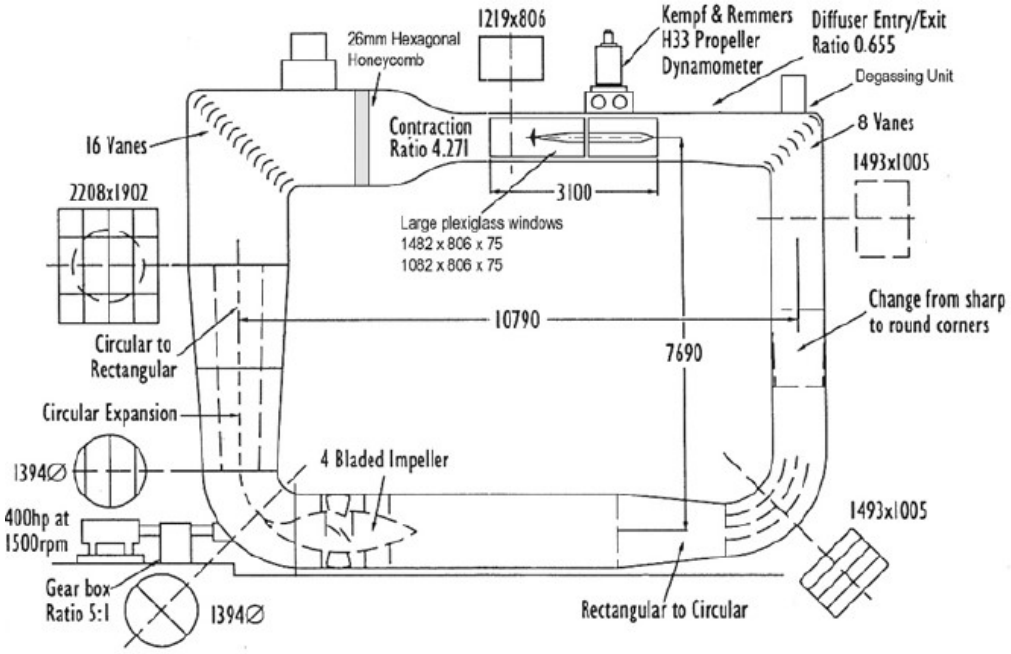

Figure 6-1 Sketch of the Emerson Cavitation Tunnel

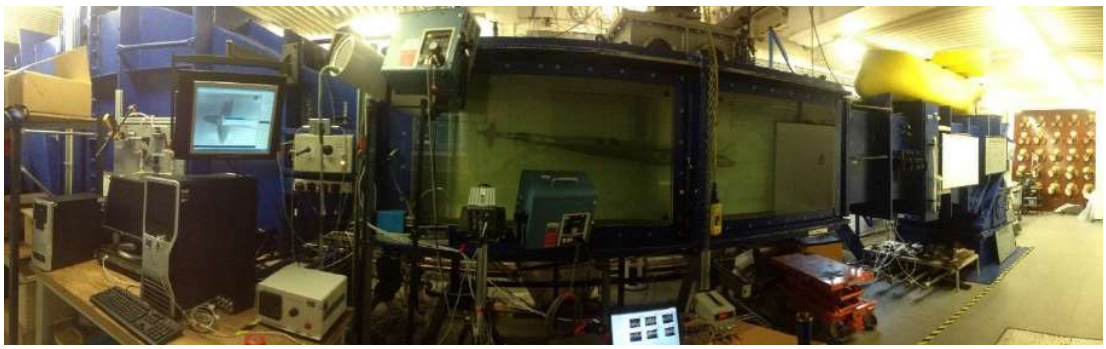

Figure 6-2 Emerson Cavitation Tunnel

Table 6-1 General Specifications of the ECT

Description	Value	Unit
Description of facility	Vertical plane, closed circulating	[-]
Test section size (LxBxH)	3.10 x 1.22 x 0.81	[m]
Test section area	0.99	[m^2]
Contraction Ratio	4.271	[-]
Drive system	4 Bladed axial flow impeller	[-]
Main pump power	300	[kW]
Main pump rotational speed	294	[rpm]
Impeller diameter	1.4	[m]
Maximum velocity	15.5	[knot]
Absolute pressure range	7.6-106	[kN/m^2]
Cavitation number range	0.5-23	[-]

6.3 Propeller – Conventional Rudder Arrangement

6.3.1 Experimental Setup

As described above, two different propeller-rudder configurations were simulated in cavitating conditions using STAR-CCM+. The first configuration has a highly skewed, 4-bladed propeller and its semi-balanced rudder with a section thickness of a 2400 GT container ship. The rudder was tested and modelled without the flap effect and hence is considered to be acting as a conventional rudder for propeller interaction. The

configuration was simulated in uniform flow conditions and tested at the ECT, (Turkmen et al, 2018).

The model propeller and rudder geometries were provided by KAMOME Propeller Co, LTD. The Controllable Pitch Propeller (CPP) model of a 250mm diameter with four built-in blades and high skew was used ahead of the rudder as shown in Figure 6-3.

Figure 6-3 Propeller-Conventional Rudder Arrangement

The cavitation tunnel tests were conducted at 5 different test conditions, representing the equivalent full-scale operational conditions of the basis container ships. Table 6-2 shows the test condition settings for advance velocity ratio (J), tunnel speed (V), shaft rotational speed (n), and tunnel (P_{tun}) and vacuum pressure (P_{vac}) and tunnel temperature (T).

Table 6-2 Test Conditions

Test Condition	***J***	***V***	***n***	***Ptun***	***Pvac***	***T***
		(m/s)	*(rpm)*	*(mmHg)*	*(mmHg)*	*(^{O}C)*
Cond' 1	0.000	0.000	1200	830.7	-200	17.1
Cond' 2	0.154	0.925	1438	830.7	-200	17.1
Cond' 3	0.260	1.560	1438	830.7	-200	17.1
Cond' 4	0.501	3.000	1438	830.7	-200	17.1
Cond' 5	0.494	3.970	1925	830.7	-400	17.1

The aft end and propeller arrangements of the conventional rudder (without the flap) was represented with the model rudders and propellers of a 2400 GT container ship with a scale ratio of 13.2 and fitted downstream of the H33 K&R dynamometer of ECT in reverse Open Water Test (POT) condition as shown in Figure 6-4.

While the measuring section of the ECT usually allows a reasonable size dummy hull with a properly scaled aft end arrangement, in this investigation, a simple wake simulation arrangement was used. In this arrangement, the wake of the H33 dynamometer was combined with the wake of a vertical plate of 0.85m length and 0.02m thickness which was placed between the trailing edge of the dynamometer strut and the model propellers with a diameter of 250mm, as shown in Figure 6-4. The wake plate was also covered with a sand paper of grit P36 to trip the wake flow in turbulent regime.

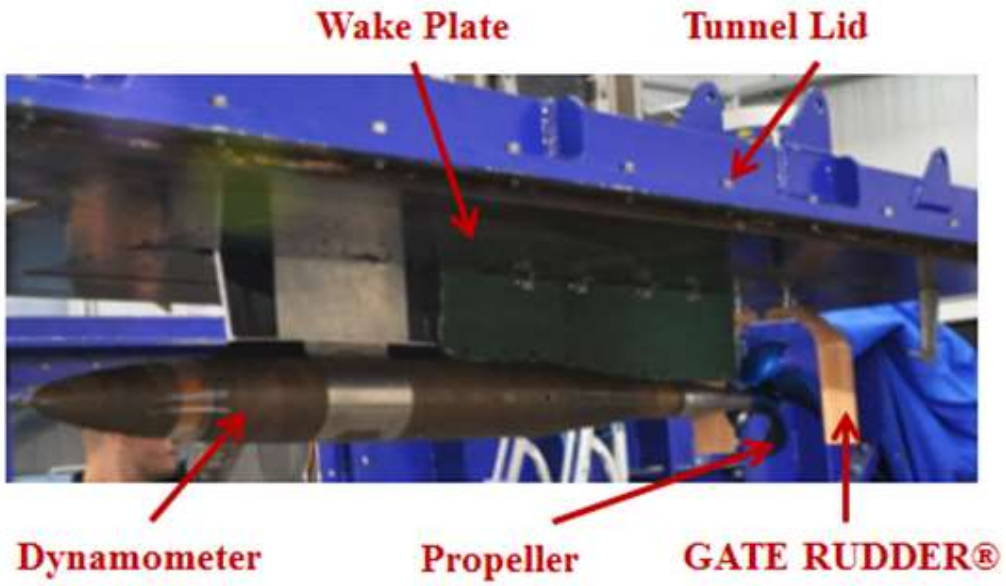

Figure 6-4 ECT test set-up including wake plate (Yilmaz et, al., 2018)

During the tests, propeller thrust and torque as well as the shaft rpm were recorded. The URN characteristics were also recorded by using a hydrophone located inside the tunnel. The cavitation observations were recorded via high speed video and still cameras from the side and bottom windows for each test condition. The oxygen content and temperature of the tunnel water were also monitored.

During the tests the associated test data for propeller performance, cavitation observations and URN were collected for each test condition and analysed for comparisons with corresponding CFD studies.

6.3.2 Computational Fluid Dynamics Approach (CFD)

Although 5 different operating conditions were simulated during the cavitation tunnel tests, only one cavitating condition, which produced the strongest tip vortex cavitation (Condition 5), was used to compare with the CFD simulations as shown in Table 6-3;

Table 6-3 EFD and CFD Conditions

Conditions	J	V	n	σ_n
	[-]	[m/s]	[rpm]	[-]
EFD Condition 5	0.494	3.970	1925	1.714
CFD Condition 5	0.500	3.000	1440	1.730

where, J is the advance velocity ratio (or coefficient) of the propeller, V is the tunnel in-flow speed, n is the propeller shaft rotational speed and σ_n is the propeller cavitation number based on the shaft speed as described at Table 6-3.

6.3.2.1 Computational domain

For modelling of the rotational motion, the overset mesh method was used to eliminate the data transfer problems of the sliding mesh approach. These may occur between the rotating and stationary domains during the stretching of tip vortices from the tip of the propeller blades through the rudder geometry. Tip vortices cannot be transferred from the rotating domain to stationary domain which includes the rudder geometry due to the presence of the interface surface.

Consequently, for the propeller-rudder interaction simulations the two flow domains, which are the background and overset regions, were prepared as shown in Figure 6-5.

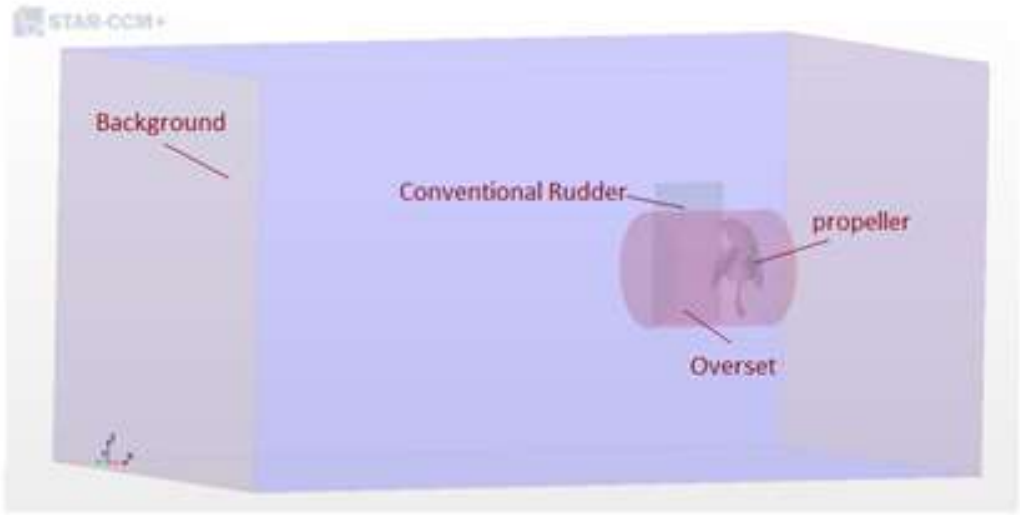

Figure 6-5 Flow Domain for Propeller and Conventional Rudder Configuration

6.3.2.2 Mesh Generation

A suitable mesh arrangement was generated for the simulation of the sheet cavitation on the propeller blade surfaces. While a 0.006D surface size for the mesh generation was applied on the propeller surfaces in general, a smaller surface size with a 0.004D was preferred for a volumetric control region around the propeller tip with a cylinder geometry.

Following the sheet cavitation simulations, new mesh refinements using MARCS were applied for the propeller-rudder interaction simulations. For this purpose the field function was prepared by modifiying the earlier defined field function of the cavitation simulations for the isolated propellers, which was described in Section 5.3.1.2 of Chapter 5, as follows;

Modified Field Function 2:

${WallDistance} < 0.1 && ${WallDistance} > 0.002 && ${Qcriterion} > 20000 ? 0.00035 : 0.0035

The field function modifications are conducted based on the below criteria:

1. As introduced in the latest version of the MARCS, the "Q-Criterion" is used instead to define the region where the tip vortices are produced and hence used for the mesh refinement.
2. Besides the change of the parameter, the field function is also modified using the "Wall Distance" function to exclude redundant mesh cells, already captured in the previous iteration on the wall surfaces of the propeller (blades and hub). The parameter "Wall Distance" is used as the limitation of the refined region, and provides a means to reduce the total number of cells and use a smaller surface size for the mesh refinement.
3. While "0" was used for the last digit for the previous version of the field function, 0.0035 is used for this modified version. The field function dictated that each mesh cell, where the Q-Criterion is above 20000 [s^{-2}], will be 0.35 [mm] in all three dimensions. Otherwise, the dimension of each cell will be kept the same using "0", which causes smaller cells that are not required. Using a specific number "0.0035" instead of "0" keeps the cells with 3.5 [mm] surface size where the mesh refinement is not needed.
4. Although the surface size is defined as 0.35 [mm] in that field function, the generated mesh is obtained with 0.22 [mm] surface size in the refined region in the propeller slipstream. This value is measured from the Figure 6-7(b) for the refined tip vortex region.

Within the above framework, Figure 6-6 shows the iso-surface of the Q-Criterion above 20000 [s^{-2}] from the side and top views. This value was defined by visualising an iso-surface of the Q-Criterion, which is a vortex identification method, described as follows;

$$Q = \frac{1}{2}(\|\Omega\|^2 - \|S\|^2) \qquad [6.1]$$

where Ω and S are the spin and strain-rate tensors, respectively. When Q is positive, this is a vorticity-dominated flow; a negative value implies a strain-dominated flow.

Figure 6-7 also demonstrates the generated mesh for sheet and tip vortex cavitation simulations with the application of MARCS, and use of the modified version of the field function.

This mesh refinement method was also applied in this study to simulate the tip vortex cavitation for the investigations of the propeller-rudder interaction in terms of propeller cavitation. The mesh, which was generated using MARCS, is shown in Figure 6-7 and the details of mesh generation are presented in Table 6-4.

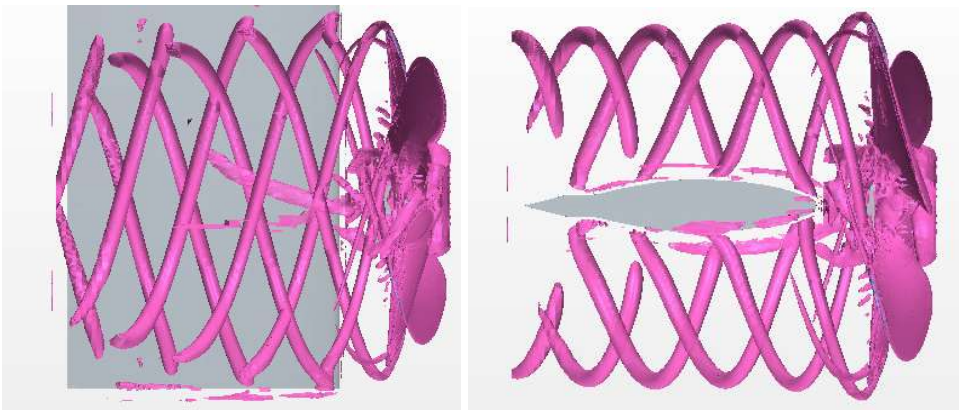

Figure 6-6 Isosurface of Q-Criterion = 20000 s^{-2}

(Left; Side view; Right; Top view)

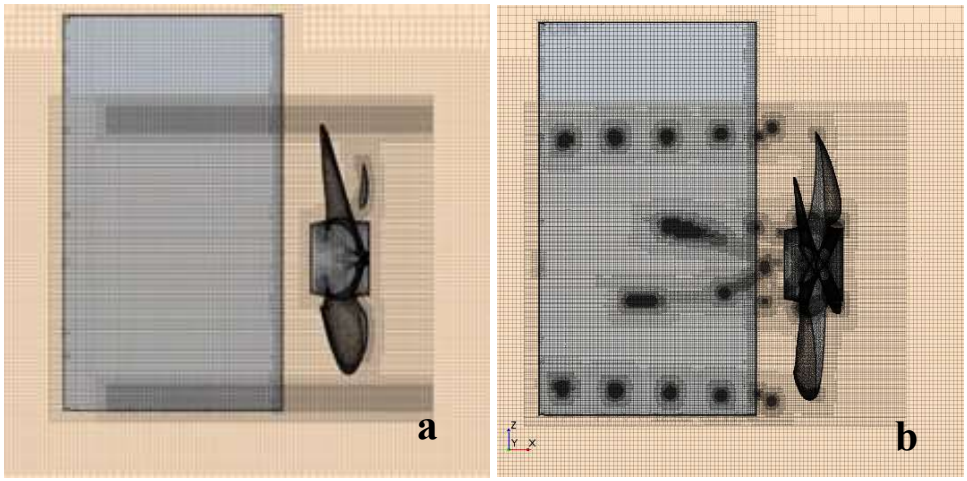

Figure 6-7 Generated mesh for Conventional Rudder-Propeller system

(**a.** Mesh for sheet cavitation; **b.** Mesh for tip vortex cavitation with MARCS)

Although the sheet cavitation could have been simulated successfully using the mesh arrangement shown in Figure 6-7(a), it was known from Section 5 that the unrefined mesh and analysis methods were not sufficient to capture the tip vortex cavitation and

to predict the propeller performance accurately. It was also shown that in order to capture a sudden pressure drop and cavity bubbles in a propeller slipstream, the adaptive mesh refinement approach (MARCS) required to be developed (as presented at Section 5 for isolated propellers). This scheme was modified, as described above, according to the requirements of the propeller-rudder interaction simulations.

Table 6-4 Mesh Details for propeller-conventional rudder arrangement

Mesh Details	Sheet	Tip Vortex (MARCS)	Unit
Surface Size (Blade)	0.5/1.5	0.5/1.5	[mm]
Surface Size (Refinement)	1.0	0.22	[mm]
Number of Cells	11,250,357	52,924,924	[-]

6.3.2.3 Simulation Setup and Boundary Conditions

The CFD simulations for the propeller-rudder arrangements and for the above described test condition were performed using STAR-CCM+.

Based on experience with the propeller rotational fluid domain used in the preceding chapters, the overset mesh method was preferred instead of the sliding mesh approach to be able to simulate the tip vortex cavitation in combination with the rudder and hence to eliminate the data transfer problems between the rotating and stationary domains.

Boundary conditions of the flow domain were defined as for the propeller cavitation simulations described and discussed in Section 5.4 of Chapter 5.

Based on the previously discussed argument regarding large scale turbulence and small-scale motions the LES turbulence models were preferred for simulating the cavitating flow, especially for the tip vortex type of cavitation. The default Schnerr-Sauer cavitation model in STAR-CCM+, again, was used for this simulation. The selected time step value was $5x10^{-5}$s, which means 833.33 time steps per revolution (24 rps rotation speed, time for one rotation 0.041666s) or 0.43 degrees revolution per time step.

In contrast to the experimental set-up as shown in Figure 6-4, the CFD simulation was conducted in uniform flow by neglecting the narrow wake produced by the dynamometer and wake plate covered with the sand paper to save time as well as due to unavailability of the wake distribution from the EFD. Also, the main interest of this study is to investigate the tip vortex cavitation dynamics interacting with a conventional section rudder and to compare these dynamics with the thinner section rudder of *The Princess Royal*, rather than to explore the effect of the above mentioned unavailable wake.

6.4 *The Princess Royal* Propeller – Rudder Arrangement

6.4.1 Experimental Setup

The Princess Royal propeller and its rudder geometry were selected for the second propeller-rudder case simulations. The simulations of this arrangement was compared with the results of the experiments conducted by the UNEW in the scope of the SONIC project. This arrangement includes the effect of the hull wake based on the dummy hull and screen mesh combination.

In SONIC, the cavitation tests were conducted in the medium size ECT of UNEW as well as in several other European test facilities, Aktas et al., (2016). The test set-up in the ECT is shown in Figure 6-8 which included a scaled dummy-hull with wake screens representing the starboard demi-hull of *The Princess Royal*, in order to simulate the wake obtained from a towing tank wake survey of the full model. A stereoscopic PIV system was used to measure wake velocities during the simulations as reported in e.g. Shi et al (2017).

During the cavitation tests, measurements were made of the underwater radiated noise, hull pressure pulses, and cavitation observations. Within the scope of this research study, only the respective propeller hydrodynamic performance data and cavitation observations are compared with the CFD calculations.

Although the ITTC preference is to use a full model of the hull in cavitation tunnel tests, a dummy hull model with an additional wake mesh was used due to limitations

of the medium size ECT facility. On the other hand, a dummy hull model provides for a better representation of the 3D flow and hull-interaction effects than a simple 2D wake screen approach which is more beneficial in terms in cost and time.

In complementing the dummy hull, a 2D wake screen (mesh) was also added ahead of the propeller plane in order to properly represent the hull wake as shown in Figure 6-8. The density and configuration of the wake meshes was adjusted during an iterative wake simulation exercise featuring the stereoscopic Particle Image Velocimetry (PIV) system of the cavitation tunnel.

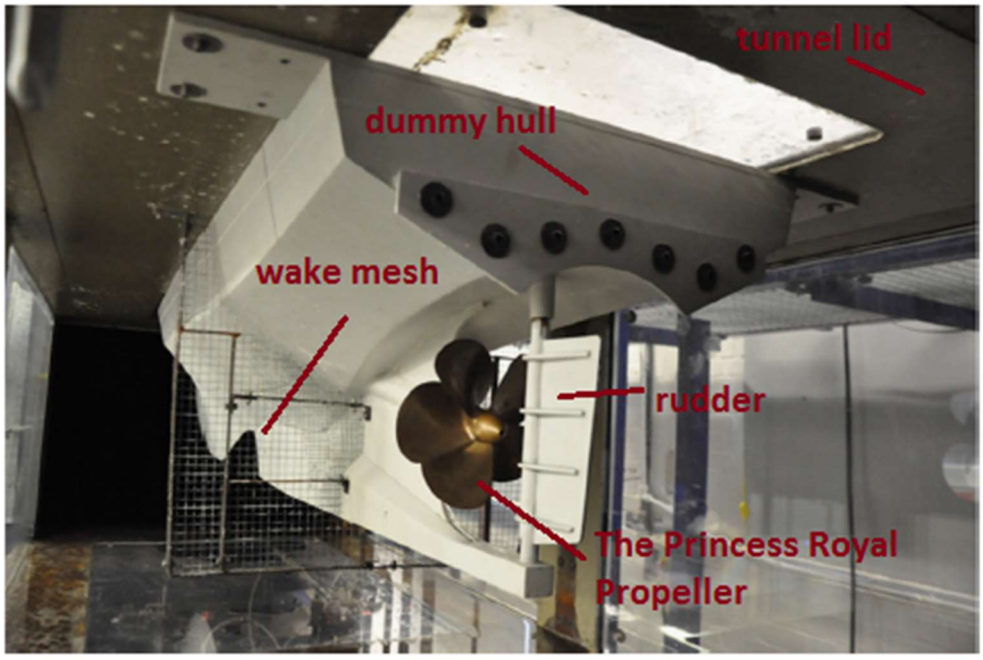

Figure 6-8 Wake Representation

The target wake for these simulations was defined by the wake measurements conducted using a 1:5 scaled model of *The Princess Royal* vessel in the towing tank of the Istanbul Technical University (ITU) without rudder and appendages by Korkut and Takinaci, (2013).

Figure 6-9 shows the wake distribution plots of the target wake (Korkut and Takinaci, 2013) and simulated wake (Aktas et. al., 2015). The plots show a high degree of similarity, especially between the 10 and 2 o'clock positions where cavitation dynamics are most severe.

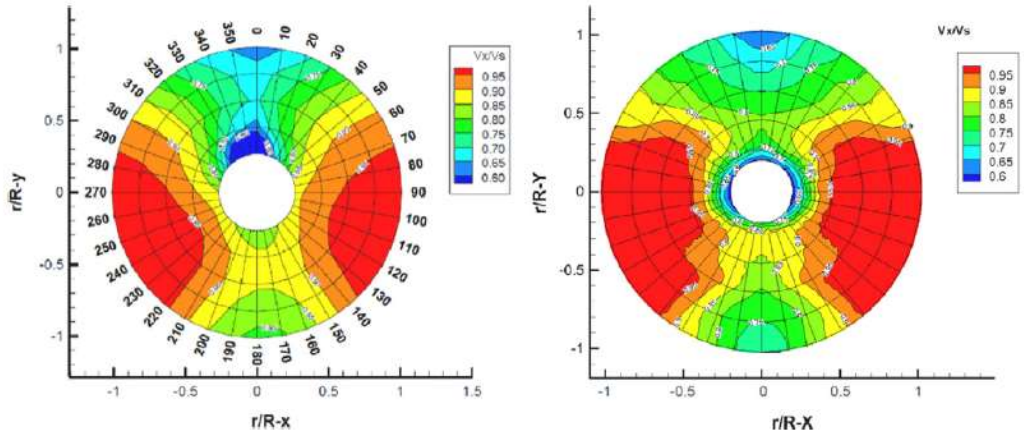

Figure 6-9 Target Wake (Left), Simulated Wake (Right) (Aktas et. al., 2015)

The cavitation tunnel tests (Table 6-5) were conducted at "Condition 4" of the sea trials based on the K_Q identity. This condition was preferred since it displayed the strongest tip vortex cavity dynamics observed during the trials and model tests. The three additional test conditions were also conducted in order to assess (15%) more heavily loaded conditions in an attempt to match the extensive cavitation observations in the full-scale.

Table 6-5 Full Scale vs. Model Scale Operating Conditions

Full Scale Operating Conditions					**Model Scale Operating Conditions**			
Condition Number	**Engine Speed (RPM)**	**Propeller Speed (RPM)**	**$10K_Q$ (-)**	**σ_N (πnD)**	**Rotational Speed (rps)**	**H_{st} (mmHg)**	**Torque (Nm)**	**15% Higher Loading Torque (Nm)**
Cond' 1	600.00	342.80	0.38	1.20	15.00	-253.85	3.84	4.41
Cond' 2	900.00	514.20	0.34	0.54	20.00	-351.31	6.07	6.98
Cond' 3	1200.00	682.10	0.32	0.30	20.00	-509.72	5.75	6.61
Cond' 4	2000.00	1141.50	0.32	0.11	30.00	-550.72	12.92	14.86

The primary cavitating condition (Condition 4) was simulated using both the CFD approach and constructed wake representation described above.

6.4.2 Computational Fluid Dynamic Approach (CFD)

The following modelling, simulations and comparisons are dedicated to “Condition 4” test case.

6.4.2.1 Computational domain

As stated earlier, the overset mesh method was selected in order to eliminate data transfer problems of the sliding mesh approach that may occur at the interface surfaces between the rotating and stationary domains for modelling of the rotation motion. Such problems may occur when stretched tip vortices pass through the rudder geometry mesh.

Accordingly, two regions were modelled, respectively, as the background (including rudder) and overset regions (including propeller) for the simulation of this propeller-rudder interaction case. Figure 6-10 shows the computational flow domain prepared for cavitation simulations of the propeller-rudder interaction case including the background and overset mesh regions including *The Princess Royal* propeller with 8 deg shaft inclination (due to the nature of the propeller-rudder arrangement for the full-scale ship) and its rudder geometry.

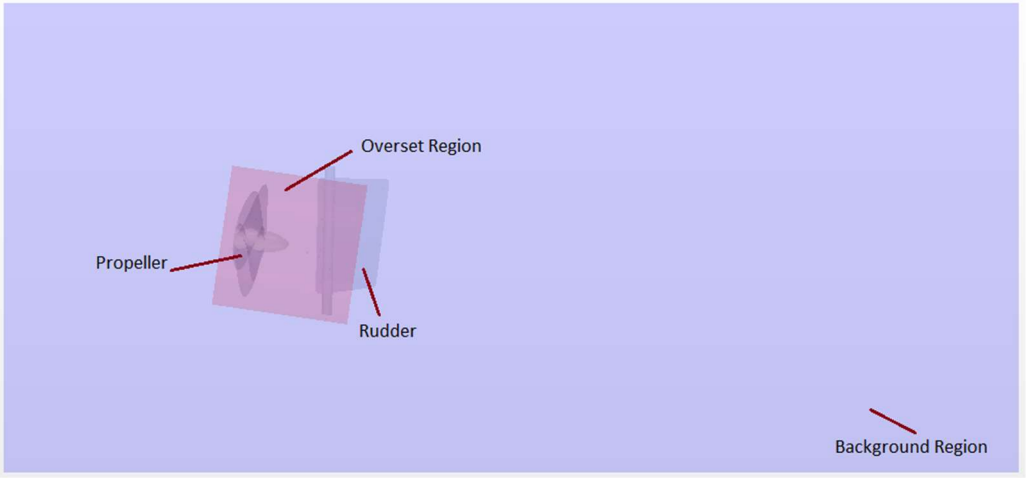

Figure 6-10 Flow Domain including Background and Overset Mesh Regions

6.4.2.2 Mesh Generation

The same mesh procedure developed for the cavitation simulations of the isolated propellers, which was presented at Section 5.3 of Chapter 5, was also applied for the propeller-rudder interaction simulations with further modifications presented in this chapter.

Firstly, a coarse mesh was generated for the sheet cavitation simulation. Then, a region was prepared by applying the Q-Criterion, to define the zone where the vortices were identified, thus generating the pink region as shown in Figure 6-11 (Left). Then, using the MARCS approach, a field function was created to generate finer meshes where the Q-Criterion was above 20000 [s^{-2}]. Having generated the finer meshes, a mesh refinement table, which included the coordinates of each cell needed to be prepared. The subsequent surface sizes, were generated automatically by STAR-CCM+ using the suitable field functions to generate the refined meshes. Figure 6-11 (Left) shows the iso-surface of the Q-Criterion above 20000 [s^{-2}] and (Right) the mesh generated using the refinement table that was prepared by using the Q-Criterion trajectory.

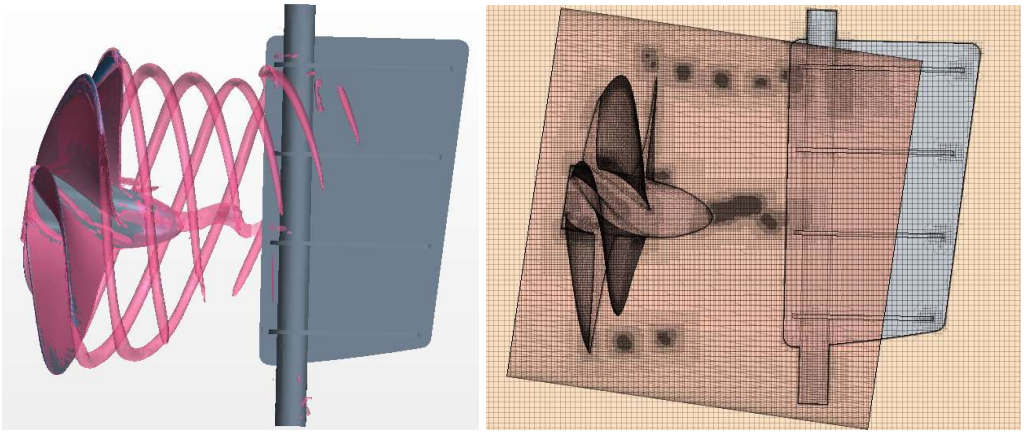

Figure 6-11 Generated Mesh for Propeller-Rudder Interaction Simulations with MARCS

In contrast to the cavitation simulations for the isolated propellers, the vortices could not be produced uniformly in the propeller slipstream due to the non-uniform flow and shaft inclination as shown in Figure 6-11. The details of the generated mesh for the sheet and tip vortex cavitation simulation are shown in Table 6-6.

Another point was the application of the mesh refinement on the propeller blade surface. This proved to be redundant and increased the total number of cells while sheet cavitation had already been successfully captured without mesh refinement on the blade surface. Using the "Wall Distance" function in the field function, the redundant mesh refinement on propeller blade surface was eliminated as stated earlier.

Table 6-6 Mesh Details for *The Princess Royal* propeller- rudder arrangement

Mesh Details	**Sheet**	**Tip Vortex (MARCS)**	**Unit**
Surface Size (Blade)	0.5/1.5	0.5/1.5	[mm]
Surface Size (Refinement)	1.0	0.22	[mm]
Number of Cells	7,925,943	48,843,117	[-]

6.4.2.3 Simulation Setup and Boundary Conditions

The propeller-rudder interaction simulations for *The Princess Royal* propeller and its rudder were conducted in STAR-CCM+ using the LES turbulence model in cavitating conditions with the Schnerr-Sauer cavitation model. The overset method was used to simulate the interaction between the propeller and rudder transferring the data from the overset region to the background mesh region as stated earlier. For the representation of the wake, a velocity distribution table, obtained from the towing tank tests results at ITU, (Section 6.4.1) were set as initial conditions on the inlet plane of the computational flow domain (Figure 6-12) including boundary conditions. Figure 6-12 also presents that the wake representation was achieved reasonably well during the cavitation simulations compared with the target wake in the towing tank, as shown ealier, in Figure 6-9.

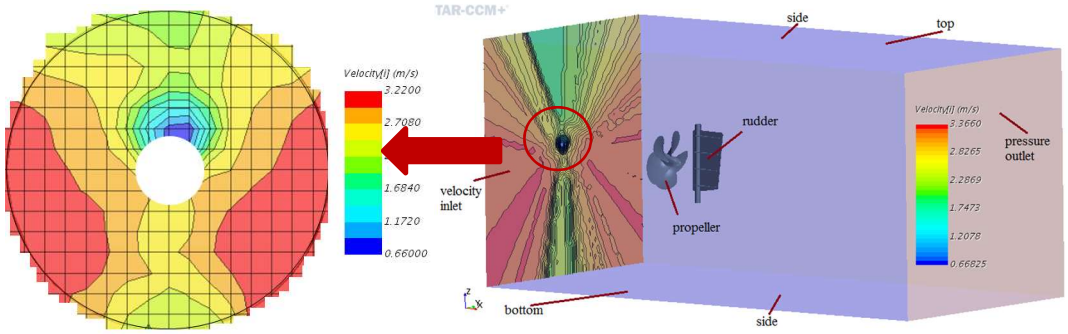

Figure 6-12 Wake Representation in STAR-CCM+ and Boundary Conditions

6.5 Results and Discussions

In this section, the earlier described two different propeller-rudder arrangements (i.e. the container propeller-conventional rudder case and *The Princess Royal* propeller-rudder case), were simulated and comparative results with the EFD data are presented and discussed. The discussion of the results include the propeller hydrodynamic performance, cavitation patterns, tip vortex cavitation, tip vortex interactions with the rudder and chordwise pressure distributions at a number of spanwise positions on the rudder surfaces for the container ship arrangement first and *The Princess Royal* arrangement to follow.

6.5.1 Propeller – Conventional Rudder Arrangement

As already stated in Section 6.3.1, although five different operating conditions, as shown in Table 6-2, were tested in the ECT, only Condition 5 was simulated and compared with the EFD which produced the strongest tip vortex cavitation as shown in Table 6-3.

Table 6-7 presents the comparative propeller performance characteristics (i.e. K_T, K_Q and η_0) based on the CFD and EFD analysis results.

Table 6-7 EFD and CFD Results Comparisons for conventional rudder-propeller arrangement

Conditions		K_T	$10K_Q$	η_0
		[-]	[-]	[-]
Conventional Rudder	EFD Analysis	0.2156	0.2910	0.5835
	CFD Analysis	0.2071	0.2717	0.6067
	Deviation	3.9%	6.6%	-4.0%

As shown in Table 6-7, although the CFD prediction of K_T shows good agreement with the experiments (EFD) with a deviation of less than 4%, K_Q could only be predicted within a deviation of % 6.6 which can be related to the geometrical differences, the presence of the wake plate and the similar (but not exact) conditions between the EFD and CFD predictions. Such aspects of this study require further investigation and fine tuning.

For the CFD-predicted cavitation patterns, Figure 6-13 shows the sheet cavitation and tip vortex cavitation, respectively, for the conventional rudder-propeller system. Figure 6-14 also presents the cavity volume change with the application of MARCS in the time history of the solution. It can be noticed that the cavity volume has increased after the application of MARCS including the combined volume of the sheet and tip vortex cavitation.

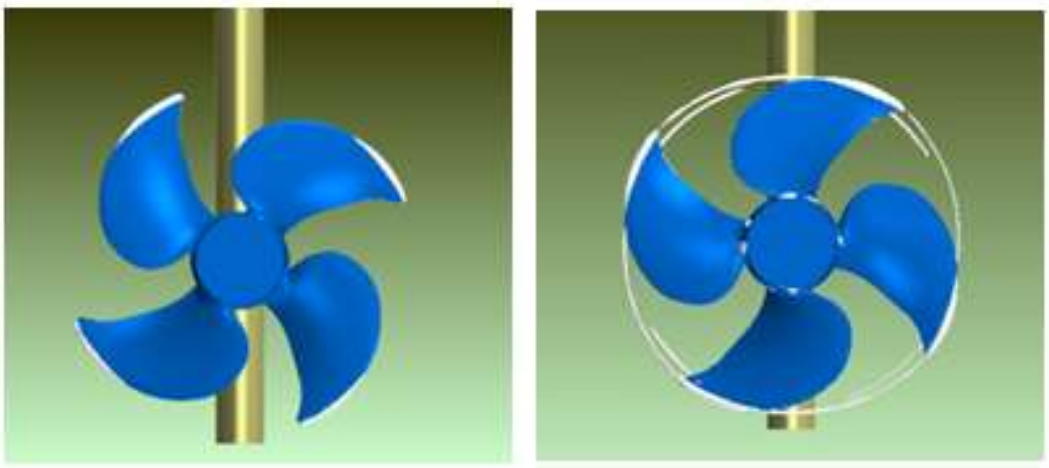

Figure 6-13 Cavitation pattern for conventional rudder and propeller system (Left; Sheet Cavitation, Right; tip vortex cavitation)

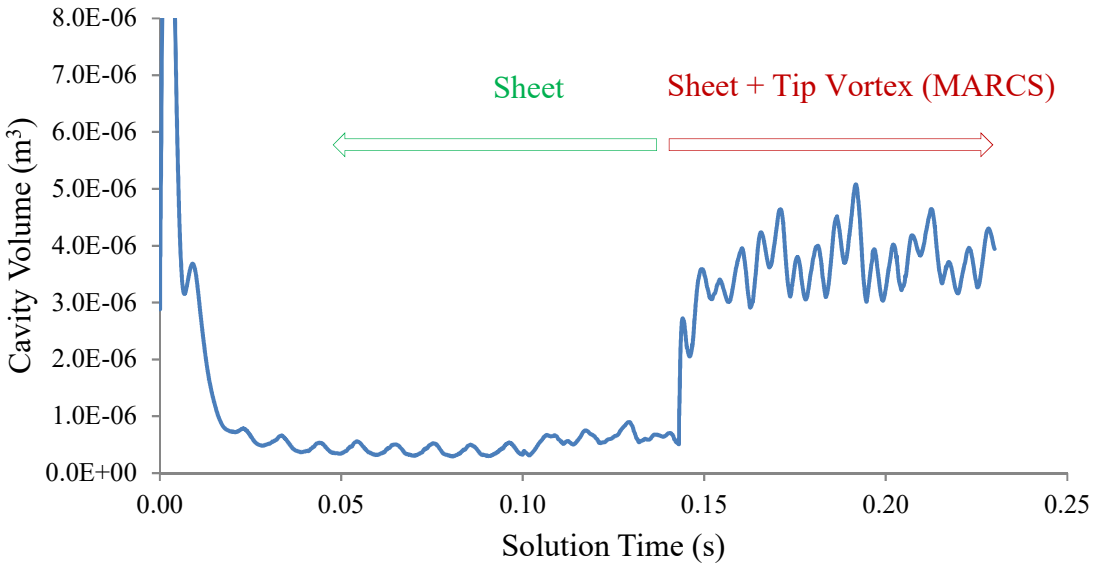

Figure 6-14 Cavity Volume Change against Solution Time without and with MARCS application

As observed during the cavitation tests with the conventional rudder-propeller system, a strong sheet cavity covered almost 15-20% of each blade surface, being more accentuated around the top dead center (i.e.high wake shadow region), as shown in Figure 6-15 (Left). Due to the effect of the wake plate, the deformation of the tip vortices at the same region was also observed and this deformation was combined with the effect of the rudder downstream, resulting in the bifurcation of the tip vortex at the rudder leading edge. In spite of the accentuated sheet cavity dynamics at the wake

shadow and deformation of the tip vortex at the rudder leading edge, the tip vortex cavitation was transported downstream through the propeller slipstream and the rudder without losing visible strength (Figure 6-15).

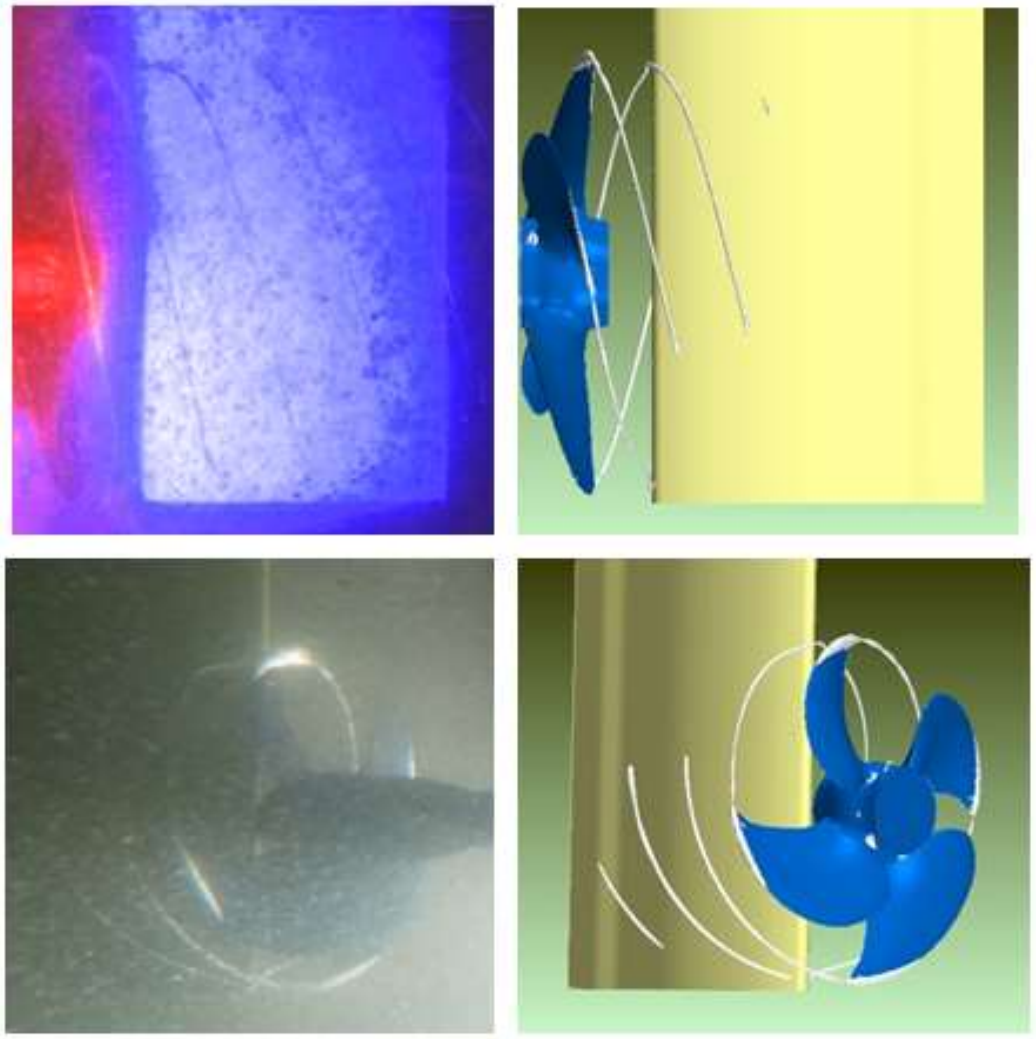

Figure 6-15 The *Propeller-Convectional Rudder Arrangement:* Cavitation Comparisons for Conventional Rudder-propeller system (Left: EFD from tunnel tests; Right; CFD predictions)

Because of the poor visual quality of the EFD observation for Condition 5, the colour of the picture on the top left of Figure 6-15 has been purposefully modified to create contrast with the rudder for better visibility of the tip vortex traces. Despite the visibility problem the comparison of the CFD predicted trajectories of the tip vortices and the sheet cavitation extent with the experimental observations looked rather encouraging.

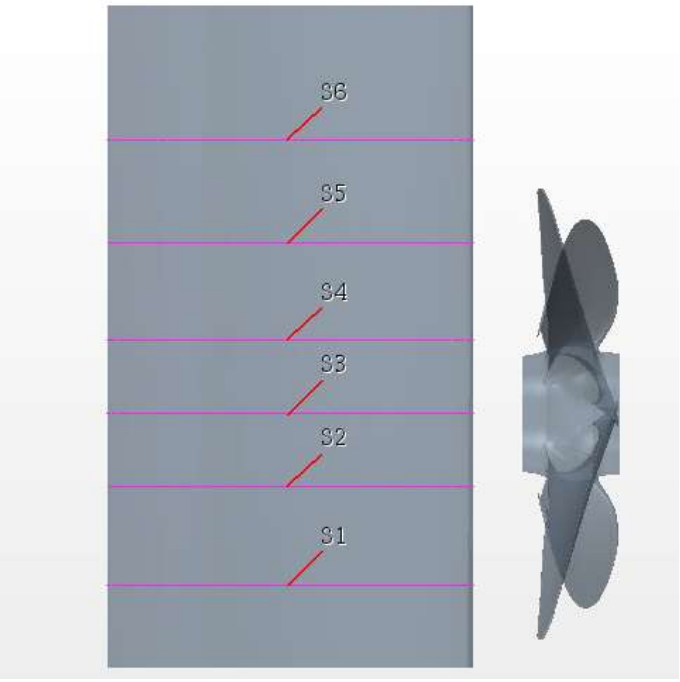

Figure 6-16 The *Propeller-Convectional Rudder Arrangement:* Section Planes (z direction) at 6 spanwise positions on rudder for pressure distribution calculations

As stated earlier, one interesting and different feature of the conventional rudder arrangement from *The Princess Royal* rudder arrangement is the profile section of this rudder with varying maximum thickess along the span compared to the flat plate type rudder of *The Princess Royal*. To demonstrate the effect of the thickness and its variation on the pressure distribution of the rudder, six different chordwise sections were specified along the rudder span (i.e. sections S1-S6 from tip to root, respectively), as shown in Figure 6-16, and the pressure distributions along the back and face of the rudder profiles at these sections are presented as shown in Figure 6-17 when the rudder is at 0^o helm angle. Sections S5-S1 and S4-S2 are placed symmetrically corresponding 0.7R and 0.3R sections of the propeller blade, respectively. S3 is also placed at the hub region in order to investigate the affect of the hub on flow characteristics.

Although the CFD results of the pressure distributions at these sections cannot be compared with the EFD due to the lack of the measurements of the pressure distributions in these tests, the general trends of these predictions were compared those with *The Princess Royal* rudder section to form an idea about the effect of the rudder thickness.

As one can see in Figure 6-17 while the pressure distribution on the rudder seems to be unaffected by the propeller's action outside the slipstream (i.e. at section 6) the remaining sections, which are inside the propeller slipstream (i.e. sections 1, 2, 3, 4 and 5), are being clearly affected, at a region from the leading edge to 0.25-0.40C of the chord. It is also interesting to note some deviation at 0.9C region as the main characteristic of the foil pressure distribution. Section 3 is in the shadow of the hub and is influenced by the relatively complex nature of the flow in this region.

Sections 1 and 2 show the influence of the change in the direction of the rotational vector in the slipsteam flow. This causes a change in the angle of attack on the sections above and below the shaft centreline and hence on which surface the suction region appears behind the leading edge.

In order to provide an insight how the propeller TVC trajectories interact with the rudder a progressive advancement of these trajectories along the rudder are presented as function of the propeller rotation in Figure 6-18 from Theta = 205 deg to 295 deg.

Finally, in order to demonstrate the accuracy and hence power of the CFD, nine simulation images are presented in Figure 6-19 while the tip vortices are approaching to the rudder and interacting with the rudder leading edge in solution time from top view. These images are also quite important for the investigations of the leading edge erosion of the rudder. Namely, in Figure 6-19, frames 4, 5 and 6, the cavitating vortex passes through a suction peak in the red ovals on the "back" surface for a right-handed propeller above the shaft. Here the free-end flares up suddenly then collapses violently as it passes out of the peak into a higher pressure region. Thus the higher pressure causes the bubbles in the vortex tube to collapse and to impart high impolsive loads on the rudder surface; this is an erosion mechanism.

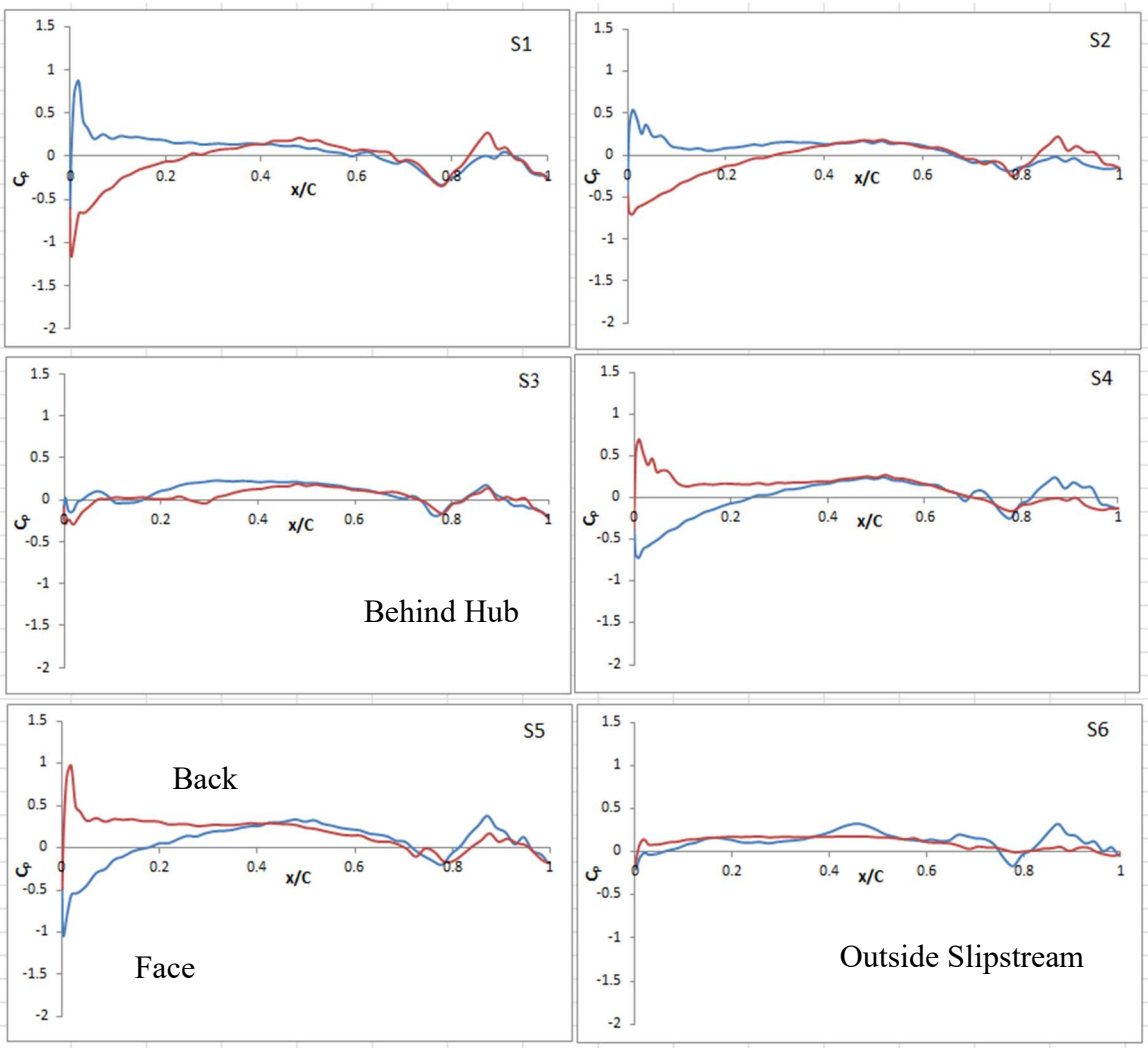

Figure 6-17 The *Propeller-Convectional Rudder Arrangement:* Chordwise pressure distribution at 6 spanwise positions for rudder (MARCS) (From top to bottom; S1-S6) (Red: Back, Blue: Face)

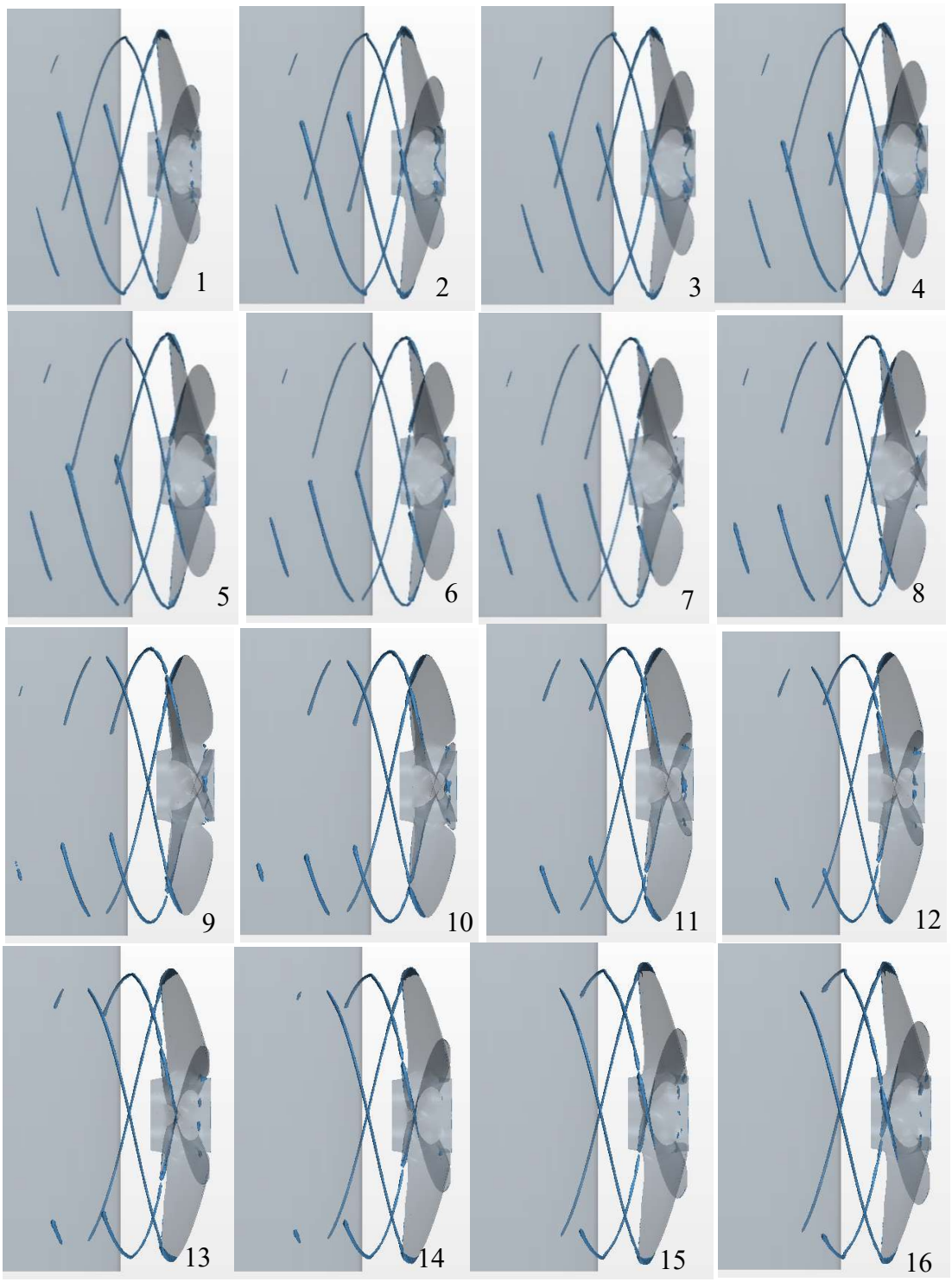

Figure 6-18 The *Propeller-Convectional Rudder Arrangement:* The deformation of the TVC in the presence of the rudder

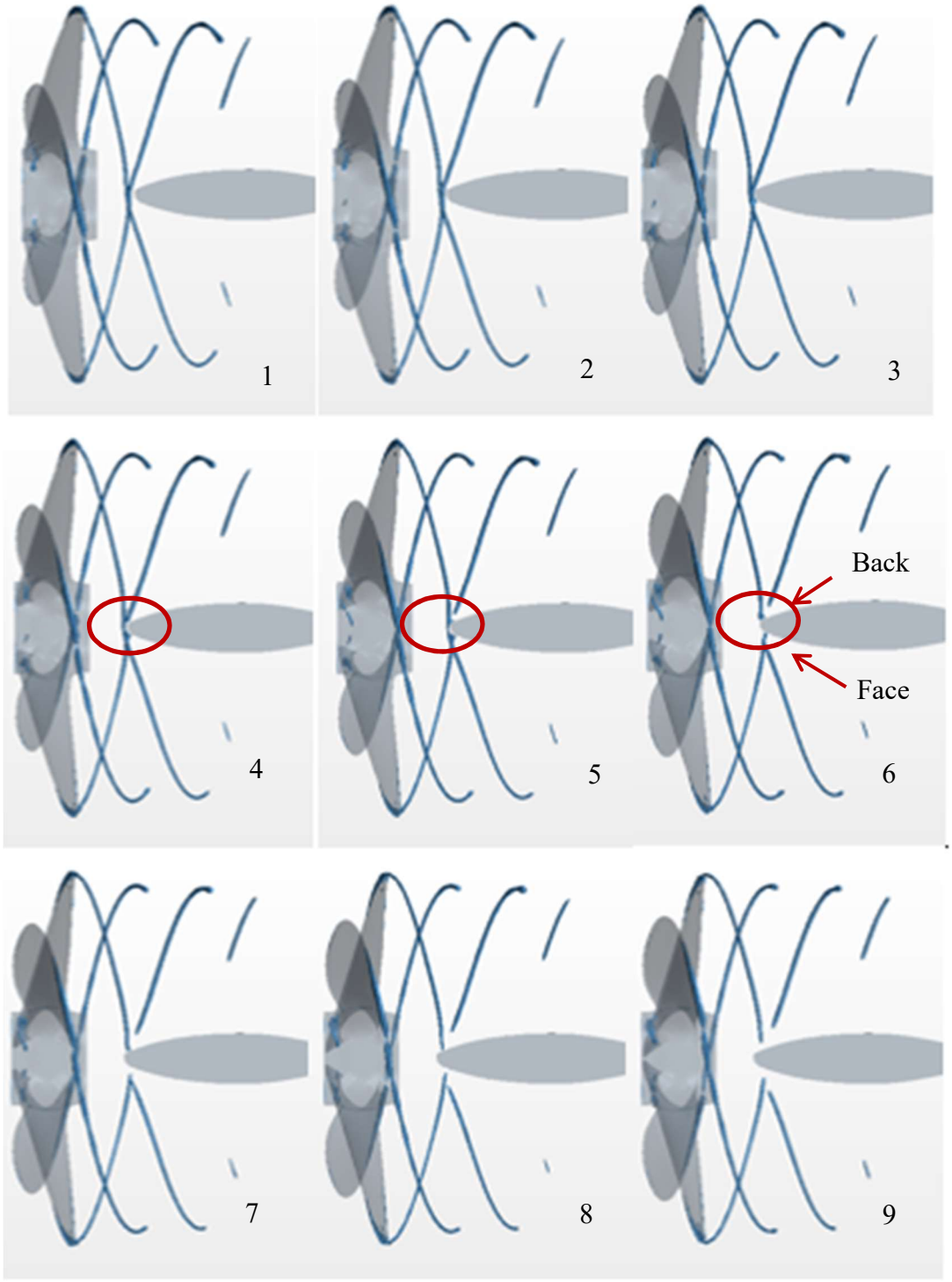

Figure 6-19 The *Propeller-Convectional Rudder Arrangement:* Vortex Interaction with Rudder Leading Edge (From Top View)

6.5.2 The *Princess Royal* Propeller – Rudder Arrangement

In presenting and discussing the propeller-rudder interaction for *The Princess Royal*, as stated earlier, only Condition 4 is considered due to the strongest tip vortex cavitation observed at the model and full-scale observations.

Experimental test Condition 4 with the engine speed of 2000 rpm was the closest to the Engine MCR (2300) condition and the full-scale propeller in this condition displayed rather large extent (almost 25-30% of the blade area), volume and intensity of the suction side sheet cavitation which can be seen at the top right corner picture of Figure 6-20. During the tests, this was extremely unsteady, breaking-up (and bursting) intermittently with cloudy appearance. This sheet cavitation terminated at the blade tip region by rolling-up in the form of a rather thick, intense and cloudy tip vortex trailing to the rudder as shown in the top left corner of Figure 6-20 and the trailing tip vortex cavitation trajectories were bursting time by time, Aktas et al. (2016).

As far as the comparison of the tunnel test observations with the full-scale cases was concerned, as shown in Figure 6-20 (top), there was a good correlation between the full-scale and model scale observations in terms of the types, strength and dynamic behaviour of the cavitation observed for the heavily loaded condition. The normal corresponding condition, yet again, simulated the similar patterns of the full-scale observations with reduced strength, Aktas et al. (2016).

Figure 6-20 also demonstrates the CFD simulation results (bottom) compared with ECT tests and full-scale cavitation observations with regards to cavitation dynamics including tip vortex cavitation particularly. Although a good agreement was obtained from the comparison between the CFD and EFD results from ECT, it was observed that sheet cavitation was under predicted when it was compared with full-scale observations (Figure 6-20, Right).

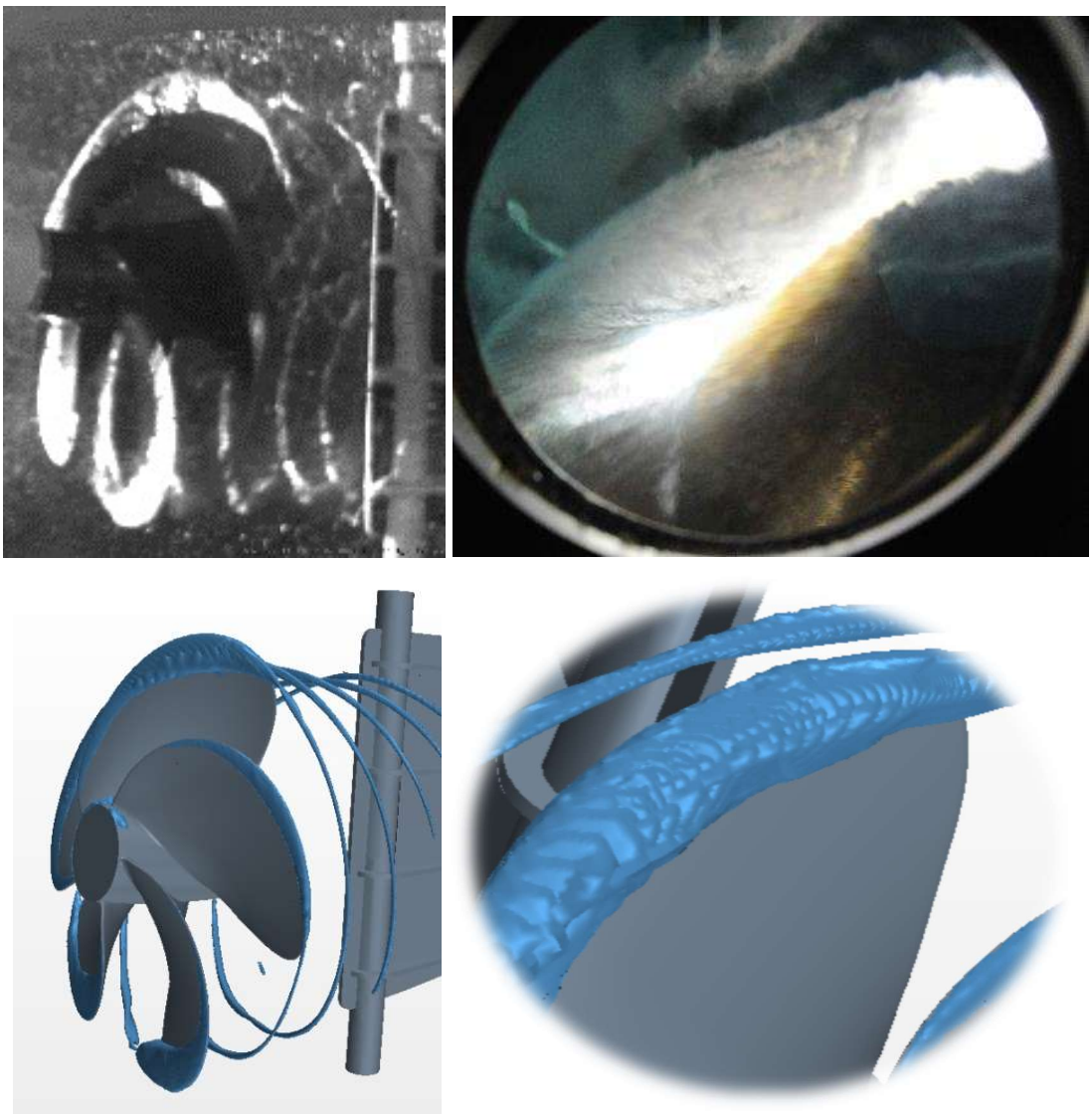

Figure 6-20 The *Princess Royal Propeller – Rudder Arrangement*: Comparison of cavitation viewings (Left; Model test, Right; Full Scale Observations for Condition 4) (Top; EFD Results, Bottom; CFD Results)

The comparison of the CFD predictions for the propeller performance with the EFD results based on the model tests at ECT are presented in Table 6-8 including the difference (deviation) between the two sets results. As shown in this table, although the CFD predictions displayed a good agreement with the experiments (EFD) regarding $K_{T,}$ for which the deviation is less than 2%, the difference in K_Q is not as good as K_T with about % 6.7 which will require further investigation and associated fine-tuning.

Table 6-8 Hydrodynamic Propeller Performance Interacting with Rudder

Cond'	Method	K_T	$10K_Q$	η_0
Cond' 4	EFD	0.2237	0.3657	49.7%
	CFD	0.2274	0.3482	51.8%
	Deviation	1.6%	-6.7%	-4.2%

In order to demonstrate the effectiveness of the MARCS on the accuracy of the propeller performance predictions the simulation results without MARCS (i.e only for sheet cavitation modelling) and with the MARCS approach (i.e. including tip vortex cavitation modelling) are given in comparison in Table 6-9. As shown in this table the deviation between the EFD and CFD results is approximately 8.0% and 8.2% for the thrust and torque coefficients, respectively, indicating the positive influence of the MARCS refinement approach. This is an added value of using MARCS for the better representation of the tip vortex cavitation extension than the other mesh refinement approaches.

Table 6-9 Propeller Performance Coefficients (Sheet vs Tip Vortex Cavitation Simulations)

	K_T	K_T%	$10K_Q$	$10K_Q$%
Sheet	0.2431	8.0%	0.3378	-8.2%
Tip Vortex	0.2274	1.6%	0.3482	-6.7%
EFD	0.2237	[-]	0.3657	[-]

As far as the CFD predicted cavitation patterns are concerned, Figure 6-21 shows the sheet cavitation and tip vortex cavitation, on the left and right, respectively while Figure 6-22 presents the cavity volume change against solution time with the application of MARCS. Similar to the results of the conventional rudder simulations the increase in the cavity volume due to the inclusion of the tip vortex cavitation is noticeable due to the use of MARCS.

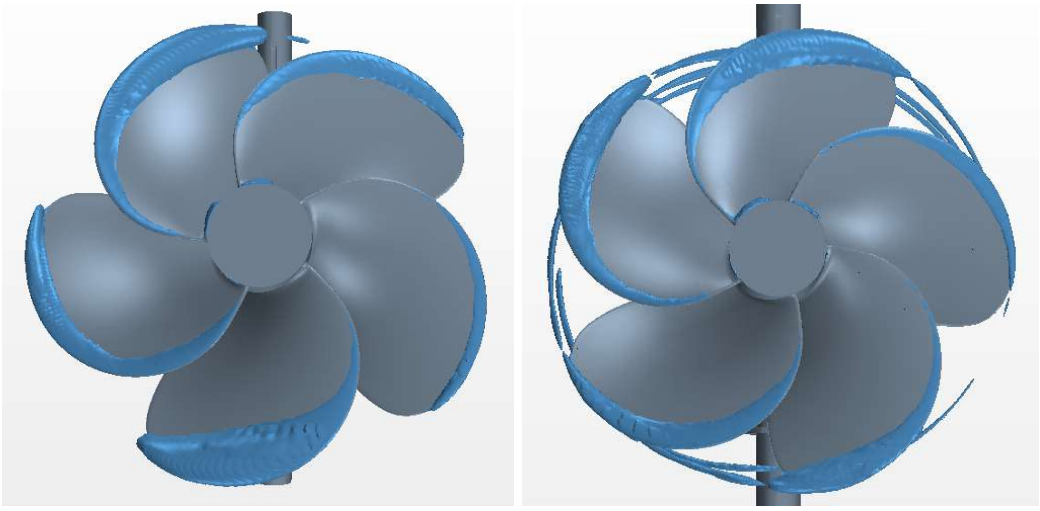

Figure 6-21 *The Princess Royal Propeller – Rudder Arrangement*: Cavitation pattern for *The Princess Royal* propeller and rudder (Left; Sheet Cavitation, Right; tip vortex cavitation (MARCS))

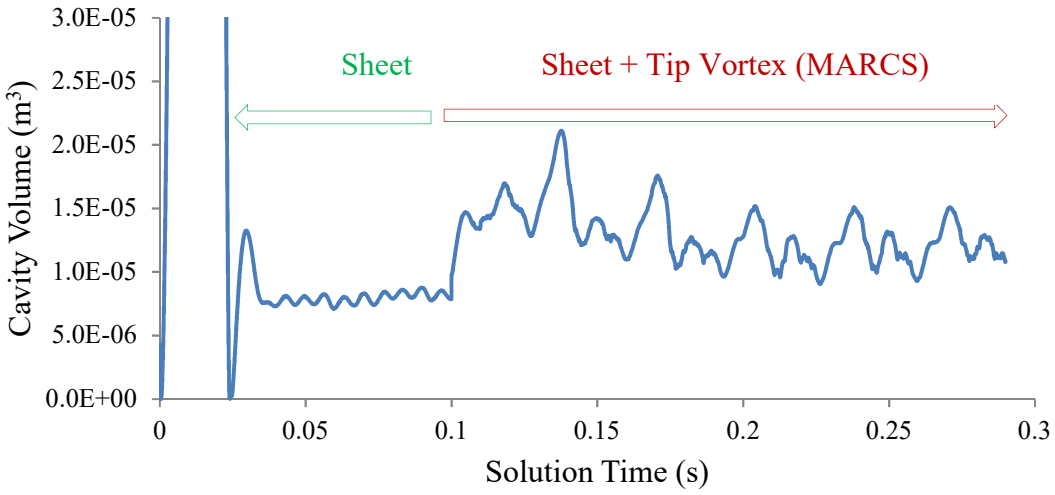

Figure 6-22 *The Princess Royal Propeller – Rudder Arrangement*: Cavity Volume Change against Solution Time without and with MARCS application

In order to investigate the effect of the rudder on the hub vortex cavitation and the tip vortex cavitation trajectories of *The Princess Royal* model propeller, further simulations were conducted with and without the rudder of this vessel. These simulations were conducted under the same cavitating conditions in the presence of the wake, which was implemented as an initial condition from the inlet patch of the flow domain, and the simulation results are presented in Figure 6-23 regarding the cavitation images while the comparative results of the propeller performance are shown in Table 6-10.

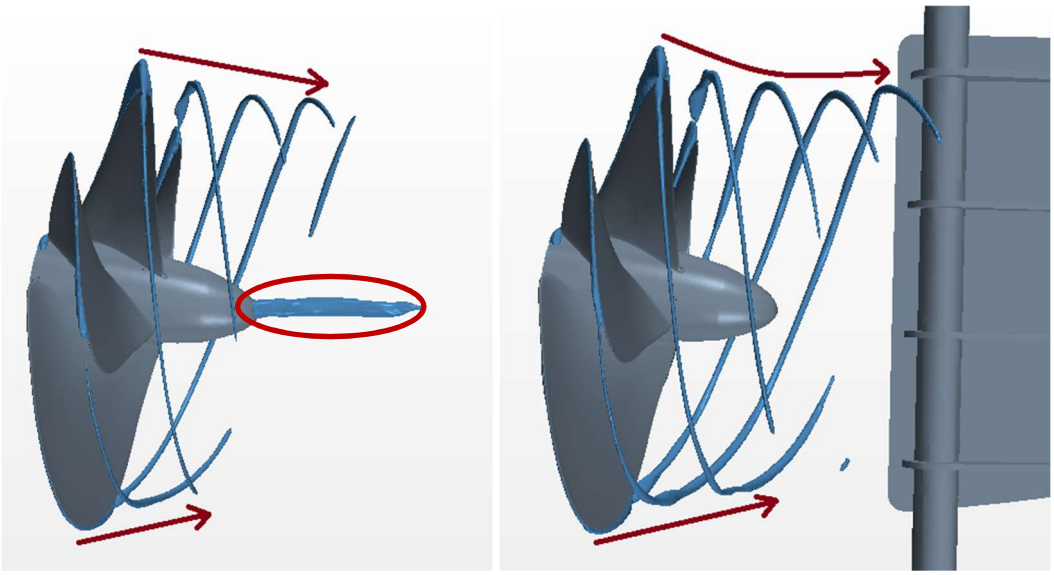

Figure 6-23 The *Princess Royal Propeller*: Cavitation Pattern Comparisons including TVC between the propeller without and with rudder arrangements

Table 6-10 Hydrodynamic Propeller Performance with and without rudder

Simulation Case	K_T	$10K_Q$	η_0
EFD Results Propeller with rudder	0.2237	0.3657	0.497
CFD Results Propeller with rudder	0.2274	0.3482	0.518
CFD Results Propeller without rudder	0.2201	0.3102	0.567

Regarding the tip vortex cavitation dynamics, as shown Figure 6-23, the envelop of the trajectories appeared to be contracting continuously over the inspected (computed) zone in the case without rudder. The similar trend, initially, can be observed in the presence of the rudder, but the contraction level raises slightly as it is approaches the rudder. However, despite the change in the slope of the TVC trajectories, the strength and typical diameter of the TVC still appear to be similar for the case with and without the rudder.

On the other hand, while the TVC trajectories were still present as independent of the presence of the rudder the strong hub vortex cavitation, which was predicted for the

case with no rudder, disappeared when the rudder was presented. A similar observation was also reported in experiments as reported from literature e.g. (Atlar et al., 1998).

Regarding the propeller performance, as shown in Table 6-10, the presence of the rudder is affecting the thrust and torque with a trend that both coefficients were increased due to the reduced swirl in the propeller slipstream which also resulted in the change of the propeller efficiency.

In Figure 6-24 to Figure 6-27 the results of the CFD predicted cavitation images are compared with those of the images captured from the EFD observation videos including the sheet and tip vortex cavitation. These comparisons show that the sheet cavitation, and particularly the tip vortex cavitation, could be simulated successfully applying MARCS as the cavitation images are almost perfectly matched to the experimental images. This is despite the fact that the presence of the dummy hull and wake screen combination was not represented in the CFD modelling, and instead the simulated wake velocities obtained from the EFD were used successfully in the CFD code as the initial conditions.

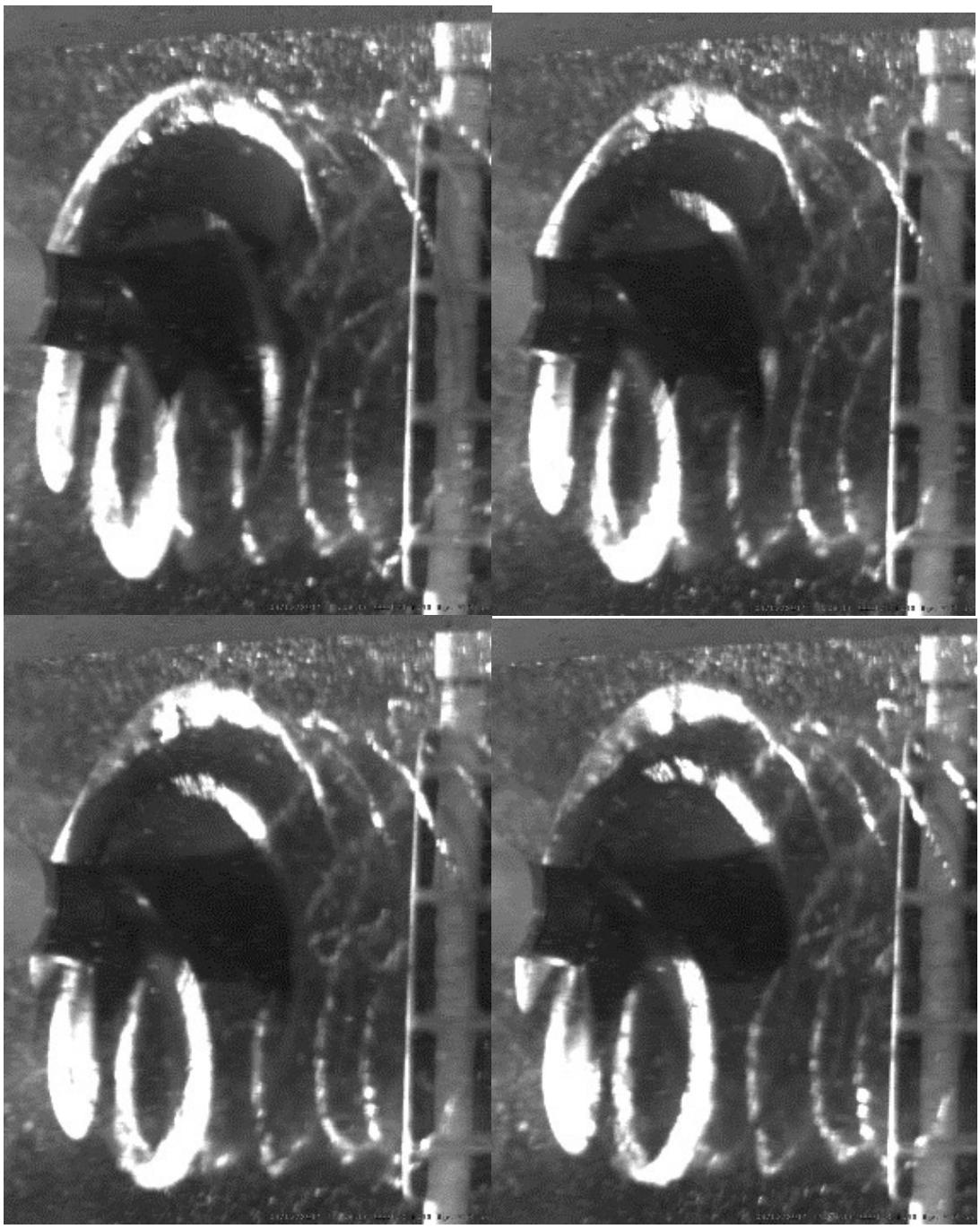

Figure 6-24 The *Princess Royal Propeller – Rudder Arrangement*: Condition 4 – EFD Results; High Speed Video Captures from Inward Camera

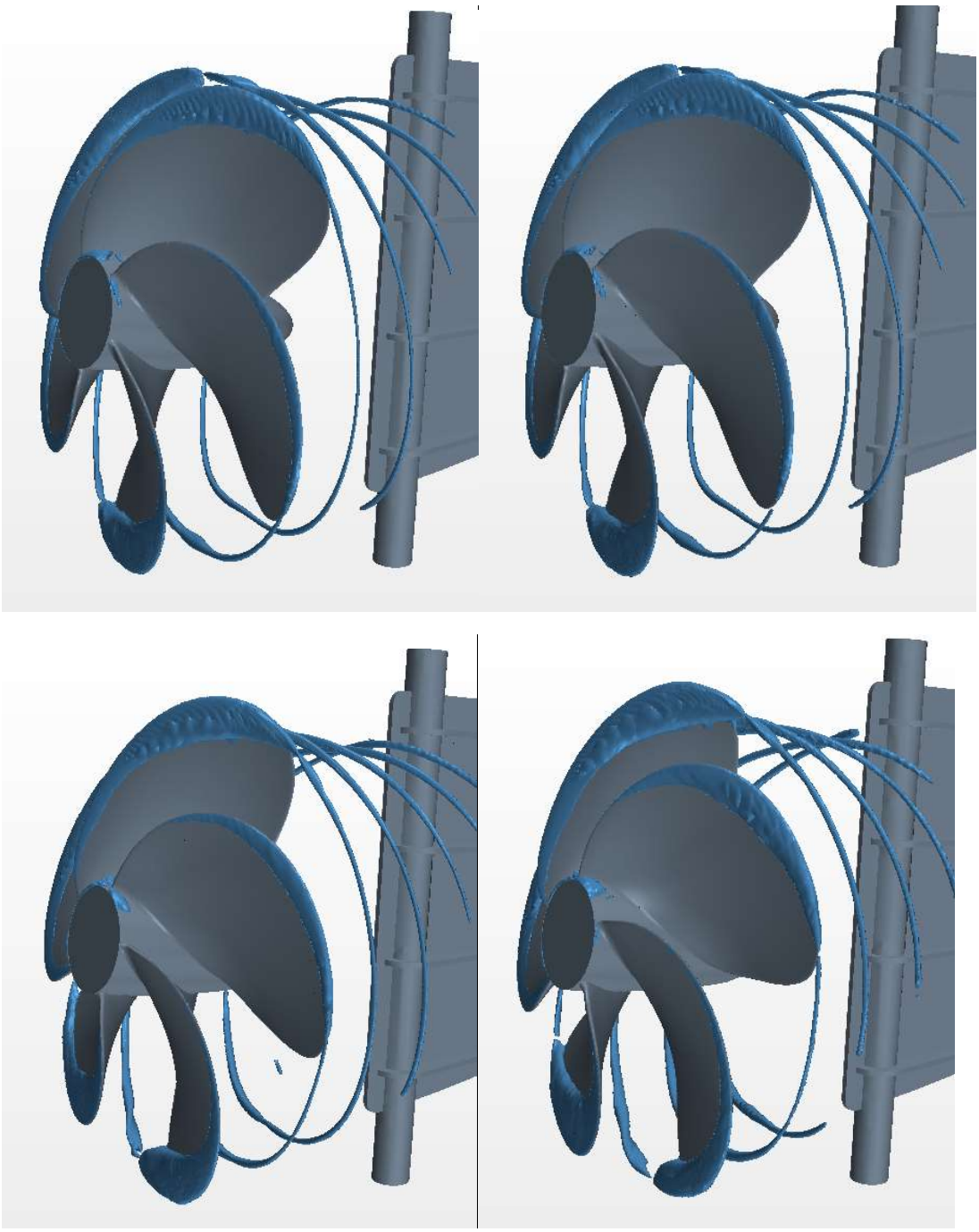

Figure 6-25 The *Princess Royal Propeller – Rudder Arrangement*: Condition 4 – CFD Results; Cavitation Pattern including extended TVC

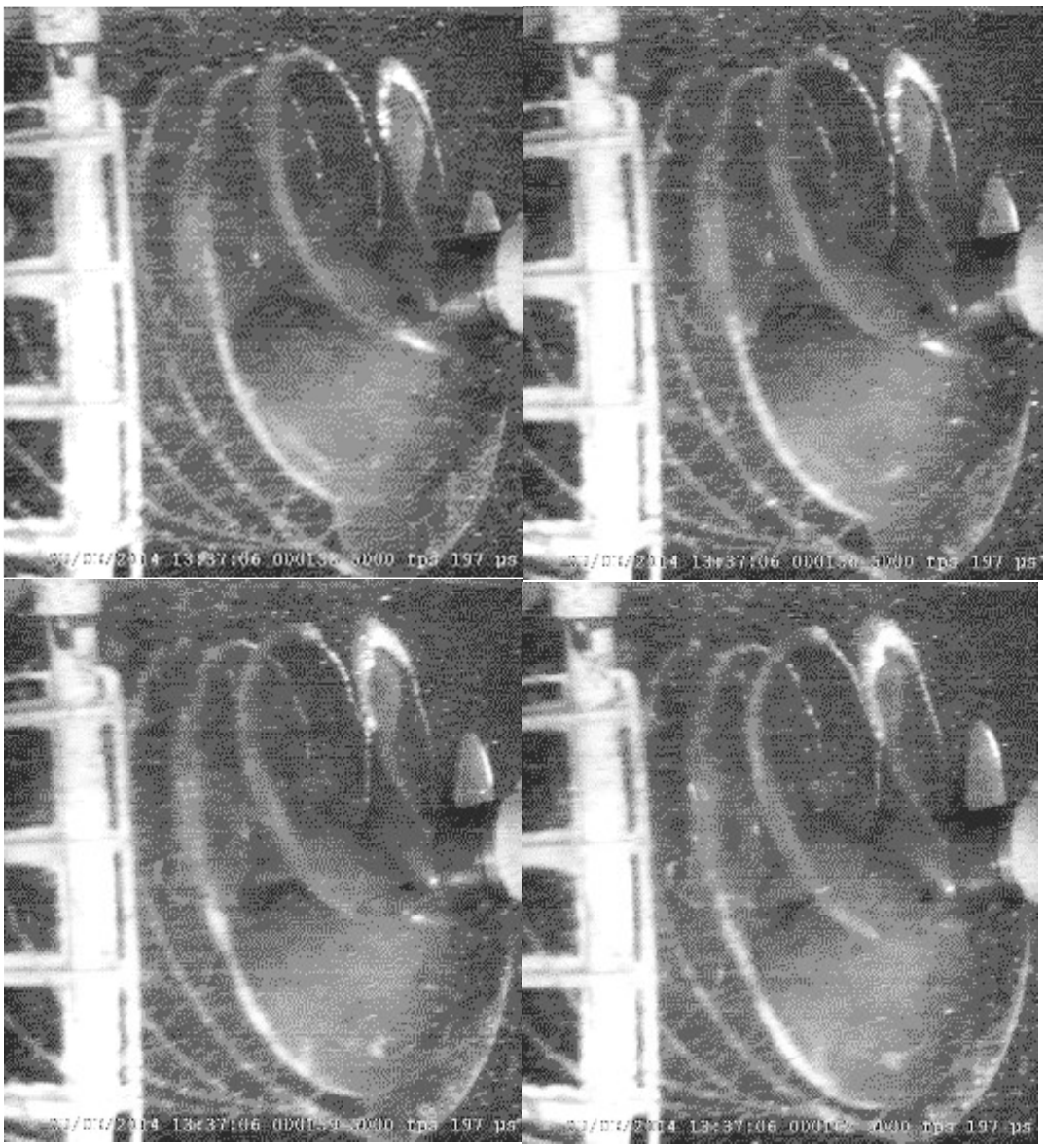

Figure 6-26 The *Princess Royal Propeller – Rudder Arrangement*: Condition 4 – EFD Results; High Speed Video Captures from Outward Camera

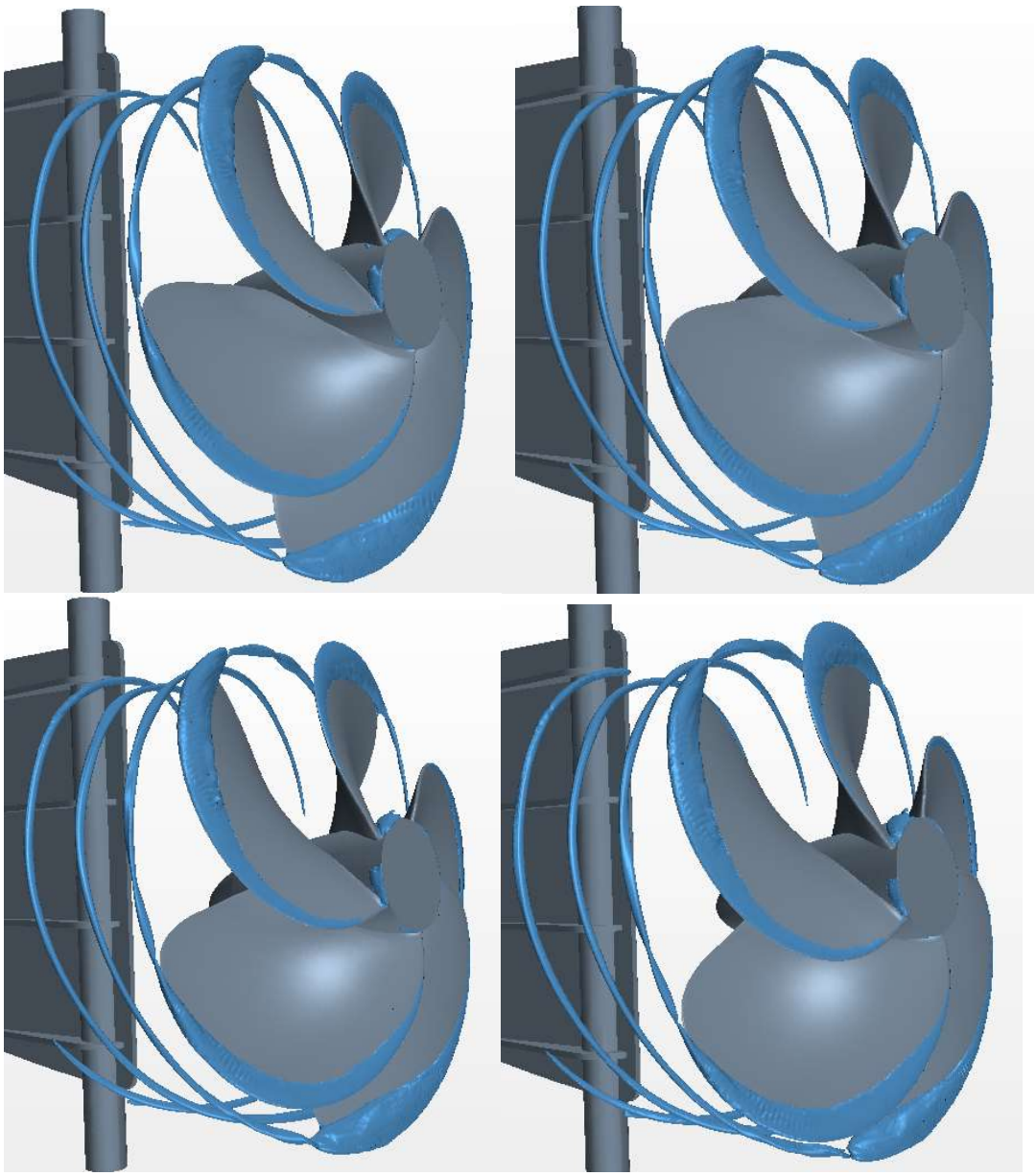

Figure 6-27 The *Princess Royal Propeller – Rudder Arrangement*: Condition 4 – CFD Results; Cavitation Pattern including extended TVC

In order to demonstrate the accuracy and hence power of the CFD two simulation images are included in Figure 6-28 to demonstrate how the cavitating slipstream interacts with the propeller at the rudder leading edge. The vortex core is seen to retard in the axial direction and deflect upwards due to the high back-pressure of the rudder leading edge pressure field. Such characteristics were identified on several vessels during rudder erosion studies, e.g. (Fitzsimmons, 2009).

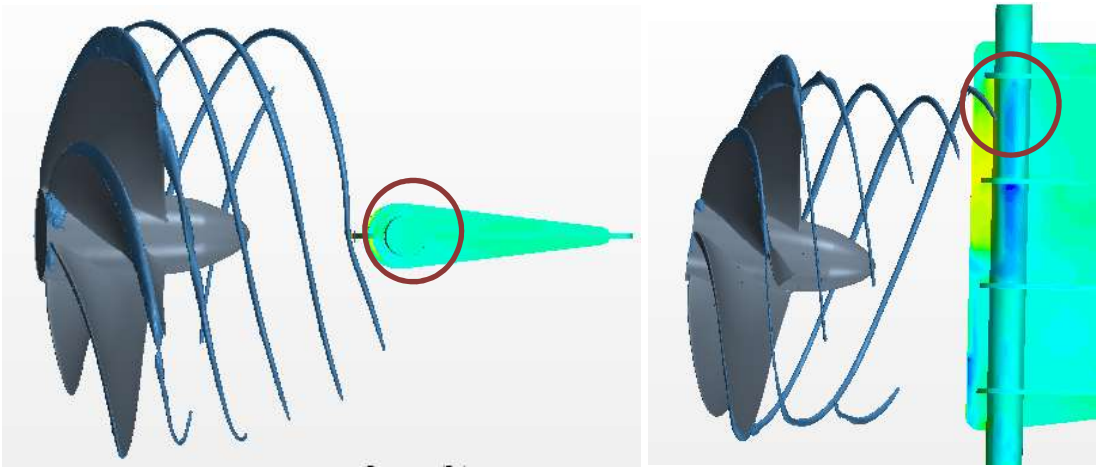

Figure 6-28 The *Princess Royal Propeller – Rudder Arrangement*: Vortex Interaction with Leading Edge

Rudder design often centres on the subject of section shape. The principal design factor is active rudder area, such that the necessary steering forces are generated to manoeuvre the vessel. The minimum thickness, requirements are governed by structural needs. Actual thickness is governed by hydrodynamic requirements since thickness change will affect the minimum drag, separation tendencies and hence stall angle and maximum lift coefficients (Molland & Turnock, 2007). Within this framework, the analysis of the data for different section shapes yields a general trend.

As stated earlier, one interesting and different feature of the conventional rudder arrangement from *The Princess Royal* rudder arrangement is the profile section of the conventional rudder with varying maximum thickness along the span compared to the flat plate type rudder of *The Princess Royal*.

To demonstrate the difference between the pressure distributions of the two rudder types, similar to the conventional rudder case, six different chordwise sections were specified according to propeller blade radii (i.e. sections S1-S6 from tip to root,

respectively), as shown in Figure 6-29, and the pressure distributions along the back and face of the rudder plate at these sections are presented as shown in Figure 6-32 when the rudder is at 0^{o} incidence.

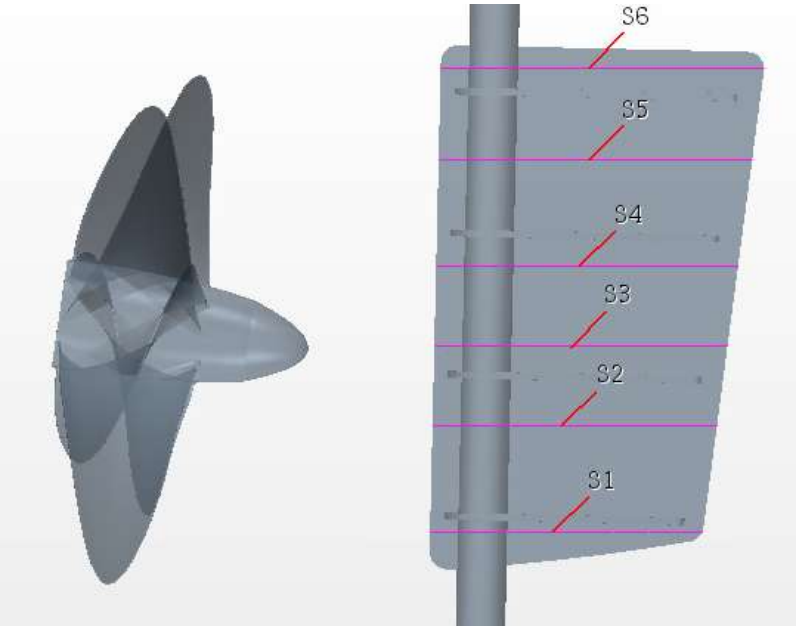

Figure 6-29 The *Princess Royal Propeller – Rudder Arrangement*: Section Planes (z direction) for pressure distribution calculations

Surface pressure distributions were calculated on the rudder, from which section results were extracted at the 6 spanwise positions (S1-S6 in as shown in Figure 6-29) for both rudders, as shown in Figure 6-32, and the comparative pressure coefficient distributions are presented in Figure 6-31 the rudder at 0^{o} incidence.

Although the CFD results of the pressure distributions at these sections cannot be compared with the EFD due to the lack of the measurements of the pressure distributions during the cavitation tests, the general trends of these predictions are compared with those of the Conventional Rudder case to form an idea about the effect of the rudder thickness.

To illustrate the effects of propeller and rudder interaction, two different rudder profiles and arrangement were investigated as shown in Figure 6-30 using the MARCS procedure. Figure 6-30 (left) shows the conventional rudder which has more thick (aerofoil) profile section compared to *The Princess Royal's* rudder on the right of

Figure 6-30 with a thin plate attached to an exposed cylindrical stock-housing and a relatively large propeller-rudder clearance.

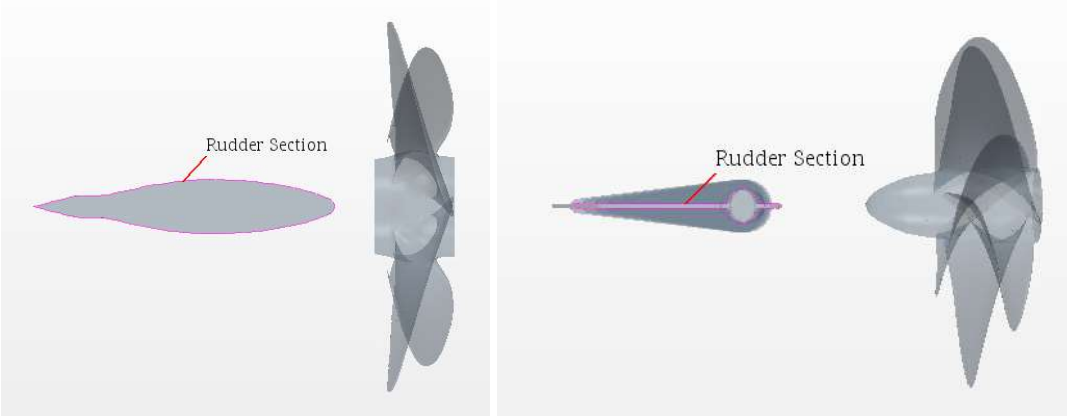

Figure 6-30 Rudder Profiles (Left; Conventional Rudder, Right; The Princess Royal Rudder)

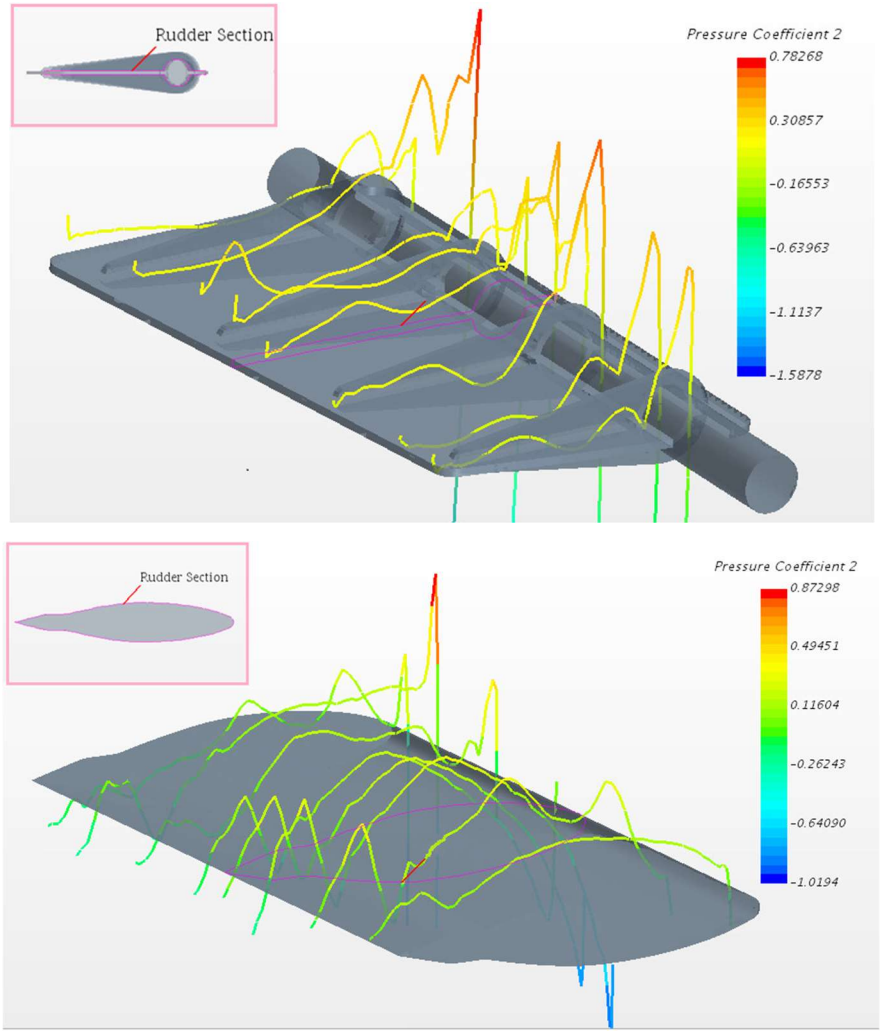

Figure 6-31 2D Pressure Distribution Plots over 3D rudder surfaces (Top; The *Princess Royal* Rudder, Right; *Conventional* Rudder)

Figure 6-31 presents the 2D pressure coefficient plot over 3D rudder surfaces for *The Princess Royal* (top) and the *conventional* rudder (bottom) geometries. This comparative image demonstrates the effect of the different rudder section shapes on the pressure distribution on rudder surfaces. The high suction pressure values have been obtained on the leading edges for both rudder geometries as shown in Figure 6-31 due to the angle of attack induced bt the rotation of the propeller slipstream. While the rudder stock bar causes a disturbance pressure increment for *The Princess Royal* rudder, a similar effect has also been observed due to the change of the rudder tail shape for the *conventional* rudder. The effect of the different section shape on the chordwise pressure distribution at 6 spanwise positions can also be seen in Figure 6-32

for *The Princess Royal* propeller – rudder arrangements similar to the containership-conventional rudder arrangemenet given in Figure 6-17.

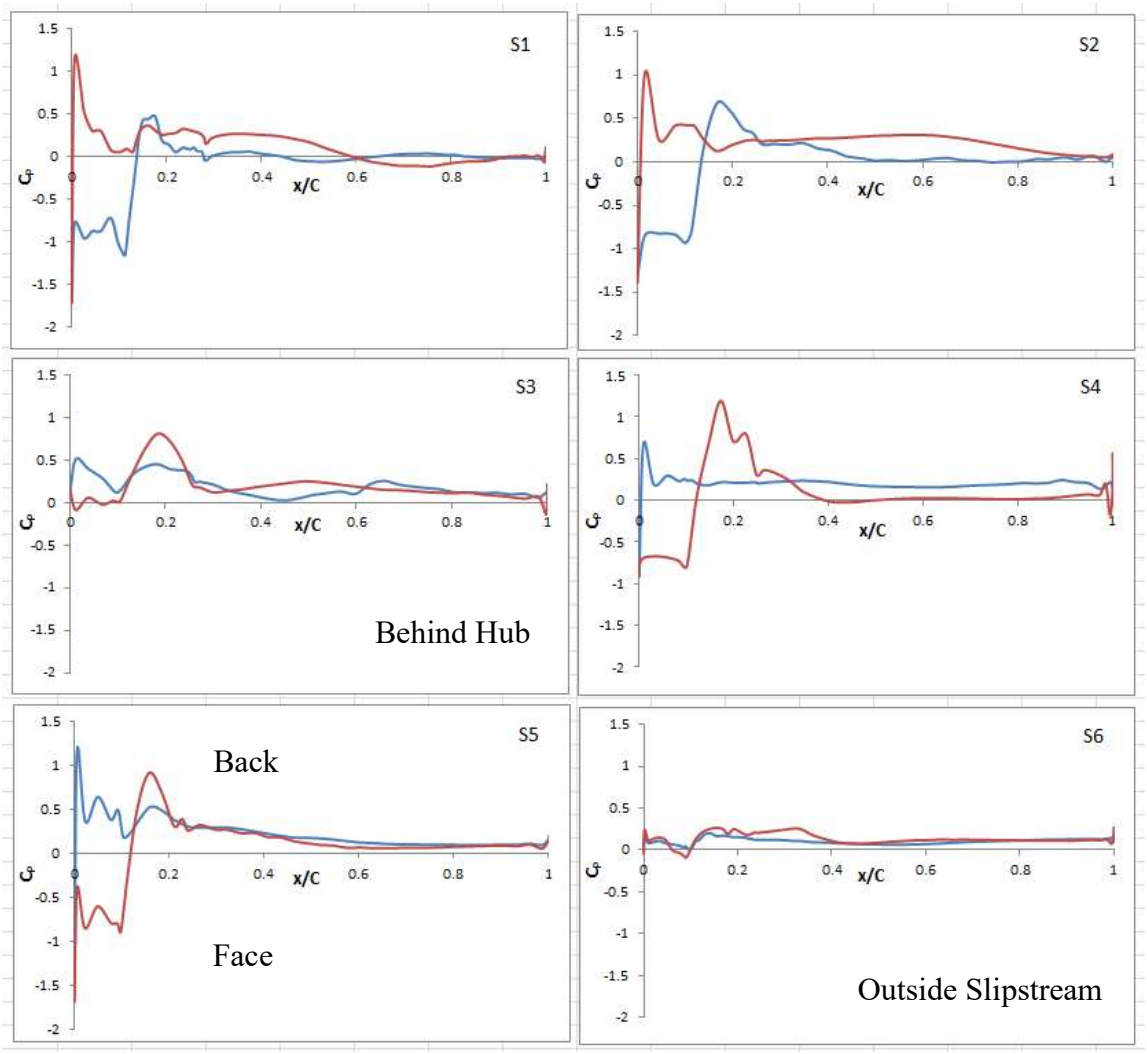

Figure 6-32 The *Princess Royal Propeller – Rudder Arrangement*: Chordwise pressure distribution at 6 spanwise positions for rudder (From top to bottom; S1-S6) (Red: Face, Blue: Back)

Figure 6-33 and Figure 6-34 show the tip vortex cavitation dynamics and resulting pressure distributions on each side of the rudder surface as viewed from the port and starboard side of the propeller-rudder system, respectively, and for different blade positions (varying from 330 deg to 60 deg). As shown in these figures while the TVC is approaching the rudder, it is rising before interacting with the rudder and the bifurcation due to the presence of the rudder is visible. Also the contrasting variation of the pressure due to the propeller's slipstream and the TVC transported at the upper and lower part of the rudder at each side can be clearly captured by the simulations.

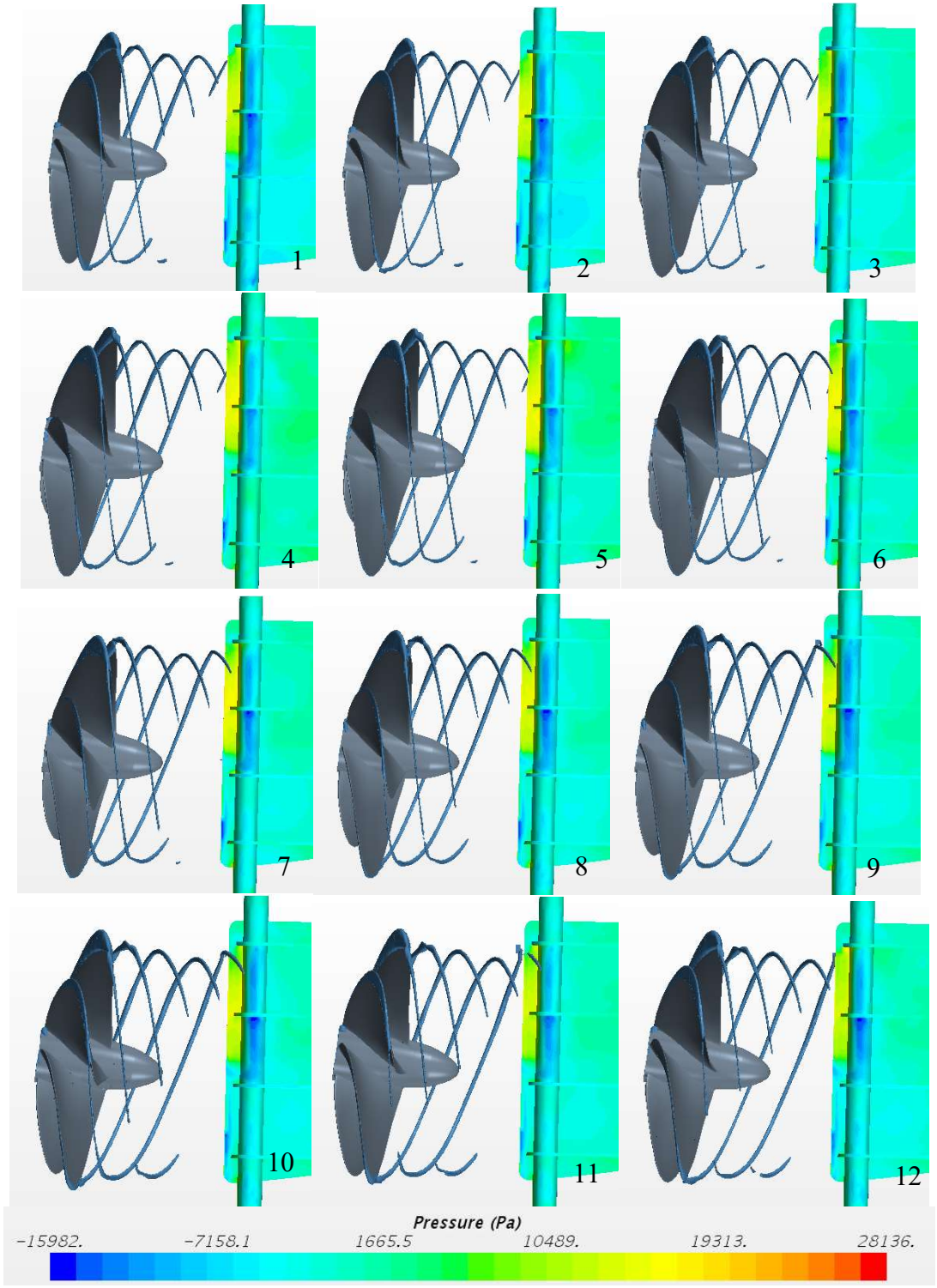

Figure 6-33 The *Princess Royal Propeller – Rudder Arrangement*: The deformation of the TVC in the presence of the rudder and pressure distribution on the rudder (Port side view)

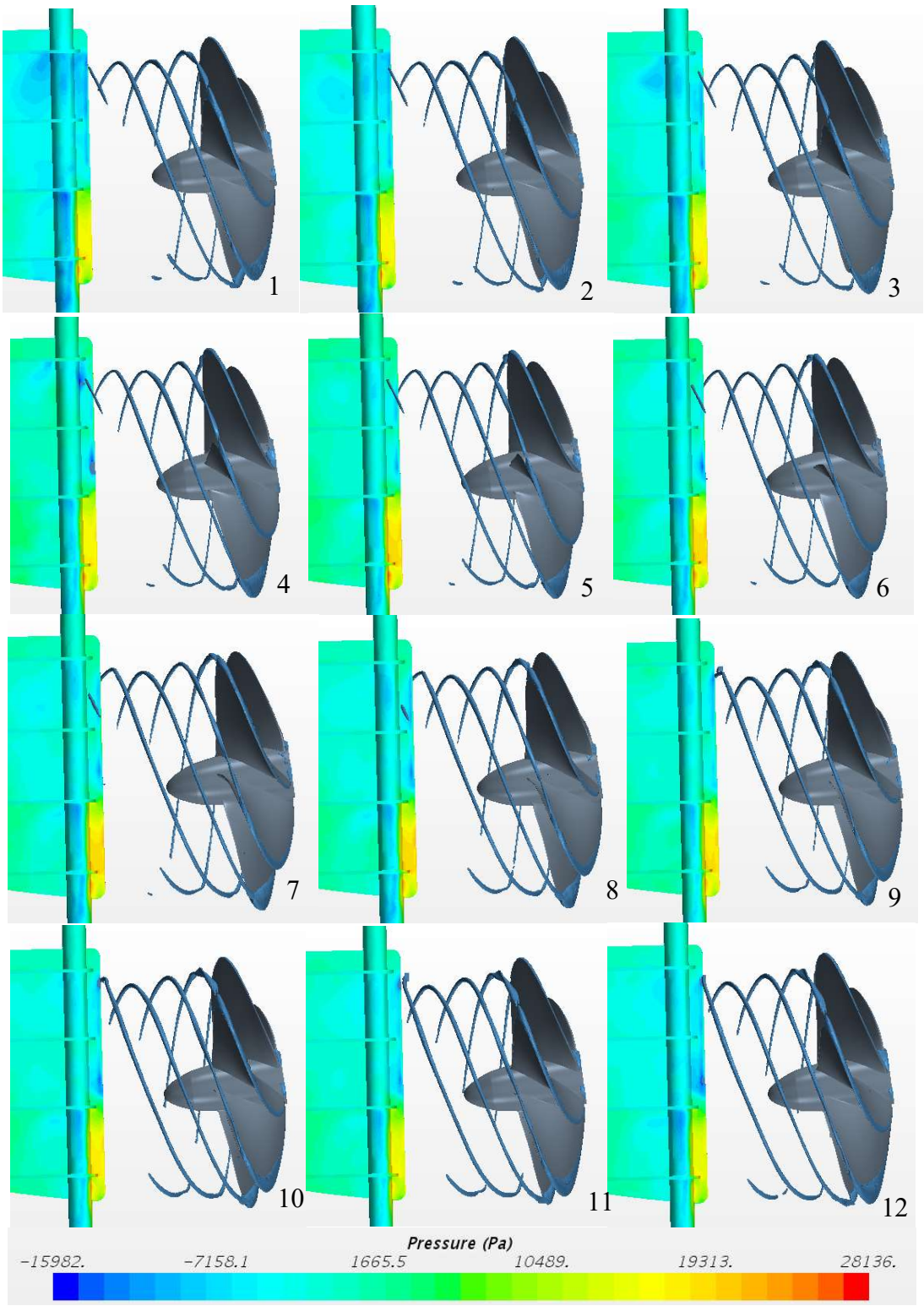

Figure 6-34 The Princess Royal Propeller – Rudder Arrangement: The deformation of the TVC in the presence of the rudder and pressure distribution on the rudder (Starboard side view)

6.6 Concluding Remarks

Chapter 6 investigated the effect of cavitation influence on the propeller-rudder interaction, in particular the effect of the tip vortex cavitation.

For this purpose two different propeller-rudder arrangements in model scale were documented and investigated. The first arrangement was that of a container ship propeller with a conventional rudder, which had aerofoil section, operating in uniform flow while the second arrangement, was that of *The Princess Royal* propeller with a flat section of rudder, operating with an inclined shaft in the presence of a simulated hull wake (non-uniform flow).

In simulating the propeller's action for the both arrangements the overset mesh method was used to model the rotational motions and to allow the extension of the cavitating tip vortex cores from the propeller tips through the rudders. This eliminated the data transfer problems associated with the sliding mesh approach. The newly developed mesh refinement technique MARCS was successfully applied for both propeller-rudder arangements to simulate the tip vortex cavity interacting with each rudder to capture the physics of the interaction accurately, in particular the tip vortex deformations in way of the rudders.

Good agreement was achieved between the CFD and EFD results for the propeller performance coefficients, especially for the prediction of K_T and sheet cavitation patterns, but particularly for the tip vortex cavitation patterns for both propeller-rudder combination simulations.

For the case of the container propeller with conventional rudder, the CFD predictions for the performance of the propeller showed good agreement with the experiments (EFD), in terms of K_T, for which the difference is less than 4%. However, K_Q could only be predicted within a %6.6 difference.

Cavitation tests (EFD) with the conventional rudder-propeller system showed the development of the TVCs from all blades combined with the sheet cavitation accentuated around the top dead centre due to the dynamometer strut and the wake

plate. The deformation of the tip vortices at the same region was also observed and this deformation was combined with the effect of the rudder in downstream resulting in the bifurcation of the tip vortex at the rudder leading edge. In spite of the accentuated sheet cavity dynamics at the wake shadow and deformation of the tip vortex at the rudder leading edge, the tip vortex cavitation was transported downstream through the propeller slipstream and the rudder without losing its strength. The CFD simulations were able to capture the above described cavitation dynamics in terms of the sheet cavitation and the TVC patterns including the deformation of the TVC trajectories approaching at the rudder leading edge.

For the case of *The Princess Royal* propeller-rudder arrangement, although the CFD predictions for the performance of the propeller showed good agreement with the experiments (EFD) in terms of K_T, for which the deviation is less than 2%, K_Q could only be predicted to within %6.7 deviation for the propeller-rudder interaction simulations. Furthermore, the new mesh adaption method showed better results for the tip vortex cavitation extent than the other mesh refinement approaches and the thrust and torque coefficients were calculated to be closer to the EFD results.

The action of *The Princess Royal*'s propeller was simulated with and without the rudder. This indicated that the CFD simulations could capture the TVC trajectories with a similar trend to the EFD observations in the presence of the rudder which displayed an initially contracting slipstream and its deformation on approaching the rudder leading edge. The comparative simulations with and without the rudder also captured the disappearance of the hub vortex cavitation due to the presence of the rudder as well as the increase in the propeller thrust and torque.

Despite there being available EFD data with regard to the pressure distributions on the rudder surfaces, the comparative CFD simulations with the two different propeller-rudder arrangements demonstrated the ability of the proposed approach to capture the physics of the propeller-rudder interaction with some anticipated details. These included the pressure variations of the two contrasting rudder sections (i.e. aerofoil section vs flat plate), the effect of the cylindrical rudder stock of *The Princess Royal* and tail end of the conventional rudder. Most noticeably the tool is able to capture the effect of the propeller slipstream and that of the transported TVC trajectories on the

pressure distribution of these rudder surfaces depending upon the blade positions in time that would be the most invaluable feedback for the cavitation erosion studies on rudders as discussed above in relation to Figure 6-19.

Chapter 7 Cavitation Influence on Propeller – Rudder – Hull Interaction

7.1 Introduction

The previous Chapter has concentrated on the cavitation influence on the propeller-rudder combination in model scale and without the actual presence of the hull. This Chapter includes the hull and investigates its combined effect in the model and full-scale by using The Princess Royal data. The main objective of this Chapter was to conduct CFD simulations to represent the physics of the propeller-rudder-hull system and their mutual interaction as realistically as possible within the limitations of the commercial CFD code (STAR-CCM+) used and the method developed (MARCS) in using the code.

To achieve the above objective, firstly, the cavitation tunnel tests conducted in the Depressurised Large Circulating Water Channel of CNR-INSEAN with the scaled model of The Princess Royal research vessel were simulated using the STAR-CCM+. The results are then compared with EFD data for one of the test conditions which displayed the strongest tip vortex cavitation presence. This is followed by further CFD simulations at full-scale for the cavitation performance of The Princess Royal, and these are compared with the full-scale results which were made available through the EU-FP7 Project SONIC.

Within the above framework, the Chapter first reviews the model test details including the test facility, model and test matrix. This is followed by the details of the CFD simulations including the computational domain, mesh generation, boundary conditions and simulation set-up. The Chapter next presents a review of the data for The Princess Royal full-scale trials and this is followed by the details of the full-scale CFD simulation, i.e. the description of the computational domain, mesh generation, boundary conditions and simulation set-up.

Having described the details of the EFD and CFD, the Chapter continues with the presentations and discussions of the results, first at model scale and then at full-scale by comparing the CFD simulation results with the EFD (model & full-scale) by mainly focusing on the cavitation simulations but also including the propeller performance and hull-pressures (in model scale). The Chapter finishes with concluding remarks based on the investigations conducted in this Chapter.

7.2 Model Scale Investigations

7.2.1 Experimental Fluid Dynamics Approach (EFD)

In order to expand the investigation of the propeller-rudder interaction further by including the effect of the hull, the natural candidate for the EFD data would be *The Princess Royal*'s data because of the Author's access to most of the data available for this vessel through the FP7-SONIC Project. Amongst the available data sources, it was specified that the model tests conducted in the Large Circulation Channel of CNR-INSEAN could be a good candidate to simulate in this research study due to the availability of a range of good visual observations of the cavitation patterns, especially with the tip vortex cavitation extensions downstream of the propeller. The EFD data from this facility also included the effect of the free surface.

In the following, therefore, a review of these model tests including the general descriptions of the CRN-INSEAN test facility, the model, test matrix and arrangements are presented based on the SONIC Project Report, (2012).

7.2.1.1 Review of Model Tests at CNR-INSEAN Facility

The Large Circulating Water Channel of CNR-INSEAN is a vertical plane, free surface, variable-pressure recirculating channel, having a capacity of 4 million of litres test water. The test section of the facility has 10 m length, 3.6 m width and 2.25 m maximum water depth. The facility is driven by two 4-bladed axial flow impellers operating in two separate and parallel trunks and developing a power of 435kW at 1500 rpm. The maximum water speed in the test section is 5.2 m/s. The facility can be

depressurized down to 30 mbar, by fitting a movable cover to the test section. Further information is available at www.insean.it. (Figure 7-1)

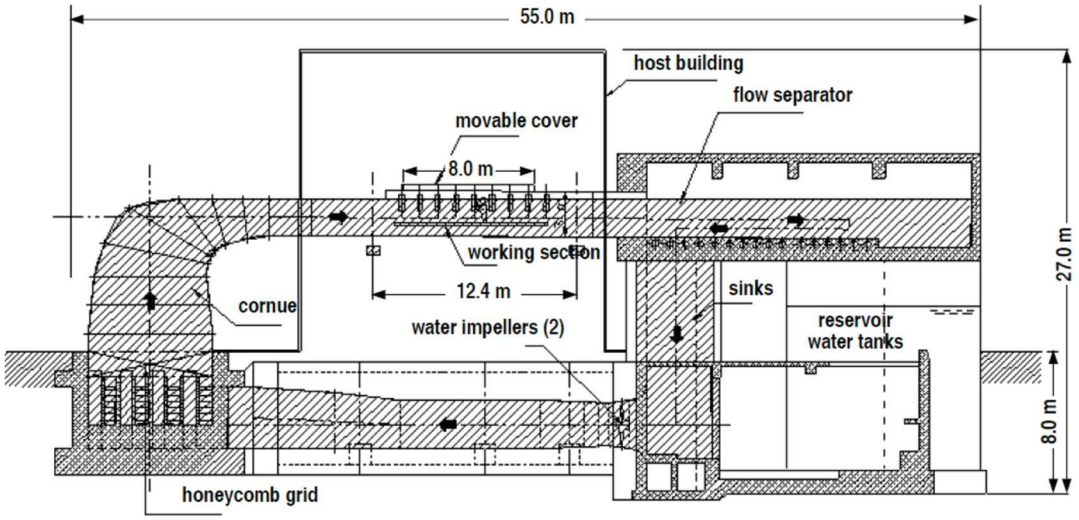

Figure 7-1 The Large Circulating Channel of CNR INSEAN

For the tests, one demi-hull of *The Princess Royal* vessel and its propeller were used in model scale with a scale factor $\lambda = 3.4$, by taking advantage of the symmetry principle for the catamaran configuration of this vessel. Figure 7-2 shows the demi-hull model, which was made from fiberglass and the aft end details of the model. Table 7-1 contains the general specifications of *The Princess Royal* in the full-scale and model scale.

Figure 7-2 The Princess Royal research Vessel and the Propeller

Table 7-1 General Specifications of the Princess Royal Research Vessel

	Full scale	Model scale
Length overall	18.88 m	5.55 m
Length between perpendiculars	16.45 m	4.84 m
breadth moulded at design waterline	7.03 m	2.07 m
breadth extreme	7.34 m	2.16 m
depth moulded	3.18 m	0.93 m
Demi-hull separation	4.9 (CL)	0.72 (to symmetry plane)
Draught (lightship) Amid	1.65 m	0.48 m
Draught (lightship) AP	1.70 m	0.5 m
Draught (lightship) FP	1.60 m	0.47 m
Number of propellers	2	1

The original test matrix was prepared using the four most representative and reliable runs of the full-scale trials selected by the SONIC project partners and which corresponded to the engine speeds of 600, 900, 1200 and 2000 rpm, with a reduction gear ratio of 1:1.75, as shown Table 7-2. In the table U is the cruising speed, V_M is the model testing velocity defined as $U/(\lambda)^{0.5}$, n is rotation speed of the propeller, J is the advance ratio defined as V_M/nD, where D is the propeller diameter, P_0 is the static pressure in the test section at the propeller immersion.

The cavitation tests were performed with an oxygen content of 0.25 mg/l, at a water temperature of about 14 °C.

Table 7-2 Test Matrix

Cond'	U [kn]	V_M [m/s]	n [rps]	J [-]	P_0 [mbar]	Description	Test type
1	4.775	1.33	10.53	0.57	70	Flow, propeller and motor perturbation	Acoustic measurements, hull pressure fluctuations, TR visualizations
2	7.1	1.98	15.80	0.57	80	Flow, propeller and motor perturbation	Acoustic measurements, hull pressure fluctuations, and TR visualizations
3	9.35	2.61	20.96	0.56	70	Flow, propeller and motor perturbation	Acoustic measurements, hull pressure fluctuations, and TR visualizations
4	10.53	2.94	26.31	0.51	75	Flow, propeller and motor perturbation	Acoustic measurements, hull pressure fluctuations, and TR visualizations

Cavitation observations were conducted using a high speed camera located as seen in Figure 7-3 and Figure 7-4. The model was set up according to the ITTC procedure 7.5-02-03-03.3 on "Cavitation Induced Pressure Fluctuation Model Scale Experiments" (ITTC, 2014). The model was equipped with a dedicated dynamometer for the measurement of thrust and torque although no records of the thrust and torque were taken during these tests. In addition, detailed flow measurements were undertaken to qualify the characteristics of the flow in the propeller region.

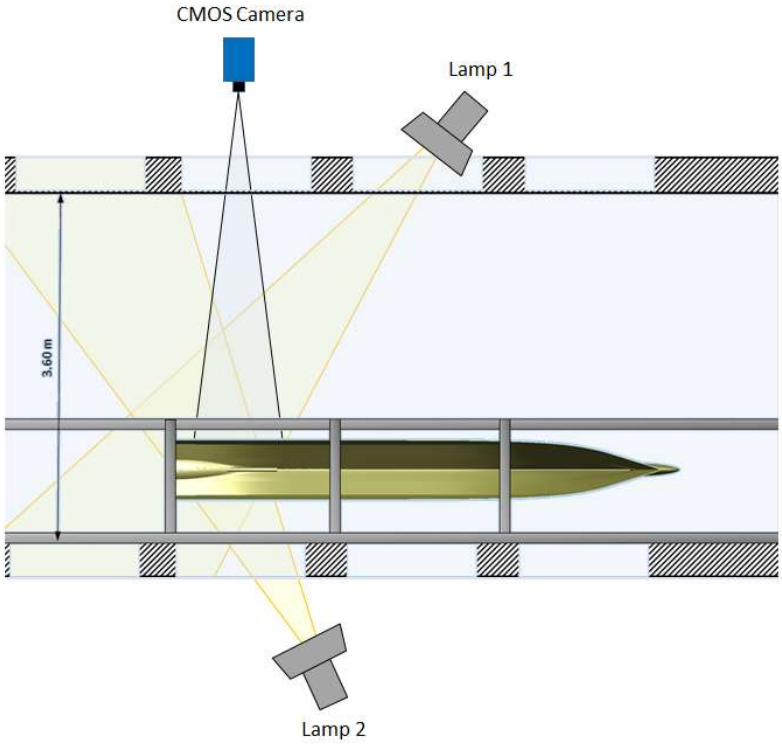

Figure 7-3 Stroscobic lights and camera arrangement

Figure 7-4 Cavitation observations: set up arrangement

The model tests also included measurement of fluctuating hull pressure at seven locations as shown in Figure 7-5.

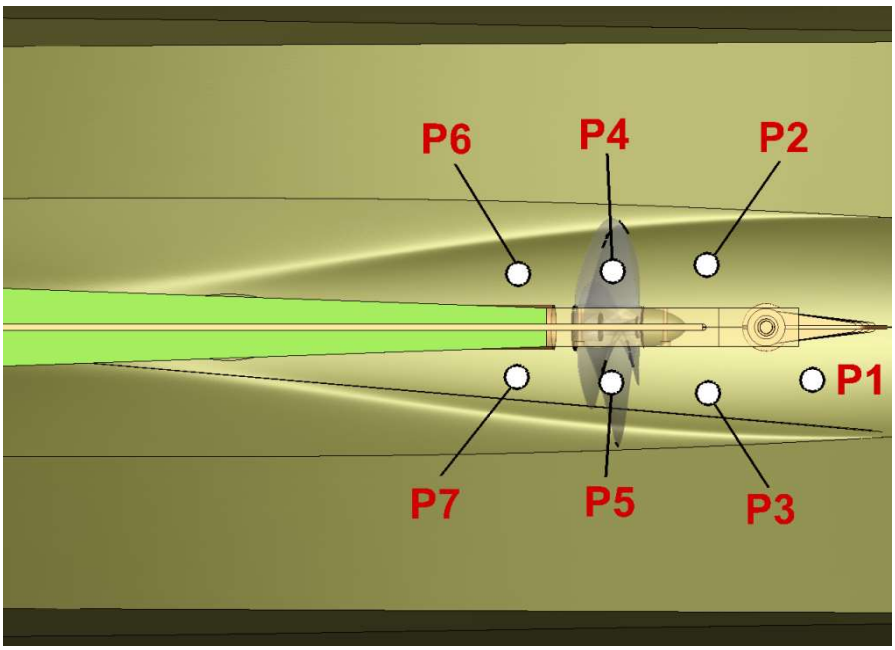

Figure 7-5 Nomenclature of Pressure sensors and relative position (SONIC Project Report, 2012)

7.2.2 Computational Fluid Dynamics Approach (CFD)

Amongst the four test conditions given in Table 7-2 “Condition 3”, which presented one of the strongest tip vortex cavitation dynamics scenarios, was selected to simulate using CFD.

During the simulation, *The Princess Royal* model and the test section details were represented as precise as possible in terms of their dimensions, location of the hull in the cavitation tunnel test section and test conditions which included the inflow speed, propeller shaft speed and tunnel free surface height, tunnel reference pressure, saturated vapour pressure and fluid temperature etc. for the proper validation study.

7.2.2.1 Computational domain

The hull geometry was placed in the computational flow domain as shown in Figure 7-6. This Figure also presents the test facility coordinate system with its origin located on the tunnel free surface at a 2.25m water depth in static condition. The hull geometry was located nearer to the right side of the tunnel with the breadth of the flow domain being 3.6m in total. The forward (inlet) boundary and aft (outlet) boundary of the computational domain was set at a distance of 2.5m from the bow of the ship and 2.0m from the aft of the ship, respectively.

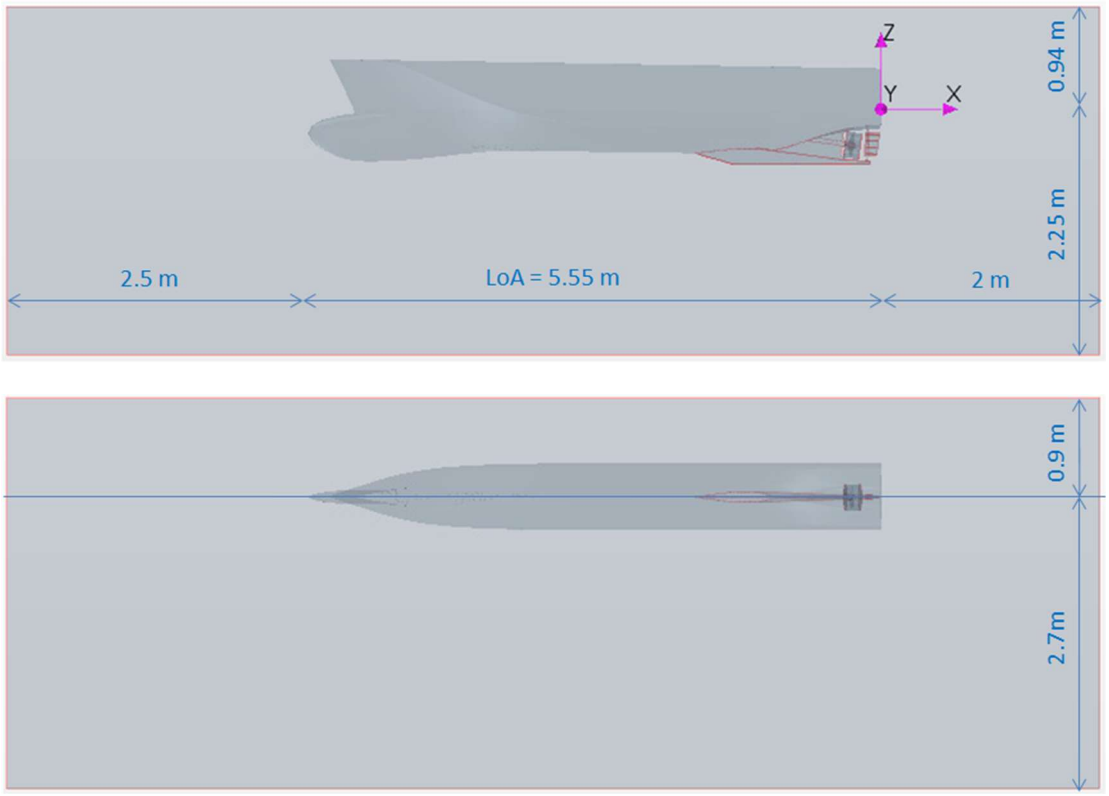

Figure 7-6 Computational Flow Domain Dimensions (Model Scale)

The computational flow domain for the simulations included a rotating region, which was represented by the sliding and overset mesh, and a stationary region to represent the background as shown in Figure 7-7. While the rotating region included the propeller geometry, the background region covered the hull, keel and rudder geometries. The overset region was prepared to cover the rudder geometry to be able to transfer the data (tip vortices) from the propeller blades through the rudder. Only one overset region, which covered the propeller and rudder geometries at the same time, could not be prepared and simulated for this case due to surface interaction problems between the propeller shaft and hull geometries causing overset mesh issues. In order to eliminate this kind of meshing problem and divergence, a combined rotation model (sliding mesh and overset mesh) was used while both regions were rotating with the propeller speed.

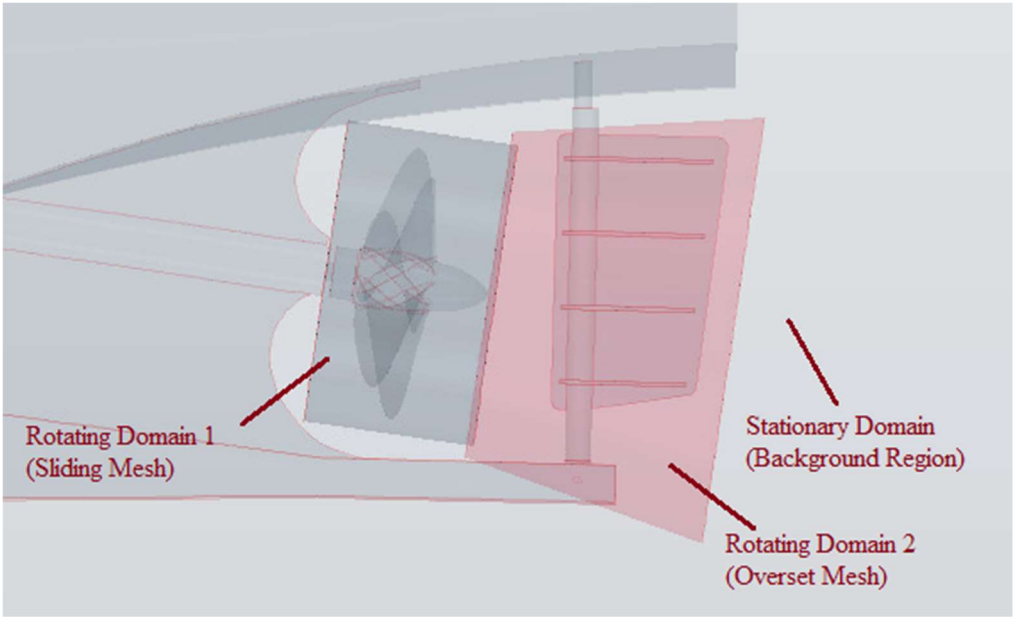

Figure 7-7 The Flow domain including Rotating (Sliding and Overset Mesh) and Stationary (Background) regions (Model Scale)

7.2.2.2 Mesh Generation

The MARCS method with its modified version, as presented in Chapter 6, had to be used for the simulation in order to compute the tip vortex cavitation trajectories from the propeller blades throughout the length of the rudder.

In order to apply MARCS, first the sheet cavitation simulations were conducted using a coarser mesh. This allowed for the specification of a region by applying the Q-Criterion, to define the zone where the vortices were identified, thus generating the pink region as shown in Figure 7-8. Then, using MARCS, a field function was created to generate finer meshes where the Q-Criterion was above 10000 [s^{-2}] for the simulation.

The details of the generated mesh for the sheet and tip vortex cavitation (with MARCS) simulations are shown in Table 7-3. For further details of the mesh generation, Table 7-4 is also included to show the number of cells for the tip vortex cavitation simulations regarding the different computational regions in the flow domain.

Finally, Figure 7-9 shows the mesh distribution generated in using MARCS for the tip vortex cavitation simulations.

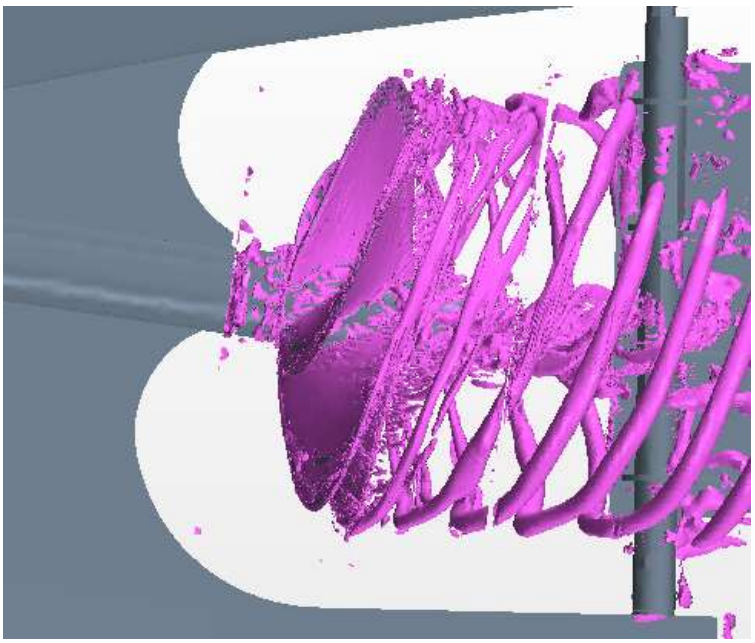

Figure 7-8 Isosurface of Q-Criterion = 10000 s^{-2} (Side view) (Model Scale)

Table 7-3 Mesh Details for the *Princess Royal* propeller-rudder-hull arrangement (Model Scale)

Mesh Details	**Sheet**	**Tip Vortex (MARCS)**	**Unit**
Surface Size (Blade)	0.5/1.5	0.5/1.5	[mm]
Surface Size (Refinement)	1.0	0.25	[mm]
Number of Cells	21,119,336	49,664,725	[-]

Table 7-4 Mesh Details for the different computational regions (Model Scale)

Number of Cells	**Tip Vortex (MARCS)**
Background Region	12,304,225
Rotating Region (Sliding Mesh)	17,507,880
Rotating Region (Overset Mesh)	19,852,620

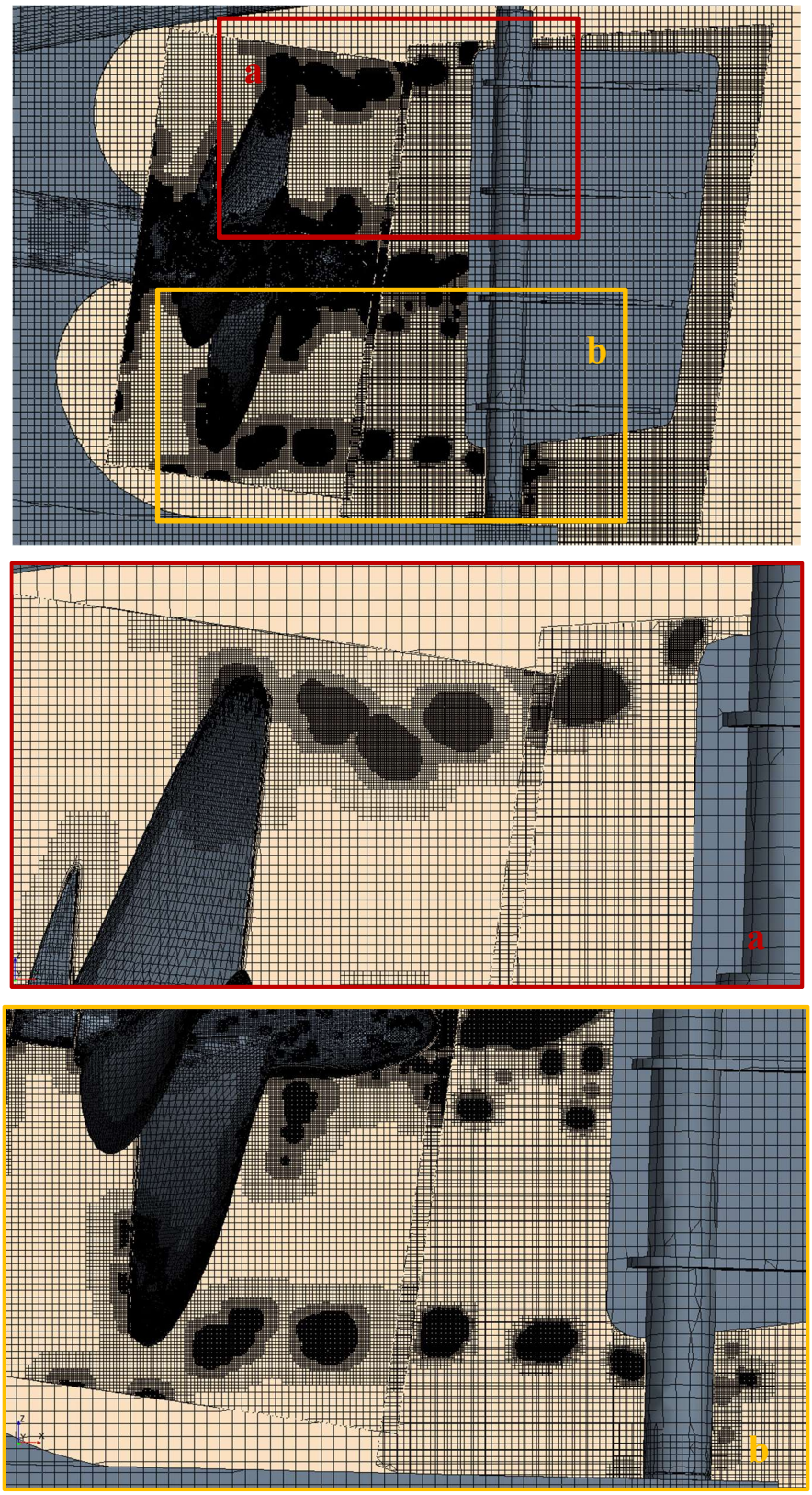

Figure 7-9 Generated mesh using MARCS (Model Scale)

7.2.2.3 Simulation Setup and Boundary Conditions

For the simulations, by considering the presence of the free surface in the testing facility, two different type fluids (water and air) and two different flow phases (water and vapour) had to be modelled. While the free surface was defined between the water and air, a multiphase interaction was described between the water and vapour phases for modelling cavitation.

Similar to the previous simulations, the cavitation was modelled using the Schnerr–Sauer cavitation model while the turbulence was modelled using the LES model.

The time step value was $5x10^{-5}$s, which means 954.198 time steps per revolution (i.e. for a rotational speed of 20.96 rps; time per revolution is 0.0477s or angular blade displacement of 0.377 degree per time step).

As stated earlier, a combined rotation system, which consisted of the sliding mesh region (including the propeller) and the overset mesh region (including the rudder), was used for modelling the rotational motion.

Besides the inlet (velocity inlet) and outlet (pressure outlet) patches of the flow domain, other tunnel walls were described as the "wall" boundary conditions to introduce the wall effect of the cavitation tunnel in accelerating the flow around the hull, propeller and rudder geometries as shown in Figure 7-10.

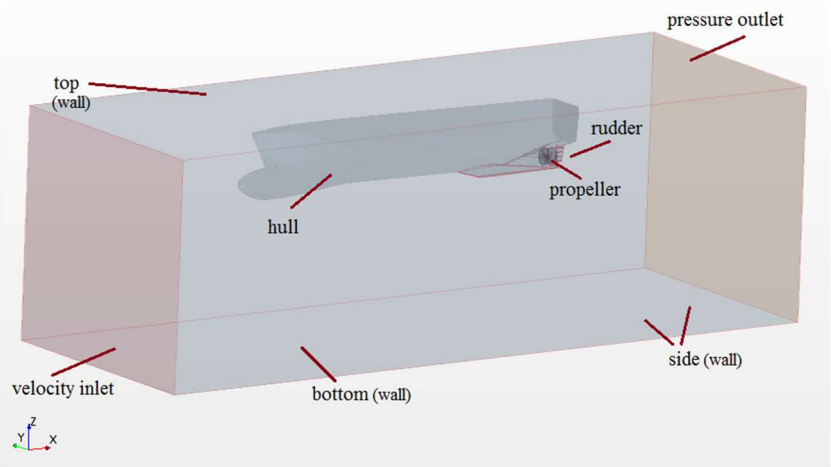

Figure 7-10 Boundary Conditions (Model Scale)

As stated earlier, the fluctuating hull pressures data were also measured during the model tests. In order to validate the pressure data to be predicted from the CFD simulations, probes (calculation points) were placed at the points corresponding to the experimental pressure pick-up points, as shown in Figure 7-5 and with the coordinates of each probe listed in Table 7-5. During the simulations the pressure data were collected from these probes in solution time by using the sheet cavitation simulations.

Table 7-5 Exact positions of the each pressure sensor

(According to Laboratory Coordinate system)

Pressure Sensors	Position (Laboratory Coordinate System)		
	X	Y	Z
P1	-0.05875	0.05101	-0.157
P2	-0.18318	-0.04991	-0.169
P3	-0.18318	0.04991	-0.170
P4	-0.24886	-0.04768	-0.178
P5	-0.24886	0.04768	-0.178
P6	-0.36515	-0.04173	-0.200
P7	-0.36515	0.04173	-0.200

Based upon the above described computational set up, the CFD simulations were conducted for "Condition-3" by following the procedure, which is shown schematically in Figure 7-11, and described in the following steps:

Step 1: Simulations start without the propeller's action and with relatively higher time step ($1x10^{-2}$s) values than those to be used for the propeller cavitation simulations. This approach provides the simulations are being converged regarding the total resistance of the ship in a short period of time, and prevents the potential divergence due to higher time step values to be used with the propeller's action.

Step 2: After the total resistance is converged, the propeller rotation is activated with the full revolution of the propeller and reduced time step ($1x10^{-3}$s). This is followed by a waiting period until the propeller thrust and torque converge.

Step 3: When the thrust and torque have converged, the propeller cavitation is activated by changing the Scaling Factor + (Chapter 3 – Equation 3.15) from 0.0 to 1.0 for simulating the cavitation with a smaller time step ($5x10^{-5}$s). Following the activation of the cavitation, the simulations are run until the sheet cavitation on the propeller blade surfaces becomes stable. Although, the cavitation dynamics can still be unsteady due to the complex flow characteristics, such as oblique flow and the presence of the hull (wake), etc., the sheet cavitation on the blade surface must be stable for the same blade positions during each rotation.

Step 4: Having established the stable state of the sheet cavitation, the MARCS procedure is applied for mesh refinement in the propeller slipstream through to the rudder, and the refined mesh is generated.

Step 5: Finally, the simulation is run using the same time step value with the refined mesh, for at least four propeller revolutions, until all the hydrodynamic outputs, such as ship resistance, propeller thrust and torque have converged. During the simulations, tip vortex cavitation will be starting to develop with the effect of the mesh refinement in the solution time.

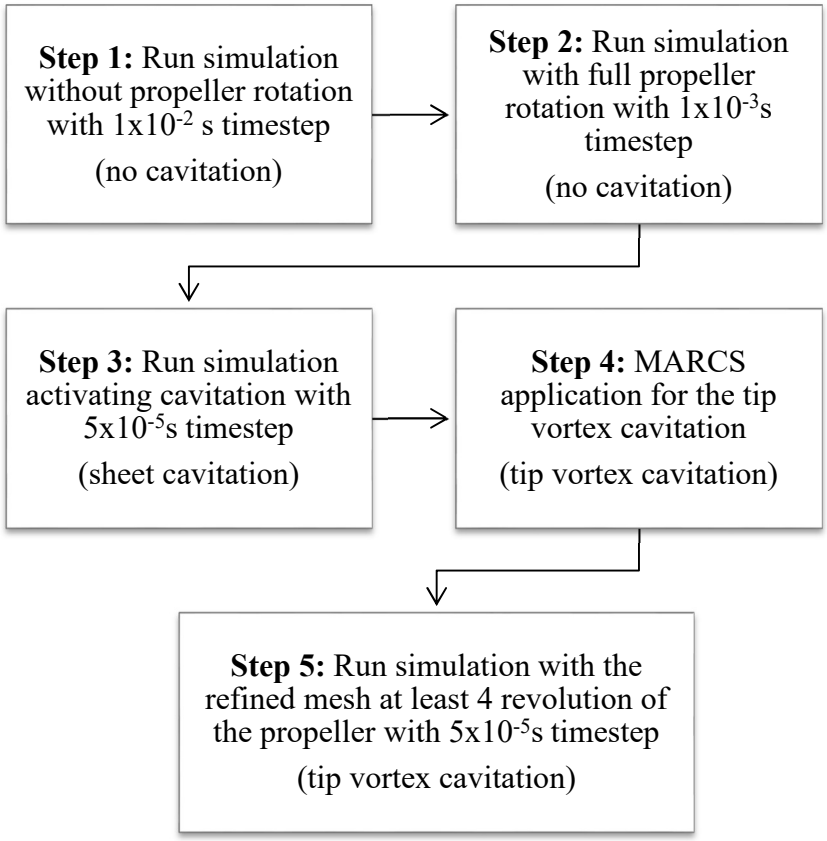

Figure 7-11 Flow chart summarising Simulation Procedure in the presence of the tip vortex cavitation (MARCS application)

7.3 Full Scale Investigations

7.3.1 Experimental Fluid Dynamics Approach (EFD) – Review of Full-Scale Trials

As stated earlier, and part of the SONIC Project, full-scale sea trials were conducted using *The Princess Royal*. The trials involved the recording of the cavitation observations from the dedicated observation windows (port holes) above each propeller of the vessel, together with propeller excited vibration measurements as well as off-board, under-water radiated noise measurements. The detailed cavitation observations were undertaken during the trials at four different operating conditions as listed in Table 7-6 by using three different cameras providing an understanding of the dynamics of the cavitation phenomena (Sampson et al., 2015).

For the full-scale simulation attempt, it was decided to use "Condition 4" which produced the strongest tip vortex cavitation dynamics at the ship and model scale and hence was the most suited to CFD modelling of developed cavitation.

Table 7-6 Full Scale Operating Conditions from *The Princess Royal* Sea Trials

Cond'	Engine RPM	Propeller RPM	Vs (knot)	V_A (m/s)	Torque (kNm)	$10K_Q$ (-)	K_T (-)
1	600	342.800	4.775	2.171	0.300	0.378	0.187
2	900	514.200	7.100	3.267	0.600	0.336	0.186
3	1200	682.100	9.350	4.348	1.000	0.318	0.185
4	2000	1141.500	15.108	7.181	2.800	0.318	0.188

7.3.2 Computational Fluid Dynamics Approach (CFD)

For the full-scale CFD simulations, *The Princess Royal*'s entire geometrical details of a demi-hull and "Condition 4" were modelled as truely as possible for the best representation of the sea trials for this operating condition.

In the following the details of the computational domain, mesh generation, simulation setup and boundary conditions are described.

7.3.2.1 Computational domain

The computational flow domain was prepared for the simulations based on the dimensions presented in Figure 7-12. The demi-hull vessel was placed at a horizontal distance of 1.5L and 2L from the inlet and outlet patches, respectively. As in the model scale simulations, the flow domain included a combined rotating region with the sliding and overset meshes and the stationary region for the background, as shown, in Figure 7-13.

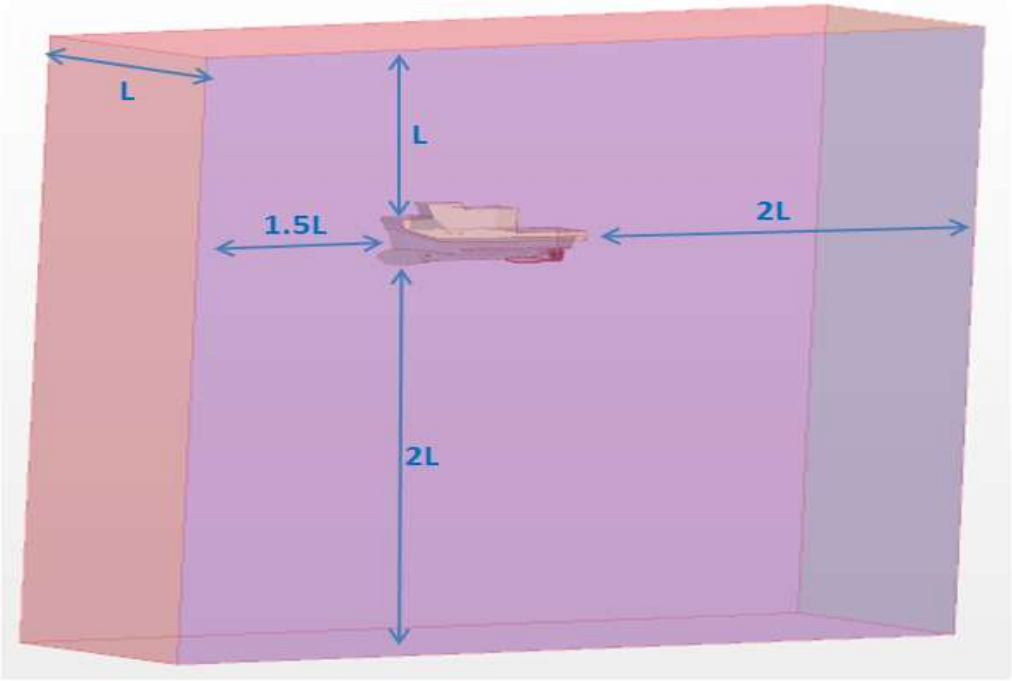

Figure 7-12 Computational Flow Domain (Full Scale)

However, in contrast to the model scale simulations, while the sliding mesh region was extended, the overset region was narrowed downstream of the propeller. This was to improve the tip vortex cavitation extension in the sliding mesh region and to reduce the total number of cells for the full-scale simulations which can be appreciated by comparing Figure 7-7 and Figure 7-13.

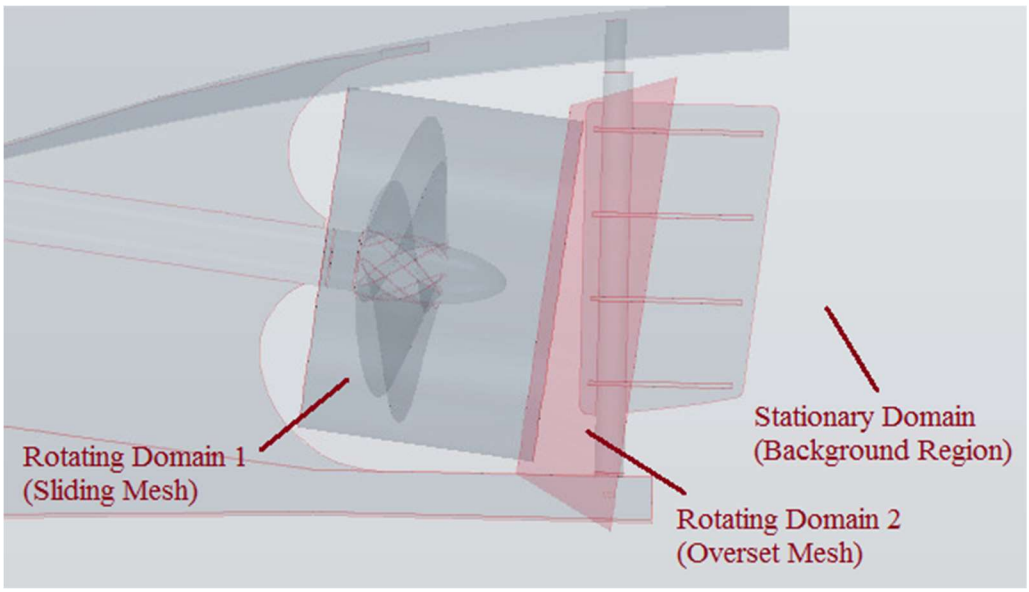

Figure 7-13 Flow domain including Rotating (Sliding and Overset Mesh) and Stationary (Background) regions (Full Scale)

7.3.2.2 Mesh Generation

The MARCS approach was also applied for the mesh generation of the tip vortex cavitation simulations in the full-scale. While Figure 7-14 presents the iso-surface of Q-Criterion (above $10000s^{-2}$), the details of the generated mesh are given in Table 7-7.

Although scale effects are not the main interest of this research study, the surface size of the refinement region, which is quite important for modelling tip vortex cavitation, has been scaled up 3 times from the model-scale to full-scale, while the geometric scale ratio (λ) was 3.4 for the model tests of *The Princess Royal* (see Table 7-3 and Table 7-7).

For further details of the mesh generation, while Table 7-8 presents the number of cells for the different computational regions in the flow domain, the generated mesh using the MARCS approach are shown in Figure 7-15.

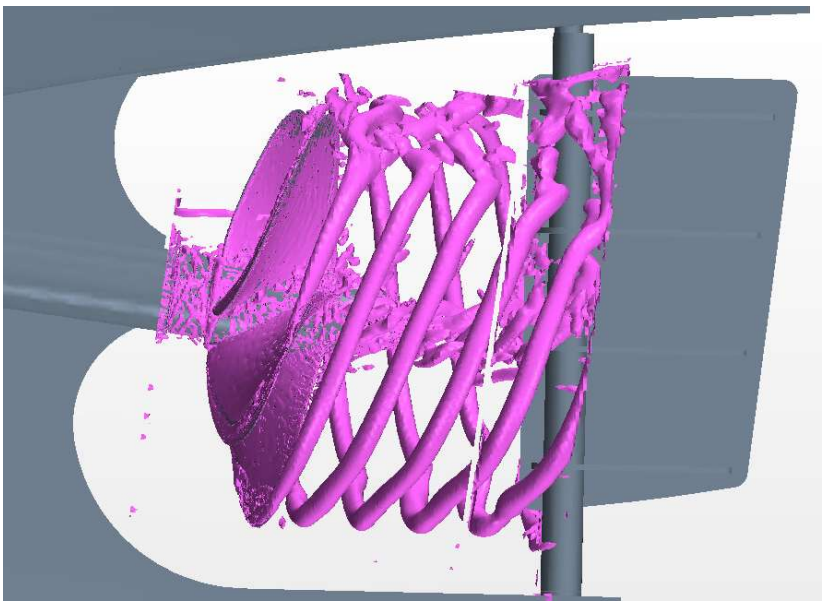

Figure 7-14 The *Princess Royal Propeller-Rudder-Hull Interaction:* Isosurface of Q-Criterion = 10000 s^{-2} (Side view) (Full Scale)

Table 7-7 Mesh Details for the *Princess Royal* propeller-rudder-hull arrangement (Full Scale)

Mesh Details	**Sheet**	**Tip Vortex (MARCS)**	**Unit**
Surface Size (Blade)	0.5/1.5	0.5/1.5	[mm]
Surface Size (Refinement)	6.0	0.75	[mm]
Number of Cells	12,114,473	74,717,905	[-]

Table 7-8 Mesh Details for the different computational regions (Full Scale)

Number of Cells	**Tip Vortex (MARCS)**
Background Region	8,156,727
Rotating Region	41,251,818
Overset Region	25,309,360

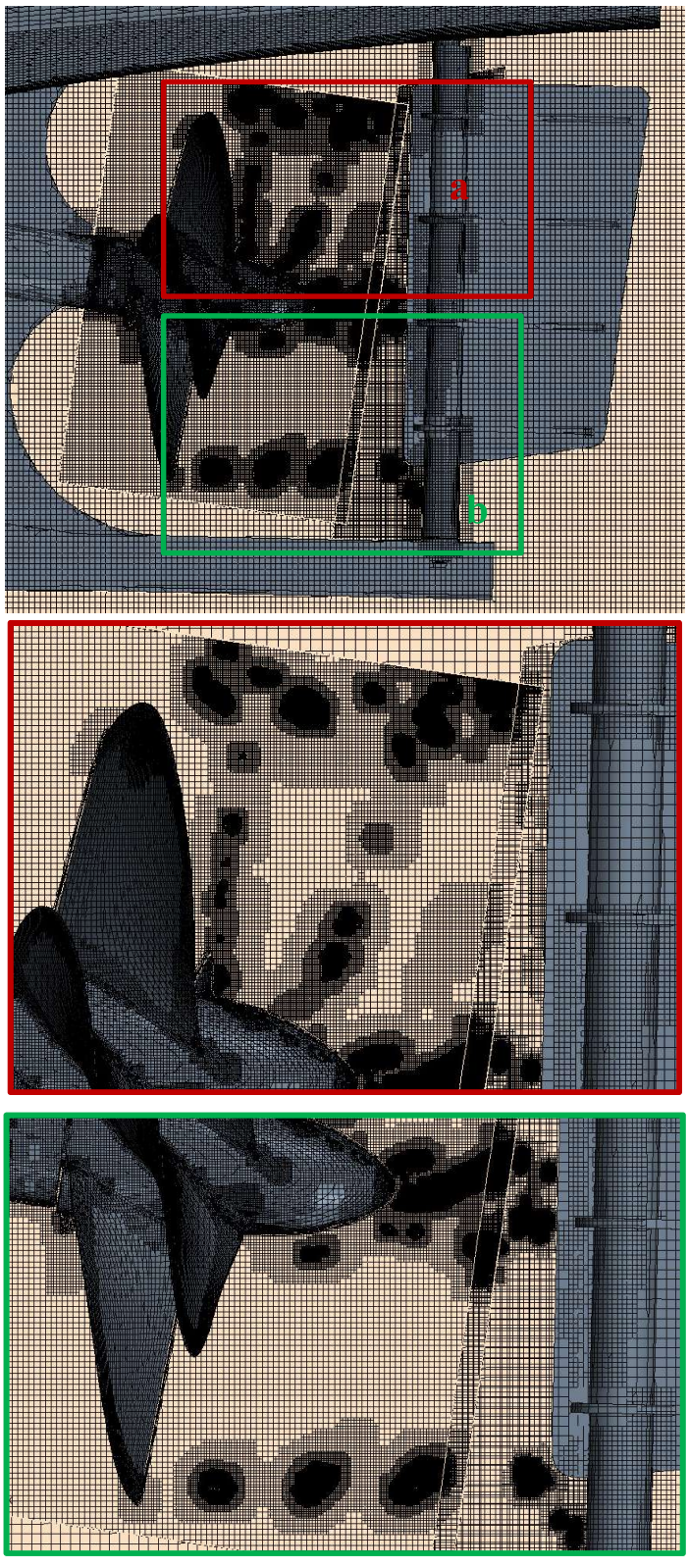

Figure 7-15 Generated mesh using MARCS (Full Scale)

7.3.2.3 Simulation Setup and Boundary Conditions

Similar to the model scale simulations, the presence of the free surface was included in the simulation setup for the full-scale simulations.

The cavitation was modelled using the Schnerr–Sauer cavitation model while the turbulence using the LES model.

The time step value was $5x10^{-5}$s, which means 1051.248 time steps per revolution (i.e. for a rotational speed of 19.025 rps; time per revolution is 0.0525s or angular blade displacement of 0.342 degree per time step).

Similar to the model scale simulations, a combined rotation system, which consisted of the sliding mesh region (including the propeller) and the overset mesh region (including a small part of the rudder), were used for modelling the rotational motion (Figure 7-13).

In contrast to the model scale simulations, besides the inlet (velocity inlet) and outlet (pressure outlet) patches of the flow domain, other 3 domain patches (side, top and bottom) were described as the "velocity-inlet" boundary conditions, as shown in Figure 7-16. The other side patch was set as the "symmetry" boundary condition since only one demi-hull was simulated of the catamaran vessel using the symmetry boundary condition in order to reduce the total number of cells.

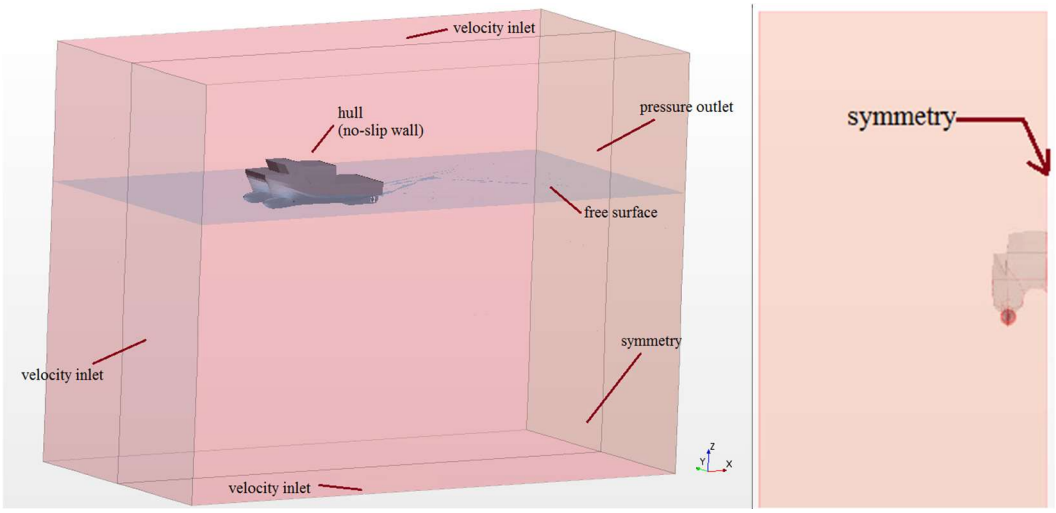

Figure 7-16 Boundary Conditions (Full Scale) (Left; Perspective view, Right; Front view)

Based upon the above described computational set up, the CFD simulations were conducted for "Condition 4" by following the same procedure for the model scale simulations in Section 7.2.2.3 and shown schematically in Figure 7-11.

7.4 Results and Discussions

In the following two sections the results of the CFD simulations in the model and full-scale are presented and discussed, separately in each section, including their comparisons with the EFD data.

7.4.1 Model Scale Investigations

In this section the simulation results for "Condition 3" are presented and discussed regarding the cavitation dynamics, hull pressure fluctuations and propeller hydrodynamic performance coefficients including the comparison with the EFD data.

The CFD predictions for the propeller performance are presented in the INSEAN facility were simulated based on the full-scale vessel speed and shaft revolution while no measurements were taken for the thrust and torque. The results in Table 7-9, therefore, only include the CFD prediction as the output.

Table 7-9 Hydrodynamic Propeller Performance for Propeller-Rudder-Hull Interaction (Model Scale)

Cond'	Method	K_T	$10K_Q$
3	CFD – Model Scale	0.183	0.267
	EFD – Model Scale	N/A	N/A

Figure 7-17 demonstrates how the free surface was presented in CFD model by displaying the volume fraction of air and water on the hull surfaces.

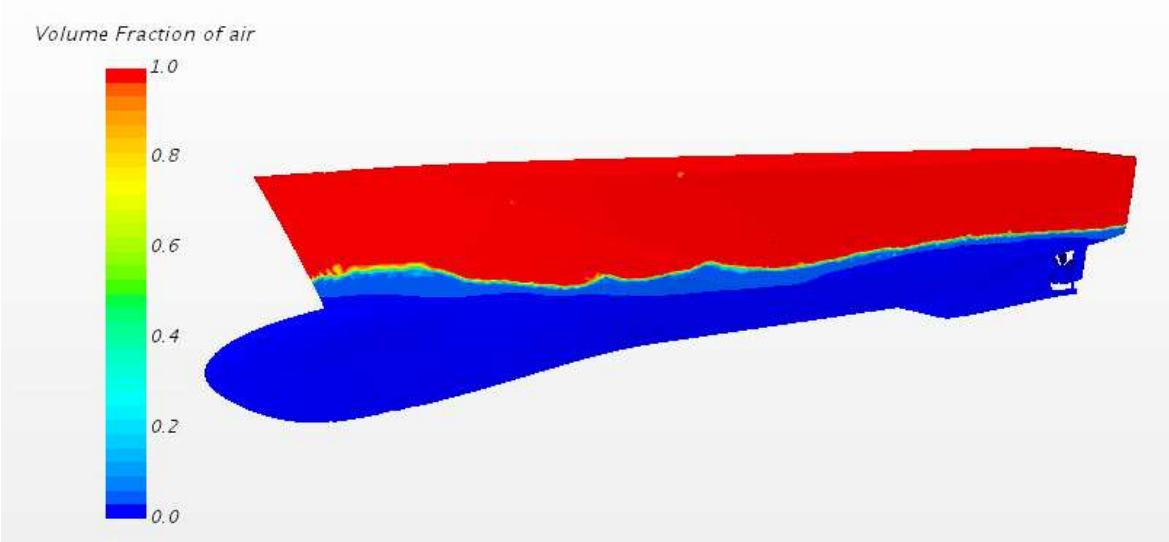

Figure 7-17 Free surface representation (Model-Scale)

For the cavitation investigations, Figure 7-18 and Figure 7-19 are included to compare the EFD recorded images with the CFD predicted images, respectively.

By concentrating on the EFD images, as shown in Figure 7-18, these twelve consecutive images were captured for the respective blade position moving from approximately θ = -10° to θ=40° (with θ=0° at TDC) to characterise the cavitation patterns observed. As shown in these images, while the tip vortex cavitation was observed at the all blade positions, in some blade passages a weak trace of the sheet cavitation was visible in a larger range of angular positions, even if its extent appeared to be much smaller. Tip vortex cavitation was observed much destabilized when the blades were meeting the hull perturbation, around the positions at 0° and 180° (in the

skeg wake shadow). Some amount of cavitation was also observed on the rudder surface (SONIC project report, 2012).

By concentrating on the CFD predicted images for the corresponding positions, as shown in Figure 7-20, similar cavitation patterns can be also observed, in general, and particularly for the tip vortex cavitation. Although both sheet and tip vortex cavitation were simulated by CFD, only the tip vortex cavitation extension could be compared with the EFD due to the lack of detailed experimental images for the sheet cavitation pattern.

As far as the tip vortex cavitation is concerned, despite the TVC being extended up to the rudder, thanks to the application of MARCS, the traces of the TVC could not be fully developed throughout the rudder. This lack of precision in the modelling can be explained with the nature of the dynamics of the TVC which can be observed from the experimental images where the tip vortices were losing their strengths as they approached the rudder, as observed in Figure 7-18. This may cause the disappearance of the tip vortices and hence a smaller surface mesh size would be needed in the refinement region in the CFD calculations to be able to capture the TVC while they are losing their strength as they approach to the leading edge of the rudder.

As shown in Figure 7-18 and Figure 7-19, it was concluded that the TVC could not be extended due to the interface problem between sliding mesh and overset mesh regions at some propeller blade positions although a combined system was used to try to eliminate this problem. The extra cavitating bubbles which were produced at the interface surface between the sliding mesh and the overset regions due to the mesh refinement with the small mesh surfaces on the interface were also observed in Figure 7-19. Unfortunately, these extra cavitating bubbles do not reflect the reality.

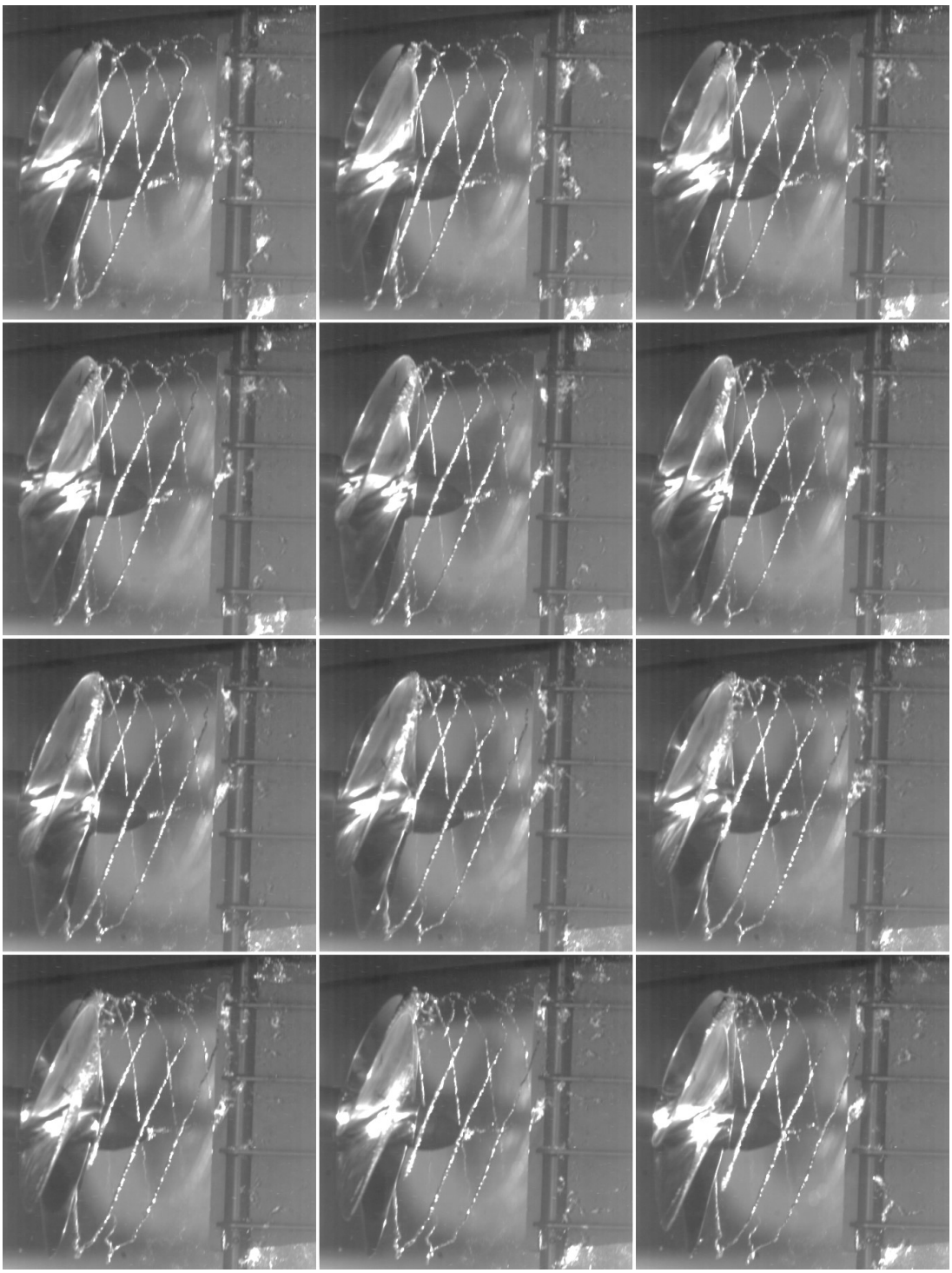

Figure 7-18 EFD Results - Cavitation observations @ V_M=2.61 m/s and n=20.96 rps (Model Scale)

Figure 7-19 CFD Results - Cavitation Patterns including tip vortex cavitation

(Model Scale)

In order to provide more focused comparison of the TVC trajectories, Figure 7-20 is included, for an overlapped comparison of the EFD and CFD results at 2 different blade positions of the propeller. In this figure, the experimental images are placed in the background, while the CFD results are brought forward. As shown in these comparative images, in spite of the under predicted tip vortex cavitation extension by the CFD, the correct trajectories of the tip vortex cavitation in the propeller's downstream is obvious confirming the ability of the MARCS mesh refinement technique when including the effect of the non-uniform hull flow.

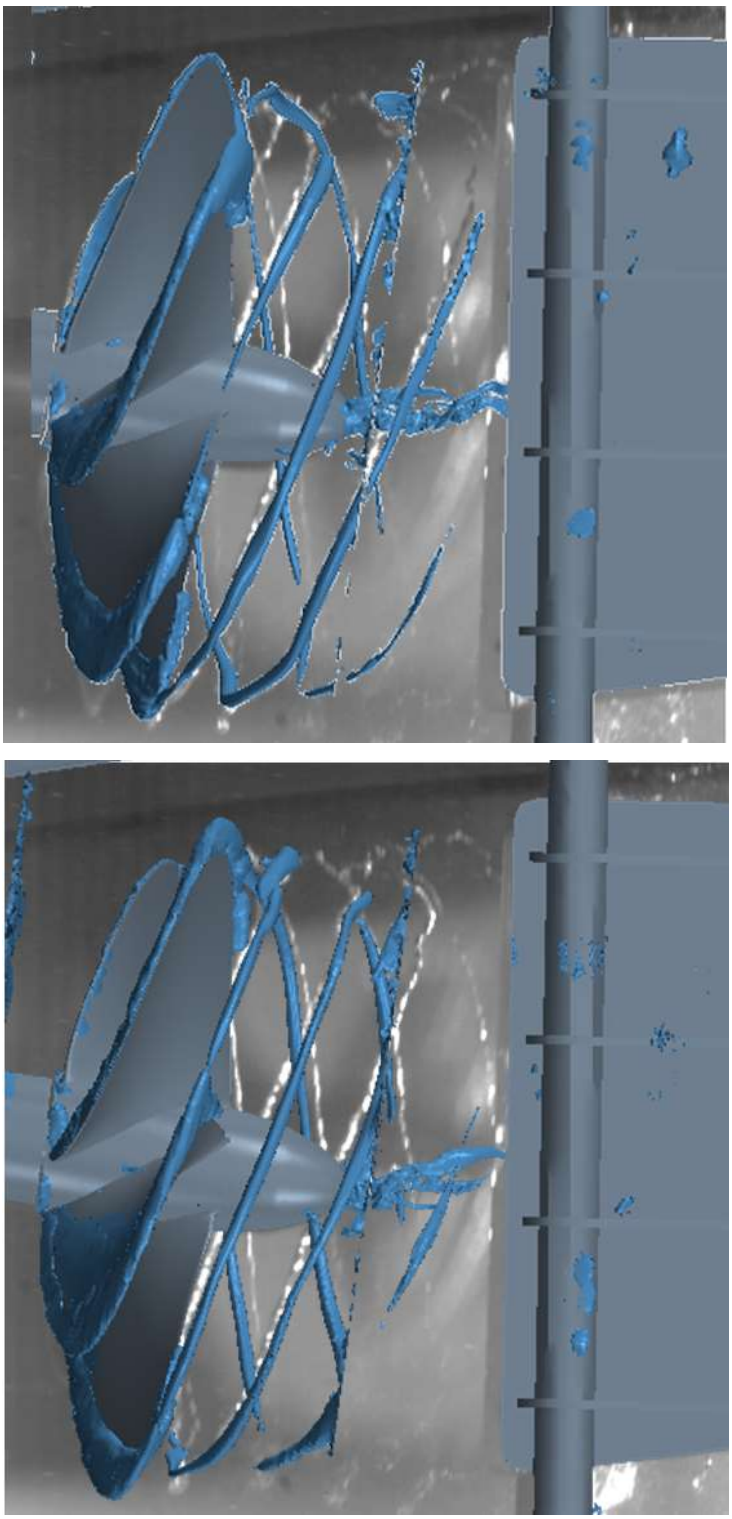

Figure 7-20 Cavitation pattern Comparisons (Model Scale) between EFD and CFD (Backward; EFD, Forward; CFD) (MARCS - tip vortex cavitation)

Based on the CFD simulations, Figure 7-21 and Figure 7-22 are also included to show the increase in the volume of cavitation due to the better modelling of the tip and hub vortex cavitation. While Figure 7-21 illustrates the predicted cavitation patterns using the coarse mesh on the left and the MARCS on the right, respectively, Figure 7-22 shows the impact of the increased cavity volume due to the tip vortex and hub vortex cavitation, using the MARCS.

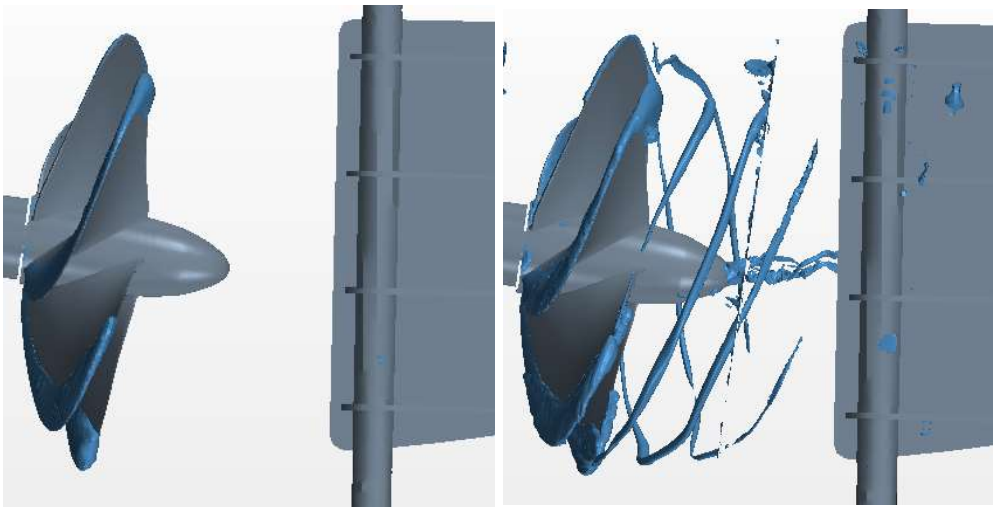

Figure 7-21 CFD Results- Cavitation pattern (Left; Sheet Cavitation, Right; tip vortex cavitation (MARCS) (Model Scale)

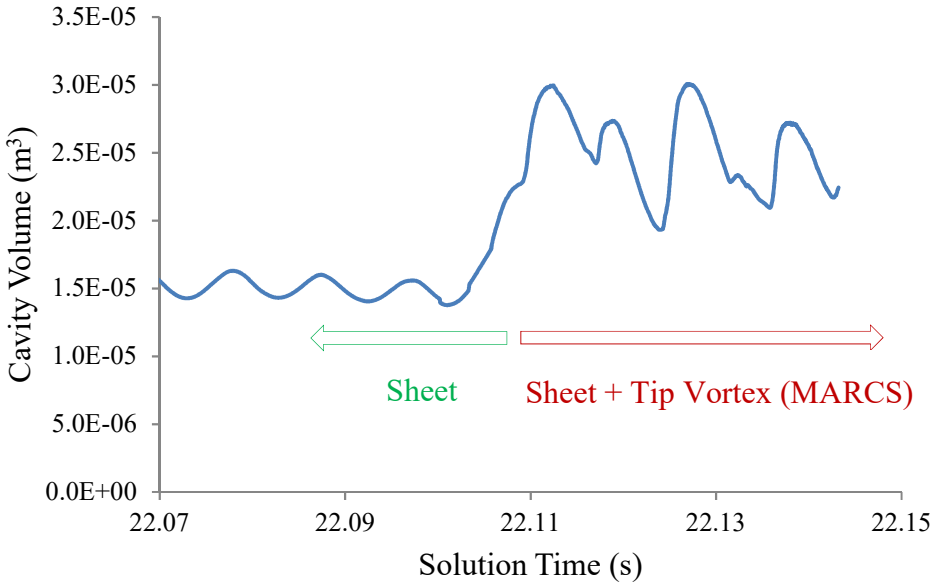

Figure 7-22 CFD Results Cavity Volume Change against to Solution Time without and with MARCS application (Model Scale)

In order to validate the CFD simulations for the fluctuating hull pressures, Figure 7-23 and Figure 7-24 are included to compare the fluctuating hull pressures predicted from the CFD simulations with the results of the EFD measurements at the six pressure probe locations as shown in Table 7-5. In these figures, while the red line demonstrates the averaged value of pressure data on the model hull surface recorded during the experiments, the black line presents the corresponding pressure data based on the CFD simulations. As shown in Figure 7-23 and Figure 7-24, although the CFD simulations generally show a reasonable correlation for the magnitudes with the experimental data for all probe locations, in some cases phase shift between the EFD and CFD results are noticeable. In these comparisons, as stated earlier, only the sheet cavitation was modelled due to the unstable cavitation dynamics of the tip vortex cavitation with the application of the MARCS.

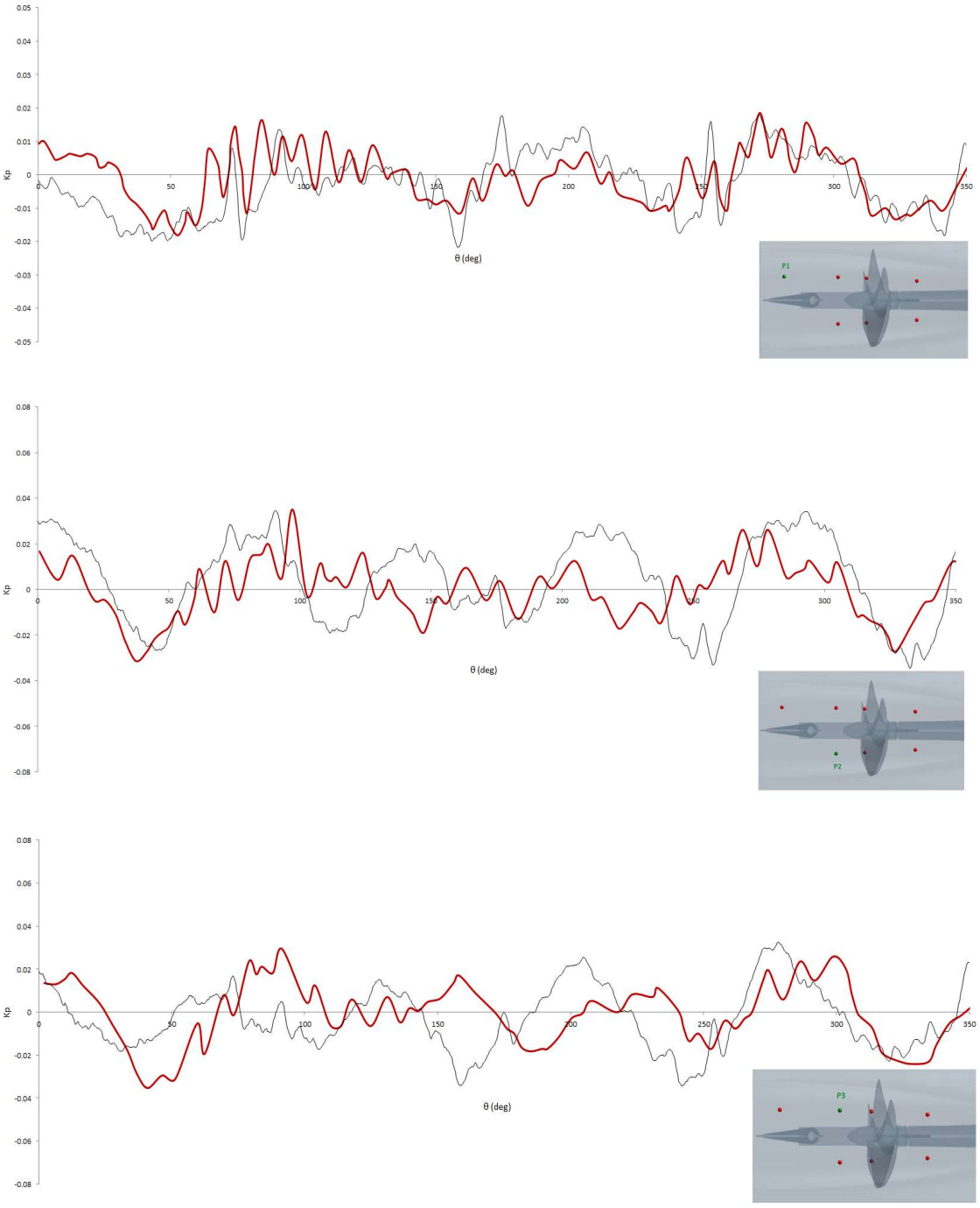

Figure 7-23 Hull Pressure Fluctuations Comparisons between EFD (Red) and CFD (Black) Results (Sheet Cavitation, From Top to Bottom; P1, P2 and P3)

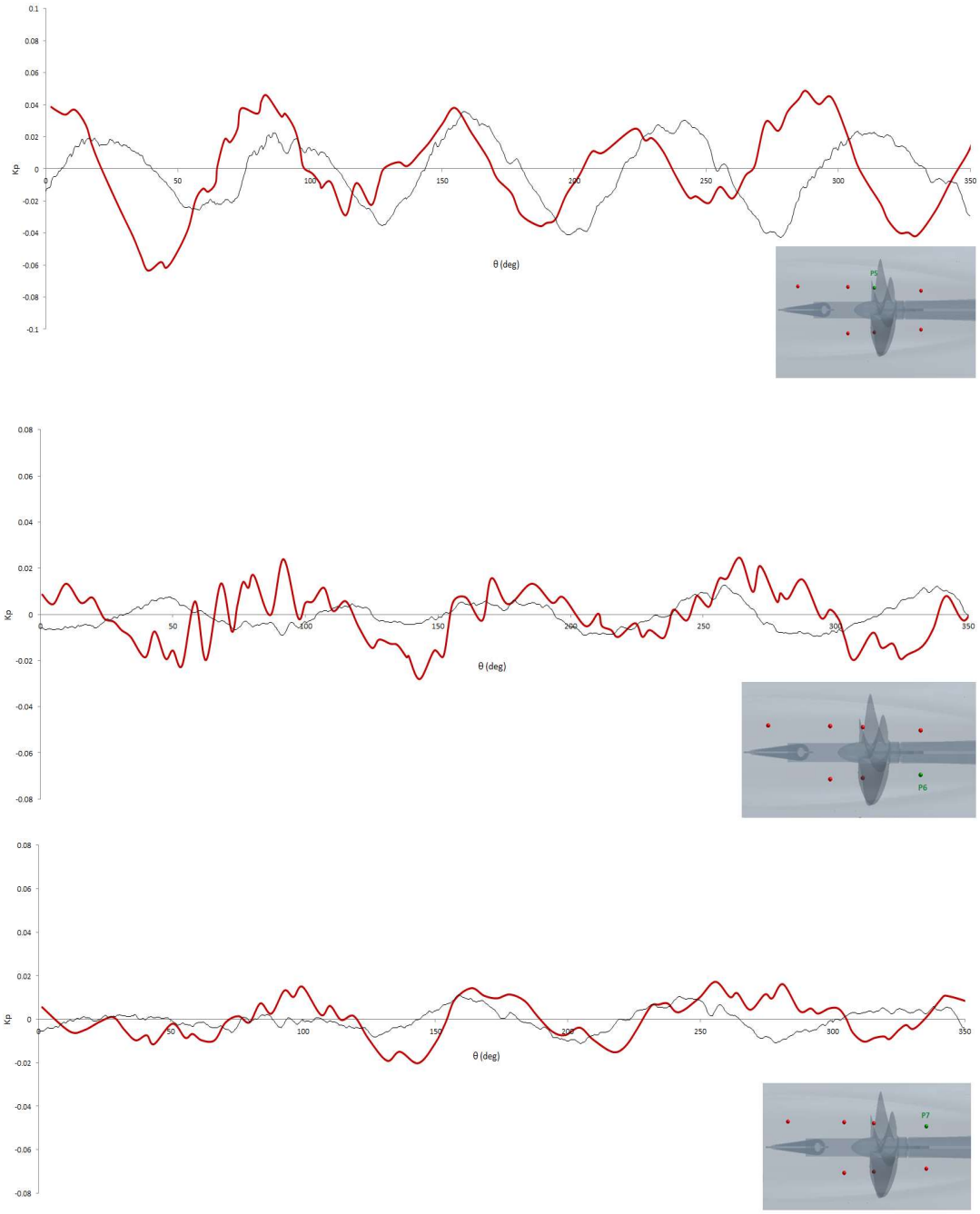

Figure 7-24 Hull Pressure Fluctuations Comparisons between EFD (Red) and CFD (Black) Results (Sheet Cavitation, From Top to Bottom; P5, P6 and P7)

7.4.2 Full Scale Investigations

In this section the full-scale simulation results for *The Princess Royal* operating in "Condition 4" are presented and discussed regarding the cavitation dynamics, propeller hydrodynamic performance coefficients including the comparison of the simulation results with the full-scale data recorded during the sea-trials.

The comparison of the CFD predictions for the propeller torque with the EFD results based on the sea trials are presented in Table 7-10 including the difference (deviation) between the two sets of the results. As shown in this table, although the CFD predictions can not be compared with the EFD results for K_T, due to the lack of the measurements during the sea trials, the difference in K_Q is approximately 9.4% deviation which will require further investigation and associated fine-tuning.

Table 7-10 Hydrodynamic Propeller Performance for Propeller-Rudder-Hull Interaction

(Full Scale)

Cond'	Method	K_T	$10K_Q$
Cond' 4	EFD – Sea Trials	N/A	0.318
	CFD – Full Scale	0.179	0.288
	Deviation	N/A	-9.4%

For the full scale computations, Figure 7-25 demonstrates how the free surface was modelled in simulations by displaying the volume fraction of the air and water on the hull surfaces respectively (from the superstructure of the hull to the keel level). While the volume fraction of the air presents the free-surface between air and water, volume fraction of water also demonstrates phase interaction between water and vapour displaying sheet cavitation pattern on blade surfaces.

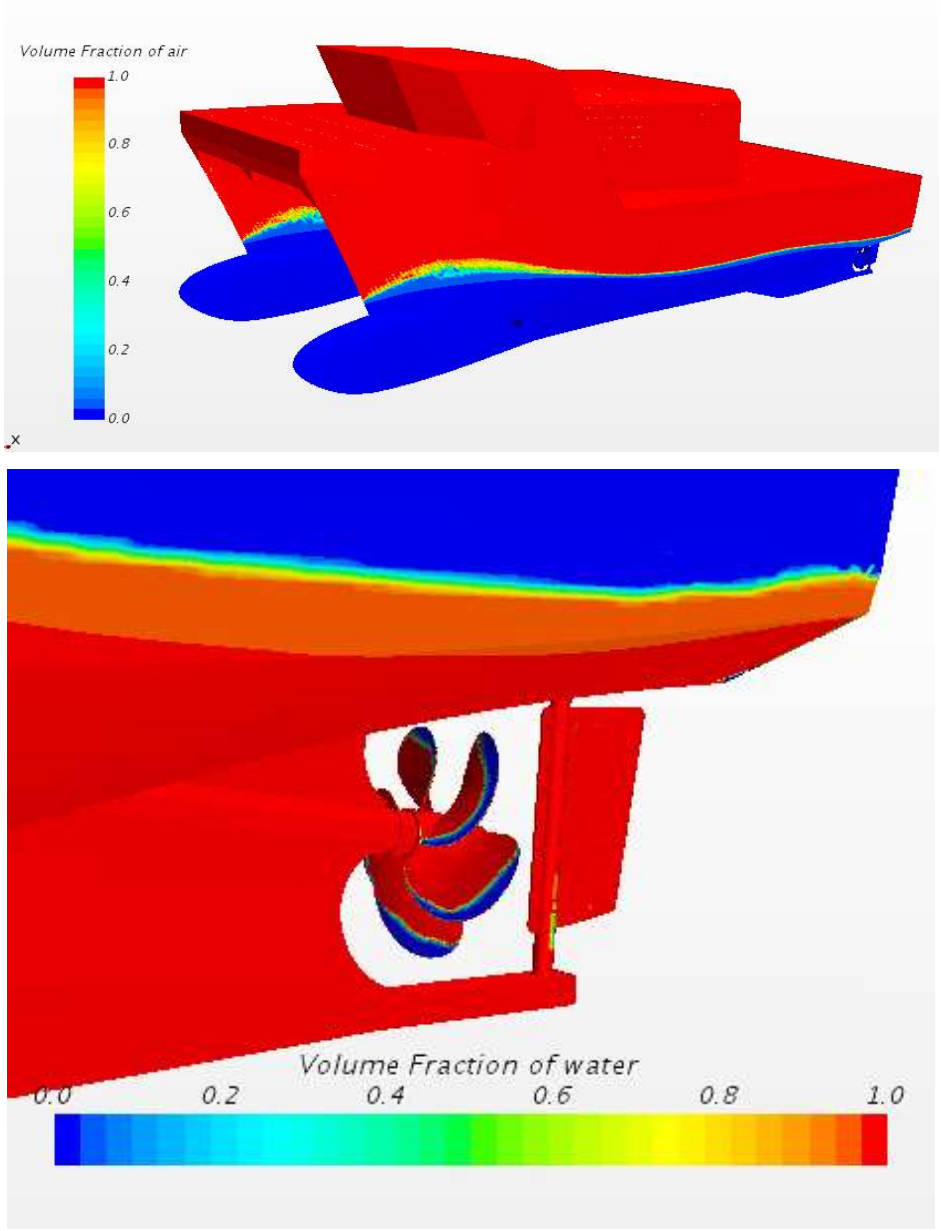

Figure 7-25 Free surface representation (Full Scale) (Top; Volume Fraction of Air, Bottom; Volume Fraction of Water including sheet cavitation on propeller blades)

For the investigation of the propeller cavitation patterns, Figure 7-26, Figure 7-27, and Figure 7-28 are included each showing the comparison of the images from the EFD and CFD results at different propeller blade positions. The EFD images are based on the full-scale trials (Sampson et al, 2015) while the CFD images from the simulations using the MARCS as described earlier.

Within the boundaries of the observation windows of *The Princess Royal*, an overall comparison of the CFD and EFD images for the three blade positions display very

encouraging similarity between them both for the sheet and tip vortex cavitation including their dynamics within the limitation of the CFD code.

As shown in these figures the full-scale images of the sheet and tip vortex cavitation reflect the true appearance of the cavitation with foamy (cloudy) appearance and its complex dynamics while the CFD predictions cannot capture such realism. However, the envelop of these cavitation patterns are still predicted remarkable well by the CFD simulations that will enable prediction of the cavity volume and deformation of the envelop in time and space which are important parameters to predict the consequences of the cavitation.

In general, the comparative images indicate that while the tip vortex cavitation has been predicted well –thanks to MARCS- with a difficult judgement on its thickness, the simulation results for the sheet cavitation somehow over predicted the sheet cavitation extent on the blade compared to the full-scale observations.

If one has a closer look at these images, firstly, Figure 7-26 represents both strong sheet and tip vortex cavitation while one blade was entering in to the wake shadow of the hull and the other one just after passing through this zone. While the entering blade was well covered with a strong sheet cavitation the strong tip vortex cavitation traces of the passing blade can be noticed in both CFD and EFD images. Although the hub cavitation cannot be seen at this shooting position in the EFD image, as reported in the trials, such strong hub vortex was existed and this was also predicted by the CFD as shown in this figure.

Figure 7-27 and Figure 7-28 further confirm the closer appearance of the cavitation images from the full-scale trials and their simulations at different blade angles. In spite of the limitations for representing the complex cavity dynamics that is associated with the cloudy appearance, it is still remarkable to observe a reasonable resemblance of the cavity envelop deformations in the CFD predictions as in the full-scale images.

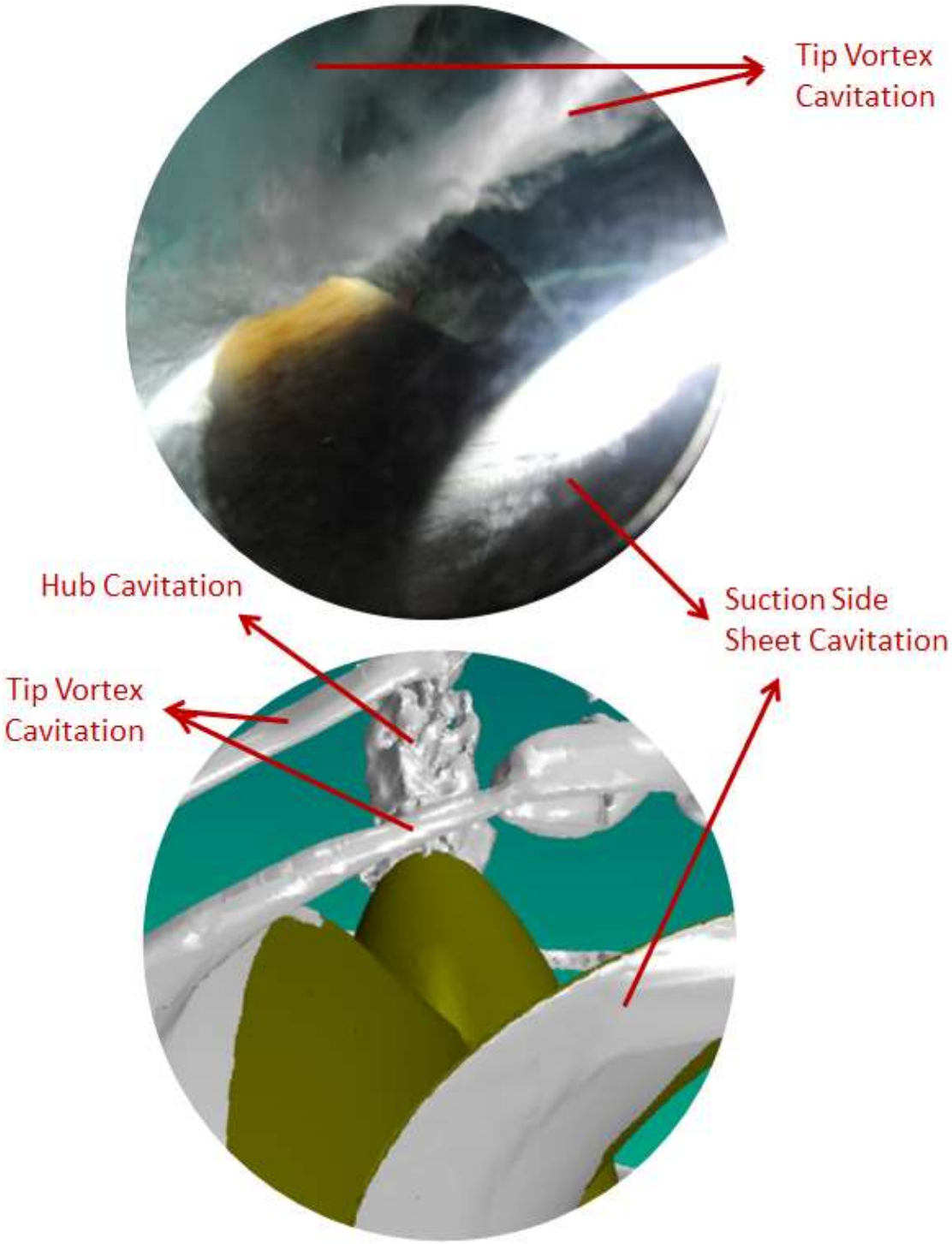

Figure 7-26 Cavitation pattern Comparisons between Sea Trials and CFD (Full Scale) (Top; Sea Trials, Bottom; CFD) (MARCS - tip vortex cavitation)

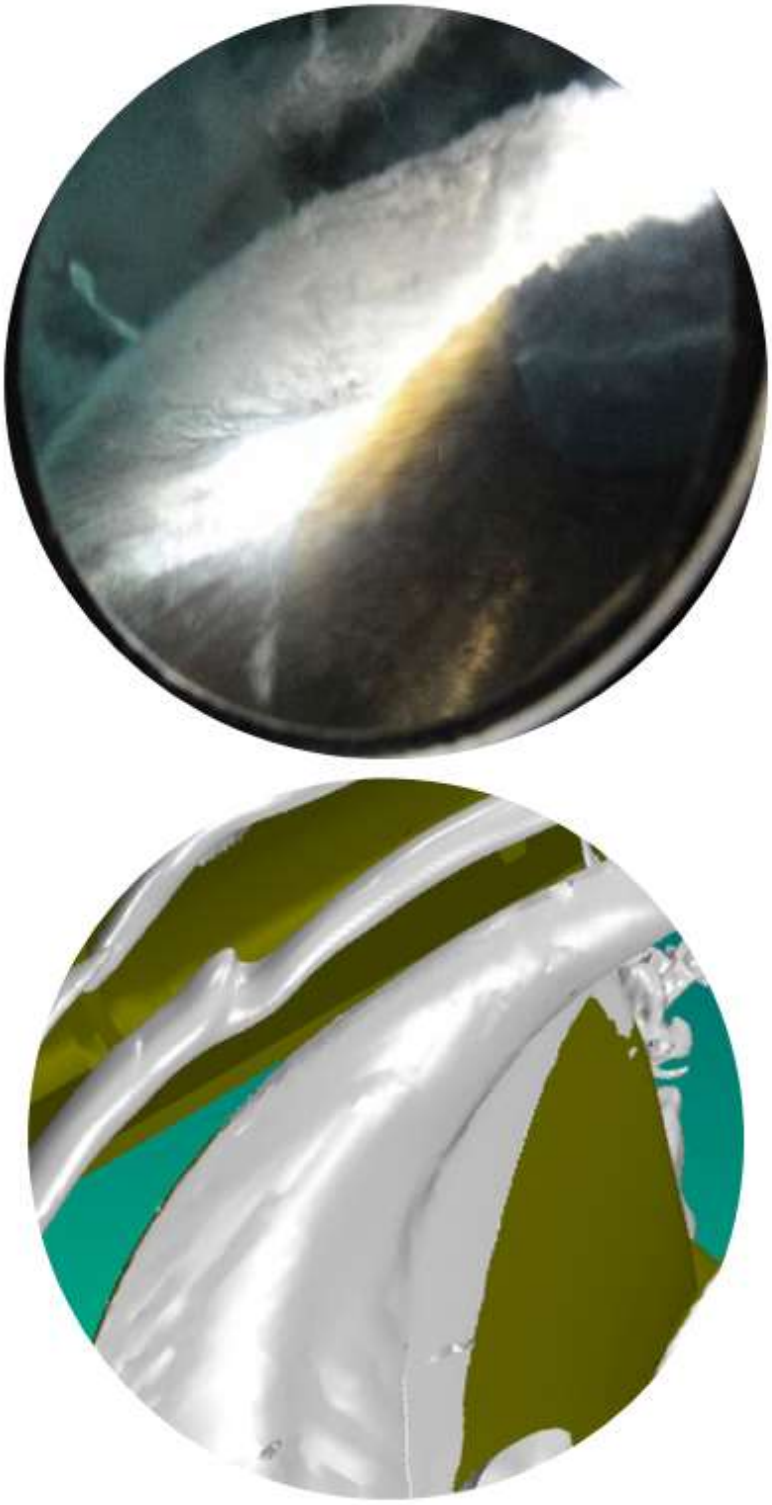

Figure 7-27 Cavitation pattern Comparisons between Sea Trials and CFD (Full Scale) (Top; Sea Trials, Bottom; CFD) (MARCS - tip vortex cavitation)

Figure 7-28 Cavitation pattern Comparisons between Sea Trials and CFD (Full Scale) (Top; Sea Trials, Bottom; CFD) (MARCS - tip vortex cavitation)

Within the framework of the aim of this research study, perhaps the ultimate way to test the capability of MARCS by using the commercial code would be to simulate *The Princess Royal's* cavitation patterns as observed from a profile view as shown in the top image (picture) of Figure 7-29. This image was captured by a video camera, which was installed on a simple streamlined body (Hydropod) and deployed overboard the vessel using a long arm, thus recording of the cavitation as well as the nearfield underwater noise of the propeller (Aktas et al, 2018). Because of the limited structural integrity of the device, the Hydropod could only be used up to a ship speed of about 9 knots beyond which it was not possible to do any observations due to bending on the arm. The full-scale image, therefore, presented in Figure 7-29 corresponds to "Condition 3" with the engine speed of 1200 rpm.

Whereas, the full-scale CFD simulations conducted are for "Condition 4" for the engine speed of 2000 rpm due to the strongest tip vortex cavitation to be able to stretch the tip vortex cavitation through the rudder. Although the Author realizes the differences between the two conditions, it is still worthy to compare the full-scale cavitation images for "Condition 3" with the CFD predictions for "Condition 4" since the main cavitation patterns for the latter condition would still be existed in the former. Therefore, the CFD predicted image for "Condition 4" is included at the bottom of Figure 7-29 for comparison.

In spite of the differences in the operating conditions, as shown in Figure 7-29, the resemblance of the main cavitation patterns for the tip vortex and sheet cavitation predicted by the CFD and full-scale observations is remarkably noteworthy. It is obvious that the simulated tip vortex cavitation traces could not be extended until the trailing edge of the rudder due to the limited overset mesh region as presented in Figure 7-13.

What was most interesting and encouraging in the full-scale simulation results was to observe the deformation of the tip vortex cavitation traces due to the presence of the rudder in the wake shadow region of the hull as encircled by yellow marker. This was a convincing indication for the capability of the methodology to capture the interaction between the propeller flow and the rudder in the presence of the non-uniform hull wake

in complementing the aim of this research study as well as the main objective of this Chapter.

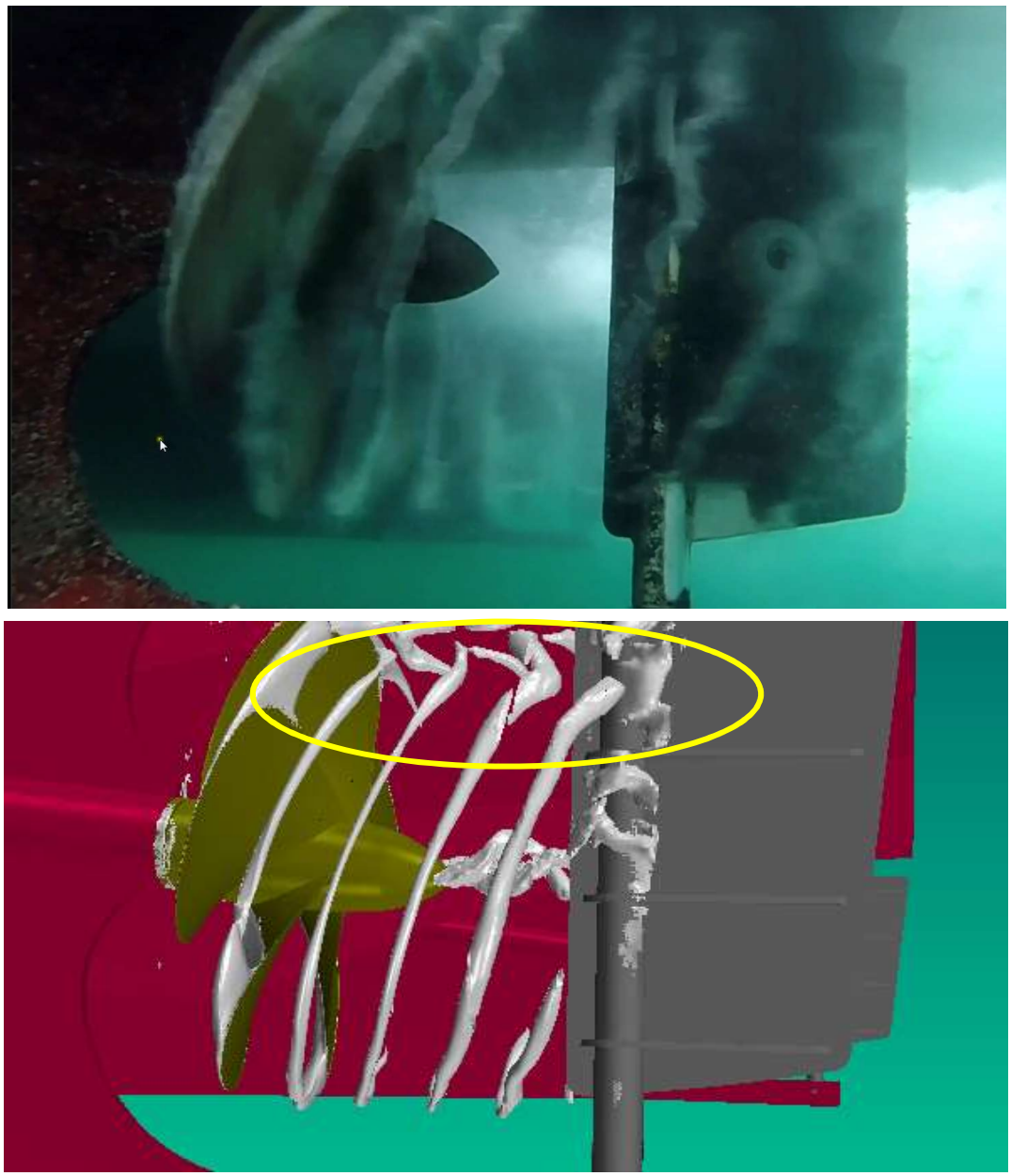

Figure 7-29 Cavitation pattern Comparisons between Sea Trials and CFD (MARCS - tip vortex cavitation) (Top; Sea Trials, Condition 3: 1200 rpm, Bottom; CFD; Condition 4: 2000 rpm)

7.5 Concluding Remarks

In complementing the aim of this research study, the main objective of this Chapter was to conduct CFD simulations to represent the physics of the cavitation influence on the propeller-rudder-hull system and their mutual interaction as realistically as possible using the newly developed MARCS meshing system within the limitations of the commercial CFD code (STAR-CCM+) used.

To achieve the above objective, firstly, the cavitation tunnel tests conducted in the Depressurised Large Circulating Water Channel of CNR-INSEAN with the scaled model of *The Princess Royal* research vessel were simulated using the commercial code, and results were compared with the test data for one of the test conditions which displayed the strongest tip vortex cavitation presence. This was followed by further CFD simulations in the full-scale for the cavitation performance of *The Princess Royal*, and comparing the results with the sea trials data of this vessel which was available through the EU-FP7 Project SONIC.

A combined rotation method including the sliding mesh and overset mesh techniques was used to model the rotational motion due to the propeller's action for both simulation cases to extend the cavitating tip vortices from propeller tip onto the rudder geometry. This was achieved by more accurate and efficient mesh generation using the MARCS approach developed in Chapter 5.

In general, although the improvements have been achieved for extending the TVC in the propeller slipstream for both simulation cases (i.e. in the model and full-scale), the interaction between the TVC and rudder could not be simulated at a desired accuracy due to the complexity of the full interaction phenomenon amongst the propeller-rudder-hull in the presence of the hull geometry and its wake.

More specifically, the results of the CFD simulations in the model scale showed good correlations with the EFD data for the cavitation patterns and in particular for the tip vortex cavitation extensions with the EFD data. Similarly, the CFD prediction of the fluctuating hull pressures, which was based on the sheet cavitation modelling, was also

in reasonable agreement with the EFD data regarding their magnitudes while there were phase shifts in some of the pressure point records.

On the other hand, the results of the full-scale CFD simulations for the performance of the propeller regarding K_Q could only be predicted with 9.4% deviation requiring further investigation.

As far as the cavitation images are concerned, an overall comparison of the predicted CFD and full-scale images for the three blade positions displayed very encouraging similarities between them both for the sheet and tip vortex cavitation including their dynamics within the limitation of the CFD procedure.

In general, the comparative images indicated that while the tip vortex cavitation pattern has been predicted well –due to MARCS- the simulation results for the sheet cavitation somehow over predicted the sheet cavitation extent on the blade compared to the full-scale observations.

What was most interesting and encouraging in the full-scale simulation results was to observe the deformation of the tip vortex cavitation traces due to the presence of the rudder in the wake shadow region of the hull. This was a convincing indication for the capability of the methodology to capture the interaction between the propeller flow and the rudder in the presence of the non-uniform hull wake in complementing the aim of this research study as well as the main objective of this Chapter.

Chapter 8 Conclusions and Recommendations

8.1 Introduction

This chapter presents a summary of the main conclusions and contributions of this research study through the evaluation of the accomplished research objectives leading to the achievement of the aim of this PhD research. This is followed by further concluding remarks on the CFD focus of this research based on the Author's experience throughout the study. Finally, recommendations are given for relevant fields of future research which are related to the work presented in this thesis.

8.2 Main Conclusions and Contributions

The first objective of this research study, which was addressed at in Chapter 2, required:

- *To review the state-of-the-art literature regarding the propeller cavitation, in particular, its effect on the interaction due to the propeller, rudder and hull, and to identify the associated research gaps*

In order to address at the above objective a "critical review" was conducted in Chapter 2, regarding the-state-of-the-art and the challenges for the numerical simulation of propeller cavitation using commercial CFD tools - including the complex interaction amongst the propeller, rudder and hull. This chapter also provided a literature review on propeller cavitation from the history of cavitation research to the-state-of-the-art developments for cavitation research using CFD methods. In the scope of the literature survey, more detailed and specific fields were also visited such as bubble dynamics, different types of cavitation, various numerical and experimental methods of cavitation and propeller-rudder-hull interaction phenomenon with regard to propeller cavitation to identify research gap(s) and hence to justify the aim and objectives of this research study.

Having conducted the literature survey it became clear that; although sheet cavitation for propellers could be simulated reasonably accurately with commercial and research CFD codes, simulating the tip vortex cavitation was still challenging for ship propellers. Within this framework, it was identified that there was a clear gap in simulating cavitation simultaneously on all blades of a ship propeller including the cavitating tip vortices in the presence of the rudder and hull especially in full-scale. This major research gap has been the Author's main motivation and hence the aim of this research study was to challenge this by pushing the limits of a state-of-the-art commercial CFD code by developing advanced meshing techniques and using available benchmark EFD data.

The second objective of the research study, which has been tackled in Chapter 3, required:

- *To develop a rational methodology for investigating propeller cavitation including the tip vortex cavitation by using computational and experimental fluid dynamics methods*

Chapter 3, therefore, presented the overall methodology used, based on CFD and EFD methods to investigate the influence of cavitation on propeller-rudder-hull interaction. Since the thesis is driven mainly by the CFD method, which required to be validated by suitable data to be obtained from EFD methods, the basis of both (CFD and EFD) methods including the available benchmark data were described in Chapter 3. The benchmark data included the three different benchmark test propellers – *PPTC VP1304, INSEAN E779A* and *The Princess Royal* Propellers – and a ship geometry – *The Princess Royal* Catamaran Research Vessel of Newcastle University.

Also, as demonstrated in this study, the use of the CFD method would require the development of an advanced mesh refinement technique (i.e. MARCS) which was described in details and applied in subsequent chapters (i.e. Chapter 5 and afterwards). Chapter 3, therefore, focused on the basics of the CFD (e.g. details of turbulence, multiphase flow, motion and cavitation modelling etc.) and those of the EFD (e.g. cavitation tunnel environment, nature of the benchmark data used etc). Finally, the validation and verification studies, that are essential for any CFD calculation, were

also presented in this chapter and discussed based on the performance simulations of the two benchmark propeller models (*INSEAN E779A* and *The Princess Royal* propellers) in non-cavitating and cavitating conditions in open water.

In essence, the work conducted in Chapter 3 has provided the Author with initial confidence in using a state-of-the-art commercial code, STAR-CCM+, to enable the Author to develop a rational methodology to tackle the aim of this research study. This also included the assurance for the provision of the experimental data from the EFD to validate the developed CFD methodology.

Furthermore, the evaluation of the validation and verification studies indicated that the deviations between calculated and measured values in non-cavitating and cavitating conditions are quite small, less than 5% for thrust and torque coefficients for all validation and verification studies. Whereas the uncertainty values presented for the tip vortex cavitation were much higher than the sheet cavitation requiring an advanced mesh refinement technique which was addressed at a later stage.

The next and third objective of the research study was addressed in Chapter 4, and required:

- *To predict propeller performance in open water conditions to verify and validate the methodology and its implementation*

In achieving the above objective the Author believed that the first, and perhaps most important building brick in the CFD modelling of the propeller-rudder-hull combination, is the correct computational modelling of the propeller in isolation (i.e. open water) and in non-cavitating condition. Chapter 4, therefore, presented the details of the computational modelling (i.e. regarding the computational domain preparation, mesh generation, boundary conditions and simulation setup etc.) for the open water performance simulations of the earlier-stated three benchmark propellers (*INSEAN E779A, PPTC VP1304* and *The Princess Royal* model propellers) in non-cavitating conditions and the comparison of the simulation results with the EFD data using the STAR-CCM+. The comparison of the CFD predictions for the performance data of the three test case propellers, which were tested in different environments, indicated good

correlations between the predictions and the EFD data, and hence providing the initial confidence in the commercial code to, next, challenge the modelling of cavitation.

The fourth and fifth objectives of the research study, which were tackled in Chapter 5, respectively, required the following:

- *To predict propeller performance especially in cavitating conditions in open water conditions*

and

- *To develop a new mesh refinement technique to improve the simulation process of propeller performance and cavitation with better accuracy including the tip vortex cavitation simultaneously from all blades*

Since the main focus of the above objectives is cavitation, Chapter 5 therefore presented and compared the results from both CFD modelling research and EFD research for cavitation development on the earlier-mentioned three benchmark model scale propeller geometries and test configurations. A new CFD model with an advanced adaptive grid has been developed by the Author and applied to all of the blades of the propeller for the improved prediction of cavitation dynamics, including tip vortex cavitation, simultaneously, from all blades and improved hydrodynamic performance of the propeller in cavitating conditions. Comprehensive details of the CFD modelling (e.g. mesh arrangements, size, time step, turbulence models etc.) of the three benchmark propellers and the simulations results for the propeller performance and cavitation images were compared with the EFD data and the results were discussed in Chapter 5.

These investigations confirmed the identified gap in the literature regarding the accurate modelling of the tip vortex cavitation and hence initiated further development into different mesh refinement approaches for tip vortex cavitation development in order to resolve the predominant issues of tip vortex extent. For this purpose, two different mesh refinement approaches were developed in Chapter 5, namely volumetric control (tube and spiral) and mesh adaption. These were used to extend the tip vortex cavitation in the propeller slipstream and to improve the hydrodynamics

performance predictions. Use of the tube and spiral geometries as volumetric control regions from the propeller tip to downstream of the propeller allowed slightly improved tip vortex extension as well as propeller performance prediction (Yilmaz et al, 2017). Ultimately, a new further enhanced scheme for Mesh Adaption Refinement Approach for Cavitation Simulations (MARCS) was developed in Chapter 5 and achieved the largest axial extent of the tip vortex cavity for the benchmark propellers as well as presenting fairly good agreement with the EFD results for cavitation dynamics and hydrodynamic performance of the propeller, (Yilmaz et al 2019). The main advantage of the MARCS approach, which is the major contribution of this research study, is that the economy of the refined mesh adaption, allows simultaneous modelling of the cavitating vortices from all of the blade tips and the hub from the propeller to the rudder. This capability facilitates to investigate the cavitation influence on the propeller-rudder-hull combination by using a state-of-the-art commercial code and hence to achieve the aim of this research study. It has the further possibility of investigating vortex-vortex interactions between the propeller tips and the rudder. A final point to note as the contribution from chapter 5 is that the new mesh refinement approach was particularly effective and attractive in simulating the tip vortex cavitation trajectories from all-blades of the 5 bladed heavily cavitating propeller (e.g. *The Princess Royal* propeller) in the uniform flow conditions with the expectation for better simulation in non-uniform flow and in full-scale.

The next and sixth objective of the research study, which was addressed in Chapter 6, required:

- *To investigate the cavitation influence on the propeller-rudder combination including the tip vortex cavitation from all blades extending in the propeller's slipstream*

Having validated the new meshing technique in the previous chapter, Chapter 6 utilized this technique to deal with the propeller cavitation simulation in the presence of the rudder to explore some fundamental aspects of the propeller slipstream-rudder interaction (including e.g. propeller performance, cavitation dynamics due the effect of the rudder, the effect of the rudder profile etc.). For this investigation two different propeller-rudder configurations, were simulated without the presence of the hull. The

first configuration involved a highly skewed, 4-bladed propeller and a conventional rudder. The rudder section thickness of a 2400 GT container ship was simulated in a uniform flow condition. The second configuration was of *The Princess Royal* propeller and its own simplified plate rudder geometry (non-aerofoil sections and exposed rudder post) operating in conditions with an inclined shaft in non-uniform flow. These two propeller-rudder configurations allowed the investigation of propeller-rudder interaction in cavitating flow conditions with strong tip vortex cavitation but also the effect of flow non-uniformity, inclination and rudder profile on this complex phenomenon. The CFD simulation results for the two configurations were compared with the experimental data of the cavitation tunnel tests conducted in the Emerson Cavitation Tunnel. The results of the findings from both simulations cases and their comparisons with the EFD data were discussed with regard to the effect of the tip vortex cavitation and differences in the propeller-rudder arrangements.

The investigations conducted in Chapter 6 confirmed that the enhanced MARCS approach was successfully applied in both propeller-rudder test cases to simulate tip vortex cavity interacting with each rudder, in particular tip vortex deformations, both axially and radially, in way of the rudders. The deformation of the cavitation tip vortex trajectories was noticeable when they approached the rudder leading edge, reflecting similar behaviour observed in the EFD images. Good agreement was also obtained between the CFD and EFD results for the propeller performance coefficients and sheet cavitation patterns, but particularly for the tip vortex cavitation patterns. For the container rudder arrangement case, in open water flow, the CFD predictions for the performance of the propeller showed good agreement with the experiments (EFD), in terms of K_T, for which the deviation is less than 4% while K_Q could only be predicted within a %6.6 deviation (Yilmaz et al, 2018b). For the more demanding simulation case of *The Princess Royal* with the rudder in non-uniform flow, although the CFD predictions for the performance of the propeller showed good agreement with the experiments (EFD) regarding K_T, for which the deviation is less than 2%, K_Q could only be predicted to within %6.7 deviation (Yilmaz et al, 2018a).

The CFD simulations with the two different propeller-rudder arrangements demonstrated further ability of the CFD tool with the use of MARCS to evaluate the

pressure distributions over the rudder blades under the effect of the propeller's slipstream including the cavitating tip vortices. Although the results could not be compared with any EFD data due to the lack of the measurements of the pressure distributions during the cavitation tests, they were compared with each other in order to investigate the effect of the different rudder profiles. The high pressure values have been obtained on the leading edges for both rudder geometries. While the rudder stock bar caused pressure increment for the *Princess Royal* rudder, the similar effect has also been observed due to the change of the rudder tail shape for the conventional rudder. This was a significant capability for future investigations of cavitation erosion and structural design of rudders.

In summary the investigations in Chapter 6 confirmed that the enhanced MARCS technique can be used effectively in a commercial CFD code for enhanced simulation of the influence of cavitation on propeller-rudder interaction phenomenon in model scale with a view to attempt to simulating the real phenomenon in full-scale.

The last and seventh objective of the research study, which has been addressed at in Chapter 7, required:

- *To simulate the performance of the ship propulsion system including the propeller, rudder and hull in model and full-scale and to investigate the cavitation influence on the combined system as realistically as possible*

Chapter 7 therefore presented the investigation of cavitation influence on the propeller-rudder-hull system, especially for representing the effect of tip vortex cavitation as realistically as possible using the newly developed MARCS meshing system and the EFD and CFD methods within the limitation of the commercial CFD code used. For this purpose two simulation studies, one of which was in model scale and the other in full-scale, were conducted for the propeller-rudder-hull arrangement of the *Princess Royal* research vessel and the results were compared with the EFD data.

For the model-scale validation study, the model test results conducted at the Large Circulation Channel of CNR INSEAN were used to represent the physics of the propeller-rudder-hull system and their mutual interaction as accurately as possible in the presence of a scaled full-hull model with free surface channel flow. The CFD

simulations were conducted with and without using the MARCS approach for comparison.

An overall comparison of the CFD predicted fluctuating hull pressures and the cavitation images with the EFD data was in good correlation for the pressure data magnitudes while there was also extremely encouraging evidence of similar cavitation patterns which captured fine details of the EFD based cavitation images.

For simulating the model scale cavitation images, although the improvements were achieved for extending tip vortex trajectories in the propeller slipstream, the interaction between tip vortex cavitation and rudder could not be simulated to the same level which the CFD simulations achieved in full-scale. This difference related to the different mesh arrangement used in the model and full-scale simulations. In the model-scale simulations, a relatively small sliding mesh region for the propeller and a large overset mesh region (covering all rudder geometry) were used for the tip vortex predictions. Despite the use of the large overset region, the mesh refinement of this region still was limited in the longitudinal axis in order to keep the total number of cells to a reasonable limit. When the CFD images were examined in the model-scale, it was noticed that the tip vortex cavitation trajectories could not be clearly extended over the rudder due to the interface problem between the sliding mesh and the overset region at some propeller blade positions although a combined system was used to eliminate this problem. This modelling difficulty was further exacerbated by the natural behaviour of the tip vortices near to the rudder (Figure 7-18), which can be observed from the EFD images, that they were losing their strength as they approached the rudder. However, this modelling difficulty could be prevented and further improved using the extended sliding mesh region and smaller surface size in the overset region that could capture relatively less strong tip vortex dynamics in the model scale.

Based upon the experience with the model scale simulations, an extended sliding mesh region and narrowed overset mesh region were used in the full-scale simulations. This arrangement was successful on the basis that while the extended sliding mesh arrangement allowed extension of the tip vortex cavitation trajectories up to the rudder, the narrowed overset mesh region helped to keep the total number of cells to a

reasonable number. Beside the change of the rotating domain size, undoubtedly, the main reason for the success of better simulations of the tip vortex cavitation in the full-scale was directly related to the greater strength of the tip vortices in the full-scale condition. Although no further simulations were conducted in the model scale with the above described revised mesh regions due to the time limitation of this research study the Author believes that the level of accuracy of the simulation in the model-scale can be as successful as in the full-scale by extending the sliding mesh region and especially using a smaller surface size in the overset region.

As far as the full-scale cavitation simulations are concerned, an overall comparison of the CFD predicted cavitation patterns with the sea-trial images for the three blade positions displayed very good similarities between them both for the sheet and tip vortex cavitation patterns including their dynamics. What was most encouraging in the full-scale simulation results was to observe the deformation of the tip vortex cavitation traces due to the presence of the rudder in the wake shadow region of the hull. This was a convincing indication for the capability of the methodology to capture the interaction between the propeller flow and the rudder in the presence of the non-uniform hull wake in complementing the aim of this research study.

Further implications of the above paragraph, and hence the further claim of this research study is that it is feasible and hence more attractive to simulate the propeller cavitation directly in the full-scale without spending additional time and effort in the model scale, with due respect to the invaluable contributions being made and still to be made by the EFD methods in the validation stage of the CFD methods.

8.3 Concluding Remarks

This research study was mainly driven by the need to assess and advance CFD methods for modelling marine propeller-hull-rudder interactions. Within this framework a wide range of CFD based investigations and hence associated simulations were conducted in this study to cover different operating conditions with different propellers, different rudders and one hull geometry to investigate the cavitation influence on a propeller-rudder-hull combination at both model and full-scale. All these simulations served a

very important purpose in achieving the main aims and objectives of this thesis as reviewed in Section 8.2. During these simulations the Author has faced various issues and drawn further comments regarding the CFD focus of the study based on her experience which are stated in the following as the concluding remarks of this thesis.

Expectedly, all of the different simulations brought a number of issues with them. Most of them were experienced at the pre-processing stage of the CFD analyses while each CFD simulation could require a different combination of numerical models (e.g. regarding turbulence, motion and cavitation etc.), and selection of proper parameters, boundary and initial conditions.

Amongst these issues, the generation of the proper mesh distribution was the most challenging part of the cavitation simulations. Ideally, a very fine mesh should be generated, especially for the CFD analysis of the complex cavitation phenomena, to capture the sudden pressure drop within the tip vortex core and the development of cavitating bubbles. Within this context, for capturing the cavitating bubbles in the propeller's slipstream in order to simulate the blade tip vortex cavitation accurately, different mesh surface sizes and refinement approaches were investigated over a long period of time. Although a very small surface size (i.e. 0.25 mm) was used for the mesh refinement in the propeller slipstream, weakly cavitating vortices were a challenge due to limited computational resources when the total number of cells was approximately 50 million.

Another complexity for the CFD simulation was the use of the overset mesh method, which was a necessity for the tip vortex cavitation especially extending the tip vortex cavitation from the propeller blades through the rudder in order to simulate the complex interaction between the tip vortex cavitation and the rudder geometry. For this purpose, the overset mesh method and a combined mesh method, which included the sliding mesh and overset mesh, were used for simulating both the propeller-rudder case and the propeller-rudder-hull case, respectively. While the use of the overset mesh method greatly increased both generated mesh size and solution time, it had a tendency to cause overset mesh errors at model scale

In addition to the mesh generation, selection of the correct turbulence model was also important to improve the CFD results in modelling cavitation. Regarding the best tip vortex cavitation extension in downstream of the propeller, three different turbulence models such as RANS, DES and LES were investigated until the best solution was achieved.

As far as the mesh generation is concerned, as developed and applied in this study, the new adaptive mesh refinement technique (MARCS) was an effective and accurate technique to simulate the propeller tip vortex cavitation particularly to trace their extensions in the propeller's slipstream. This new method gave the most accurate results for the isolated propeller simulations in uniform flow conditions, but initially, it also presented oscillating results when the simulations were conducted for the propeller-rudder interaction with the inclined shaft and in non-uniform flow conditions. However, the issue was resolved by changing Scaling Factor + inside the cavitation parameters in the Schnerr-Sauer model and the tip vortex cavitation traces could be extended up to the rudder.

Another time-demanding and essential stage of a CFD simulation is the processing phase of the simulations which generally takes the longest time of the CFD investigations. To give an example, the total CPU time allocated to run a typical cavitation simulation in Chapter 5 for the isolated propellers is approximately 7610 hours by utilising a 40-core high speed supercomputer which is corresponding to one week in real time. It must be noted that this amount of time applies only to a typical cavitation simulation for only one cavitating condition. Undoubtedly, this time increased when the simulation case became more complex including rudder, hull geometries and also free surface for the propeller-rudder-hull interaction simulations. To give an example from Chapter 7 for model scale calculations, propeller cavitation including TVC could be predicted in 24640 CPU hours which was approximately 3 times longer than the isolated propeller simulations.

Perhaps the most challenging and novel part of this study were the full-scale cavitation simulations on the propeller-rudder-hull arrangement. Having developed the new mesh refinement approach and applied on the model-scale test cases, it was quite important to further develop the applications in full-scale. Although the scale effect is

not the main interest of this research study, the investigation of the cavitation influence on the propeller-rudder-hull system were carried one step forward passing from model-scale to the full-scale.

This PhD thesis clearly presented that CFD methods can be very attractive for the investigation of the cavitation influence on the propeller-rudder-hull system while the model tests and sea trials are expensive, complex and time-consuming alternatives that every researcher cannot easily have an access to. The newly developed mesh refinement approach used in combination with a commercial CFD code has demonstrated that the physics of the complex cavitating flow can be simulated in full-scale within the limited computational resources and time constraint of this research study.

Having realised the fact that CFD can be an extremely useful tool in a researchers' hands, it must be used wisely to investigate any complex phenomena with reliable approaches, methods and validations based on dedicated EFD methods and made possible with developing computational power, technology and research effort world-wide. It is the Author's belief that the CFD will grow to be a more powerful and significant tool with such improvements, able to simulate real physical phenomena in coming years.

8.4 Recommendations for Future Work

This research study was conducted with limited computational resources and time constraint due to the nature of the PhD studies. Thus, a number of related research topics are listed in the following as recommendations for future work:

1. **Further investigations for the interaction between the sheet and tip vortex cavitation:** In the current study although the sheet cavitation on the blades and the tip vortex cavitation with its extension in the propeller's slipstream was successfully modelled the interaction between the sheet and tip vortex cavitation has not been studied in detail. Further research is therefore required to better understand this complex interaction that could be important from the

point of view of the pressure distribution on the tip region, blade tip erosion and cavitating noise.

2. **Further development of MARCS:** The new adaptive mesh refinement technique (MARCS) developed in this study could give unstable results at model scale with the inclined shaft and in non-uniform flow conditions. This would result in the appearance and disappearance of the tip vortex cavitation in solution time when the generated mesh matched with vortex trajectory and was no longer suitable, respectively, due to the rotation of the refined mesh region. The MARCS approach therefore still needs to be further developed applying re-meshing methods at each time-step to be able to keep the vortices matched with the refined mesh region in the propeller slipstream when the blade position changes in solution time.
3. **Further CFD analysis and modelling of tip vortex cavitation interaction with the rudder:** In some of the simulations conducted for the propeller-rudder combination case and the propeller-rudder-hull combination, due to the lack of the computational resources, the rotating regions (sliding mesh and overset mesh) required to be shorter to decrease the total number of cells and solution time. Therefore, the tip vortex cavitation extension could be simulated over the limited region that could not cover the entire rudder surface from the leading to the trailing edge of the rudder. Further CFD analysis and modelling work would be required to be able to extend tip vortices to investigate the deformation of tip vortex cavitation throughout the rudder. These further investigations will also help to investigate rudder erosion, cavitation noise and vibration phenomenon more accurately.
4. **Development of a more accurate full-scale analysis for the propeller-rudder-hull system:** Due to the time and resource limitations of the current study, the simulation of the cavitation on the propeller-rudder-hull system in full-scale has been a very good starting basis to investigate the cavitation influence on the propeller-rudder-hull interaction. However, this basis study should be further developed with the further development of MARCS as suggested in Paragraph 2 with more full-scale application case studies

supported by dedicated EFDs. Many full-scale studies are known to exist, however, permission to use such data is often complex.

5. **Development of a CFD model including tip vortex cavitation for under water radiated noise prediction:** Current CFD predictions of the underwater radiated noise due the propeller cavitation have been mainly based on the sheet cavitation modelling. The modelling of the tip vortex cavitation, which is the main contributor to the cavitation noise, as proposed in this research study should be combined for modelling of the cavitation noise for more accurate prediction using CFD.

   To give an example, during this PhD study, the proposed advanced meshing refinement technique was also used for an industrial research project for the underwater noise prediction. At the beginning of this project, lack of the TVC modelling, change of the cavitation volume could not be predicted well, hence the effect of the cavitation volume on noise prediction could not be estimated. After the MARCS application to the cavitation modelling, before the cavitation tunnel tests, reduction of the cavitation volume, correspondingly underwater radiated noise could be predicted. Although, this study was covering only cavitation volume reduction prediction rather than cavitating noise prediction, developing of MARCS approach and the application on cavitation noise calculations using CFD can provide more accurate prediction approach for cavitating noise predictions including tip vortex cavitation extension, even cavitating bubble collapse and rebound stages. This research study can also be expanded for the cavitating noise prediction with the better predictions of broadband pressure fluctuations, blade passing frequencies and defining the noise sources including TVC extension thanks to the MARCS approach (Aktas et al.,2018b).

6. **Development of a CFD model for rudder erosion prediction method in the presence of tip vortex cavitation interacting with rudder:** Erosion damage to the rudder leading edge is often a result of repeated impacts from the cavitating propeller-tip vortex streaming aft. A more accurate modelling of tip vortex cavitation up to the rudder leading edge might be very important for the further investigations of rudder erosion, particularly leading edge erosion, due

to the known dynamics of such distorting tip vortex cavitation. Hence, the accurate tip vortex cavitation model which was developed in this research can be critical for the rudder erosion investigations, say by investigating and extending the criteria proposed by Li, (2012).

References

Aktas, B., Atlar, M., Leivadaros, S., Sasaki, N., Fitzsimmons, P. (2018) "Hydropod: An Onboard Deployed Acoustic–Visual Device for Propeller Cavitation and Noise Investigations" IEEE Journal of Oceanic Engineering PP(99):1-15, January 2018.

Aktas, B., Atlar, M., Turkmen, S., Korkut, E., Fitzsimmons, P., (2015) "Systematic cavitation tunnel tests of a propeller in uniform and inclined flow conditions as part of a round robin test campaign" Ocean Engineering.

Aktas, B., Atlar, M., Turkmen, S., Shi, W., Sampson, R., Korkut, E., Fitzsimmons, P. (2016) "Propeller cavitation noise investigations of a research vessel using medium size cavitation tunnel tests and full scale trials", Ocean Engineering Volume 120, 1 July 2016, Pages 122-135.

Aktas, B., Yilmaz, N., Sasaki, N., Atlar, M., Tani, G., Miglianti, F., Viviani, M., Taylor, D., (2018b), "An Experimental Investigation into PressurePores Technology to Mitigate Propeller Cavitation and Underwater Radiated Noise, A. Yücel Odabaşı Colloquium Series 3rd International Meeting on Progress in Propeller Cavitation And its Consequences: Experimental and Computational Methods for Predictions, 14th – 16th November 2018, Istanbul, Turkey.

Atlar M., Aktas B., Sampson R., Seo K.C., Viola I.M., Fitzsimmons P., Fetherstonhaug C., (2013) "A Multi-Purpose Marine Science & Technology Research Vessel For Full Scale Observations And Measurements", 3rd International Conference on Advanced Model Measurement Technologies for the Marine Industry, Jan.

Atlar, M., Patience, G., (1998) "An Investigation into Effective Boss Cap Designs to Eliminate Hub Vortex Cavitation", PRADS'98, The Hague.

Atlar, M., (2000) “A History of the Emerson Cavitation Tunnel and its Role in Propeller Cavitation Research”, Iternational Conference on Propeller Cavitation , Newcastle.

Atlar, M., (2011) Recent Upgrading of Marine Testing Facilities at Newcastle University, AMT’11 – The 2nd Conference on Advanced Model Measurement Technology for the EU Maritime Industry, 4-5 April 2011, Newcastle Upon Tyne, UK, p: 1-32.

Bensow, R., Bark, G., (2010) “Simulating Cavitating Flows with Les in Openfoam”, V European Conference on Computational Fluid Dynamics, ECCOMAS CFD 2010, June, 2010.

Bertram, V., (2012) “Practical Ship Hydrodynamics”, (2nd Edition), Elsevier Ltd., UK (2012).

Boorsma, A., Whitworth, S. (2011) “Understanding the Details of Cavitation”, Second International Symposium on Marine Propulsors smp’11, Hamburg, Germany, June 2011.

Brennen, C. E., (1995) “Cavitation and Bubble Dynamics”, Oxford University Press, New York.

Bretschneider, H., Bosschers, J., Choi, G.H., Ciappi, E., Farabee, T., Kawakita, C., Tang, D., (2014) “Specialist Committee on Hydrodynamic Noise, Final Report and Recommendations to the 27th ITTC”, Copenhagen, Sweden.

Budich, B., Schmidt, S., J., Adams, N.,(2015) “Numerical Investigation of a Cavitating Model Propeller Including Compressible Shock Wave Dynamics”, Fourth International Symposium on Marine Propulsors smp’15, Austin, Texas, USA, June, 2015.

Burrill, L. C., Emerson, A., (1962-63) “Propeller Cavitation - Further Tests on 16in Propeller Models in the King's College Cavitation Tunnel”. Trans. NECI, 79, 1962-63.

Burrill, L.C., (1943) “Developments in propeller design and manufacture for merchant ships”. Transactions of the Institute of Marine Engineers, 1943.

Burrill, L.C., (1951) “Sir Charles Parsons and Cavitation”. Transactions of the Institute of Marine Engineers 63 (1951) 149–167.

Carlton, J. (2007). Marine Propellers and Propulsion, Elsevier Ltd.

Carlton, J., Radosavlijevic, D., Whitworth, S., (2009) “Rudder-Propeller-Hull Interaction: The Results of Some Recent Research, In-Service Problems and their Solutions”, 1st International Symposium on Marine Propulsors smp’09, June 2009, Trondheim, Norway.

Euler, M., (1756) “Théorie plus complete des machines qui sont mises en movement par la reaction de l’eau [The most complete theory of machines that are set in motion by the reaction of water]”, L’Académie Royale des Sciénces et Bélles Léttres, Berlin.

Felli, M., Falchi, M., (2011) “Propeller tip and hub vortex dynamics in the interaction

with a rudder”, Exp Fluids DOI 10.1007/s00348-011-1162-7.

Felli, M., Guj, G., Camussi, R., (2008) “Effect of the Number of Blades on Propeller Wake Evolution”, Experiments in Fluids, March 2008, Volume 44, Issue 3, pp 409-418.

Ferziger, J. H., Peric, M., (2002) “Computational Methods for Fluid Dynamics”, Springer, Third, Rev. Edition.

Fine, N. and Kinnas, S.A., (1993) “A boundary element method for the analysis of the flow around 3D cavitating hydrofoils”. J. Ship Research **37**, 213–224.

Fine, N. E. (1992) “Nonlinear Analysis of Cavitating Propellers in Non-uniform Flow”, PhD thesis, Department of Ocean Engineering, MIT.

Fitzsimmons, P. A., (2009) “Cavitation Development on Propulsors and Rudders”, 13th International Congress International Maritime Association of Mediterranean, 12-15 October 2009, Istanbul, Turkey.

Fujiyama, K., Kim, C-H., Hitomi, D., (2011) “Performance and Cavitation Evolution of Marine Propeller using Numerical Simulations”, The 2nd International Symposium on Marine Propulsors, smp’11, Hamburg, Germany, June 2011. Workshop: Propeller Performance.

Gaggero, S., Tani, G., Viviani, M. and Conti, F., (2014) “A Study on The Numerical Prediction of Propellers Cavitating Tip Vortex”, Ocean Engineering 92(2014)137–161.

Goodrich, G. J., Molland A. F., (1979) “Wind Tunnel Investigation of Semi-Balanced Ship Skeg Rudder”, Trans. RINA, Vol. 121.

Guilmineau, E., Deng, G., Leroyer, A., Queutey, P., Visonneau, M., Wackers, J., (2015) “Influence of the Turbulence Closures for the Wake Prediction of a Marine Propeller”, ERCOFTAC Workshop Direct and Large-Eddy Simulations 10, May 2015, Limassol, Cyprus.

Hallander, J., (2017) “Systematic Cavitation Tunnel Tests with a Propeller in Uniform and Inclined Flow Conditions as Part of a Round Robin Campaign”, The 5th International Conference on Advanced Model Measurement Technology for the Maritime Industry (AMT’17), Glasgow, UK.

Hallander, J., (2017) “Systematic Cavitation Tunnel Tests with a Propeller in Uniform and Inclined Flow Conditions as Part of a Round Robin Campaign”, The 5th International Conference on Advanced Model Measurement Technology for the Maritime Industry (AMT’17), Glasgow, UK.

Hallander, J., (2017) Systematic Cavitation Tunnel Tests with a Propeller in Uniform and Inclined Flow Conditions as Part of a Round Robin Campaign, The 5th International Conference on Advanced Model Measurement Technology for the Maritime Industry (AMT’17), Glasgow, UK.

Han, J-M., Kong, D-S., Song, I-H., (2001) “Analysis of the Cavitating Flow Around the Horn-Type rudder in the Race of a Propeller”, CAV2001:sessionB9.005.

Hess, J.L., Valarezo, W.O., (1985) “Calculation of Steady Flow about Propellers by Means of a Surface Panel Method”, AIAA, Paper No. 85, 1985.

Hill, J.G., (1949), “The design of propellers”, Trans. SNAME, 57, 1949.

Holden, K., (1981) “Effect of propeller design parameters on noise induced by cavitation”, in: A.C. Nilsson, N.P. Tyvand (Eds.), Noise Sources in Ships I:Propellers, Nordforsk, Miljovardsserien, Sweden.

Hsiao, C. T., Pauley, L. L., (1998) “Numerical Computation of Tip Vortex Flow Generated by a Marine Propeller", 1998 ASME Fluids Engineering Division Summer Meeting FEDSM'98 June 21 - 25, 1998 Washington D.C.

Hsiao, J. T., Chahine. G.L., (2008) “Scaling of Tip Vortex Cavitation Inception for a Marine Open Propeller”, 27th Symposium on Naval Hydrodynamics Seoul, Korea.

ITTC Report, (2002) “Recommended Procedures testing and Extrapolation Methods Propulsion; Cavitation. Description of Cavitation Appearances”, in ITTC – Recommended Procedures, 7.5-02-03-03.2, Propulsion Committee of 23rd ITTC. p. 7.

ITTC Report, (2014) "Cavitation Induced Pressure Fluctuation Model Scale Experiments", in ITTC Recommended Procedures, 7.5-02-03-03.3.

ITTC Report, (2017a) “Specialist Committee on Hydrodynamic Noise, Final Report and Recommendations to the 28th ITTC”.

ITTC Report, (2017b) “Propulsion Committee, Final Report and Recommendations to the 28th ITTC”.

Keller, J. (1966) auf’m. Enige Aspecten bij het Ontwerpen van Scheepsschroeven. Schip enWerf, No. 24, 1966.

Kinnas, S., Hsin, C-Y., (1992) A Boundary Element Method for the Analysis of the Unsteady Flow Around Extreme Propeller Geometries, AIAA Journal, 30, 3, March, 688-696.

Kinnas, S.A., Fine, N.E., (1994) "A Nonlinear Boundary Element Method for the Analysis of Unsteady Propeller Sheet Cavitation", Proceedings of Nineteenth Symposium on Naval Hydrodynamics, Office of Naval Research, National Academy Press, pp. 717-737.

Knapp, R. T., Daily, J. W., Hamitt, F. G., (1970) "Cavitation", New York, McGraw-Hill.

Knapp, R.T. Hollander, A., (1948) "Laboratory investigations of the mechanism of cavitation", Trans. ASME 70, 419–435.

Konno, A., Wakabayashi, K., Yamaguchi, H., Maeda, M., Ishii, N., Soejima, S., Kimura, K., Yamguchi, H., Maeda, M., Ishii, N., Soejima, S., Kimura, K., (2002) "On the Mechanism of the Bursting Phenomena of Propeller Tip Vortex Cavitation", J. Mar. Sci. Technol. 6, 181–192. doi:10.1007/s007730200006

Korkut, E., (1999), "An Investigation Into The Scale Effects on Cavitation Inception and Noise in Marine Propellers", School of Marine Science and Technology Technology, Newcastle University, Philosophy of Doctorate Thesis.

Kracht, A. M., (1995) "Cavitation on Rudders" An International Conference on Propeller Cavitation (PROPCAV'95) to celebrate 100 years of Propeller Cavitation Research 16-28 May 1995, Newcastle Upon Tyne, UK.

Kuiper G., (1981) "Cavitation Inception on Ship Propeller Models", Wageningen.

Lafeber, F., H., and Lloyd, T., (2017) "Round Robin Test on the Underwater Radiated Noise of a Cavitating Ship Propeller in Open Water", The 5th International Conference on Advanced Model Measurement Technology for the Maritime Industry (AMT'17), Glasgow, UK.

Lauterborn, W., Bolle, H., (1975) “Experimental Investigations of Cavitation-Bubble Collapse in the Neighborhood of a Solid Boundary”, Journal of Fluid Mechanics, Vol. 72, part 2, pp, 391-399.

Lee, C-S., (1979) “Prediction of steady and unsteady performance of marine propellers with or without cavitation by numerical lifting surface theory”, PhD thesis, MIT, Department of Ocean Engineering.

Lee, H., (2002) “Modeling of Unsteady Wake Alignment and Developed Tip Vortex Cavitation”, PhD Dissertation, University of Texas at Austin.

Lee, H., Kinnas, S. A., (2004) “Application of a Boundary Element Method in the Prediction of Unsteady Blade Sheet and Developed Tip Vortex Cavitation on Marine Propellers”, Journal of Ship Research, Vol. 48, No. 1, March 2004, pp. 15–30.

Lee, H., Kinnas, S. A., Gu, H., Natarajan, S., (2003) “Numerical Modeling of Rudder Sheet Cavitation Including Propeller/Rudder Interaction and the effects of a tunnel”, the 5th International Symposium on Cavitation (CAV2003), Osaka, Japan, November 1-4, 2003.

Leonard, A. (1974) “Energy cascade in large eddy simulations of turbulent fluid flows”, Adv. Geophys., 18A, 237

Li, Z., (2012) “Assessment of Cavitation Erosion with a Multiphase Reynolds-Averaged Navier-Stokes Method” PhD thesis, Delft University of Technology

Lloyd, T., Vaz, G., Rijpkema, D., Reverberi, A., (2017) “Computational fluid dynamics prediction of marine propeller cavitation including solution verification”, Fifth International Symposium on Marine Propulsors smp’17, Espoo, June 2017

Lloyd, T., Vaz, G., Rijpkema, D., Schuiling, B., (2015) “The Postdam Propeller Test Case in Oblique Flow: Prediction of Propeller Performance, Cavitation Patterns and Pressure Pulses”, The 2nd International Workshop on Cavitating Propeller Performance, Austin, Texas, 4th June 2015.

Mascio, A. D., Dubbioso, G., Muscari, R., (2015) “CFD Analysis of Propeller-Rudder Interaction”, The 25th International Ocean and Polar Engineering Conference, 21-26 June, Kona, Hawaii, USA.

Molland, A. F. and Turnock, S. R., (1991) “Wind tunnel investigation of the influence of propeller loading on ship rudder performance”, Southampton, UK. University of Southampton 151pp. (Ship Science Reports, 46) ,

Molland, A.F. and Turnock, S.R., (1992) “The prediction of ship rudder performance characteristics in the presence of a propeller”, Wilson, P.A.(ed.) In Manoeuvring and Control of Marine Craft. Proceedings of the Second International Conference, held in Southampton, UK, 14-17 July 1992. Computational Mechanics Publications. pp. 475-492.

Morgut, M., Nobile, E., (2012) “Numerical predictions of cavitating flow around model

Scale propellers by CFD and advanced model calibration”, Hindawi Publish. Corp. Int.

J. Rotating Mach. 2012, 618180. https://doi.org/10.1155/2012/618180. 11 pages.

Muzaferija, S., Papoulias, D., Peric, M., (2017) “VOF Simulations of Hydrodynamic Cavitation Using the Asymptotic and Classical Rayleigh-Plesset Models”, 5th International Symposium on Marine Propulsion smp’17, Espoo, Finland, June 2017.

Natarajan, S. (2003) “Computational Modelling of Rudder Cavitation and Propeller/Rudder Interaction”, Master Dissertation, The University of Texas at Austin.

Paik, K. J., Park, H. G., Seo, J. (2013) “RANS simulation of cavitation and hull pressure fluctuation for marine propeller operating behind-hull condition”, Int. J. Nav. Archit. Ocean Eng. (2013) 5:502~512 pISSN: 2092-6782, eISSN: 2092-6790.

Park, C., Seol, H., Kim, K., Seong, W., (2009) “A Study on Propeller Noise Source Localization in a Cavitation Tunnel”, Journal of Ocean Engineering, Volume 36, Issues 9-10, Pages 754-762.

Parkin, B.R. (1952) “Scale effects in cavitating flow”, Ph.D. Thesis, Calif. Inst. of Tech.

Parsons, C., (1897) “The Application of the Compound Steam Turbine to the Purpose of Marine Propulsion”, TINA, 38, 232-242.

Peng, H., Qiu. W., Ni, S., (2013) “Effect of Turbulence Models on RANS Computation of Propeller Vortex Flow”, Journal of Ocean Engineering, Volume 72, Pages 304-317.

Pennings, P., Westerweel, J., Terwisca, T., (2016) “Cavitation tunnel analysis of radiated sound from the resonance of a propeller tip vortex cavity”, International Journal of Multiphase Flow, 83 (2016) 1–11.

Pereira, F., Felice, F. D., Salvatore, F., (2016) “Propeller Cavitation in Non-Uniform Flow and Correlation with the Near Pressure Field”, Journal of Marine Science and Engineering, 4, 70; doi:10.3390/jmse4040070

Pereira, F., Salvatore, F., Felice, F. D., (2004) “Measurement and Modeling of Propeller Cavitation in Uniform Inflow”, Journal of Fluids Engineering, Vol. 126.

Phillips, A. B., Turnock, S. R., Furlong, M., (2010) “Accurate Capture of Propeller-Rudder Interaction using a Coupled Blade Element Momentum-RANS Approach”, Journal of Ship Technology Research, Schiffstechnik, Volume 57, 2010 – Issue 2.

Phillips, A.B., Turnock, S.R., (2011) “Application of the VORTFIND algorithm for the

identification of vortical flow features around complex 3D geometries”. Int. J. Numer.

Meth. Fluid. 2011 (00), 1–25.

Phillips, A.B., Turnock, S.R., 2011. Application of the VORTFIND algorithm for the identification of vortical flow features around complex 3D geometries. Int. J. Numer. Meth. Fluid. 2011 (00), 1 – 25.

Plesset, M. S. & Prosperetti, A. (1977) “Bubble Dynamics and Cavitation”, The Annual Review of Fluid Mechanics, Vol 9.

Plesset, M. S., (1948) “Dynamics of Cavitation Bubbles”, ASME J. Appl. Mech., 16, 228-231.

Plesset, M. S., Prosperetti, A., (1977) “Bubble Dynamics and Cavitation”, Ann. Rev. Fluid Mech. 1977. 9: 145-85

Plesset, M., S., (1970) “Cavitation Erosion in Noaqueous Liquids”, Journal of Basic Engineering, 92(4), 807-813.

Postdam Evaluation Reports Case 1 (2015)

Postdam Evaluation Reports, (2015) 4th International Symposium on Marine Propulsors, smp’15, Austin, Texas, June 2015.

Postdam Propeller Test Case Reports (2011), Report 3752, 3753 & 3754.

Prandtl, L., Tietjens, O.G., (1934) “Applied Hydro- and Aeromechanics”. United Engineering Trustees, 1934; also Dover, 1957.

Princess Royal Propeller Test Report (2017)

Rayleigh, L., (1917) “The pressure developed in a liquid during the collapse of a spherical cavity”, Phil. Mag., 34.

Reynolds, O., (1873) “The causes of the racing of the engines of screw steamers investigated theoretically and by experiments”, Trans. INA.

Roache, P. J., (1998) “Verification and Validation in Computational Science and Engineering”, Hermosa Publishers, Albuquerque, New Mexico.

Salvatore, F., Streckwall, H., Terwisga, T. (2009) “Propeller Cavitation Modelling by CFD- Results from the VIRTUE 2008 Rome Workshop”, 1st International Symposium on Marine Propulsors smp’09, Trondheim, Norway.

Sampson, R. and Turkmen, S. and Aktas, B. and Shi, W. Fitzsimmons, P. and Atlar, M. (2015) On the full scale and model scale cavitation comparisons of a Deep-V catamaran research vessel. In: Proceedings of the second Workshop on Cavitation and Propeller Performance. SMP, [S.I.]. ISBN 9780996459433.

Schneer, G. H., Sauer, J., (2001) “Physical and Numerical Modeling of Unsteady Cavitation Dynamics”, ICMF-2001, 4th International Conference on Multiphase Flow, New Orleans, USA, May 27-June 1, 2001

Schnerr, G. H. & Sauer, J. (2001) “Physical and Numerical Modelling of Unsteady Cavitation Dynamics”, International Conference on Multiphase Flow, New Orleans, USA.

Sharma, S.D., Mani, K., Arakeri, V.H., (1990) “Cavitation noise studies on marine propellers”, J. Sound Vib. 138 (1990) 255–283. doi:10.1016/0022-460X(90)90542-8.

Shi, W., Aktas, B., Atlar, M., Vasiljev, D., Seo, K. (2017) “Stereoscopic PIV aided wake simulation of a catamaran research vessel using a dummy-hull model in a medium size cavitation tunnel” Journal of Marine Science and Technology, October 2017.

SJTU, (2017) The Princess Royal Propeller Test Report.

SONIC (2012) 'Suppression Of underwater Noise Induced by Cavitation', in European Union Framework programme 7. FP7-SST-2012-RTD-1-SST.2012.1.1-1. - Assessment and mitigation of noise impacts of the maritime transport on the marine environment (coordinated topic within the framework of the ‘Ocean of Tomorrow’), FP7, Grant agreement no: 314394.

STAR-CCM+ User Guide, (2018)

Stern, F., Wilson, R.V., Coleman, H. W., Paterson, E.R, (2001) “Verification and Validation of CFD Simulations - Part1: Methodology and Procedures”, Journal of Fluids Engineering, Vol. 123.

Strscheletsky, M. (1950), “Hydrodynamische Grundlagen zur Berechnung der Schiffschranben”, G. Braun, Karlsruhe, 1950.

Szantyr, J. A. (2007a) “Mutual hydrodynamic interaction between the operating propeller and the rudder”, Archives of Civil and Mechanical Engineering, Vol. VII 2007 No. 3.

Szantyr, J. A. (2007b) “Dynamic Interaction of the Cavitating Propeller Tip Vortex with the Rudder”, Polish Maritime Research 4(54) 2007 Vol 14; pp. 10-14 DOI: 10.2478/v10012-007-0033-x.

Tani, G., Aktas, B., Viviani, M., Atlar, M., (2017a), “Two Medium Size Cavitation Tunnel Hydro-Acoustic Benchmark Experiment Comparisons as Part of a Round Robin Test Campaign”, Ocean Engineering 138 (2017) 179–207.

Tani, G., Aktas B., Vivani, M., Atlar, M., (2017b), “Hydro-acoustic Characterization of “The Princess Royal” Propeller as Part of a Round Robin Test Campaign”, The 5th International Conference on Advanced Model Measurement Technology for the Maritime Industry (AMT’17), Glasgow, UK.

Thornycroft, S. J., Barnaby, S. W. (1895) “Torpedo- boat destroyers”, Minutes of the Proced. Inst. Civil Engrs, p.50

Turkmen, S., Fukazawa, M., Sasaki, N., Atlar, M. (2018) “Cavitation Model Tests and Full-Scale Review of the First Gate Rudder System Installed on the 400TEU Container Ship” A. Yücel Odabaşı Colloquium Series 3rd International Meeting on Progress in Propeller Cavitation And its Consequences: Experimental and Computational Methods for Predictions, 14th – 16th November 2018, Istanbul, Turkey.

van Manen, J. D., van Oossanen, P., (1988) “Chapter VI – Propulsion”, Lewis, E. V. (ed.) In Principles of Naval Architecture Vol II – Resistance, Propulsion and

Vibration, The Society of Naval Architects and Marine Engineers 601 Pavonia Avenue Jersey City, NJ

Vaz, G., Bosschers, J., Modelling, (2006) “Three dimensional sheet cavitation on marine

propellers using a boundary element method” In: Sixth International Symposium on

Cavitation CAV2006, Wageningen, The Netherlands.

Vaz, G., Hally, D., Huuva, T., Bulten, N., Muller, P., Becchi, P., Herrer, J. L. R., Whitworth, S., Mace, R., Korsstrom, A., (2015), “Cavitating Flow Calculations for the E779A Propeller in Open Water and Behind Conditions: Code Comparison and Solution Validation.

Viitanen, V, M, Siikonen, T., (2017) “Numerical Simulation of Cavitating Marine Propeller Flows”, 9th National Conference on Computational Mechanics, MekIT’17.

Weitendorf, E. A., (2001) “On the History of Propeller Cavitation and Cavitation Tunnels”, CAV2001:sessionB9.0001

Wilson, R.V., Stern, F., Coleman, H. W., Paterson, E.R, (2001) “Comprehensive Approach to Verification and Validation of CFD Simulations—Part 2: Application for Rans Simulation of a Cargo/Container Ship”, Journal of Fluids Engineering, Vol. 123.

Windt, J., Bosschers, J., 2015. Influence of local and adaptive mesh refinement on the tip vortex characteristics of a wing and propeller. In: VI International Conference on Computational Methods in Marine Engineering, (MARINE 2015).

Yilmaz, N., Atlar, M., Fitzsimmons, P. A. (2018), “An Improved Tip Vortex Cavitation Model for Propeller-Rudder Interaction”, 10th International Cavitation Symposium (Cav’18), Baltimore, USA, May 2018.

Yilmaz, N., Atlar, M., Khorasanchi, M., (2019) “An Improved Mesh Adaption and Refinement Approach to Cavitation Simulation (MARCS) of Propellers”, Journal of Ocean Engineering, (1 January 2019)

Yilmaz, N., Khorasanchi, M., Atlar, M. (2017), “An Investigation into Computational Modelling of Cavitation in Propeller’s Slipstream”, 5th International Symposium on Marine Propulsion (Smp’17), Helsinki, Finland, June 2017.

Yilmaz, N., Turkmen, S., Aktas, B., Fitzsimmons, P., Sasaki, N., Atlar, M., (2018), “Tip Vortex Cavitation Simulation of a Propeller in a Gate Rudder System”, A. Yücel Odabaşı Colloquium Series 3rd International Meeting on Progress in Propeller Cavitation And its Consequences: Experimental and Computational Methods for Predictions, 14th – 16th November 2018, Istanbul, Turkey.

Young, Y.L., Kinnas S, A., (2001) “A BEM for the Prediction of Unsteady Midchord Face and/or Back Propeller Cavitation”, J. Fluids Eng 123(2), 311-319, Jan.